STUDIES ON LUMINESCENT PROPERTIES OF Eu^{3+} ACTIVATED MOLYBDATE AND TUNGSTATE BASED NOVEL RED PHOSPHORS

Thesis submitted to the Faculty of Science under
University of Kerala for award of the degree of

Doctor of Philosophy
in
Physics

Mariyam Thomas

MATERIALS SCIENCE AND TECHNOLOGY DIVISION
NATIONAL INSTITUTE FOR INTERDISCIPLINARY SCIENCE AND TECHNOLOGY (CSIR - NIIST)
THIRUVANANTHAPURAM
KERALA

August 2012

To my beloved parents…

DECLARATION

I hereby declare that this thesis entitled "**Studies on Luminescent properties of Eu^{3+} activated Molybdate and Tungstate based Novel Red Phosphors**" is an independent work carried out by me for the degree of Doctor of Philosophy in Physics of University of Kerala under the guidance of **Dr. Peter Koshy**, Chief Scientist (Rtd.), National Institute for Interdisciplinary Science and Technology, Thiruvananthapuram and **Dr. P. Prabhakar Rao**, Senior Principal Scientist, National Institute for Interdisciplinary Science and Technology, Thiruvananthapuram. I further declare that this thesis or part of it has not previously been formed the basis for the award of any degree or diploma.

21.08.2012
Thiruvanathapuram **Mariyam Thomas**

राष्ट्रीय अंतःविषय विज्ञान तथा प्रौद्योगिकी संस्थान
NATIONAL INSTITUTE FOR INTERDISCIPLINARY SCIENCE AND TECHNOLOGY
वैज्ञानिक तथा औद्योगिक अनुसंधान परिषद् | Council of Scientific and Industrial Research
इन्दुस्त्रिअल एस्टेट पी.ओ, पप्पनाम्कोड़े, तिरुअनंतपुरम, भारत 695019 | Industrial Estate P.O, Pappanamcode,Thiruvananthapuram,India 695019

21.08.2012

CERTIFICATE

This is to certify that this thesis entitled "**Studies on Luminescent properties of Eu^{3+} activated Molybdate and Tungstate based Novel Red Phosphors**" is an authentic record of bonafide research work carried out by Mrs. MariyamThomas, National Institute for Interdisciplinary Science and Technology, Thiruvananthapuram for the degree of Doctor of Philosophy in Physics of University of Kerala under our guidance and supervision.

Dr. Peter Koshy
Chief Scientist (Rtd.)

Dr. P. Prabhakar Rao
Senior Principal Scientist

Tel: 91 471 2490674 Fax: 91 471 2491895, 2491712, 2490389, (D) 2515239/256/384 Email: spo@niist.res.in Website: http//www.niist.res.in

ACKNOWLEDGEMENTS

At this moment of accomplishment, first of all I wish to thank God Almighty, for choosing me to be a part of this beautiful world and for all the blessings in my life.

I am extremely indebted to my guide Dr. Peter Koshy who has accepted me as his student and group member. I wish to thank him for his consistent support, valuable guidance, discussions and encouragements. With a great feel of pleasure I would like to express sincere gratitude to Dr. P. Prabhakar Rao, who also has guided me with whole hearted support. I wish to thank him for all discussions, valuable suggestions and abiding guidance.

I wish to pass on my thankfulness to Dr. Suresh Das Director, NIIST, and former directors Dr. T. K. Chandrashekar and Dr. B. C Pai for the infrastructural facilities provided. I sincerely thank Dr. K. G. K. Warrier, Dr. M. T. Sebastian, Dr. U. Syamaprasad and Dr. Manoj Rama Varma and all the Scientists of Materials Science and Technology Division for extending the research facilities.

I am privileged to thank Kerala State Council for Science, Technology and Environment (KSCSTE) for the financial support granted to me to carry out my research work through Junior Research Fellowship, 2007. Also I am thankful to Council for Scientific and Industrial Research (CSIR) for providing me all the facilities and infrastructure to perform my research work.

I am grateful to Mr. M.R Chandran and Mrs. Lucy Paul for giving me an insight into the morphology of the samples through the SEM analysis and also for the moral support. Let me also express my sincere thanks to Mr. M. R. Nair and Mr. V. Sreekantan for their persistent and instantaneous helping hands. I wish to thank Mr. P. Guruswamy for rendering the XRD data of the samples during the earlier stages of my research work.

This research work is an outcome of a team work where lot many were there on and off the scene with valuable and untiring support. Words are indeed insufficient to express my feeling of happiness for having a bunch of friends who are really making my life more colorful, vibrant and special. On this occasion, I wish to thank my senior colleagues Dr. Deepa M and Dr. Sibi K. S for the love and care that they have showered on to me during my research life. I am expressing my heartfelt thanks to all my colleagues Mrs. Sandhya Kumari,

Mr. Radhakrishnan, Mr. Mahesh, Mr. Vaisakhan Thampi, Mr. Shanoj, Ms. Sumi, Mrs. Sameera, Mrs. Reshmi, Ms. Linda Francis, Ms. Vineetha James, Ms. Divya, Ms. Ramya, Ms. Gayathri, Ms. Liji Nirmal who are there with me for the last years of my research life with whole hearted support and love. My special thanks are due to my roommates Ms. Raji, Mrs. Deepa, Mrs. Sandhya, Mrs. Neenu, Mrs. Sasikala who have been there to cherish my mind with fresh thoughts and lighter moments.

I wish to thank Krishna chechi and family for their prayerful support. I owe to Ms. Dhanya, Ms. Divya, Ms. Sheethu, Mrs. Reshmi, Mr. Manu, Mr. Dhanesh, Mr. Jobin, Dr. Biju, Dr. Savitha for the fruitful discussions they had with me and also for extending facilities to me. I am extending my special thanks to Dr. V. K Vaidian, Dr. Jayasree V, Dr. V. M Anand Kumar, Dr. Jojo P. J and Mr. Aneez Fayaz for their background support and encouraging words of happiness.

Let me extend my sincere thanks to my grandparents, who dreamt a lot and prayed for me. I wish to thank my parents and brother, who are there with me all the times, who moulded me with their advices, who attracted me with their simplicity of life, enduring love and care. I would like to extend my special thanks to my in laws, for their valuable support and prayers. I wish to express a word of gratitude to all my cousin brothers, sisters and family members. I wish to extend my thankfulness to my husband, Mathew George who has extended his full support for completing this research work.

At the end, I would like to thank all those people who were there with me to make this thesis possible and made my research life an unforgettable experience. Also I am extending my gratitude to all those (if any) who are missed from my list some how. Thank you all.

Mariyam Thomas

PREFACE

Inorganic luminescent materials have wide applications in many optoelectronic devices such as displays, sensors, light emitting diodes etc. An extensive research is going on in the field of white light generation from phosphor converted white light emitting diodes (pc-WLEDs) owing to their wide applications and advantages such as high luminous efficacy, low power consumption, long lifetime, high color rendering index (CRI), environmental friendliness etc. White light can be generated by mixing the primary colors and consequently the main approaches for generating white light are: mixing outputs of red, green and blue (RGB) LEDs, using an ultraviolet (UV) LED to stimulate red, green and blue phosphors and using a blue emitting diode that excites yellow or red and green phosphors. Each of these approaches has potential advantages and technical challenges. Among these approaches, phosphor converted WLEDs (pc-WLEDs) will yield a white output with good color rendering index, color reproducibility and are optically more stable under different driving currents. Development of novel phosphors for pc-WLED applications is one of the key challenging areas in this regard.

The phosphor materials being used currently for solid state lighting (SSL) based on near UV InGaN LEDs (λ_{em}: 370 - 410 nm) are $BaMgAl_{l0}O_{17}$: Eu^{2+} (blue), ZnS: Cu^{2+}, Al^{3+} (green) and Y_2O_2S: Eu^{3+} (red) and that for blue LED chip, the phosphors are $SrGa_2S_4$: Eu^{2+} (green) and SrY_2S_4: Eu^{2+} (red). However, the present red phosphors (mostly sulfides) have major limitations such as weak absorption in near UV region, inadequate lifetime under UV irradiation and chemical instability. In addition to these the brightness of red phosphors are about eight times less than that of green and blue phosphors. Consequently the problems of red phosphors are one of the major hurdles in the advancement of WLEDs which necessitates the development of novel, stable and efficient red phosphors to make pc-WLEDs a reality for general illumination.

From a practical point of view a light source comprising a red line emitter at 610 - 615 nm is the best compromise between luminous efficacy and color rendering. Eu^{3+} ions are considered to be preferable choice of activators for red luminescence as they exhibit a high lumen equivalent, quantum efficiency and photostability. However a drawback is the weak absorption of Eu^{3+} in the blue and even in the near UV region. The main strategy to solve this problem has been to choose suitable host materials that have broad - intense charge transfer (CT) absorption bands in the near UV and capable of efficiently absorbing the emission from InGaN based LEDs. Of many host lattices, molybdates and tungstates are superior because of good chemical, thermal and hydrolytic stability and the presence of broad - intense CT band

in the near UV region. A recently adopted strategy is to convert near UV or blue light via the 4*f*–4*f* transitions of Eu^{3+} located at 394 ($^7F_0$–$^5L_6$) and 465 nm ($^7F_0$–$^5D_2$), which are rather intense in molybdates and tungstates. Among Eu^{3+} doped molybdate and tungstate based red phosphors, $CaMo/WO_4$: Eu^{3+} are superior but charge compensation is required for their better luminescence performance. Keeping all these facts in mind, in the current research work an attempt has been made to develop novel red phosphors based on molybdate and tungstate host lattice. The idea is to modify the lattice of $CaMo/WO_4$: Eu^{3+} and their CT band position. No charge compensation approach is required here.

The present research work has been divided into three parts. In the first part, Eu^{3+} activated molybdate/tungstate based Powellite/Scheelite type red phosphors, $Ca(La/Gd)_{1-x}NbMo/WO_8$: xEu^{3+} (CL/GNM and CL/GNW) have been synthesized via solid state reaction (SSR) route. The structural, microstructural and photoluminescence properties were studied in detail. The optimum red luminescence of these phosphors with activator concentration is studied. The investigations on its luminescent properties revealed that these samples are well excitable under near UV and blue irradiations via intra configurational *f-f* transitions of Eu^{3+}. For both molybdates and tungstates, the excitation band corresponding to charge transfer transitions are clearly observable and are stronger in the case of molybdate based samples than tungstates. Moreover, the CT band of molybdate samples is positioned at a lower energy region compared to the corresponding tungstates leading to a more probable host sensitized energy transfer process in the case CL/GNM samples. As the activator ions (Eu^{3+}) are distributed in the non centrosymmetric sites in the lattice of both CL/GNM and CL/GNW phosphors, they emit sharp red light via $^5D_0$ - $^7F_2$ transitions. The lifetimes of Eu^{3+} states in the current phosphors are in the order of milli seconds. The red emission lines of these phosphors are characterized by good color purity and quantum efficiency (*Chapters 3 and 4*).

Second and third part of the research work was concerned with the attempts for improving luminescent properties of the aforementioned red phosphors. An improvement in the red emission of phosphors is possible by red shifting the CT band position. For this purpose, a suitable codopant (Bi^{3+}) is incorporated in the optimized red phosphors (CL/GNM and CL/GNW). The luminescence properties of the phosphors with respect to Bi^{3+} codoping are investigated in detail. The variation of different attributes of the phosphors such as asymmetry ratio, lifetime and absorption strength etc. with respect to Bi^{3+} codoping is discussed. The red shifting of CT band position of both molybdates (313 nm to 330 nm) and tungstates (290 to 324/327 nm) is accomplished by Bi^{3+} codoping. Both the position and intensity of CT band of the phosphors played a key role in controlling their luminescence

behavior. In the case of tungstate based red phosphors the Bi^{3+} codoping not only red shifted the CT band position but also intensified the CT transitions. In addition to this, Bi^{3+} codoping influenced the microstructure of both phosphors progressively. The extent of agglomeration of both phosphors reduced to a great extent through Bi^{3+} incorporation, which also had a direct contribution to their luminescence enhancement. Consequently an improvement in the red emission intensity of both CL/GNM and CL/GNW phosphors happened (~2 times). The details of the role of Bi^{3+} in both lattices and variation in the luminescence properties with respect to Bi^{3+} codoping are included in this section (*Chapter 5*).

The effect of physical properties of the phosphors on their luminescence properties are studied in the third part. This is motivated by the fact that in addition to the position and intensity of CT band, the physical properties of phosphors such as crystallinity, surface area, morphology and distribution of activator etc. have crucial roles in determining their luminescence properties. These properties can be controlled by the variation in the synthesis method and heat treatment process. Thus the optimized red phosphors are synthesized via citrate gel (CG) route. Effect of heat treatment process on their luminescence properties is also studied. The phosphor particles attained uniform particle shape as well as narrow size distribution via the CG route and the average particle size is reduced from 5 μm to 100 nm - 1 μm. An enhanced red emission (~4 times) is achieved by the variation in the synthesis method and heat treatment process. The lifetime variation of the phosphors with respect to heat treatment process revealed the possibility of overlapping of CT states of the host lattice with *f-f* levels of Eu^{3+} and hence the non radiative energy transfer process. These phosphors are characterized by longer lifetime than their SSR analogues (*Chapter 6*).

A brief outline of the thesis covering the aforementioned research work is as follows. First chapter presents a brief introduction to the state of the art in research efforts on red phosphors for pc-WLED applications. The details of the synthesis methods and characterization techniques are included in the second chapter. The results and discussion of three parts of the research work on red phosphors are included in the consecutive chapters (Chapters 3 to 6). Major conclusions and future scope of the current research work are presented in the last chapter (Chapter 7).

To sum up, luminescent properties and its improvement factors of many Eu^{3+} activated molybdate and tungstate based novel phosphors were studied. The red phosphors developed in this study are characterized by strong red emission under both near UV and blue excitations with comparable CIE color co ordinates to that of NTSC standard red phosphors and these could be promising red phosphors for pc-WLED applications.

Mariyam Thomas

CONTENTS

LIST OF TABLES

LIST OF FIGURES

ABBREVIATIONS

CCT	:	Correlated Color Temperature
CG	:	Citrate Gel
CIE	:	Commission Internationale de I' Eclairage
CN	:	Co ordination Number
CRI	:	Color Rendering Index
CT	:	Charge Transfer
CTB	:	Charge Transfer Band
CTS	:	Charge Transfer States
EM	:	Emission
EX	:	Excitation
FT- IR	:	Fourier Transform Infrared
FWHM	:	Full Width at Half Maximum
LMCT	:	Ligand to Metal Charge Transfer
NTSC	:	National Television Standards Committee
OLED	:	Organic Light Emitting Diodes
PC- WLED	:	Phosphor Converted White Light Emitting Diode
PL	:	Photoluminescence
SEM	:	Scanning Electron Microscopy
SSL	:	Solid State Lighting
SSR	:	Solid State Reaction
UV	:	Ultraviolet
XRD	:	X ray Diffraction

CHAPTER 1

INTRODUCTION AND LITERATURE REVIEW

Inorganic luminescent materials have wide applications in many optoelectronic devices such as displays, sensors, light emitting diodes etc. The research on solid state lighting based on phosphor converted white light emitting diodes (pc-WLEDs) has gained an incredible drive in the past decade due to their inherent advantages and wide applications. pc-WLEDs have several advantages over conventional lighting technologies: long lifetime, high luminescence efficiency, low power consumption etc. are some of them. This chapter narrates an introduction to solid state lighting, ways of white light generation and basic concepts of phosphors including energy processes, performance requirements, need for development of new red phosphors etc. The state of the art in research efforts on red phosphors, specifically Eu^{3+} activated molybdate and tungstate based phosphors for pc-WLED applications is also included and the chapter ends up with an overview of the current research work.

1.1 Solid State Lighting

Energy is one of the major inputs for economic development of any country. An important and mounting use of energy is the generation of electricity. Efficient use of electricity necessitates persistent energy conservation efforts. Energy efficiency is achieved when energy usage in a specific product is reduced without affecting output or user comfort levels. About 20% of electricity is used for lighting. The most widely used sources of artificial illumination are incandescent and fluorescent lamps. Conventional incandescent and fluorescent lamps rely on either heating or discharge of gases. Both phenomena are associated with large energy losses that occur because of the high temperatures and large Stokes shifts involved. There is a considerable scope of reducing energy consumption through energy efficient lighting schemes. Solid state lighting (SSL) is emerging as a highly proficient field and a possible substitute to existing lighting technologies. The research on SSL has gained incredible drive in the past decade due to their inherent advantages of high light efficiency, low energy consumption, long service lifetime and durability compared to conventional light sources (Nakamura S *et al* 1994; Aanegola S *et al* 2003; Narukawa Y *et al* 2004; Rohwer L. S *et al* 2003). Lighting applications that use light emitting diodes (LEDs), organic light emitting diodes (OLEDs) or light emitting polymers are commonly referred to as solid state lighting (SSL). Unlike incandescent or fluorescent lamps, which create light with filaments and gases encased in a glass bulb, solid state lighting consists of semiconductors that convert electricity into light.

In 1907, H. J. Round reported on light emission from a silicon carbide junction diode, which is the first light emitting diode (LED) ever. Independently, Losev observed emission from ZnO and SiC diodes, as published in 1927 (Zheludev N *et al* 2007). At that time the potential of the technology was not realized and the inventions remained largely unnoticed. It was not until 1962 that the first practical visible spectrum LED was developed, by Nick Holonyak at General Electric. In the decades that followed, LEDs were used extensively in numerical displays and signaling applications because the wavelengths produced by semiconductor lasers have generally been longer than 0.7 μm. However this situation was completely changed with Shuji Nakamura's invention, who successfully fabricated double hetero structure InGaN/GaN blue LED chips for the first time in 1993 and later in 1994 succeeded in producing high power blue InGaN/AlGaN LEDs suitable for commercial applications (Nakamura S *et al* 1994; 1997), which made it possible to use LEDs for general lighting. The operation of LEDs is based on spontaneous light emission in semiconductors, which is due to the radiative recombination of excess electrons and holes that are produced

by the injection of current. Therefore, LEDs are not limited by the fundamental factors that still existed in conventional incandescent lamp and compact fluorescent lamp (Schubert E. F *et al* 2005). Thus SSL offer unprecedented promises that include three major benefits: (i) Huge energy savings enabled by efficient conversion of electrical energy to optical energy (ii) Substantial positive contributions to sustainability through reduced emissions of global warming gases, acid rain gases and toxic substances such as mercury (iii) The creation of new paradigms in lighting driven by the unique controllability of solid state lighting sources. Due to the powerful nature of these benefits, the transition from conventional lighting sources to SSL is virtually assured.

SSL based on white light emitting diodes (WLEDs) have got much attention in recent years because of their wide applications as well as their advantages over conventional light sources such as high color rendering index (CRI), long lifetime, high luminescence efficiency, low power consumption, environment friendliness etc (Krames M. R *et al* 2007; Yamada M *et al* 2005). First WLED was developed by Nichia Chemical Co. in 1996 by means of a blue InGaN LED chip coated with yttrium aluminum garnet yellow phosphor ($Y_3Al_5O_{12}:Ce^{3+}$, YAG: Ce) (Nakamura S *et al* 1997). The main drawbacks of YAG based WLEDs are poor color rendering and serious thermal quenching of luminescence. When the chip is driven under certain current, blue light is emitted by the InGaN chip through electron hole recombination in p - n junctions. Some of the blue light from the LED excites the YAG: Ce phosphor to emit yellow light and then the rest of the blue light is mixed with the yellow light to generate white light. Until now, the conventional white light sources have almost reached their physical limit of efficiency while white LEDs have not. The luminescence efficiency of semiconductor based white LEDs can be greatly improved by reducing the non radiative recombination of electron hole pairs in the p - n junctions and designing a new structure to enhance external quantum efficiency. Based on the physical principles, the luminous efficiency of white LEDs can approach 200 lm/W by the year of 2020 which will be far greater than that of incandescent lamps and fluorescent lamps (Shur M.S *et al* 2005). A comparison of luminous efficacies of different lighting sources is presented in Table 1.1.

Table 1.1 Luminous efficacies of various lighting sources

Lighting Source	Incandescent	Linear Fluorescent	Compact Fluorescent	LED (Commercial)	LED (Lab)
Luminous Efficacy (lm/W)	5-15	90	40 - 60	30 – 80	150

1.2 White Light Generation: Different Approaches

Generally there are three different approaches which can be used for generating white light based on LEDs. They are; (1) by mixing reds, greens and blues, i.e., outputs of red, green, blue (RGB) LEDs (2) by using an ultraviolet (UV) LED to stimulate RGB phosphors and (3) by using a blue emitting diode that excites a yellow emitting phosphor embedded in the epoxy dome; the combination of blue and yellow light makes a white emitting LED. The different approaches for white light generation are schematically represented in Fig. 1.1.

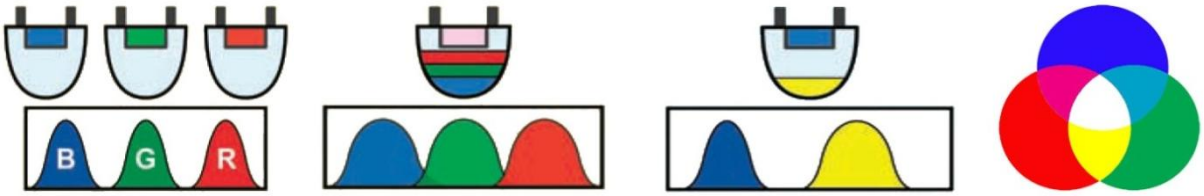

Fig. 1.1 Different approaches to generate white light.

Each of these approaches has potential advantages and clear technical challenges. Mixing the emission from red, blue and green colored LEDs is the most straightforward technique since there is no quantum deficit arising from Stokes shift and hence offers infinitely graduated color and white point control. However this form requires independent output power control on each LED and moreover there is a gap in the operating voltage between them making the operation quite cumbersome. The instability of color temperature also exists for RGB LED approach due to the degradation of different color LEDs with variations of driving current. White LEDs can be fabricated by coating UV LED chips with white light emitting single phased phosphors or RGB tri color phosphors. Here UV light is completely absorbed by the single phosphor or mixed RGB phosphors and the output appears white. The quantum deficit between the UV pump and the phosphors especially the low energy red phosphor, dissipates significant energy and makes this approach inherently less efficient than the RGB LED scheme for generating white light.

However, the UV LED approach has the advantage that color can be controlled by the phosphor mix at least at one point in time and at one temperature and hence the color rendering should be excellent. Today's commercial pc-WLEDs normally use a 450 - 470 nm blue GaN LED chip covered by a yellowish phosphor coating, which is usually made of YAG:Ce. The pc-WLEDs made by means of blue LED + YAG: Ce yellow phosphors suffer some weaknesses, such as poor color rendering index and low stability of color temperature. Since the white light is generated by the combination of blue light emitted by an LED chip

and yellow light emitted by YAG:Ce phosphors, deterioration of the chip or YAG:Ce phosphors would cause some significant color changes (Steigerwald D. A *et al* 2002). Despite the variation of driving current, WLEDs are optically much more stable. It is considered that WLEDs might be the direction of SSL development for their high efficiency and easy fabrication. In order to make SSL based on pc-WLEDs a reality for general illumination we have to overcome many significant technical challenges and development of luminescent materials (phosphors) is one of the key challenging areas.

1.3 Phosphors: Basic Concepts

Phosphors are materials that exhibit the phenomenon of phosphorescence, which is a form of luminescence. Luminescence is emission of light by a material as a consequence of absorbing energy. It differs from incandescence, which is a process in which solids emit light by reason of their high temperatures (Hill C. G. A 1984). It arises when atoms of a solid become energized in some way without appreciably heating the bulk material. These atoms then release the excess energy in the form of ultraviolet, visible or infrared radiation (Nalwa H.S *et al* 2003). Depending on the excitation source there are different kinds of luminescence namely; chemiluminescence, electroluminescence, photoluminescence where the excitation sources are chemical reaction, electric field, electromagnetic radiation respectively.

Generally the term photoluminescence take into the account of two phenomena such as fluorescence and phosphorescence shown in Fig. 1.2. Fluorescence corresponds to emission process involving a spin allowed (singlet, S – singlet, S) transition and is characterized by short lifetime of about $\leq 10^{-8}$s. On the other hand phosphorescence corresponds to emission process involving a spin forbidden (singlet, S – triplet, T) transition and is characterized by long lifetime of about $\geq 10^{-8}$s. Since inorganic phosphors for WLED applications are excited by the radiative emission of LED chips, the luminescence of the phosphors is expressed as photoluminescence (PL) (Feldmann C *et al* 2003).

Phosphors are usually made from a suitable host material (H), to which an activator (A) is added. The host materials are typically oxides, nitrides, oxynitrides, sulfides, selenides, halides or silicates of zinc, cadmium, manganese, aluminum, silicon or various rare earth metals. The activators are luminescent centers, where the electrons radiatively relax and prolong the emission time (afterglow). They are often impurity metal cations such as Mn^{2+}, Sb^{3+}, Ce^{3+}, Eu^{2+}, Tm^{3+}, Er^{3+}, $Tb^{3+,}$ Pr^{3+}, Eu^{3+} etc. If activator does not absorb the excitation radiation effectively, it is possible to excite the activator by indirect means. In such cases, sensitizers (S) play the role. Sensitizers are ions or ionic groups incorporated in the host lattice which absorb the radiation and it can return to the ground state in three ways; by

radiation, by the dissipation of excitation energy in the form of heat and by transfer of excitation energy to the activator (Blasse G 1979). The physical phenomenon associated with a phosphor material is briefly represented in Fig. 1.3.

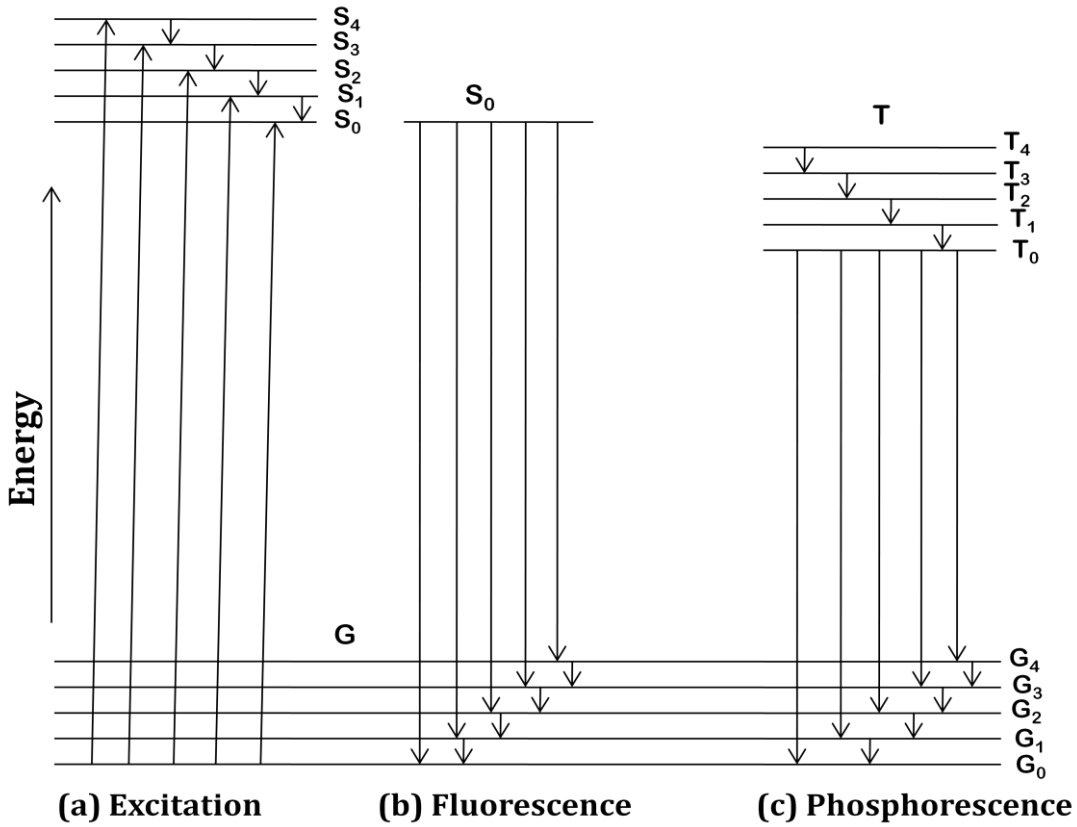

Fig. 1.2 Energy process involved in excitation, fluorescence and phosphorescence.

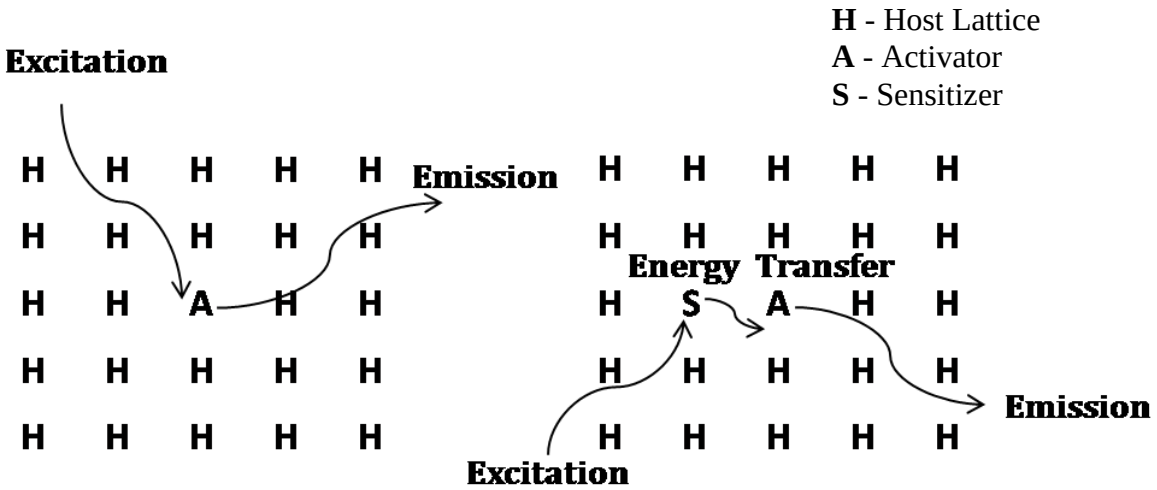

Fig. 1.3 Physical phenomenon associated with a phosphor.

1.3.1 Energy process in a phosphor

The sequences of energy processes that occur within a phosphor include (Nalwa H. S *et al* 2003):-

- Absorption of energy (from a variety of sources).
- Excitation within the activator center to form an excited state (10^{-11} s).
- Relaxation of the excited state (energy is lost to the vibrational states of the lattice) (10^{-8} s).
- Emission of a lower energy photon from the excited state, and relaxation to the original (ground) state (10^{-9} - 10 s).

In a phosphor, absorption of energy may occur in the host or directly in the activator center (the added transition metal ion). But it is the activator center (site) which becomes excited whether by transfer of energy from the host or not. There may be several excited states possible but only the lowest excited state is involved in photon emission. If more than one excited state does occur, each excited state relaxes to the next lower energy excited state until the final excited state is reached, whereupon photon emission occurs in due time. Whether upper excited states are involved depends upon the original energy of the exciting photon. This energy may exceed the minimum energy needed for excitation and the excess energy causes the upper excitation states to become populated or even ionized.

The configurational co-ordinate diagram is usually used to describe the PL mechanism of an activator (Nalwa H. S *et al* 2003). As shown in Fig. 1.4, the total energy E of the activator is plotted as a function of r, the distance between metal cations and anions in the lattice. The horizontal dashed lines in ground state and excited state curves denote the vibrational states. r_0 and r_1 represent the equilibrium distances of the ground state activator and the excited state activator respectively. When the activator absorbs some radiation light, an expansion of the lattice occurs in the vicinity of the activator ion and the activator is raised to the excited state (Blasse G *et al* 1970).

The excitation (EX) and emission (EM) processes are illustrated by vertical arrows, showing that the nucleus of the activator stays at approximately the same position during these processes. This is the so called Franck Condon principle, which is based on the fact that an atomic nucleus is 10^3-10^5 times heavier than an electron, and an electron moves much faster than a nucleus (Shigeo Shionoya W. M. Y 1999). The energy difference between EX and EM is known as the Stokes shift. When the temperature of the phosphor exceeds a specific value, the vibrational energy makes the excited activator reach the Q point of the

excited state curve and then the activator returns to ground state without radiation, which is called temperature quenching.

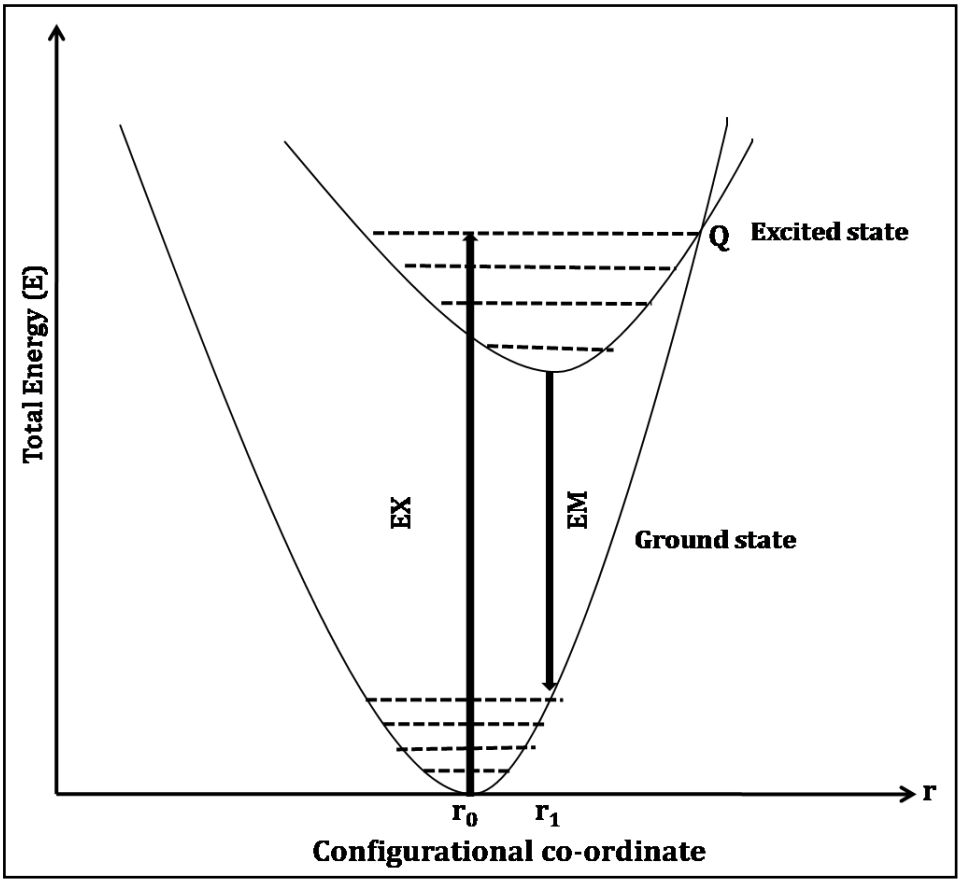

Fig. 1.4 Configurational co-ordinate model.

The principal localized luminescent centers can be classified by their electronic transitions as follows (below, an arrow to the right (→) indicates optical absorption and to the left (←), emission) (Shigeo Shionoya W. M. Y 1999):

(i) $1s \leftrightarrow 2p$; F.

(ii) $ns^2 \leftrightarrow ns\ np$; Ga^+, In^+, Tl^+, Ge^{2+}, Sn^{2+}, Pb^{2+}, As^{3+}, Sb^{3+}, Bi^{3+}, Cu^-, Ag^-, Au^-, etc.

(iii) $nd^{10} \leftrightarrow nd^9(n+1)s$; Cu^+, Ag^+ and Au^+.

(iv) $3d^n \leftrightarrow 3d^n$, $4d^n \leftrightarrow 4d^n$; first and second transition metal ions.

(v) $4f^n \leftrightarrow 4f^n$, $5f^n \leftrightarrow 5f^n$; rare earth and actinide ions.

(vi) $4f^n \leftrightarrow 4f^{n-1}5d$; Ce^{3+}, Sm^{2+}, Eu^{2+}, Tm^{2+}, Yb^{2+}.

(vii) A charge transfer transition or a transition between an anion *p* electron and an empty cation orbital. eg: Intra molecular transitions in complexes such as VO_4^{3-}, MoO_4^{2-} and WO_4^{2-}.

Rare earth and transition metal ions are most frequently used activators in phosphors and are characterized by an incompletely filled 4*f* shell. The 4*f* orbital is shielded from the surrounding, by the filled $5s^2$ and $5p^6$ orbitals. Therefore the influence of crystal lattice on the optical transitions within the $4f^n$ configuration is small but essential. Intra configurational 4*f*-4*f* optical (electric dipole) transitions are strongly forbidden by the parity selection rule (Blasse G 1994).

When an atom is free or in a spherical symmetry field, its electronic states are denoted by a set of the quantum numbers S, L and J in the LS coupling scheme. Here S, L and J denote the quantum number of the spin, orbital and total angular momentum respectively. Then the selection rules for electric dipole and magnetic dipole transitions in the LS coupling scheme are given by;

$$\Delta S = 0, \Delta L = 0, \pm 1 \quad (1.1)$$

$$\Delta J = \pm 1, 0 \ (J = 0 \rightarrow J = 0, \text{Not allowed}) \quad (1.2)$$

If the spin orbit interaction is too large to use the LS coupling scheme, the JJ coupling scheme might be used in which many (S, L) terms are mixed into a J state. In the JJ coupling scheme therefore the ΔS and ΔL selection rules in Eqn. (1.1) and (1.2) are less strict and only the ΔJ selection rule applies.

The parity selection rule will be relaxed in some cases especially when the rare earth ion occupies a site without inversion symmetry. In such cases, uneven components of crystal field mix a small amount of opposite parity wave functions (like 5*d*) into the 4*f* wave functions. i.e., the forbidden 4*f*-4*f* transition steals some intensity from the allowed 4*f*-5*d* transitions. The selection rule for the partially allowed electric dipole *f-f* transition is $|\Delta J| \leq 6$ (J = 0 – 0, 1, 3, 5 are forbidden).

The allowed optical transitions of rare earth ions are inter configurational and are of two types. They are charge transfer (CT) transitions ($4f^n \rightarrow 4f^{n+1}L^{-1}$, where L = ligand) and $4f^n \rightarrow 4f^{n-1}5d$ and are corresponding to broad absorption bands. These are parity allowed magnetic dipole transitions (Blasse G 1994).

1.4 Basic Terminology

A good illuminating source for sophisticated applications like indoor lighting requires warm white light with an excellent color rendering index, high luminous efficacy and good output color purity. Basic terms associated with lighting sources specifically pc-WLEDs are briefly given below.

1.4.1 CIE chromaticity coordinates

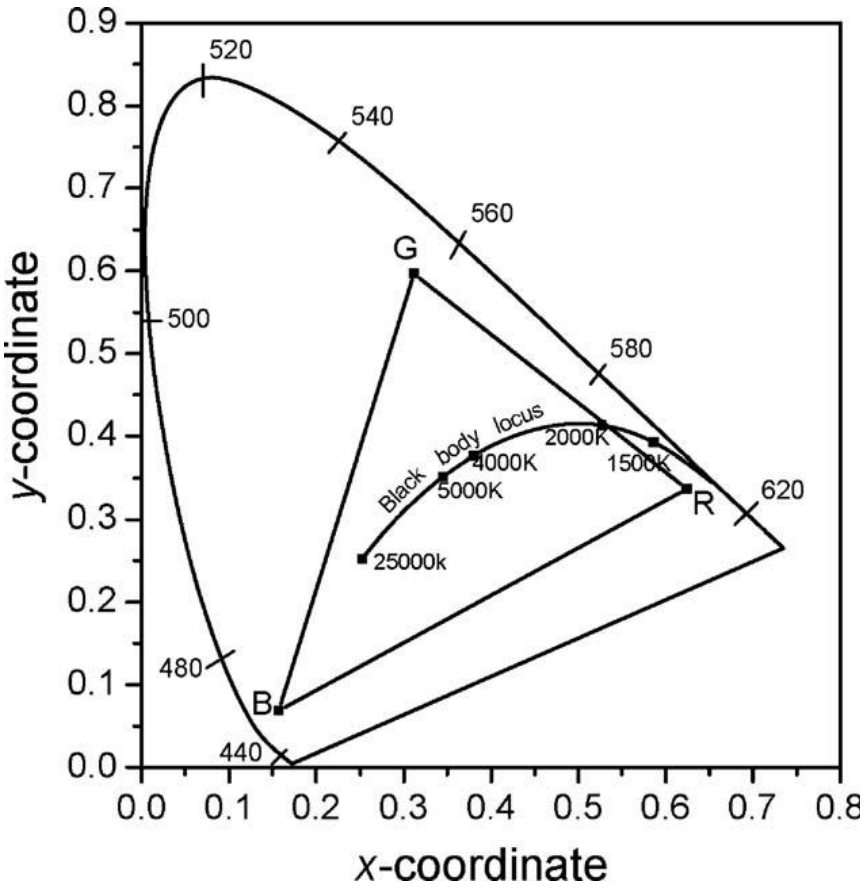

Fig. 1.5 CIE chromaticity co-ordinate diagram.

The Commission Internationale de l' Eclairage (CIE) system is the most common method to describe the composition of any color in terms of three primaries as shown in Fig. 1.5 (Zhang Q. Y *et al* 2002). Artificial colors denoted by X, Y, Z also called tri stimulus values, can be added to produce real spectral colors. By a piece of mathematic legerdemain, it is necessary only to quote the quantity of two of the reference stimuli to define a color since the three quantities (x, y, z) are made always to sum to 1 (Stevens W. R 1969). The x, y, z, i.e., the ratios of X, Y, Z of the light to the sum of the three tri stimulus values, are the so-called chromaticity coordinates (Kaufman J. E *et al* 1972). (*x,y*) is usually used to represent the color. NTSC standard color coordinates of red is (0.67, 0.33).

1.4.2 Correlated Color Temperature (CCT)

Color temperature (Kelvin) is the absolute temperature at which a blackbody radiator must be operated to have a chromaticity equal to that of the light source (Kaufman J. E *et al* 1972). The light of an incandescent bulb is thermal radiation and the bulb is very close to an

ideal black body radiator, so its color temperature is the temperature of the filament. Many other light sources such as fluorescent lamps emit light by ways other than thermal radiation. Color temperature values associated with light sources other than incandescent lamps are correlated color temperature (CCT) and not true color temperatures. Correlated color temperature is the temperature of a blackbody whose chromaticity most nearly resembles that of a light source (Kaufman J. E *et al* 1972). Light sources with a higher CCT are said to be "cool" in appearance, while those with lower CCT are characterized as "warm".

1.4.3 Color Rendering Index (CRI)

CRI is a measure of the degree to which the perceived colors of objects illuminated by the source conform to those of the same objects illuminated by a reference source for specified conditions (Kaufman J. E *et al* 1972). It indicates how well a light source renders colors on a scale of 0 - 100, compared to a reference light source. The test procedure established by the International Commission on Illumination (CIE) involves measuring the extent to which a series of eight standardized color samples differ in appearance when illuminated under a given light source, relative to the reference source. The average shift in those eight color samples is reported as Ra or CRI. In addition to the eight color samples used by convention, some lighting manufacturers report an R9 score, which indicates how well the light source renders a saturated deep red color. A CRI of 100 would represent that all color samples illuminated by a light source in question would appear to have the same color as those same samples illuminated by a reference source.

1.4.4 Luminous Efficacy

Luminous efficacy is a figure of merit for light sources. The luminous efficacy of a light source is defined as the ratio of the total luminous flux (lumens) to the power (watts or equivalent) (Kaufman J. E *et al* 1972). Depending on context, the power can be either the radiant flux of the source's output or the total electric power consumed by the source. The lumen is defined as 1/683 W of monochromatic green light at a frequency of 540 x 10^{12} Hz (corresponding to a wavelength of about 555 nm where the human eye is most sensitive). This means that the theoretically attainable maximum value assuming complete conversion of energy at 555 nm would be 683 lm/W. The luminous efficacies that can actually be attained vary depending on the lamps, but always remain far below this ideal value. The luminous efficacy is always in contradiction with CRI, because a high CRI value requires proper spectral dispersion over all the visible range which would make the luminous efficacy far below 683 lm/W. Thus balanced values of these two parameters are adopted for different lighting occasions.

1.5 Performance requirements for color conversion phosphors

In pc-WLEDs, the phosphor (wavelength converters) absorbs the short wavelength emission from the primary LED chip and down converts it to a longer wavelength. The output of a WLED strongly depends on the performance of these conversion phosphors. Even though a large number of conversion phosphors are available, only limited number of them is suitable for wavelength conversion. The basic and key performance requirements for a phosphor for pc WLED are enlisted below (Smet P. F *et al* 2011):

- ✓ An emission spectrum that, in combination with the emission of the other components (LED, other phosphors) leads to a pure white emission with a specific color rendering and color temperature.
- ✓ An excitation spectrum showing good overlap with the pumping LED and large absorption strength.
- ✓ An emission spectrum, excitation spectrum and a quantum efficiency that remain unchanged at elevated temperature.
- ✓ A quantum efficiency approaching unity, thus maximizing the overall electrical to optical conversion efficiency of the entire LED phosphor package.
- ✓ An excellent chemical and temperature stability.
- ✓ Absence of emission saturation at high fluxes.

1.6 Need for developing new red phosphors

In order to make SSL based on pc-WLEDs as the source of general lighting, it is necessary to overcome many challenges. Developing conversion phosphors is one of the key challenging areas in this field. The phosphors for pc-WLEDs must combine high quantum efficiency and absorption for UV and blue radiation with the ability to withstand high temperature generated by the LED without degrading and quenching the luminescence, and moreover it should be chemically stable. Thus novel phosphor materials with improved properties are greatly in demand, for which choice of host lattice and activator is very important.

The first pc-WLED was based on blue GaInN LED pumping a YAG: Ce^{3+} yellow phosphor. The output of this LED phosphor combination is termed as 'lunar white' (Bando K *et al* 1998). It suffers some weaknesses such as poor color rendering index (CRI) because of the deficiency in the red spectral region and low stability of correlated color temperature (CCT). Achieving lower CCTs and higher CRIs require red phosphors to compensate for the spectral deficiencies of standard pc LEDs. There are two ways to generate warm white light: One is to combine an UV chip with tricolor (red, green and blue) phosphors and the other is

to compensate the red light deficiency of YAG:Ce^{3+} based LED with a separate red emitting phosphor (Kim J. S *et al* 2004). Both these approaches demand stable and efficient red phosphors.

The current phosphor materials used for SSL based on near UV InGaN LEDs (λ_{em} : 370-410 nm) are $BaMgAl_{10}O_{17}$: Eu^{2+} for blue, ZnS: Cu^{2+}, Al^{3+} for green and Y_2O_2S: Eu^{3+} for red and that for blue LED chip, the phosphors are $SrGa_2S_4$: Eu^{2+} for green and SrY_2S_4: Eu^{2+} for red (Nishida T *et al* 2003). Among these phosphors, the brightness of red phosphors is about 8 times less than that of green and blue phosphor materials. From the view point of SSL applications, it is necessary to develop novel red luminescent materials because in the currently developed red phosphors, the quantum efficiency and luminous efficacy for red emission is limited.

The well known red emitting phosphors for pc-WLEDs are usually sulfide semiconductors such as $Zn_{1-x}Cd_xS$: Ag (Huh Y. D *et al* 2003), SrY_2S_4: Eu^{2+} (Huh Y. D *et al* 2004), CaS: Eu^{2+} (Kato K *et al* 1983), SrS: Eu^{2+} (Yamashita N *et al* 1995), $Ca_{1-x}Sr_xS$: Eu^{2+} (Hu Y. S *et al* 2005), Ba_2ZnS_3: Mn (Thiyagarajan P *et al* 2006) etc. However, they suffer from poor chemical and photo stability, high cost or unsatisfactory efficiency. Efficient red emitting phosphors are still commercially limited to Eu^{2+} doped CaS and SrS, but their hygroscopic nature needs to be overcome by a complicated treatment. Y_2O_2S:Eu^{3+} also shows efficient red emission, but it lacks chemical stability, efficient absorption in the near UV region, adequate lifetime and brightness. Moreover, Y_2O_2S based red phosphors decompose and will produce sulphide gas which is harmful to the environment.

For these reasons, there is an urgent need to explore the possibility of designing a stable red phosphor with intense absorption in the near UV or blue region to increase the overall white light efficiency and lifetime. The research efforts on red phosphors for pc-WLEDs are included in later section.

1.7 Luminescence properties of Eu^{3+}

The characteristic properties of rare earth ions are attributable to the presence of deep lying 4*f* shell which is not entirely filled. Since the presence of the crystal lattice scarcely affects the position of these levels, there is a close resemblance between the energy level diagram of the free ion and that of the incorporated ion. Eu^{3+} ion has six electrons in the 4*f* shell and corresponding energy level diagram is shown in Fig. 1.6. The diagram shows that in addition to the discrete 4*f* levels there are other levels present. These are represented schematically as broad - hatched bands. The energy levels of these bands depend to a great extent on the host lattice. The bands referred to fall into two groups. In the first group one of

the 4*f* electrons is raised to the higher 5d level: $4f^{n} \rightarrow 4f^{n-1}5d$. This 5*d* level can be strongly influence by the host lattice. In the second group one of the electrons of the surrounding anions is promoted to the 4*f* shell of the Eu^{3+} ion (charge transfer state). Obviously the position of this energy band depends on the surrounding ions (Blasse G 1994).

The luminescence properties of trivalent europium (Eu^{3+}) ions have got technological importance because it has been widely applied to phosphors for color displays and fluorescent lamps. The emission of Eu^{3+} ion consists of usually lines in the red spectral region. These lines correspond to transitions from the excited $^5D_0$ level to the ^7F_J (J = 0, 1, 2, 3, 4, 5, 6) levels of $4f^6$ configuration.

Since the $^5D_0$ level will not split by the crystal field (because J = 0), the splitting of emission transitions yields the crystal field splitting of the ^7F_J levels (Blasse G 1994). The emission wavelengths of Eu^{3+} are determined primarily by their local environment in host crystals. When the Eu^{3+} ion occupies a site with inversion symmetry, the $^5D_0$-$^7F_1$ magnetic dipole transition (usually observed at ~592 nm) is dominating and $^5D_0$-$^7F_2$ electric dipole transition (with emission wavelengths of approximately 610 - 620 nm) dominates when it occupies a site without inversion symmetry (Blasse G 1979).

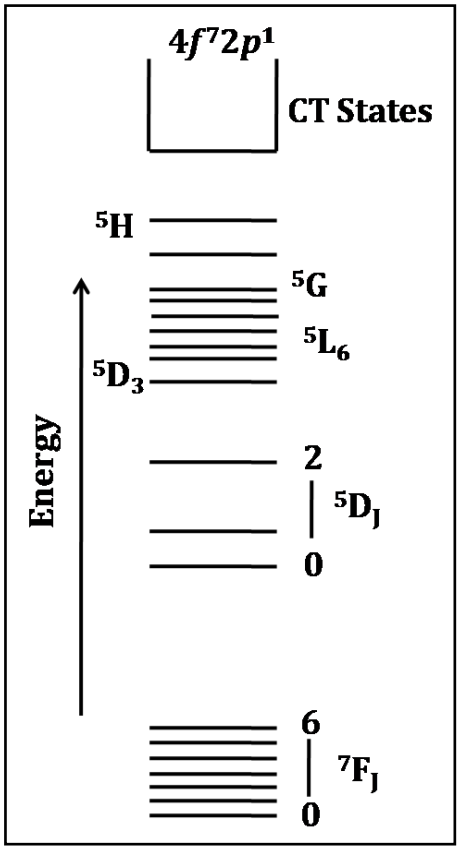

Fig. 1.6 Energy level diagram of Eu^{3+} ion.

Actually, both the electric dipole and the magnetic dipole transitions appear simultaneously in practical inorganic luminescent materials although their intensities are different. The luminescence intensity ratio of $^5D_0$-$^7F_2$ (electric dipole) transition to $^5D_0$-$^7F_1$ (magnetic dipole) transition called as asymmetry ratio gives a measure of the degree of distortion from inversion symmetry of the local environment around the Eu^{3+} ions in the host matrix. Eu^{3+} doped red phosphors are of great interest for the application in near UV LEDs, since they exhibit a high lumen equivalent, quantum efficiency and photostability at the same time. Moreover, from a practical point of view a fluorescent light source comprising a red line emitter emitting at 610–615 nm is the best compromise between luminous efficacy and color rendering (Ronda C 2008).

1.8 Crystal structure of ABO_4 type Molybdates and Tungstates

Binary oxides with the general formula ABO_4 in which A and B cations can be multivalent and compositely substituted, have several common structure types. The common crystal structures of ABO_4 oxides are zircon type, scheelite type and wolframite type. ABO_4 oxides such as silicates, phosphates, arsenates, vanadates and chromates are iso structural with zircon ($I4_1/amd$, No.141). A few ABO_4 oxides such as germanates, molybdates and tungstates crystallize in the scheelite structure ($I4_1/a$, No.88). Large number of molybdates, tungstates and tantalates crystallize with the wolframite structure (P2/c, No.13) and relatively few ABO_4 oxides exist as M' fergusonite structures ($P2_1/c$, No.14). Many of ABO_4 oxides transform from zircon or scheelite structures to M' fergusonite under pressure and the fergusonite structure can be viewed as a distorted scheelite structure (Lia H *et al* 2007).

In the scheelite type structure, the A cations are surrounded by eight oxygen atoms with two different distances, the B cations coordinate with four oxygen atoms, and the oxygen anions are connected with two A ion and one B ion. The BO_4 tetrahedra in scheelite structure are more distorted and are densely packed than the zircon structure. The scheelite structure is characterized by the layered stacked cell and so it can be readily distinguished from the other structures exhibited by ABO_4 oxides. The layered stacked cell of scheelite type ABO_4 oxides is reflected in general larger c axis parameter relative to other non layered structures. In view of the structural diversity, A/B ions variety, various properties and applications ABO_4 oxides are important materials from both theoretical and technological standpoints (Lia H *et al* 2007).

We can consider $CaMoO_4$ and $CaWO_4$ as representatives of scheelite type molybdates and tungstates family. Both $CaMoO_4$ and $CaWO_4$ crystallizes in the same scheelite type structure with a space group $I4_1/a$, No.88, particularly the crystal structure of $CaMoO_4$ is

known as powellite and that of $CaWO_4$ as scheelite. The lattice parameters (*a, b*) in both scheelite and powellite are the same, but *c* is larger in powellite and it has been observed that the *c*/*a* ratio is usually larger for molybdates than for tungstates in scheelite type compounds. The crystal structure of $CaMoO_4$ can be explained by the CaO_8 polyhedra and MoO_4 tetrahedra as the building blocks.

The CaO_8 polyhedra share four of its edges with four other CaO_8 polyhedra extending in the c directions. Each oxygen atom of the CaO_8 polyhedra is connected to one Mo atoms. Thus each oxygen atom is coordinated with two of Ca and one Mo atoms (Achary S.N *et al* 2006). A typical three dimensional representation of $CaMoO_4$ unit cell is shown in Fig.1.7. In other words, a cubic close packing of Ca^{2+} and MoO_4 or WO_4 tetrahedral units in an ordered manner can explain the scheelite structure.

The crystallographic details of both $CaMoO_4$ and $CaWO_4$ are enlisted in Table 1.2. The oxygen position parameters are variables for both $CaMoO_4$ and $CaWO_4$ and the refined oxygen parameters for $CaMoO_4$ at 25°C are (0.146, 0.006, 0.2083) (Achary S.N *et al* 2006) and that for $CaWO_4$ are (0.1504, 0.0085, 0.2111) (Zalkin A *et al* 1964).

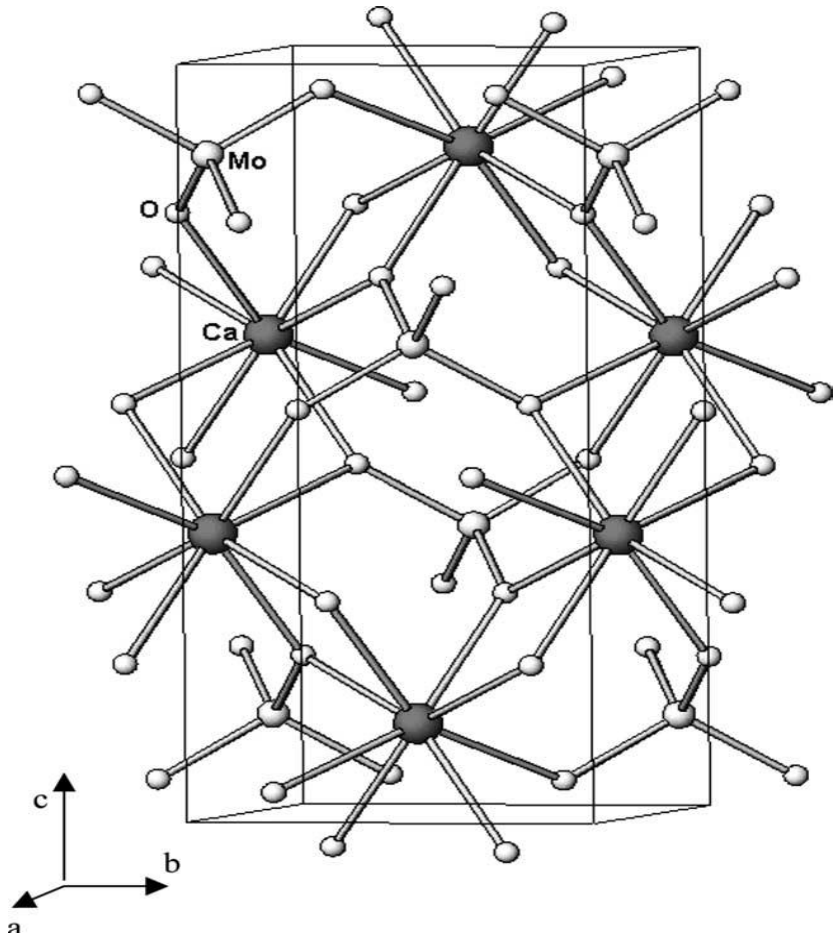

Fig. 1.7 Crystal structure of $CaMoO_4$ at room temperature (25°C).

Table 1.2 Crystallographic details of $CaMoO_4$ and $CaWO_4$

	$CaMoO_4$	$CaWO_4$
JCPDS File no.	29-0351	41-1431
Crystal structure	Powellite	Scheelite
Unit cell	Tetragonal	Tetragonal
Space group	$I4_1/a(88)$	$I4_1/a(88)$
Lattice parameters (Å)		
a	5.23	5.24
c	11.43	11.37
Crystallographic positions	Ca : 4b (0, ¼, ⅝)	Ca : 4b (0, ¼, ⅝)
	Mo : 4a (0, ¼, ⅛)	W : 4a (0, ¼, ⅛)
	O : 16f (x, y, z)	O : 16f (x, y, z)

1.9 Research efforts on red phosphors for pc-WLEDs: Literature Review

Selection of both host lattice and activator ion (luminescence center) has utmost importance in the design of phosphors for pc-WLEDs. Extensive research is going on in the field of developing novel and stable phosphors particularly red phosphors for pc-WLEDs. Host lattices such as fluorides, oxyfluorides, nitridosilicates, oxonitridosilicates and many oxides such as alkaline earth borates, tellurates, vandates, molybdates, tungstates etc. have been explored by the research community. Most trivalent rare earth ions (with Ce^{3+} as the major exception) yield a set of relatively narrow emission lines due to internal $4f^n$- $4f^n$ transitions, and are widely used as the activators for red emission. Eu^{3+}, Sm^{3+}, Pr^{3+} and Dy^{3+} are commonly used line emitting centers. On the other hand broad band emitting Ce^{3+}, Mn^{2+}, Eu^{2+} are also used as dopants for red emission. The current status and research efforts on these red phosphors for pc-WLEDs are briefly reviewed here.

Complex fluorides and oxyfluorides such as $NaYF_4$: Yb^{3+}, Er^{3+} and YOF: Yb^{3+}, Er^{3+} can emit one photon of shorter wavelength via absorption of two or more exciting photons with longer wavelengths through an energy transfer up conversion (UC) process (Menyuk N *et al* 1972; Kramer K. W *et al* 2004; Li Z. H *et al* 2007). When doped with Eu^{3+} or Tb^{3+}, these compounds show down conversion (DC) luminescence (Wang H. Y *et al* 2005) and have applications in various fields of electronics, dielectrics, optics, optoelectronics and

photonics (Fergus J. W *et al* 2000; Fujihara S *et al* 2001). Eu^{3+}doped $NaYF_4$ and YOF nano crystallites were also seen to be good red emitters (Zeng *et al* J. H 2009).

Another class of red phosphors includes silicates, nitridosilicates and oxonitridosilicates. Among the silicates, Ca_2SiO_4:Eu^{3+} red phosphor materials synthesized by the flux fusion reaction method with dominated emission peak at 612 nm under 400 nm excitation is suitable for trichromatic WLED based on UV InGaN chip. Here charge compensation approach is utilized for the improved luminescence and the luminescent intensity of Ca_2SiO_4:Eu^{3+} with Li^+ as a charge compensator was much stronger than that with Na^+, K^+ and Cl^- as charge compensators (Quanmao Y.U *et al* 2008). The synthesis of silicates based phosphors is cumbersome and these phosphors are facing thermal quenching at temperatures above 100°C.

Nitridosilicates and oxonitridosilicates such as $M_2Si_5N_8$: Eu^{2+}/Ce^{3+} (Hoppe H. A *et al* 2000), $MSi_2O_{2-\delta}N_{2+2/3\delta}$: Eu^{2+}/Ce^{3+} (M = Ca, Sr, Ba) (Li Y. Q *et al* 2005; Bachmann V *et al* 2006), $CaSiN_2$: Eu^{2+}/Ce^{3+} (Lee S. S *et al* 1997; Le T. R *et al* 2006), $MgSiN_2$: Eu^{2+} (Dubrovskii G. P *et al* 1981; Gaido G. K *et al* 1974), $MYSi_4N_7$: Eu^{2+}/Ce^{3+} (M = Sr, Ba) (Li Y. Q *et al* 2004 a, b), SiAlON: RE (RE = Eu^{2+}, Ce^{3+}, Yb^{2+}, Tb^{3+}, Pr^{3+}, Sm^{3+}) (Xie R. J *et al* 2002; Xie R. J *et al* 2004), SiAlON: Eu^{2+} (Hirosaki N *et al* 2005) and $CaAlSiN_3$: Eu^{2+} (Uheda K *et al* 2006 a) are studied extensively and they emit visible light efficiently under near UV or blue light irradiation. They are characterized by good thermal and chemical stability.

Eu^{2+} activated nitrides namely $M_{1-x}Eu_xSiN_2$ ($0 < x \leq 0.1$; M = Sr, Ba) are essentially broad emitting phosphors. $Ba_{1-x}Eu_xSiN_2$ ($0 < x \leq 0.1$) shows a broad emission (500–750 nm) with maxima from ~600 to 630 nm and $Sr_{1-x}Eu_xSiN_2$ ($0 < x \leq 0.1$) shows a broad emission (550–850 nm) with maxima from ~670 to 685 nm with increasing Eu^{2+} concentration. The strong excitation bands of these phosphors in the wavelength range of 300–530 nm are favorable properties for pc-WLED applications (Duan C. J *et al* 2008). Synthesis of nitrides is difficult to some extent which requires glove box handling of precursors and high firing temperatures. Requirements of high purity raw materials are essential and oxygen impurity is also always a concern.

Alkaline earth borates and rare earth doped tellurates (Ln_2TeO_6) are also suitable inorganic phosphors for pc-WLED applications. (Li P. L *et al* 2008; Kim K *et al* 2008; Llanos J *et al* 2008). $LiBaBO_3$:Sm^{3+} red phosphor (597 nm) can be effectively excited by UV light and its emission intensity was enhanced via charge compensation method (Li P *et al* 2009). The tellurate phosphor namely La_2TeO_6: Eu^{3+} exhibits an excitation spectra with three bands corresponding to the excitations of electrons from Eu^{3+} 4*f* ground state to different

excited 4*f* levels of Eu^{3+} and its emission spectrum is characterized by an intense peak centered at 616 nm due to $^5D_0 \rightarrow {}^7F_2$ transition of Eu^{3+} ions. $Eu_{0.1}Gd_xLa_{1.9-x}TeO_6$ ($0.02 \leq x \leq 0.1$) phosphors also emit intense peak centered at 616 nm under an excitation of 395 nm (Llanos J *et al* 2009). The major limitation of these phosphors is the thermal quenching behavior even at a lower temperature less than 100°C.

Table 1.3 Characteristics of some commercially available red phosphors
(O: Good; M: Medium; X: Bad)

Composition	Intensity	Width	Durability	Thermal quenching
(Sr, Ca)S/Eu	O	Broad	*X*	X
$(Ca,Sr)_2Si_5N_8/Eu$	M	Broad	M	M
$CaAlSiN_3/Eu$	O	Broad	O	O
La_2O_2S/Eu	M	Narrow	M	M
$3.5MgO\ 0.5MgF_2.\ GeO_2/Mn$	M	Narrow	O	O
$(Sr,Ca,Ba,Mg)_{10}(PO_4)_6Cl_2/Eu,Mn$	M	Broad	O	O
$Ba_3MgSi_2O_8/Eu,Mn$	O	Broad	M	M
K_2SiF_6/Mn	O	Narrow	O	O
$(Sr,Ba)_3SiO_5/Eu$	O	Broad	X	O

Among various activators, Mn^{2+} ions could have red emission due to the spin and parity forbidden $^4T_1\ (^4G) \rightarrow {}^6A_1\ (^6S)$ transition and the emission is usually very weak under near UV excitation. Duan et al. reported a novel red phosphor CaZnOS: Mn^{2+} with strong excitation bands in 350–500 nm region due to the $d \rightarrow d$ transitions of Mn^{2+} (Duan C.J *et al* 2009). While for BaZnOS: Mn^{2+} in the same wavelength region, the excitation efficiency of Mn^{2+} is quite low. The strong excitation band of Mn^{2+} in CaZnOS is because of the lifting of spin and parity prohibitions of Mn^{2+} *d-d* transition via the deviation from pure tetrahedral symmetry as a consequence of mixed MnS_3O coordination (Duan C. J *et al* 2009). It is suggested that manipulating coordination of the Mn^{2+} ion by mixing different anions is one way for

designing more novel Mn^{2+}doped phosphors for WLED applications (Duan C. J *et al* 2009). Owing to the weak excitation bands of Mn^{2+}, sensitizers with high transition efficiency such as Eu^{2+} or Ce^{3+} with the 4*f*-5*d* allowed transition are normally used to improve the intensity of Mn^{2+} emission (Ye S *et al* 2008 a, b). Since not all of the energy absorbed by Eu^{2+} transfers to Mn^{2+}, the residual emission energy of Eu^{2+} would cause poor color purity of red emission. In some hosts such as $CaSiO_3$: Eu^{2+}, Mn^{2+} the energy absorbed by Eu^{2+} could be efficiently transferred to Mn^{2+} (Ye S *et al* 2008 b). Commercially available some red phosphors and their characteristics are enlisted in Table 1.3.

Even though an extensive study is going on the field of red phosphors as mentioned; efficient red phosphors for pc-WLED applications are of great demand. Efforts are there to overcome the drawbacks of current red phosphors and to develop novel red phosphors. In this scenario, Eu^{3+} activated phosphors particularly in which the Eu^{3+} occupies a non-centrosymmetric site in the host, have got more technological importance as Eu^{3+} exhibit characteristic red emission via $^5D_0 \rightarrow {}^7F_2$ transition (Reddy K. R *et al* 1996). Consequently, the effect of Eu^{3+} doping in various host matrices has been studied and their photoluminescence properties have been analyzed. However a drawback is the weak absorption of Eu^{3+} in the blue and even in the near UV region. The main strategy to solve this problem has been to choose suitable host materials that have broad and intense charge transfer (CT) absorption bands in the near UV and capable of efficiently absorbing the emission from InGaN based LEDs. Of many host lattices, molybdates and tungstates are superior because of good chemical, thermal and hydrolytic stability and the presence of broad and intense CT band in the near UV region (Neeraj S *et al* 2004 a; Wang Z *et al* 2007). Recently adopted strategy is to convert near UV or blue light via the 4*f* - 4*f* transitions of Eu^{3+} located at 394 ($^7F_0$–$^5L_6$) and 465 nm ($^7F_0$–$^5D_2$), which are rather intense in molybdates and tungstates. Research efforts on the Eu^{3+} activated molybdate and tungstate based red phosphors reviewed and are presented as follows:

Eu^{3+} activated $CaMoO_4$ and $CaWO_4$ are superior phosphors in the family of powellite type molybdates and scheelite type tungstates respectively. Hu et al have first studied $CaMoO_4$: Eu^{3+} and indicated that $CaMoO_4$: Eu^{3+} shows desirable absorption in the near UV region with excellent thermal, chemical stability than the well known red phosphor, Y_2O_2S:Eu^{3+} (Hu Y. S *et al* 2005). The red emission is originated from $^5D_0$-$^7F_2$ transition of Eu^{3+} and the near UV excitation performs at around 395 nm through $^7F_0$-$^5L_6$ absorption of Eu^{3+}. However, the brightness of $CaMoO_4$: Eu^{3+} is inadequate for application in WLEDs. In line with this many research groups were engaged in modifying and improving the

luminescence behavior of $CaMoO_4$: Eu^{3+} red phosphors. In order to improve the luminescent properties, Li and co-workers (Li X *et al* 2007) used alkaline metal ions for charge compensation. Liu et al have investigated the effect of different charge compensation models on the luminescent property of Eu^{3+} doped $CaMoO_4$ and found Na^+ is regarded as the optimal charge compensation for molybdate phosphor (Liu J *et al* 2007). Wang et al obtained enhanced emission intensity of Eu^{3+} by co doped Sm^{3+}, Bi^{3+} and Eu^{3+} in molybdate (Wang Z *et al* 2006, Wang J. G *et al* 2005, 2006). Ci et al synthesized the series $Ca_{1-x}Mo_{1-y}Si_yO_4$: xEu^{3+} phosphors and investigated its luminescence properties in detail (Ci Z P *et al* 2008). To further improve the emission intensity of $CaMoO_4$: Eu^{3+}, Na^+, Bi^{3+} are used as a co-activator and Si as a substituting element for the host lattice (Xie A *et al* 2009). The substitution of Y^{3+} and Gd^{3+} to $CaMoO_4$: Eu^{3+} phosphor is studied; and in $(Ca_{1-x-y},Ln_y)MoO_4$: xEu^{3+} red phosphor, the partial site of Ca^{2+} is replaced by Ln^{3+} (Y, Gd) which results in some changes in the lattice structure around the luminescent center ions (Eu^{3+}) and an enhancement in the luminescent intensity (Linga Y. Y *et al* 2010).

In addition to the charge compensation approach, the effect of morphology, particle size and shape of phosphors on the luminescence behavior is also investigated by many research groups and for this purpose the synthesis method is altered from conventional solid state reaction to facile hydrothermal method. Submicro sized $CaMO_4$: RE^{3+} (M= Mo, W; RE= Eu^{3+}) were synthesized by hydrothermal method (Lei F *et al* 2008). The luminescence quantum efficiency is calculated as 17.13% for $CaWO_4$: Eu^{3+} and 12.78% for $CaMoO_4$:Eu^{3+}. Furthermore, it is found that Eu^{3+} ions in $CaWO_4$ are located in a more polarizable environment than that $CaMoO_4$. Low temperature synthesis via a facile hydrothermal method at 120°C and photoluminescent properties of $CaMoO_4$:Eu^{3+} red phosphor with uniform micro assemblies is reported (Yu F *et al* 2011). The alkaline source used in the reaction process was found to play a critical role in the formation of different morphologies of spherical, shuttle like and cake like nature. The morphology of the samples influenced its luminescence emission intensity to a great extent.

Another aspect for improving the luminescence performance of Eu^{3+} activated $CaMoO_4$ based red phosphors is the reduction of Eu^{3+} site symmetry (Sohn K. S *et al* 2003, 2006) and can be achieved by structural adjustment of the phosphor. Zhang *et al* introduced Na^+ ions to $CaMoO_4$: Eu^{3+} lattice for reducing the crystal symmetry of Eu^{3+}, which lead to an enhanced red emission via the structural adjustment of the phosphor (Zhang Z. H *et al* 2009). The possibility for strong coupling between NbO_4 and Eu^{3+} is made utilized for the enhancement of emission intensity of $CaMoO_4$: Eu^{3+}. For which Nb^{5+} is incorporated into $CaMoO_4$ lattice

resulting to $Ca_{1-x}Mo_{1-y}Nb_yO_4$: xEu^{3+} lattice leading to an enhancement in the emission intensity under both near UV and blue excitations and excellent color purity (Yan S. X *et al* 2007).

Energy transfer process via codoping suitable ions to the phosphor is the other way for modifying their luminescence properties. In this regard Sm^{3+}, Bi^{3+} ions are codoped to $CaMoO_4$: Eu^{3+} phosphor (Jin Y *et al* 2011). The dynamical process of energy transfer in $CaMoO_4$: Eu^{3+}, Sm^{3+} is explained and these phosphors are well excitable under 405 nm (Jin Y *et al* 2011). With the codoping, the excitation spectra of the phosphor is extended to longer wavelength region and become better matching for the near UV LED excitation (Cao F.B *et al* 2009; Okamoto S *et al* 2007). It was found that both the polarization effect of Bi^{3+} on the charge transfer state (CTS) of MoO_4 and the $6s \rightarrow 6p$ transition of Bi^{3+} play roles in the red shift of the absorption band at UV region. Eu^{3+} and Sm^{3+} codoped micro/nanosized $MMoO_4$ (M = Ca, Ba, Sr) phosphors with various shapes (nanoflakes, microflowers, cubes, and spheres) have been synthesized via a facile hydrothermal method with surfactant free environment and studied the energy transfer mechanism (Jin Y *et al* 2008).

Many molybdate based red phosphors are there which include phosphors with high valence transition metal groups such as $Gd_2Mo_3O_9$: Eu^{3+} (Zhao X. X *et al* 2007), $(Li_{0.333}Na_{0.334}K_{0.333})Eu(MoO_4)_2$ (Wang Z. L *et al* 2005), $Na_5Ln(MoO_4)_4$: Eu^{3+} (Ln = La, Gd and Y) (Guo C.F *et al* 2009 a), $BaGd_2(MoO_4)_4$: Eu^{3+} (Guo C.F *et al* 2009 b) etc. All of them have narrow line shaped excitation peaks at near UV (λ_{ex} = 365‑410 nm) and are ascribed to the parity forbidden *4f‑ 4f* transitions. Nassau et al. (Nassau K *et al* 1965) gave a survey of the structure of tungstates and molybdates with the formula $RE_2(AO_4)_3$ (A = Mo, W) along the rare earth series. $Gd_2(MoO_4)_3$ was researched as one member of an isotypic series of ferroelectric rare-earth molybdates and was first prepared by Borchardt (H.J. Borchardt *et al* 1963). A series of the red phosphor $Gd_{2-x}Eu_x(MoO_4)_3$ for GaN based WLED by sol-gel method has been reported (Guoa C *et al* 2008). Results indicate that phosphors $Gd_{2-x}Eu_x(MoO_4)_3$ prepared by sol-gel method have a narrow size distribution, favorable size, homogeneous shape and high luminescent intensity, which is better than those of the phosphors prepared by solid state method. The phosphor $Gd_{1.2}Eu_{0.8}(MoO_4)_3$ shows a higher luminescent intensity than that of phosphor Y_2O_2S: $0.05Eu^{3+}$ under the excitation of near UV and blue light. It has also been observed that the quenching concentration in $Gd_2(MoO_4)_3$:Eu^{3+} is much higher than in $CaMoO_4$: Eu^{3+} due to the large distance between rare earth in the latter case (X. Zhao *et al* 2007). To broaden the excitation bands at the near UV region and to enhance the red emission intensity of Eu^{3+} efficiently upon near UV

excitation, Bi^{3+} is used in $LiEuMo_2O_8:Eu^{3+}$ (Ye S *et al* 2009) phosphors. It has been reported by Sivakumar and Varadaraju that ordered double perovskite $(Ba,Sr)_2CaMoO_6:Eu^{3+}$, Li^+ phosphors have an intense broad absorption band at 200 - 450 nm contributed primarily by the CTS of MoO_6 groups (Sivakumar V *et al* 2008). Recently Ye et al. investigated this system further, and found that Eu^{3+} prefers the B site (Ca^{2+}) in this double perovskite system (general formula ABO_3 for simple perovskite), and the linear Mo-O-Eu configuration for Eu^{3+} at the B site benefits the ET from the CTS of MoO_6 to Eu^{3+} through an exchange mechanism (Ye S *et al* 2008). A strong quenching among the CTS of MoO_6 groups was also found, which results in little CTS energy transfer to Eu^{3+}.

The optical properties of trivalent rare earth ions (RE^{3+}) in tungstate materials with scheelite ($CaWO_4$) structure have been widely investigated (Strek W *et al* 2001; Nosenko A *et al* 2000; Do Y. R *et al* 2000; Shi F *et al* 1998) especially due to their attractive third order nonlinear dielectric susceptibilities (Kuleshov N. V *et al* 1997). Luminescence properties of Eu^{3+} activated $CaWO_4$ is studied systematically (Zhu C.Q *et al* 2008) and is considered as a potential red phosphor for pc-WLED applications. Powell and co-workers (Treadaway M. J *et al* 1974; Tyminski J. K *et al* 1982) had studied the luminescent properties and energy transfer of $CaWO_4$: Eu^{3+} systems. The effect of charge compensation (Li^+, K^+, Na^+) on the luminescence behavior of $CaWO_4$: Eu^{3+} is investigated and Li^+ codoping made the emission intensity much stronger (Shi S *et al* 2008 a). The effect of Li^+, Zn^{2+} and Mg^{2+} charge compensation on luminescent properties of $CaWO_4$: Eu^{3+} is also investigated (Shi S *et al* 2008 b). The improved luminescence performance of $CaWO_4$: Eu^{3+} via Bi^{3+} codoping under an excitation of 277 nm is reported (Pode *et al* 1997).

Many attempts have been made to study the effect of variation of synthesis method on its luminescence behavior. $CaWO_4$: RE (RE = Tb^{3+}, Eu^{3+} and Sm^{3+}) were prepared by the aqueous sol-gel method using tartaric acid as a complexing agent. The formation of nanocrystals with an average particle size of less than 250 nm is confirmed. Photoluminescence study under excitation at 280, 360 and 460 nm showed that $CaWO_4$: Eu^{3+} compound emission was by a factor of 10 to 100 more intense than that of other $CaWO_4$: RE samples (Žalga A *et al* 2009). Monodispersed, non agglomerated and homogenous $CaWO_4$: Ln^{3+} (Ln: Eu, Sm, Dy) are synthesized by solvothermal method without further heat treatment process (Wang W *et al* 2010).

In addition to this, many other tungstates based red phosphors are studied in detail. The correlation between the crystal structure and luminescence properties of Eu^{3+} doped metal tungstates phosphors of the general formula, $A_{4-x}(WO_4)_3$ (A= Li, Na, K) is reported and the

high doping concentration of Eu^{3+} increased the absorption of UV light without any detectable concentration quenching effect (Lee G. H *et al* 2011). Many other tungstate based red phosphors such as $Gd_{0.2}(WO_4)_3$: Eu^{3+}, Sm^{3+}, $Na_{0.5}Gd_{0.5}WO_4$: xEu^{3+} (Yan B *et al* 2011), $Gd_{2-x}WO_6$: Eu^{3+} (Lei F *et al* 2008), $Ca_3Ln_2W_2O_{12}$ (Zeng Q *et al* 2008) etc. are studied systematically. The photoluminescence spectrum of $Gd_{0.2}Sm_{0.3}Eu_{1.5}(WO_4)_3$ contains board excitation bands extending from 330 to500 nm, resulting from the strong crystal field imposed on the Sm and Eu sites (Wei Q *et al* 2009). Moreover, boric acid as a flux is effectively improving the photoluminescence intensity. A series of Eu^{3+} doped tungstate red phosphors, $Ca_3Ln_{2-x}Eu_xW_2O_{12}$ (Ln = La, Gd, and Y) also show intensely red emission under 395 nm excitation and superior high-temperature behavior (Zeng Q *et al* 2008). Making use of properties of tungstates and molybdates, a few tungsto - molybdates solid solution phosphors are there. Variation of luminescence property with respect to W^{6+} and Mo^{6+} in $Ca_{0.54}Sr_{0.22}Eu_{0.08}La_{0.08}(MoO4)_{0.4}(WO4)_{0.6}$ red phosphors are effectively investigated (Cao F. B *et al* 2009).

In conclusion, major efforts have been made by many research groups around the world in the development of novel red phosphors for pc-WLED applications and to study the mechanism involved. But still current red phosphors have to overcome some drawbacks such as less brightness, inadequate lifetime under near UV excitations, chemical instability, inefficient absorption in the UV region etc. There are plenty of scopes for improvement of current red phosphors or development of novel, stable and efficient red phosphors. With this back ground of research efforts on red phosphors for pc-WLED applications, in the current research work an attempt has been made to develop Eu^{3+} activated novel red phosphors based on molybdate and tungstate host lattice (ABO_4). The idea is to modify the host lattice of $CaMo/WO_4$ by adding $La/GdNbO_4$ and no charge compensation approach is required here. The luminescence properties of Eu^{3+} and basic structural details of molybdates and tungstates selected for the research work has been briefly presented in the earlier sections and the coming section reveals an overview of the current research work.

1.10 Research Work: An overview

With the basic understanding of the importance of SSL and the demand of stable red phosphors for making them as a source of general illumination, development of novel red phosphors for pc-WLEDs is set as the major objective of the current research work. For this molybdates/ tungstates with powellite/ scheelite structure are selected as host lattices; Eu^{3+} as activator ion and studied their luminescent properties in detail. The properties such as good chemical stability, broad and intense charge transfer (CT) band in the near UV region and the

ability to capture radiation from a GaN based LED over a range of wave lengths etc. make powellite/ scheelite type molybdates/ tungstates as good host lattices for phosphor materials. Eu^{3+} is a preferable choice as an activator as it exhibits a high lumen equivalent, quantum efficiency and photostability at the same time. Moreover, from a practical point of view a fluorescent light source comprising a red line emitter emitting at 610 - 615 nm is the best compromise between luminous efficacy and color rendering.

The present research work has been divided into three parts. In the first part, Eu^{3+} activated molybdate and tungstate based powellite/ scheelite type [$Ca(La/Gd)_{1-x}NbMo/WO_8$: xEu^{3+}] red phosphors have been synthesized via solid state reaction (SSR) route and the structural, microstructural and photoluminescent properties were studied in detail. It is observed that these phosphors emit strong red light (613 nm) under both near UV (394/395 nm) and blue (465 nm) excitations. The luminescence properties of the phosphors with respect to activator concentration are studied and optimized. *Chapter 2* briefly includes the different synthesis routes and characterization techniques utilized for the research work and *Chapter 3* (Molybdates) and *Chapter 4* (Tungstates) cover the details of the first part of research work.

Second and third part of the research work is an attempt to study various factors affecting the luminescent behavior of optimized red phosphors and the steps to improve their luminescence properties. Generally the position and intensity of charge transfer band of the phosphors play an important role in their luminescence behavior. We can improve the red emission of phosphors by red shifting the CT band position. For this, suitable codopant (Bi^{3+}) is incorporated in the aforementioned optimized red phosphors and studied their luminescence properties. By Bi^{3+} codoping we were able to red shift the CT band of both molybdate and tungstate red phosphors and hence an improvement in their red emission also (~2 times). The details of role of Bi^{3+} in both lattices and variation in the luminescence property with respect to Bi^{3+} codoping are included in the second part (*Chapter 5 (A & B)*).

In addition to position and intensity of CT band, the physical properties of phosphors such as crystallinity, surface area, morphology and distribution of activator etc have crucial role in determining their luminescence properties. These properties can be controlled by the variation in the synthesis method and heat treatment process. Thus an effort has been taken to synthesise the optimized red phosphors via citrate gel route. Effect of heat treatment process on their luminescence properties is also studied. Morphological improvement as well as enhanced red emission (~4 times) is achieved by the variation in the synthesis method and heat treatment process. These phosphors are characterized by sharp red emission with longer

lifetime and better color purity. The effect of variation in the synthesis method and heat treatment process on the luminescence properties of the developed red phosphors cover the third part of the research work [*Chapter 6 (A & B)*].

Precisely, during the present research work an attempt has been made to study he luminescent properties and their improvement factors of Eu^{3+} activated molybdate and tungstate based novel phosphors. The current red phosphors are characterized by strong red emission under both near UV and blue excitations and these could be promising red phosphors for pc-WLED applications.

CHAPTER 2

SYNTHESIS METHODS AND CHARACTERIZATION TECHNIQUES

Synthesis of phase pure materials and their characterization is a very important aspect for materials research. For the current research work on Eu^{3+} activated novel red phosphors two different methods of synthesis are adopted namely, solid state method and citrate gel method. Various techniques are used for structural, microstructural and optical characterization of these phosphors. This chapter outlines various methods of synthesis and characterization techniques employed for the development of Eu^{3+} activated molybdate and tungstate based novel red phosphors.

2.1 Introduction

Synthesis of high quality, phase pure inorganic materials is one of the most important aspects of material science research. The proper choice of the chemical precursors and the preparation technique are essential to obtain a material with the desired chemical and physical properties and it is well known that material's performances are closely related to the ways that they are processed (Kong L.B *et al* 2008). The solid samples can be synthesized in variety of shapes and sizes depending upon their requirements such as single crystals, amorphous solids, thin films, thick films, polycrystalline powder etc. Several methods available to synthesize high quality samples in bulk and thin film forms are, Solid State Reaction (SSR), Vapor Phase Transport (VPT), Co-precipitation, Citrate gel, Sol gel, Physical Vapor Deposition (PVD), Chemical Vapor Deposition (CVD), Pulsed Laser Deposition (PLD), Chemical Solution Deposition (CSD), Metal Organic Chemical Vapor Deposition (MOCVD), Sputtering, Flux Growth Technique, Electrochemical Methods etc.

Various techniques are there for structural and microstructural characterization of as prepared materials with desired properties. The structural characterization techniques include X ray Diffraction (XRD), Neutron Diffraction (ND) and Electron Diffraction (ED) while microstructural characterization methods are Scanning Electron Microscopy (SEM), Atomic Force Microscopy (AFM), Lateral Force Microscopy (LFM), Scanning Tunneling Microscopy (STM), Magnetic Force Microscopy (MFM), Transmission Electron Microscopy (TEM) etc. The optical properties such as UV Visible absorption and photoluminescence can be recorded by Spectrophotometer and Spectrofluorimeter respectively.

For the present research work of studies on luminescent properties of Eu^{3+} activated molybdate and tungstate based novel red phosphors, Solid State Reaction (SSR) and Citrate Gel (CG) routes are selected as the synthesis methods and the crystalline structure, morphology, absorbance and luminescent properties of these phosphors were characterized by powder X ray diffraction (XRD), Scanning Electron Microscopy (SEM), UV Visible absorption spectroscopy and Photoluminescent spectroscopy. This chapter overviews various methods of synthesis and characterization techniques employed for the development of Eu^{3+} activated novel red phosphors.

2.2 Synthesis Methods

2.2.1 Solid State Reaction Route

Most of the inorganic phosphors were synthesized conventionally via a solid state reaction process because of its facile operation. In solid state reaction route, powders are used as raw materials and solid - solid reaction occurs between these powders. Up to now, this

method has been the most widely and intensively used approach for the preparation of phosphors including oxides, (oxy) nitrides and fluorides because it is comparatively simple and very suitable for mass production. Because of the refractory nature of alumina and RE oxides, conventional solid state reaction synthesis of oxide based phosphors like YAG requires temperature higher than 1000°C. The solid state reaction is controlled by atomic diffusion between different raw materials. Hence, repeated grinding and heating are required. Furthermore, a controlled atmosphere is necessary to master the valence of the activator and the stoichiometry of the host lattice. The particle size of the phosphor prepared by this method is relatively large and less controllable. In solid state reaction method, the solid reactants react chemically without the presence of any solvent at high temperatures yielding a product which is stable. There are two factors, namely thermodynamic and kinetic, which are important in solid state reaction; the former determines the possibilities of any chemical reaction to occur by the free energy considerations which are involved while the later determines the rate at which the reaction occurs (Engler E.M 1987; West A. R 1984). The atoms diffuse through the material to form a stable compound of minimum free energy. In order to prepare a single phase sample, the conditions during any reaction are very important. During synthesis the parameters such as temperature, pressure, gas flow and time for the reaction are to be varied according to the phase requirements in the sample. The major advantage of solid state reaction method is that the final product in solid form is structurally pure with the desired properties depending on the final sintering temperatures. This method is environment friendly and non toxic or unwanted waste is produced after the SSR is complete.

The steps involved in solid state reaction for synthesis of phosphors are schematically illustrated in Fig. 2.1. They are;

(1) Selection and weighing of raw materials

Take appropriate high purity (99.99%) fine grain powders as starting materials (reagents) in stoichiometric proportions depending upon the composition and weigh all of them as per the calculations performed.

(2) Mixing and drying

The stoichiometrically weighed reactants are mixed together in an agate mortar with acetone as the mixing medium. After mixing, the powder is kept in a hot air oven at 100°C for 30 min. This process is repeated three times so as to get a homogeneous, finely powdered mixture. For solid state diffusion mechanism, the growth of the reaction product in powder system occurs at the contact points. The homogeneity of mixing is one of the most important factors which decide the ability of a process to produce homogeneous, single phase powder.

The size and distribution of the reactant particles are important factors for deciding the degree of homogeneity.

A homogeneous mixture has great influence on the diffusion distances and the number of contacts between the reactant particles. The presence of agglomerates results in porosity of the final product. Therefore it is necessary to mix the reactants to a high level and to powder them repeatedly. During mixing process, these agglomerates get broken and defects are introduced into the grains which enhance the diffusion mechanism.

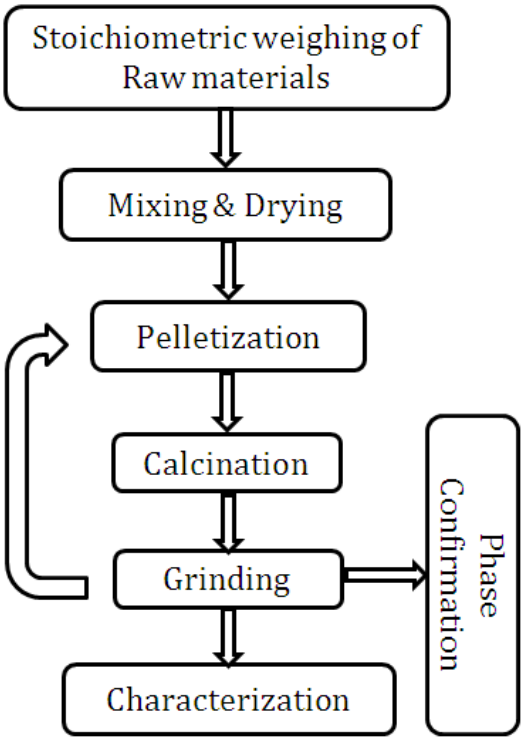

Fig. 2.1 Schematic illustration of phosphor preparation by solid state reaction route.

(3) Pelletization

The homogenously mixed powders are pelletized to enhance intimate contact of reactants and minimize contact with the crucible. Organic binder may be used to help keep pellet together.

(4) Calcination

Calcination is an intermediate heating at a lower temperature through which chemical reactions between solid starting materials usually in the form of mixed powders take place. The reactants normally consist of oxides, carbonates, nitrates, sulphates etc. It involves heat treating a powder or mixture of powders at a temperature well below its melting point for

effective decomposition, to liberate unwanted gases and/or chemically bound waste, solid state reactions and structural transformations to produce the desired composition and phase product. The kinetics of solid state reactions occurring during calcinations may be controlled by any one of the three processes:- (i) the reaction at the interface between the reactant and solid product (ii) heat transfer to the reaction surface (iii) gas diffusion or permeation from the reaction surface through the porous product layer.

(5) Grinding

The grinding of calcined pellets has an effective role in deciding the degree of homogeneity. Generally grinding to somewhere around 1 to 10 μm is advisable. Grinding the solid reactants to very fine powder (<1 μm) can lead to the formation of agglomerates that result in non uniform packing. Agate mortar with pestle is used for grinding the powder reactants. Finally the grinded, reacted powders were analyzed by X ray diffraction technique and analyze the structural formation. If the required phase purity of the phosphor materials is not achieved, repeat the calcination process twice / thrice with intermittent grinding till the completion of reaction.

2.2.2 Citrate Gel Route

In conventional synthesis routes, the reactants are mixed together manually by grinding the mixture of starting materials or mechanically by ball milling process and the subsequent reaction rate depends on a large degree on the particle size of the reactants, the degree of homogenization achieved on mixing and the intimacy of contact between the grains, as well as the obvious effect of temperature.

By chemical methods of preparation, it is possible to achieve a high degree of homogenization together with a small particle size and faster reaction rates. Various chemical methods include sol gel, citrate gel, co precipitation and combustion methods etc that ensure easy mixing of precursor solutions at the molecular level, provides a high degree of homogeneity at low processing temperatures, and makes doping of activators, coactivators or sensitizers straightforward and effective (Dhage S. R *et al* 2003, 2004 (a), (b); Gaikwad A. H *et al* 2004).

The citrate gel route includes the following steps and is schematically illustrated in Fig. 2.2.

- Select highly pure (99.99%) raw materials of corresponding metallic cations for the necessary phosphor material. (Nitrates, Chlorides).
- Stoichiometrically weigh and make the cationic solution in distilled water.
- Prepare the citrate solution by dissolving appropriate molar ratio of citric acid in distilled water (1:2).

- After completing homogenization of citrate solution, dissolve all the cationic solution in citrate solution (1:5).
- Keep for constant stirring for 1 hour for homogenous mixing.
- Concentrate the solution by keeping it in the water bath (maintained at 100°C) for 3 hours leading to the formation of gel.
- Dry the viscous gel to form a brown product and then powder it by grinding in an agate mortar, which is the precursor.
- Heat treat the precursor at various temperatures to get the required phase pure phosphors.

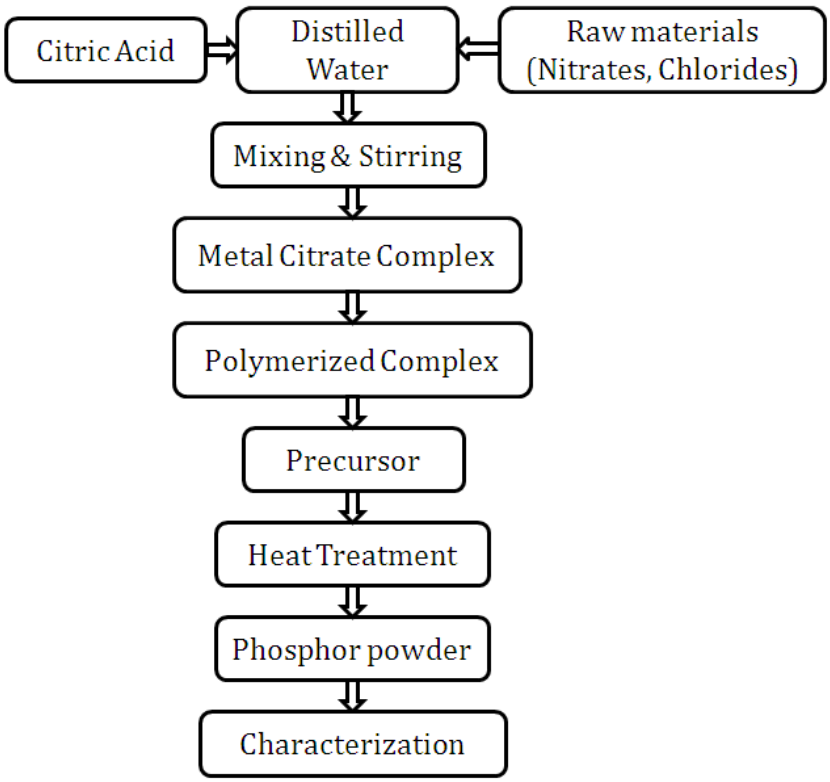

Fig. 2.2 Schematic illustration of phosphor preparation by citrate gel route.

2.3 Characterization Techniques

2.3.1 Structural Characterization – X ray Diffraction (XRD)

X rays are electromagnetic radiation with typical photon energies in the range of 100 eV - 100 keV. For diffraction applications, only short wavelength X rays (hard X rays) in the range of a few angstroms to 0.1 angstrom (1 keV - 120 keV) are used. Because the wavelength of X rays is comparable to the size of atoms, they are ideally suited for probing

the structural arrangement of atoms and molecules in a wide range of materials. The energetic X rays can penetrate deep into the materials and provide information about the bulk structure. X rays primarily interact with electrons in atoms. When X ray photons collide with electrons, some photons from the incident beam will be deflected away from the direction where they originally travel. If the wavelength of these scattered X rays did not change (meaning that X ray photons did not lose any energy), the process is called elastic scattering (Thompson Scattering) in that only momentum has been transferred in the scattering process. These are the X rays that we measure in diffraction experiments, as the scattered X rays carry information about the electron distribution in materials. On the other hand, in the inelastic scattering process (Compton Scattering), X rays transfer some of their energy to the electrons and the scattered X rays will have different wavelength than the incident X rays. Diffracted waves from different atoms can interfere with each other and the resultant intensity distribution is strongly modulated by this interaction. If the atoms are arranged in a periodic fashion, as in crystals, the diffracted waves will consist of sharp interference maxima (peaks) with the same symmetry as in the distribution of atoms. Measuring the diffraction pattern therefore allows us to deduce the distribution of atoms in a material (Cullity B. D 1978).

.

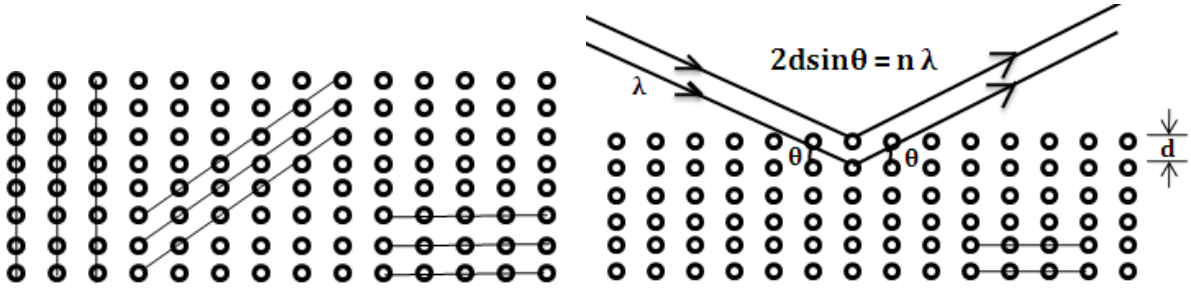

Fig. 2.3 Illustrations of lattice planes and Bragg's Law.

The peaks in an X ray diffraction pattern are directly related to the atomic distances. The interaction of X rays with the periodic arrangement of atoms arranged in two dimensions can be illustrated as follows. The atoms, represented as spheres in Fig. 2.3, can be viewed as forming different sets of planes in the crystal. For a given set of lattice planes with an inter planar distance d, the condition for a diffraction (peak) to occur can be written as;

$$2d\sin\theta = n\,\lambda \qquad (2.1)$$

which is known as the Bragg's law, after W.L. Bragg, who first proposed it. In the equation, λ is the wavelength of the X ray, θ the scattering angle, and n an integer representing the order of the diffraction peak. The Bragg's Law is one of most important laws used for interpreting

X ray diffraction data (Warren B. E 1969). Although we have used atoms as scattering points in this example, Bragg's Law applies to scattering centers consisting of any periodic distribution of electron density. In other words, the law holds true if the atoms are replaced by molecules or collections of molecules such as colloids, polymers, proteins and virus particles.

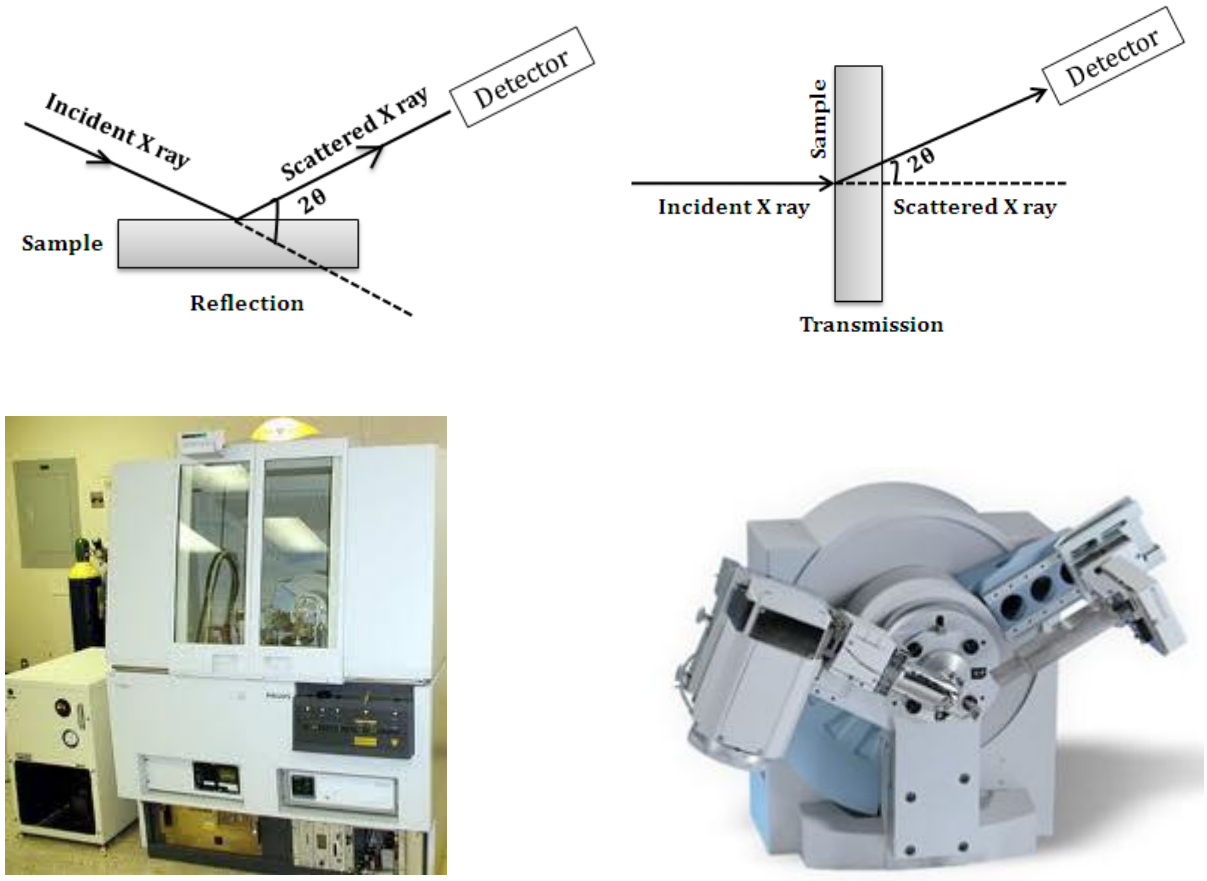

Fig. 2.4 Reflection and transmission geometry in X ray diffraction and Goniometer in PANalytical X'pert PRO X ray diffractometer.

Powder XRD (X ray Diffraction) is perhaps the most widely used X ray diffraction technique for characterizing materials. As the name suggests, the sample is usually in a powdery form consisting of fine grains of single crystalline material to be studied. The term 'powder' really means that the crystalline domains are randomly oriented in the sample. Therefore when the 2D diffraction pattern is recorded, it shows concentric rings of scattering peaks corresponding to the various d spacings in the crystal lattice. The positions and the intensities of the peaks are used for identifying the underlying structure (phase) of the material. Powder diffraction data can be collected using either transmission or reflection geometry, as shown in Fig.2.4.

Powder diffraction data are usually presented as a diffractogram in which the diffracted intensity is shown as function either of the scattering angle, 2θ or interplanar spacing, d. The diffractogram data can be analysed for phase identification and for calculation of lattice parameters, extent of crystallinity, crystallite size and strain present in the lattice. For the structural characterization of phosphor materials, here PANalytical X'pert PRO Xray diffractometer is used. The instrumental parameters are summarized in Table 2.1.

Table 2.1 Instrumental parameters of PANalytical X'pert PRO X ray diffractometer

Diffractometer system	PANalytical X'pert PRO
Configuration	Flat sample stage
Goniometer	Theta – theta mode
Goniometer radius	240 mm
Scan Type	Continuous
Divergence slit type	Fixed
Divergence slit width	0.5°
Measurement temperature	25°C
Specimen length	10 mm
Anode material	Cu
K Alpha1	1.5406 Å
Generator settings	30 mA, 40 kV
2θ offset	Zero

2.3.2 Microstructural Characterization – Scanning Electron Microscopy (SEM)

Electron Microscopy can be defined as a specialized field of science that employs the electron microscope as a tool and uses a beam of electrons to form an image of a specimen (Bozzola J. J *et al* 1992; Heath J. P 2005). In contrast to light microscopy which uses visible light as a source of illumination and optical lenses (glass) to magnify specimens in the range between approximately 10 to 1,000 times their original size, electron microscopy is operated in the vacuum and focuses the electron beam and magnifies images with the help of electromagnetic lenses. The electron microscope takes advantage of the much shorter

wavelength of the electron compared to the wavelengths of visible light (Flegler S. L *et al* 1993). When the accelerating voltage is increased in electron microscope, the wavelength decreases and resolution increases. In other words, increasing the velocity of electrons results in a shorter wavelength and increased resolving power (Flegler S. L *et al* 1993). The scanning electron microscope (SEM) is primarily used for the study of surface morphology of solid specimens, which gives image at very high magnification and high resolution. Due to the manner in which the image is created, SEM images have a characteristic three dimensional appearance and are useful for judging the surface structure of the sample.

Electrons in scanning electron microscopes are accelerated at voltages in the range of 2 to 40 kV. An electron beam < 0.01mm in diameter is focused on the specimen. These fast primary electrons (PE) interact in various ways with the surface layers of the specimen. The zone, in which such interaction occurs, and in which different signals are produced, is called "interaction volume" or "electron diffusion cloud". The size of the interaction volume is proportional to the energy of primary electrons and its shape is determined depending upon scattering processes by the mean atomic number. Secondary electrons (SE), back scattered electrons (BSE) are produced flowing off as specimen current. In addition X rays, Auger electrons, and cathodoluminescence are produced. Although secondary electrons are produced in the entire interaction volume, they can only escape from surface layers. Secondary electrons are very slow, their escape energy is ≤ 50 eV. Approximately half of all secondary electrons are produced very near to the point of impact of primary electrons. The SE signal, comprising all essential information on topography, produces electron-micrographs of high resolution.

The basic parts of a scanning electron microscope includes electron optical column, vacuum system, signal detectors and display system. Schematic illustration of a SEM is shown in Fig. 2.5. The primary function of the lenses is to demagnify the electron beam. The vacuum system consists of two pump systems. Scan generator coils control the magnifications. Electrons in the electron gun are emitted from the cathode and accelerated by the anode to the energy 1 – 50 keV. The electron beam is condensed by the condenser lenses (one or two). Magnetic field produced by the scan coils deflects the electron beam back and forth. The electron beam focused by the objective lens to very fine spot (1-5 nm) scans the sample surface in a raster pattern. Primary electrons interact with the atoms of the sample surface causing emissions of the secondary electrons which are detected and producing the image. The backscattered electrons of the electron beam may also be detected. The

backscattered electron image is used for contrasting the sample regions, having different chemical compositions.

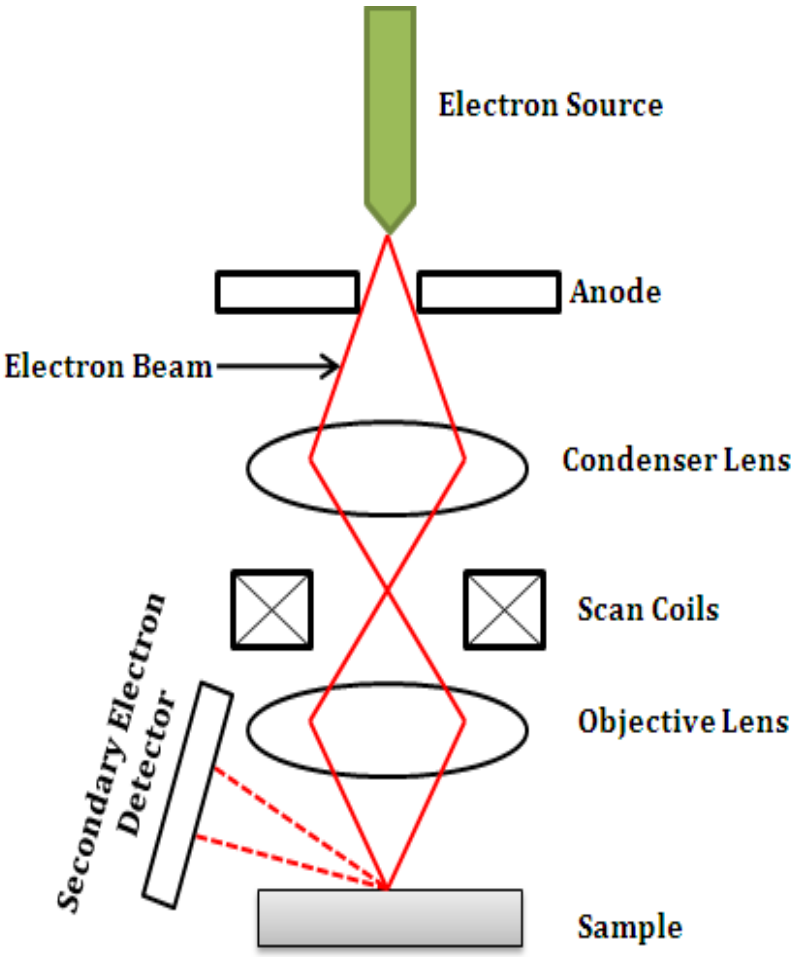

Fig. 2.5 Schematic presentation of a Scanning Electron Microscope.

For microstructural analysis using SEM, non conductive solid specimens should be coated with a layer of conductive material except when observed with Variable Vacuum or Environmental SEM. Such coatings are made on the surface of non conductive samples using gold or palladium (Goldstein J. I *et al* 1981).

The microstructural analysis of the as prepared phosphors was carried out by JEOL JSM- 5600 LV scanning electron microscope. The details of the instrumental settings are summarized in Table 2.2.

Table 2.2 Instrumental parameters of JEOL JSM- 5600 LV scanning electron microscope

Scanning Electron Microscope	JEOL JSM- 5600 LV (High vacuum mode)
Mode of Imaging	Secondary Electron
Resolution	3.5 nm
Accelerating Voltage	0.5 - 30 kV
Working depth	5 - 48 mm (min)
Magnification	x18 to x 3,00,000
Probe Current	10^{-12} -10^{-6} A
Filament	Tungsten Hair pin
Temperature	15 - 25°C
Specimen Holder	10 mm dia X 10 mm height (min)

2.3.3 Optical Characterization – UV Visible Absorption Spectroscopy

UV Visible absorption spectroscopy is a powerful analytical tool to understand the optical properties of materials and to identify inorganic and organic materials. UV Visible absorption spectroscopy involves absorption of UV/ Visible light by a molecule causing the excitation of an electron from ground electronic state to excited electronic state. UV Visible absorption spectrum is a plot of degree of absorption of sample against the wavelength of the incident radiation. It may include both broad and sharp lines of absorption. In practice it is found that the ultraviolet and visible spectrum of most molecules consists of a few humps rather than sharp lines. The main reason for the band absorption is that an electronic level transition is usually accompanied by a simultaneous change between the more numerous vibrational levels. Thus a photon with too little energy to be accepted by the molecule for a 'pure' electronic transition can be utilized for a transition between one of the vibrational levels associated with the lower electronic state to one of the vibrational levels of a higher electronic state. A typical spectrophotometer set up for UV Visible absorption is shown in Fig. 2.6. In absorption spectrophotometer, the photon energy of the radiation incident on the sample is selected by a scanning monochromator (Ronda C 2007; Henderson B *et al* 1989; Yen W. M *et al* 2004)

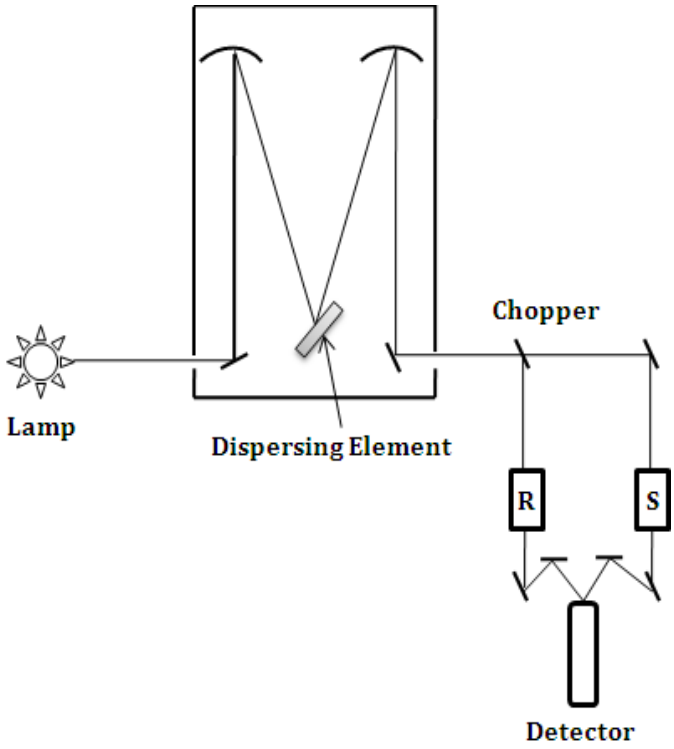

Fig. 2.6 Schematic illustration of a UV Visible absorption spectrophotometer.

The radiation selected by the monochromator is passed through a chopper that alternately directs the radiation along a reference beam path (going through compartment R) and through a path containing the sample (compartment S). One detector alternately records the signals from both beam paths. The transmittance T(λ) is defined as the ratio of the intensity of the light passed through the sample I(λ) to the intensity of the reference signal I_0 (λ). In a transmission spectrum, T is plotted as a function of wavelength (an equivalent quantity). Instead of transmittance the absorbance or optical density, A is often the quantity plotted on the y axis.

It is related to the transmittance by the equation,

$$A = - \log_{10} (T) \qquad (2.2)$$

Absorption spectroscopy is used to measure the transmitted signal for transparent (non-scattering) samples such as single crystals or solutions. An alternative for strongly scattering materials such as polycrystalline powders is diffuse reflection spectroscopy. The difference in set ups for absorption and reflection spectroscopy is in the detection compartment. When diffuse reflection spectroscopy is used, the backscattered signal is detected and compared to the backscattered signal from a reference material. Polycrystalline powders of MgO or $BaSO_4$ can be used as a reference. These materials scatter all the light in the wavelength range 200–3000 nm. The reflectance, R, defined as I/I_0 (λ), is plotted on the y axis.

The absorbance of the phosphors was recorded by Shimadzu UV 2401 spectrophotometer. The instrumental parameters of Shimadzu UV 2401 are enlisted in Table. 2.3.

Table. 2.3 Instrumental parameters of Shimadzu UV 2401 spectrophotometer

Spectrophotometer Model	UV 2401
Lamps	Tungsten, Deuterium
Detector	PMT
Wavelength Range	190-900 nm
Wavelength Reproducibility	0.1 nm
Wavelength Precision	0.3 nm
Monochromator	High performance holographic grating (single)
Power Needed	240 V

2.3.4 Optical Characterization – Luminescence Spectroscopy

Luminescence spectroscopy is a collective name given to three related spectroscopic techniques. They are molecular fluorescence spectroscopy, molecular phosphorescence spectroscopy and chemiluminescence spectroscopy. The basic process involved in phosphors is phosphorescence (photoluminescence), here phosphorescence spectroscopy can be referred as luminescence spectroscopy (Pelant I *et al* 2012). Photoluminescence spectra are measured using compact commercial equipment called spectrofluorimeters. Their main elements are also shown in Fig. 2.7.

The sample is excited with a lamp which is followed by a monochromator (the excitation monochromator) or a laser beam. The emitted light is collected by a focusing lens and analyzed by means of a second monochromator (the emission monochromator) followed by a suitable detector connected to a computer. Two kinds of spectra, (i) emission spectra and (ii) excitation spectra can be recorded. In emission spectra, the excitation wavelength is fixed and the emitted light intensity is measured at different wavelengths by scanning the emission monochromator. An emission spectrum yields information on the energetic positions of the optical transitions that are involved in the emission of light. From emission spectra, no information about the absolute value of the transition strengths can be obtained but

comparison of relative intensities (after correction for instrumental response) is straightforward for transitions originating from the same level. In this case, the observed intensities $I_{em}(\lambda)$ for transitions to various levels are proportional to the corresponding radiative transition rates.

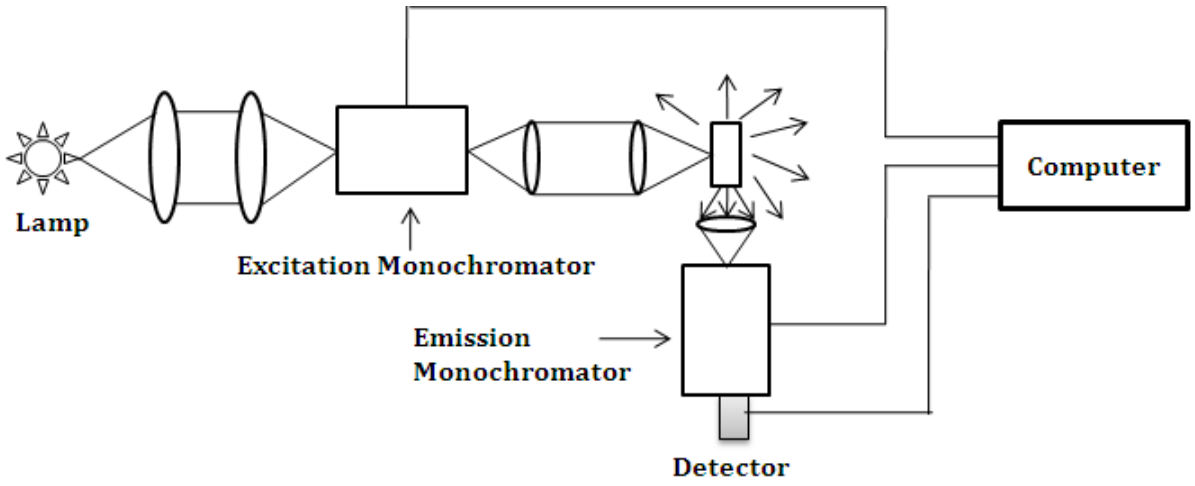

Fig. 2.7 Schematic illustration of a photoluminescence spectrofluorimeter.

In excitation spectra, the emission monochromator is fixed at any emission wavelength while the excitation wavelength is scanned in a certain spectral range. In contrast to an absorption spectrum, an excitation spectrum yields information on the energetic position of absorption bands that lead to emission of the chosen wavelength.

The different experimental set ups for absorption/ reflection and emission/ excitation spectroscopy lead to a different performance. Excitation and emission spectroscopy have very low background levels and a much higher sensitivity. They are used in combination with samples containing very small quantities of luminescent species. Absorption and diffuse reflection spectroscopy have much larger background and noise levels and are used for more concentrated samples. Both types of techniques also show different requirements for the equipment used. For absorption and diffuse reflection spectroscopy, the requirements for the output powers of lamps and the sensitivity of the detector are less demanding than for emission and excitation spectroscopy. Collimated radiation from the excitation source is measured in the former two techniques while in the latter, diffuse and spectrally resolved emission radiation of much lower intensity has to be detected.

The photoluminescence properties of developed red phosphors are recorded by Horiba Yvon Fluorolog® 3 spectrofluorimeter. The instrumental parameters of Horiba Yvon Fluorolog® 3 spectrofluorimeter are enlisted in Table. 2.4.

Table.2.4 Instrumental parameters of Fluorolog® 3 spectrofluorimeter

Spectrofluorimeter	Fluorolog® 3 (FL3-22)
Source	450 W Xe Lamp
Excitation Monochromator	Double
Emission Monochromator	Double
Sample Compartment Module	T Box
Detector	PMT (R928P)

2.3.5 Lifetime Measurement – Phosphorimeter

Luminescence lifetime is the time required for the luminescence intensity to decay from the initial value to 1/e of that value (e = 2.718...). Lifetimes can be measured by pulsed luminescence experiment. The Phosphorimeter is used to record the lifetime of luminescence. The lifetime of Eu^{3+} activated red phosphors were recorded by the Phosphorimeter attached to Fluorolog® 3 spectrofluorimeter. The Phosphorimeter includes a pulsed Xe lamp, gating electronics to control the size and temporal displacement of the detection window. It is a part of dual lamp house that contain both pulsed and continuous Xe lamps, electronics and cables. By software control it is possible to switch between pulsed and continuous lamps. For the lifetime measurement the sample is excited with pulsed light. The emitted phosphorescence is measured by a photon counting detector (R928) with variable delay and open window between pulse and detection.

A typical sequence of data acquisition starts with a flash from the pulsed lamp, sensed by the control module at time t = 0. The light enters excitation spectrometer, where it is dispersed. Monochromatic light from the spectrometer excites the sample.

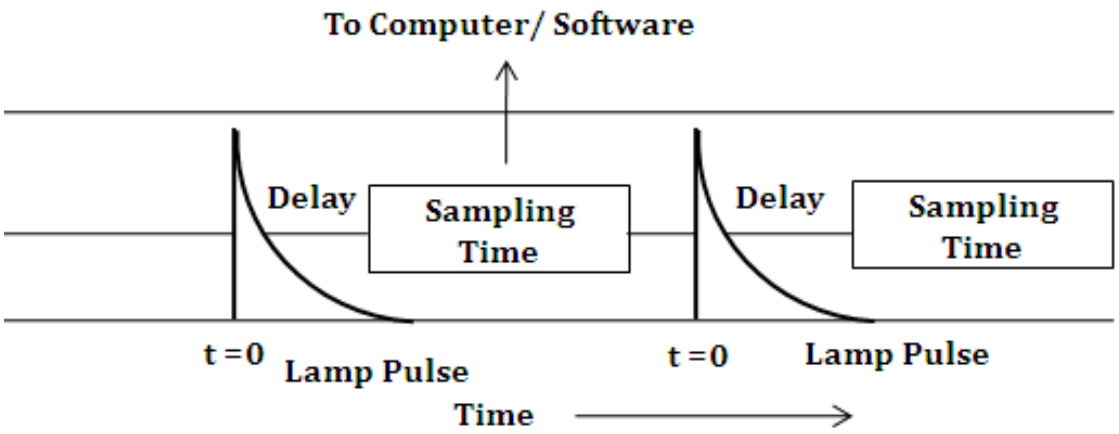

Fig. 2.8. The sequence of excitation, delay and sampling in lifetime measurement.

Luminescence emission from the sample then passes through emission spectrometer to photomultiplier tube detector. The control module includes a gate and delay generator, allowing the signal at detector to be integrated only during a specific period after flash (Delay after flash), for a predetermined length of time (Sample window). Any signal arriving before or after the gating is ignored. This sequence of excitation, delay and collection is repeated for each lamp pulse (Fig. 2.8). The total signal is accumulated for a pre determined number of pulses and the data is saved to the disk. The data can be manipulated and luminescence lifetime of the corresponding sample can be calculated.

CHAPTER 3

LUMINESCENT PROPERTIES OF POWELLITE TYPE NOVEL RED EMITTING PHOSPHORS; $Ca(La/Gd)_{1-x}NbMoO_8$: xEu^{3+}

Luminescent properties of molybdate based powellite type novel red phosphors, $Ca(La/Gd)_{1-x}NbMoO_8$: xEu^{3+} are investigated. Phosphors are excitable under near UV and visible irradiations matching well with the emission lines of near UV and blue LED chips and they emit strong red light (613 nm) under these excitations via $^5D_0$ - $^7F_2$ transitions of Eu^{3+}. Optimum luminescence behavior of the current phosphors with respect to activator concentration (Eu^{3+}) and its mechanism are discussed. These phosphors are characterized by sharp red emission lines with good color purity. These materials could be promising red phosphors for generating white light via phosphor converted white light emitting diodes.

J. Solid State Chem. *182 [1] (2009) 203.*

3.1 Introduction

Inorganic luminescent materials have wide applications in many optoelectronic devices such as displays, sensors, light emitting diodes etc. An extensive research is going on in the field of white light generation via inorganic phosphor converted white light emitting diodes (pc-WLEDs) owing to their ample applications and advantages. High luminous efficacy, low power consumption, long lifetime, high color rendering index (CRI), environmental friendliness etc are some of their advantages (Hu Y *et al* 2005; Yan S *et al* 2007). Commercially available WLED comprises of a blue InGaN chip (450- 470 nm) with a yellow phosphor (YAG: Ce^{3+}) which lacks good CRI (< 80) due to the deficiency in the red region (above 600nm) (Nakamura S *et al* 1997). To improve the CRI a variety of other approaches for white light generation were realized, such as the pumping of red, green and blue phosphors with an ultraviolet (UV) LED (λ_{em}: 370-410 nm) or using a blue LED in conjunction with green ($SrGa_2S_4$: Eu^{2+}) and red (SrY_2S_4: Eu^{2+}) phosphors (Huh Y *et al* 2004). Of these approaches, the combination of a near UV LED and the tri color phosphors may be the most convenient way to obtain high quality WLEDs. The current phosphor materials used for SSL based on near UV InGaN based LEDs are $BaMgAl_{l0}O_{17}$: Eu^{2+} for blue, ZnS: Cu^{2+}, Al^{3+} for green and Y_2O_2S: Eu^{3+} for red and that for blue LED chip, the phosphors are $SrGa_2S_4$: Eu^{2+} for green and SrY_2S_4: Eu^{2+} for red (Nishida T *et al* 2003). However, sulfide based red phosphors have some drawbacks such as poor absorbance in near UV region, low chemical stability, hazardous decomposition products such as sulfide gas (which is harmful to the environment) and inadequate lifetime under UV irradiations. Therefore it is necessary to develop novel, stable and efficient red phosphors for LED applications that can be effectively excited in the near UV and visible regions.

Finding novel families of phosphor materials with high absorption in the near UV and blue spectral region and reduced degradation by UV radiation are the key challenges to overcome. In order to identify novel and potential red phosphors for pc-WLEDs, the selection of host material and activator is important. Recently, oxide phosphors have gained much attention because of their higher chemical stability than their sulfide counter parts (Gundiah G *et al* 2008; Minami T *et al* 2003). Among these molybdates and tungstates with powellite/scheelite structure are considered as good host lattice under near UV or blue excitation because of high chemical stability, broad and intense CT band arising from MoO_4/WO_4 tetrahedron unit in the near UV region and the capability of efficiently capturing radiation from a GaN based LED over a range of wave lengths. (Zhang Z. J *et al* 2007; Macalik L *et al* 2004 ; Zhou Y *et al* 2010 ; Lei S *et al* 2010).

Eu^{3+} is a preferable choice as an activator for red emission in various host lattices, which has been used in most commercial red phosphors. This is because in Eu^{3+} ions, the lowest excited levels ($^5D_0$) of the $4f^6$ configuration is situated below the $4f^5 5d$ configuration and it mainly shows very sharp $^5D_0$-$^7F_2$ red emission lines when it occupy the lattice sites without inversion symmetry (Kodaira C. A *et al* 2003). Eu^{3+} exhibits a high lumen equivalent, quantum efficiency and photostability at the same time. Moreover from a practical point of view a fluorescent light source comprising a red line emitter emitting at 610 - 615 nm is the best compromise between luminous efficacy and color rendering (Ronda C 2008).

However, the main drawback of Eu^{3+} is the weak absorption in the blue and even in the near UV region. An important strategy to solve this problem is to develop materials that have broad and intense CT absorption bands in the near UV and are capable of efficiently absorbing the emission from InGaN based LEDs. Such materials include oxysulfides, vanadates, molybdates, tungstates etc. where the oxygen to Eu^{3+} CT band is very intense and broad and the position is at rather low energy. A recent idea is to convert near UV or blue light via the 4*f*-4*f* transitions of Eu^{3+} located at 394 ($^7F_0$–$^5L_6$) and 465nm ($^7F_0$–$^5D_2$), which are rather intense in molybdates and tungstates (Neeraj S *et al* 2004). Following the excitation process, Eu^{3+} relaxes non radiatively to the $^5D_0$ state which is the emitting energy level.

In order to explore a desirable red luminescence, great efforts have been made based on molybdate host lattice. $CaMoO_4$ is important among metal molybdate families that have potential applications in various fields such as in photoluminescence (Graser R *et al* 1975), microwave applications (Johnson L. F *et al* 1962), white light emitting diodes (Hu Y *et al* 2005) and laser materials (Barbosa *et al* 2002). Hu et al (Hu Y. S *et al* 2005; Lopez M. D *et al* 2004; Zhao X. X *et al* 2007; Zhang N *et al* 2007) mentioned $CaMoO_4$: Eu^{3+} that can have red emission by exciting at 394 nm and its luminescence properties were studied. Neeraj et al. improved these molybdate based systems by doping Eu^{3+} in $AB(WO_4)_{2-x}(MoO_4)_x$ and $ABMoO_4$ (A = Na, B = Gd, Y, Bi) (Chiu C. H *et al* 2007; Wang Z. L *et al* 2007; Neeraj S *et al* 2004; Kim T. Y *et al* 2007). It is considered that the central Mo metal ion is coordinated by four O^{2-} ions in tetrahedral symmetry. Hence $(MoO_4)^{2-}$ is relatively stable and can be opted for the host material. Still the brightness of molydate based current red phosphors is limited. This demands the development of novel, stable and efficient red phosphors with improved performance than the existing red phosphors for the advancement of pc-WLEDs.

In this regard, an attempt has been made to synthesize and study the luminescence properties of molybdate based powellite type Eu^{3+} activated novel red phosphors, $Ca(La/Gd)_{1-x}NbMoO_8$ for pc-WLED applications. The crystalline structure, morphology and

absorbance of these phosphors were characterized by powder X ray diffraction (XRD), scanning electron microscopy (SEM), and UV Visible absorption spectroscopy. Investigations on their photoluminescent properties indicated that the phosphors emit strong red light under both near UV (394/395 nm) and blue (465 nm) excitations and these materials could be promising red phosphors for use in generating white light in pc- WLEDs. This chapter elucidates the experimental details, structural, microstructural and luminescent properties of the developed novel red phosphors.

3.2 Experimental

Powellite type red emitting phosphors with the general composition: $CaLa_{1-x}NbMoO_8$: xEu^{3+} (x = 0.01, 0.03, 0.05, 0.1) (CLNM) and $CaGd_{1-x}NbMoO_8$: xEu^{3+} (x = 0.05, 0.1, 0.15, 0.20, 0.25, 0.30) (CGNM) were prepared by solid state reaction using $CaCO_3$, La_2O_3/Gd_2O_3, Nb_2O_5, MoO_3 and Eu_2O_3 (Chemicals are from Acros Organics and Sigma Aldrich with 99.99% purity) as the starting materials. The stoichiometric amounts of these materials were weighed and then thoroughly wet mixed in an agate mortar with acetone as the wetting medium. The mixing was followed by drying in an air oven. The mixing and drying were repeated thrice to obtain a homogenous mixture and was calcined at 1200°C for 6 h in a platinum crucible in an air atmosphere furnace.

The crystal structure as well as the phase purity of the calcined samples were examined by recording the powder X ray diffraction patterns using a PANalytical X'pert Pro diffractometer with Ni filtered CuKα radiation (λ= 1.54056Å). The structural refinement of all the XRD patterns for $Ca(La/Gd)_{1-x}NbMoO_8$: xEu^{3+} were further performed by the Rietveld analysis using the X'pert plus program. The morphological analysis of the powder samples was done by a scanning electron microscope (JEOL, JSM- 5600LV). The UV Visible absorption of the samples was recorded by UV-Vis Spectrophotometer (Shimadzu UV-2401). Photoluminescence excitation, emission spectra were recorded using a Horiba Yvon Fluorolog® 3 Spectrofluorimeter with a 450W xenon flash lamp as the exciting source. To record the emission spectra, the excitation wavelength is fixed at 394/395 and 465 nm respectively and the emitted light intensity is measured at the wavelength range of 500 - 750 nm. For recording excitation spectra, the emission monochromator is fixed at 613 nm emission wavelength and the excitation wavelength is scanned in 200 - 500 nm spectral range. Both the excitation and emission spectra are recorded by fixing the excitation and emission monochromator slit widths at 0.5 and 1 nm respectively. The CIE chromaticity coordinates of the phosphors were also calculated. Luminescence lifetime of the phosphors was recorded by the phosphorimeter attached to Fluorolog® 3 spectrofluorimeter.

3.3 Results and Discussion

3.3.1 Powder X ray diffraction analysis

The powder X ray diffraction patterns of CLNM (x = 0.01, 0.03, 0.05, 0.1) and CGNM (x = 0.05, 0.1, 0.15, 0.20, 0.25, 0.30) samples are shown in Fig. 3.1 and Fig. 3.2 respectively. The presence of sharp and intense peaks in the XRD patterns indicates the crystalline nature of the samples. The obtained patterns were found to be similar to that of the earlier reported for $CaMoO_4$ (Ravindran Nair K *et al* 2008) and all the peaks in the XRD patterns are indexed with the $CaMoO_4$ (JCPDS file no. 29-0351) tetragonal powellite structure with the space group $I4_1/a$. The prominent peaks correspond to (112), (004), (200), (204), (220), (116) and (312) lattice planes (Ravindran Nair K *et al* 2008). There are no traces of extra peaks from impurities in the pattern. Thus all the samples are single phase forming solid solutions of CLNM and CGNM.

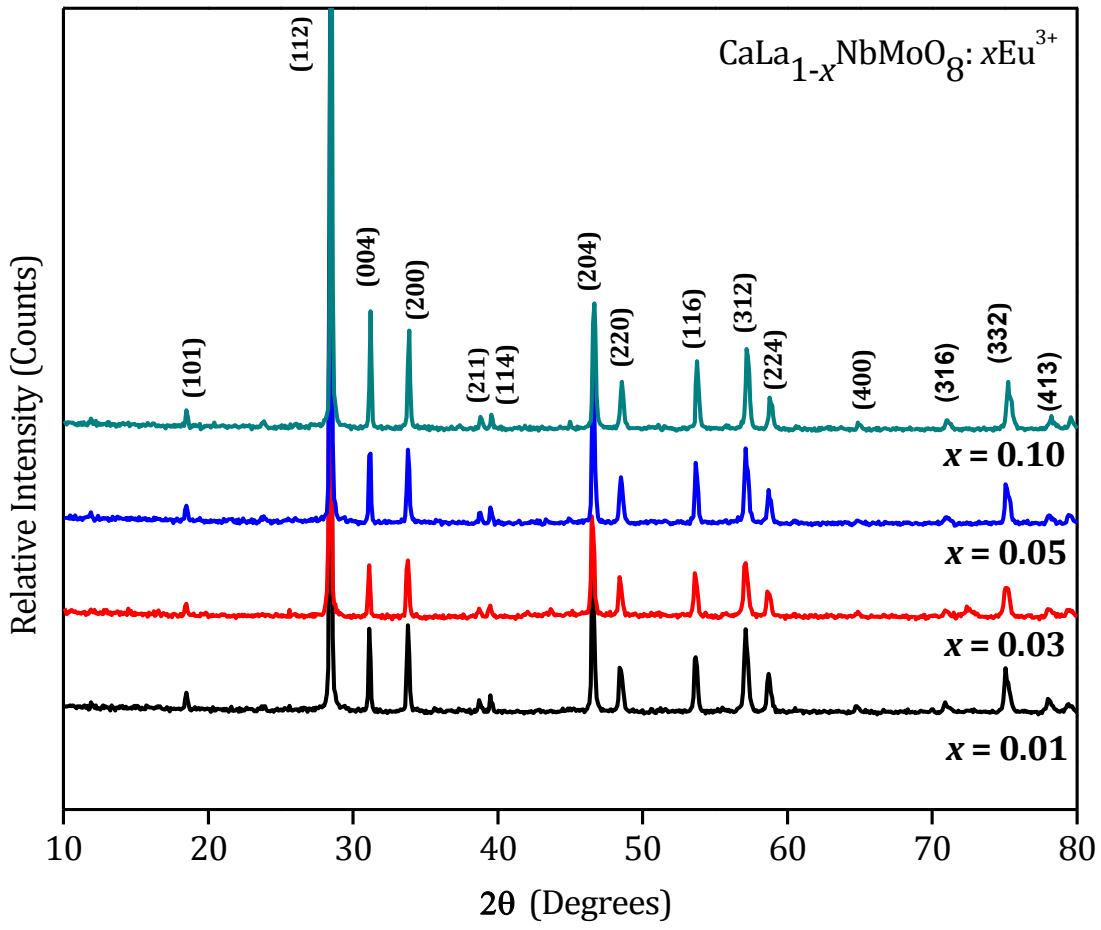

Fig. 3.1 Powder X ray diffraction patterns of $CaLa_{1-x}NbMoO_8$: xEu^{3+} (x = 0.01, 0.03, 0.05, 0.1).

In CLNM and CGNM lattices, A site is shared by Ca^{2+}, La^{3+}/Gd^{3+} and Eu^{3+} ions and is surrounded by eight oxygen atoms forming AO_8 polyhedra. Nb^{5+} and Mo^{6+} ions share B sites and are four coordinated forming BO_4 tetrahedra. Each oxygen atom of the AO_8 polyhedra is connected to one Nb/Mo atoms. Thus each oxygen atom is coordinated with two A atoms and one Nb/Mo atom. The cubic close packing of A atoms and Nb/MoO_4 tetrahedral units in an ordered manner form the powellite structure. Since the ionic radii of Eu^{3+} (r = 1.07Å when coordination number (CN) = 8) is close to that of La^{3+} (r =1.16 Å when CN = 8) and Gd^{3+} (r =1.05 Å when CN = 8); Eu^{3+} ion prefers to occupy La^{3+}/Gd^{3+} site in CLNM and CGNM lattices respectively.

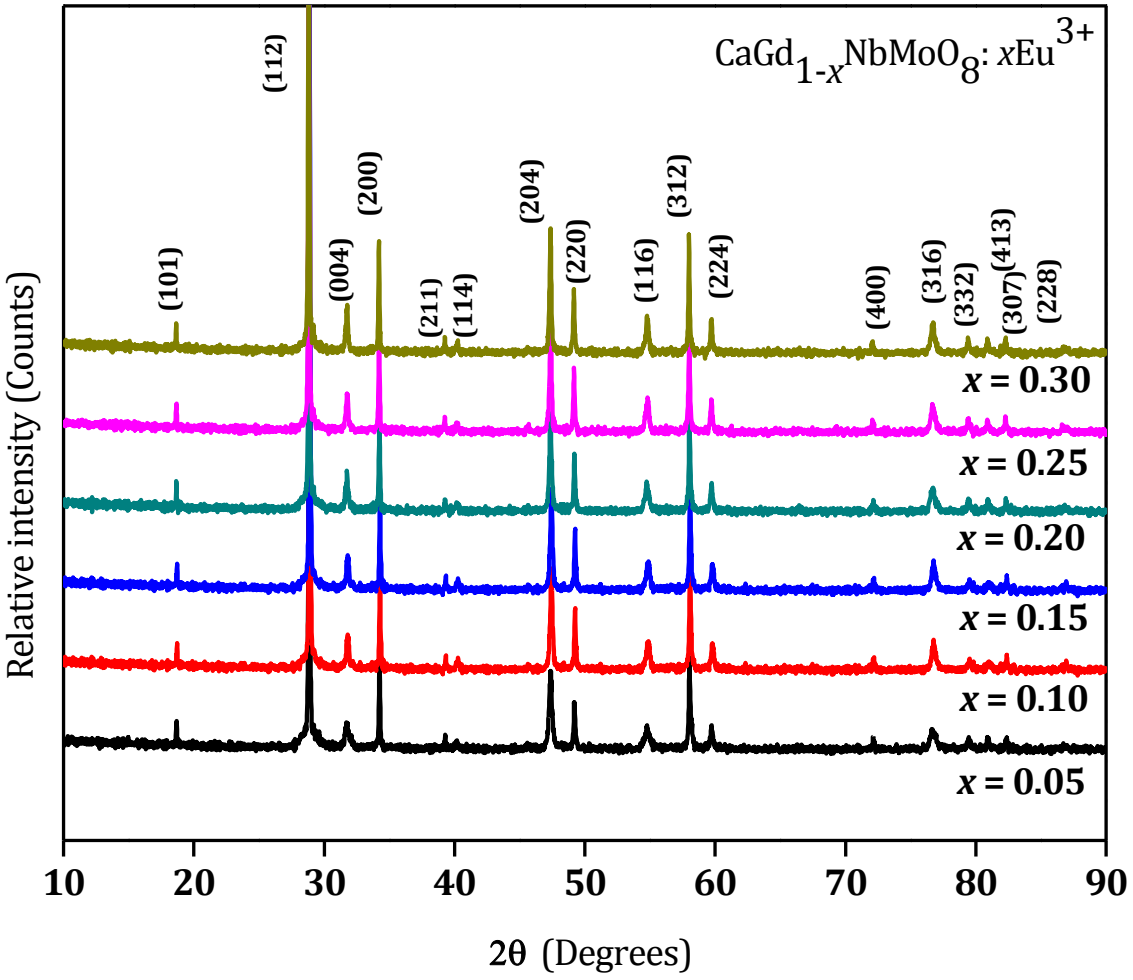

Fig. 3.2 Powder X ray diffraction patterns of $CaGd_{1-x}NbMoO_8$: xEu^{3+} (x = 0.05, 0.10, 0.15, 0.20, 0.25, 0.30).

The structural refinement of all the XRD patterns for CLNM and CGNM phosphors were performed by the Rietveld analysis using the X'pert plus program. The starting model for the refinement of the phases was taken from the reported crystal structure of $CaMoO_4$. For

CLNM and CGNM samples, Ca and La/Gd/Eu are at (4b: 0, 1/4, 5/8) sites, Nb and Mo at (4a: 0, 1/4, 1/8) sites and O at (16f: x, y, z), Z = 4 in the space group $I4_1/a$, no.88 (Zhang Z. J *et al* 2007; Achary S. N *et al* 2006). The profile was fitted using Pseudo Voigt profile function. Fig. 3.3 and Fig. 3.4 shows the typical best fit that was observed, calculated, the difference powder diffraction profiles and the expected Bragg reflections for $CaLa_{0.97}NbMoO_8$: $0.03Eu^{3+}$ and $CaGd_{0.70}NbMoO_8$: $0.30Eu^{3+}$. The expected Bragg peak positions are marked below the profile fit as vertical bars.

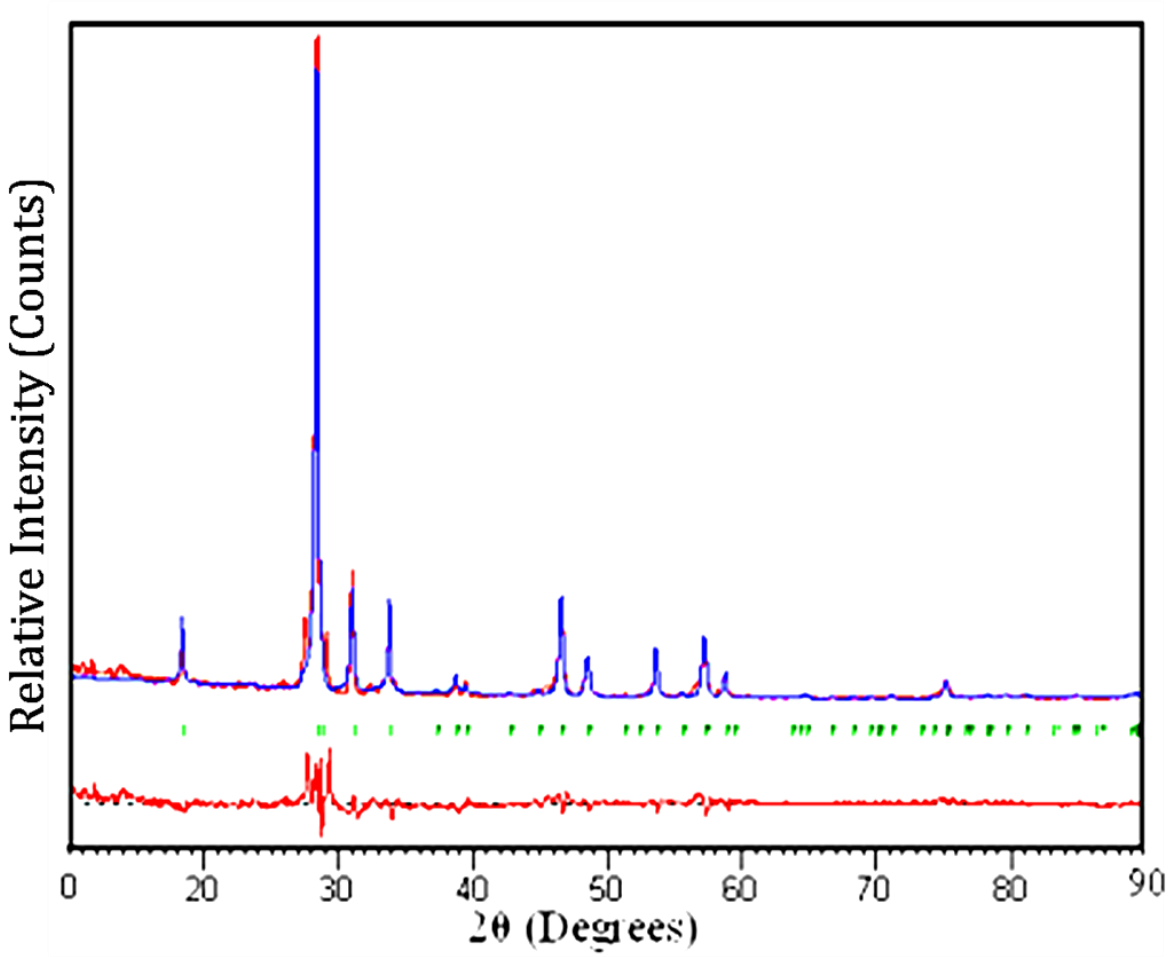

Fig. 3.3 Observed (red), calculated (blue) and difference (red) powder X ray diffraction profiles obtained from the Rietveld refinement of XRD data for $CaLa_{0.97}NbMoO_8$: $0.03Eu^{3+}$.

The R factors, the refined oxygen coordinates, lattice parameters and other parameters obtained from the Rietveld refinement of the powder diffraction data for some of the compositions of CLNM and CGNM phosphors are given in Table 3.1. The refined R values suggest that the refinement is in good agreement with the space group in all respects.

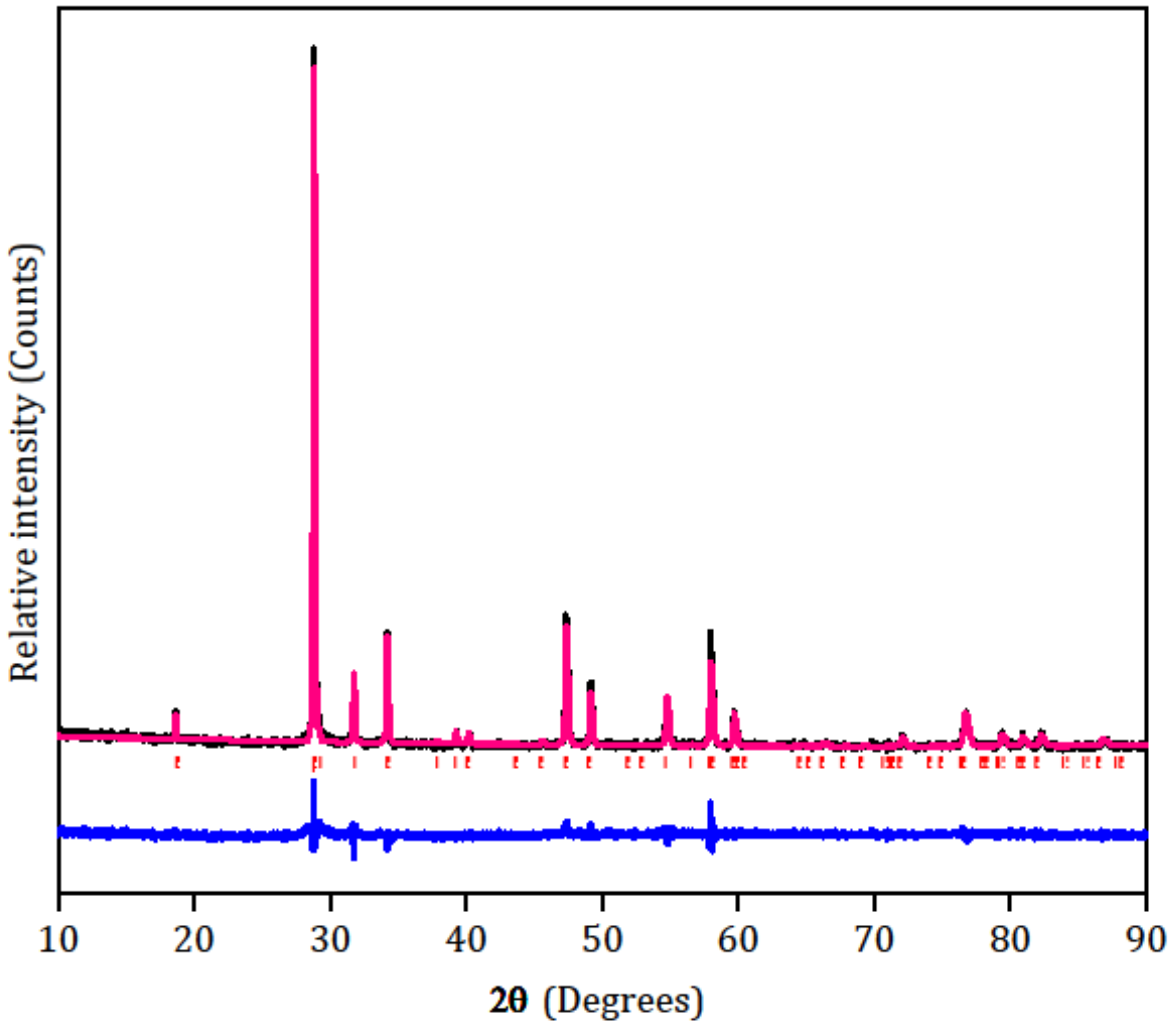

Fig. 3.4 Observed (pink), calculated (black) and difference (blue) powder X ray diffraction profiles obtained from the Rietveld refinement of XRD data for $CaGd_{0.70}NbMoO_8$: $0.30Eu^{3+}$.

From the refined cell parameters it is clear that the lattice parameters and unit cell volume of CLNM samples decreases with the increase of Eu^{3+} concentration. This is due to the lower ionic radius of Eu^{3+} compared to that of La^{3+}. i.e., the ionic radius of Eu^{3+} (r = 1.07 Å, when coordination number (CN) = 8) is smaller than that of La^{3+} (r = 1.16 Å, when CN = 8). While the refinement result of CGNM samples show that with respect to Eu^{3+} doping, both the lattice parameters and unit cell volume is increasing. For CGNM phosphors, the degree of increase of lattice parameters and unit cell volume with respect to Eu^{3+} doping marginal. This observation further confirms the effective incorporation of Eu^{3+} ions in La^{3+} /Gd^{3+} sites in CL/GNM samples respectively. In CGNM lattice, Eu^{3+} is substituting a lower ionic radius site [Gd^{3+} (r = 1.05 Å when CN = 8)] and hence Eu^{3+} ion's local environment can be slightly distorted compared to that of CLNM lattice. Since the unit cell volume of CGNM

phosphor is lower compared to that of CLNM phosphor, $CaGdNbMoO_8$ host lattice is stiffer than that of $CaLaNbMoO_8$ lattice.

Table 3.1 Variation of lattice parameters, Oxygen coordinates, R factors, and other parameters obtained from Rietveld analysis of $CaLa_{1-x}NbMoO_8$: xEu^{3+} and $CaGd_{1-x}NbMoO_8$: xEu^{3+}.

	$CaLa_{1-x}NbMoO_8$: xEu^{3+}			$CaGd_{1-x}NbMoO_8$: xEu^{3+}		
x	0.03	0.05	0.10	0.10	0.25	0.30
Lattice parameters (Å)						
a	5.3199	5.3167	5.3160	5.2326	5.2345	5.2346
c	11.5200	11.5140	11.5010	11.2559	11.2567	11.2569
Unit cell Volume ($Å^3$)	326.03	325.47	325.02	308.19	308.43	308.45
Oxygen position co ordinates						
x	0.1499	0.1499	0.1499	0.1499	0.1499	0.1499
y	0.0069	0.0069	0.0069	0.0069	0.0069	0.0069
z	0.2099	0.2099	0.2099	0.2099	0.2099	0.2099
Residues (%)						
R_{exp}	11.58	8.67	9.47	8.15	8.29	8.37
R_p	6.15	5.19	9.66	7.63	7.88	7.81
R_{wp}	9.41	9.41	12.52	9.84	10.10	10.12
Number of variables	12	12	12	12	12	12

3.3.2 Microstructural characterization

Scanning electron micrographs of selected compositions of both CLNM (magnification: 2,500) and CGNM (magnification; 5,000) phosphors are presented in Fig. 3.5 and Fig. 3.6. The microstructure reveals the crystalline nature of particles. The particles are agglomerated to some extent. The increase of crystallinity and de agglomeration is observed with the increase of Eu^{3+}concentration in both host lattices. The particles are in the scale of 1–5 μm in average size with homogenous nature.

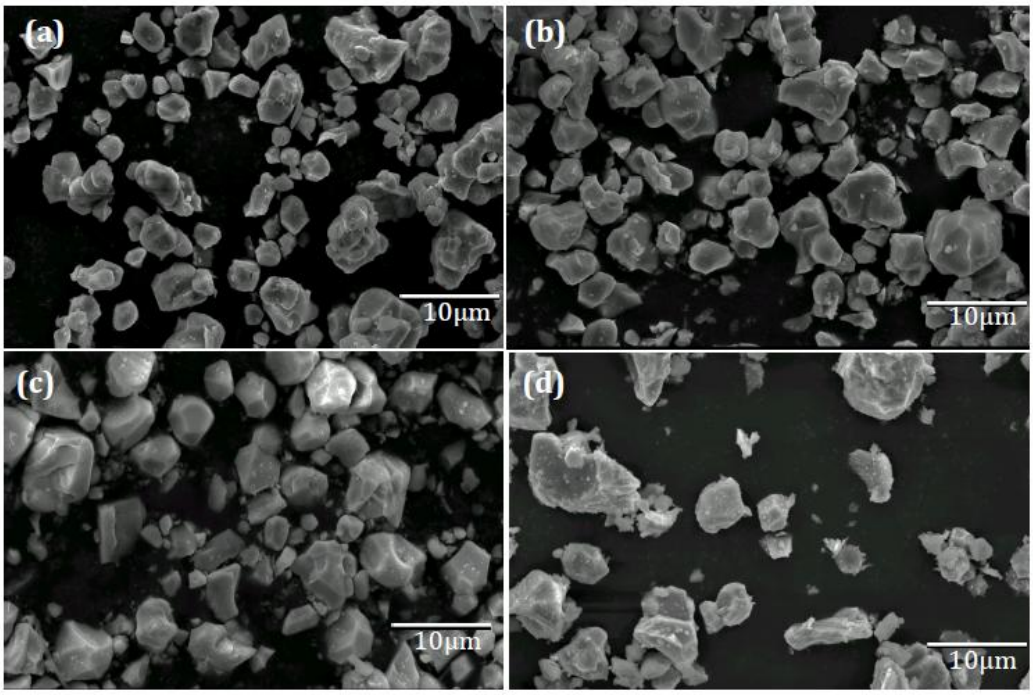

Fig. 3.5 Scanning electron micrographs of phosphor powders of $CaLa_{1-x}NbMoO_8$: xEu^{3+} with varying Eu^{3+} concentrations: (a) $x = 0.01$, (b) $x = 0.03$, (c) $x = 0.05$, and (d) $x = 0.1$.

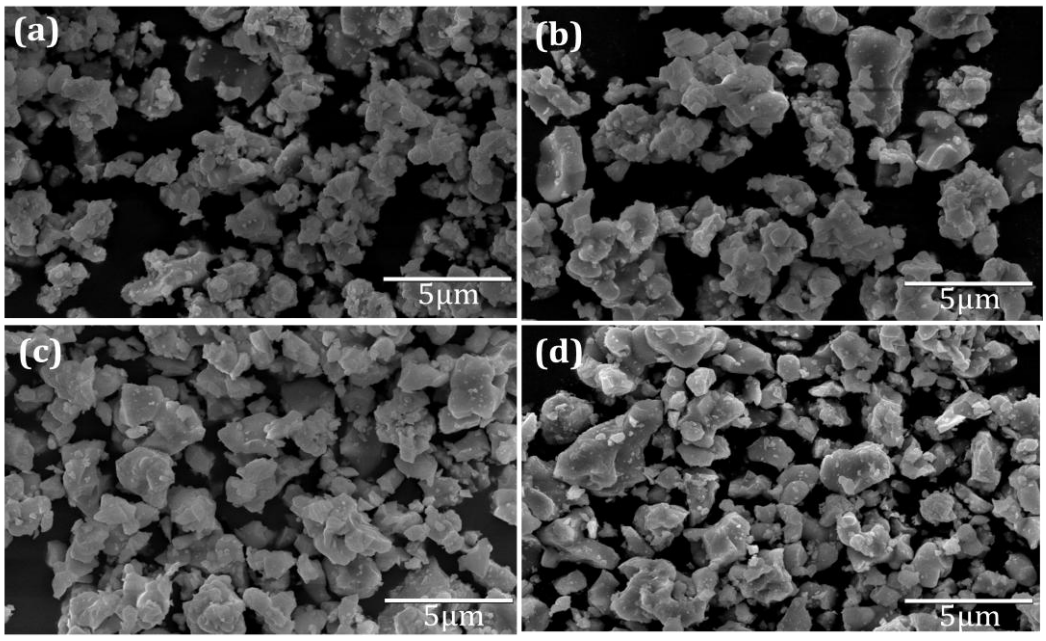

Fig. 3.6 Scanning electron micrographs of phosphor powders of $CaGd_{1-x}NbMoO_8$: xEu^{3+} with varying Eu^{3+} concentrations: (a) $x = 0.15$, (b) $x = 0.20$, (c) $x = 0.25$, (d) $x = 0.30$.

3.3.3 UV Visible absorption

The UV Vis absorption spectra of CLNM (x = 0, 0.05) and CGNM (x = 0.0, 0.20, 0.30) phosphors are shown in Fig. 3.7 and Fig. 3.8. For both phosphors the absorption spectral profile is almost similar except some variation in the relative absorbance. The absorption spectra include strong and broad band of absorption in UV region (200- 375 nm). This region of absorption can be arising from the ligand to metal charge transfer (LMCT) transitions of MoO_4/NbO_4 and O^{2-}-Eu^{3+} groups in the host lattice (i.e., charge transfer from O^{2-} to Mo^{6+}/Nb^{5+} atoms in the MoO_4/ NbO_4 groups respectively) (Thomas M *et al* 2009). For Eu^{3+} doped samples the absorption peaks correspond to intra configurational *f-f* transitions of $^7F_0$-$^5L_6$ (394, 395 nm) and $^7F_0$- $^5D_2$ (464, 465 nm) are also observable.

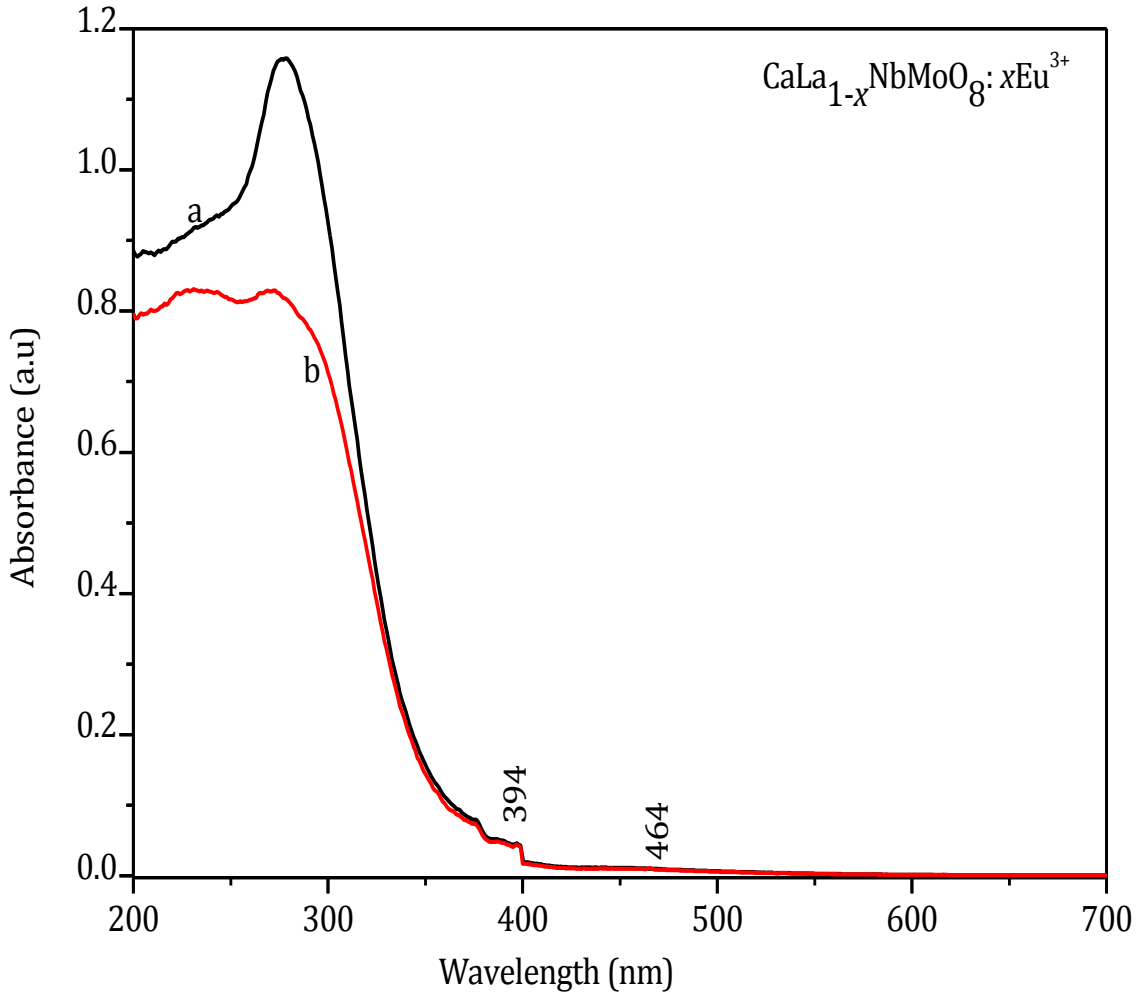

Fig. 3.7 UV-Vis absorption spectra of $CaLa_{1-x}NbMoO_8$: xEu^{3+} (a) x = 0, (b) x = 0.05.

It can be seen from Fig. 3.7 that the intensity of absorbance for $CaLaNbMoO_8$ (host lattice) is greater than that of the Eu^{3+} doped sample, indicating an efficient energy transfer

from the CT states to the Eu^{3+} emitting levels. The Eu^{3+} intra configurational *f-f* transitions have lower intensity compared to the CT band of absorption. It can be due to the lower doping concentration and forbidden parity selection rule. The degree of absorption of Eu^{3+} levels is increasing with Eu^{3+}doping concentration of the samples for CGNM phosphors.

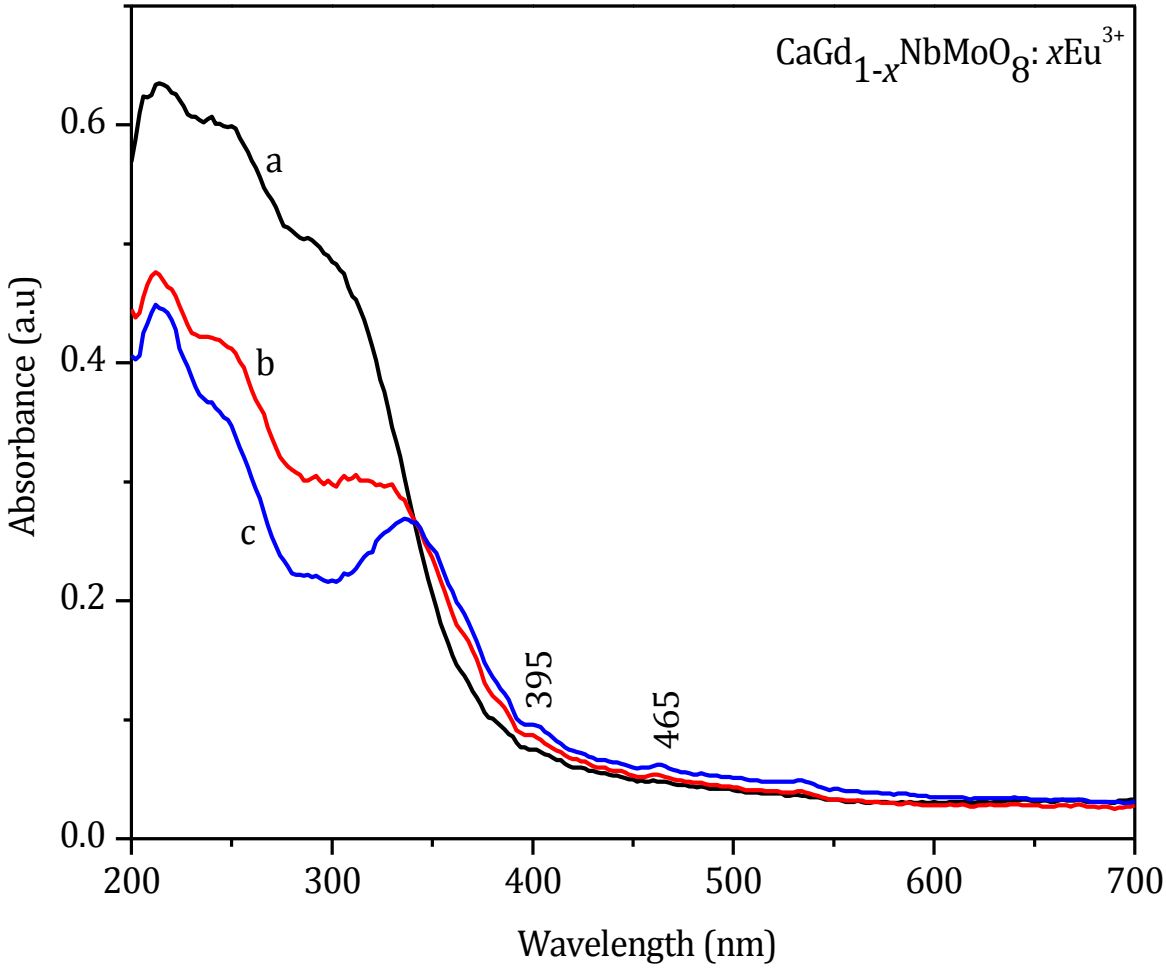

Fig. 3.8 UV-Vis absorption spectra of $CaGd_{1-x}NbMoO_8$: xEu^{3+}
(a) x = 0.10, (b) x = 0.20 (c) x = 0.30.

Thus from the absorption spectral analysis it is expected that these phosphors are excitable under both near UV and blue irradiation, which is one of the main prerequisites for a phosphor material for pc WLEDs.

3.3.4 Photoluminescence properties

3.3.4.1 Excitation spectra

Fig. 3.9 and Fig. 3.10 present the excitation spectra of both CLNM (x = 0.01, 0.03, 0.05, 0.1) and CGNM (x = 0.05, 0.1, 0.15, 0.2, 0.25, 0.30) samples for an emission at 613 nm. The excitation spectra of CLNM and CGNM phosphors include both broad band (240-360

nm, peaking around 313 nm) and sharp peaks (beyond 360 nm) of excitation. It has been reported that the excitation spectra of $CaMoO_4$: $0.05Eu^{3+}$ shows a dominant broad band, which corresponds to the combination of CT transitions from Eu^{3+}- O^{2-} and $(MoO_4)^{2-}$ groups (Hu Y *et al* 2005; Hu Y. S *et al* 2005). Also $LaNbO_4$ shows strong absorbance at 260 nm corresponding to the CT band in NbO_4 group (Hsiao Y. J *et al* 2007). Thus it can be assumed that the observed broad band in the excitation spectra corresponds to the combinations of the CT transitions from Eu^{3+}- O^{2-}, MoO_4 and NbO_4 groups. For both CLNM and CGNM phosphors the excitation spectral profile are closely similar and the positions of CT band is also the same (313 nm).

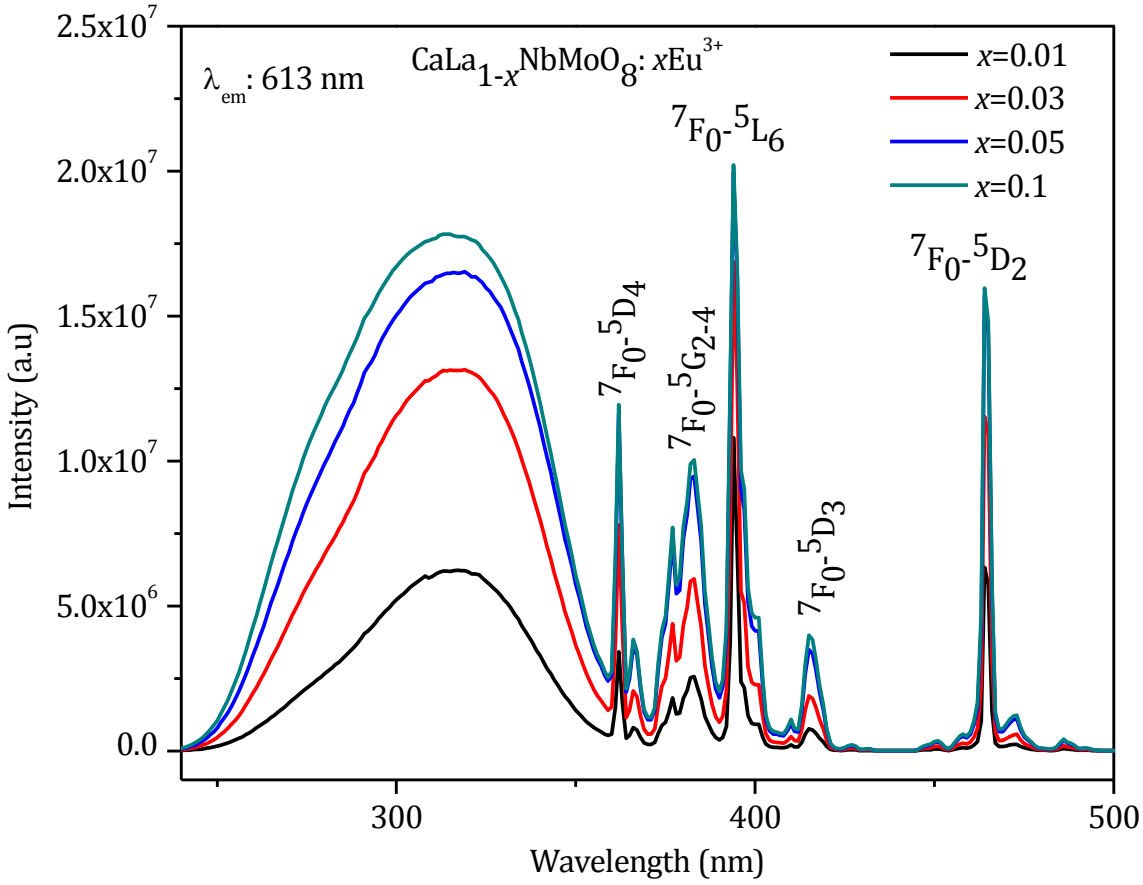

Fig. 3.9 Excitation spectra of $CaLa_{1-x}NbMoO_8$: xEu^{3+} for an emission at 613nm.

The CT band position of a phosphor material is closely related to the degree of covalency of ligand – metal and Ln^{3+}- Eu^{3+}- O^{2-} (in the present case, Ln^{3+} = La^{3+}/Gd^{3+}) bonds present in the lattice. Here same ligands of MoO_4 and NbO_4 are present in the host lattices of both CLNM and CGNM phosphors, further the electronegativity values of other host cations such as of $La^{3+}$and Gd^{3+} (1.1 and 1.2) are almost comparable. This can lead to similar extent

of electronic interactions in both lattices. Thus the observation of similar energy position of CT band in both phosphors is obvious.

The sharp peaks beyond 360 nm are due to the intraconfigurational (*f–f*) transitions of Eu^{3+}, including the peaks with maxima at 362 nm ($^7F_0$ - $^5D_4$), 384 nm ($^7F_0$ - $^5G_{2,4}$), 394/395 nm ($^7F_0$ - $^5L_6$), 412 nm ($^7F_0$ - $^5D_3$), 464/465 nm ($^7F_0$–$^5D_2$) respectively (Thomas S. M *et al* 2008; Wang J *et al* 2005). Among them, the intensity of the peaks at 394/395 and 464/465 nm excitation wavelengths (which are emission wavelengths of near UV and blue LED chips), is much stronger than the other transitions of Eu^{3+}. This implies that molybdate based powellite type CLNM and CGNM phosphors can be effectively excited by the radiations in the near UV and blue wavelength regions.

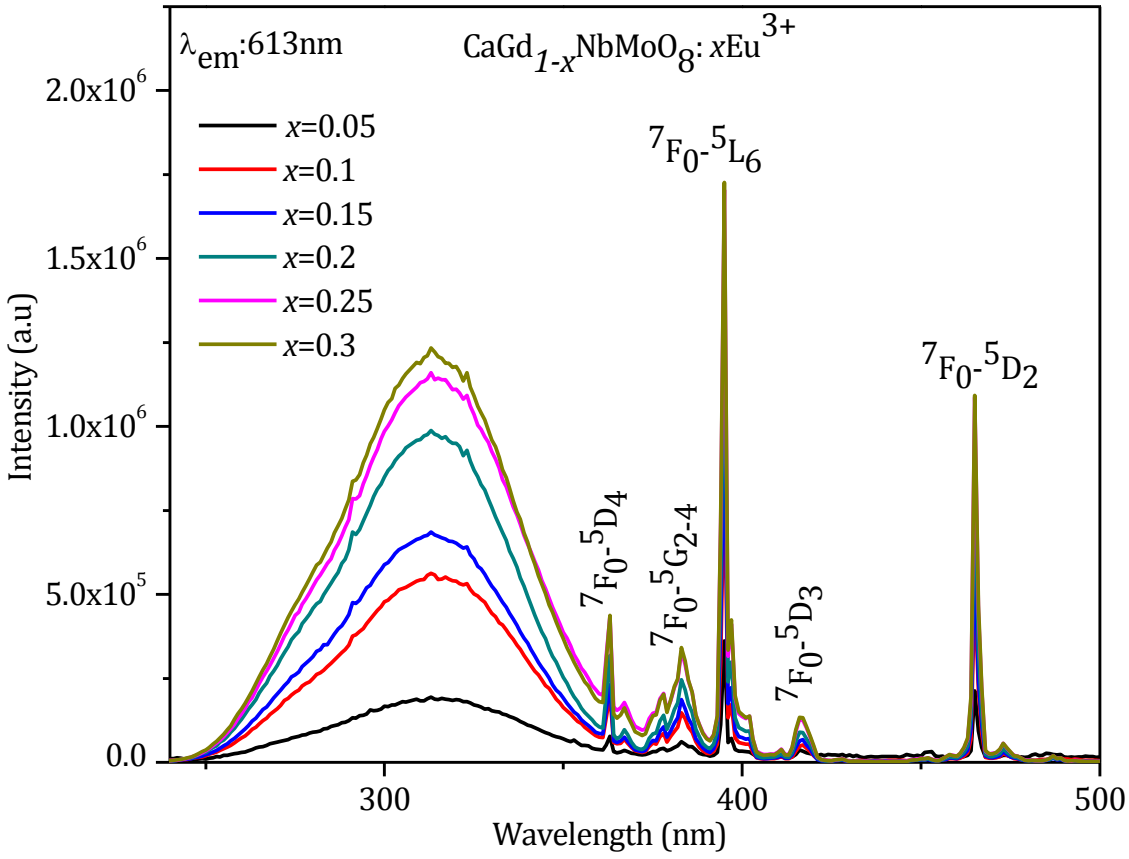

Fig. 3.10 Excitation spectra of $CaGd_{1-x}NbMoO_8$: xEu^{3+} for an emission at 613nm.

It is also observed that absorption peaks of intra configurational 4*f* transitions of Eu^{3+} increase with increasing doping concentration of Eu^{3+}, indicating the effective incorporation of Eu^{3+} in the host lattice. The increase of absorption/excitation strengths of $^7F_0$-$^5L_6$ and

$^7F_0$-$^5D_2$ transitions can contribute to enhanced red emission from CLNM and CGNM phosphors with respect to Eu^{3+} concentration under both near UV and blue excitations.

3.3.4.2 Emission spectra

Fig. 3.11 and Fig. 3.12 show the emission spectra of CLNM (x = 0.01, 0.03, 0.05, 0.1) and CGNM (x = 0.05, 0.1, 0.15, 0.2, 0.25, 0.30) phosphors under near UV and blue excitations. The major emission peaks are observed at 580, 591, 612, 613, 623 nm and all these are characteristic emission peaks of Eu^{3+} ion corresponding to $^5D_0$-^7F_J (J =0, 1, 2) transitions (Zhang Z. J *et al* 2007).

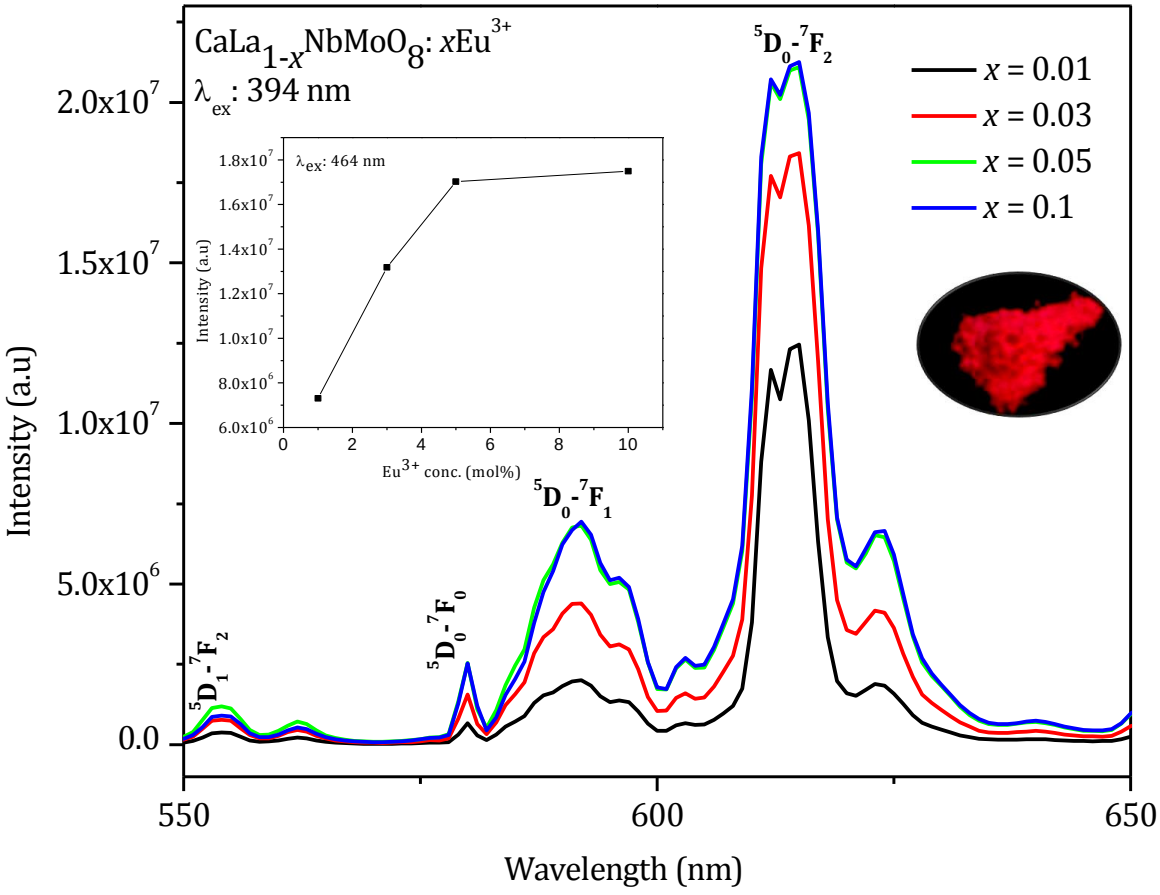

Fig. 3.11 The emission spectra of $CaLa_{1-x}NbMoO_8$: xEu^{3+} under 394 nm excitation (Inset shows the relative intensity variation of 613 nm peak under 464 nm excitation and photograph of $0.1Eu^{3+}$ doped sample under UV irradiation).

Of these emission peaks, the red emission peak at 613 nm is more dominant than the other peaks and is due to the electric dipole transition ($^5D_0 - {}^7F_2$) of Eu^{3+}. Also the emission corresponding to the magnetic dipole transitions ($^5D_0 - {}^7F_1$) in the orange region (590 nm) is weak. In terms of the Judd‑ Ofelt theory, the magnetic dipole transition is always allowed and is insensitive to the site symmetry (Hu Y *et al* 2005). Generally for Eu^{3+} ions, the electric

dipole transitions ($^5D_0$ – $^7F_2$) leading to red emission (613 nm) are forbidden due to its violation of parity selection rule. However, these electric dipole transitions will be allowed only when Eu^{3+} occupies a site without an inversion center (Blasse G 1979). Subsequently when Eu^{3+} ions occupy inversion center sites, the $^5D_0$-$^7F_1$ transitions should be relatively strong, while the $^5D_0$-$^7F_2$ transitions should be relatively weak. Here in the case of CLNM and CGNM phosphors it is clear that Eu^{3+} mainly occupies a site without an inversion center and consequently they emit strong red light at 613 nm. The emission lines for both CLNM and CGNM phosphors are similar for near UV (394/395 nm) and blue (464/465 nm) excitations. However, it is seen that the red light under near UV excitation is more intense than that under blue excitation.

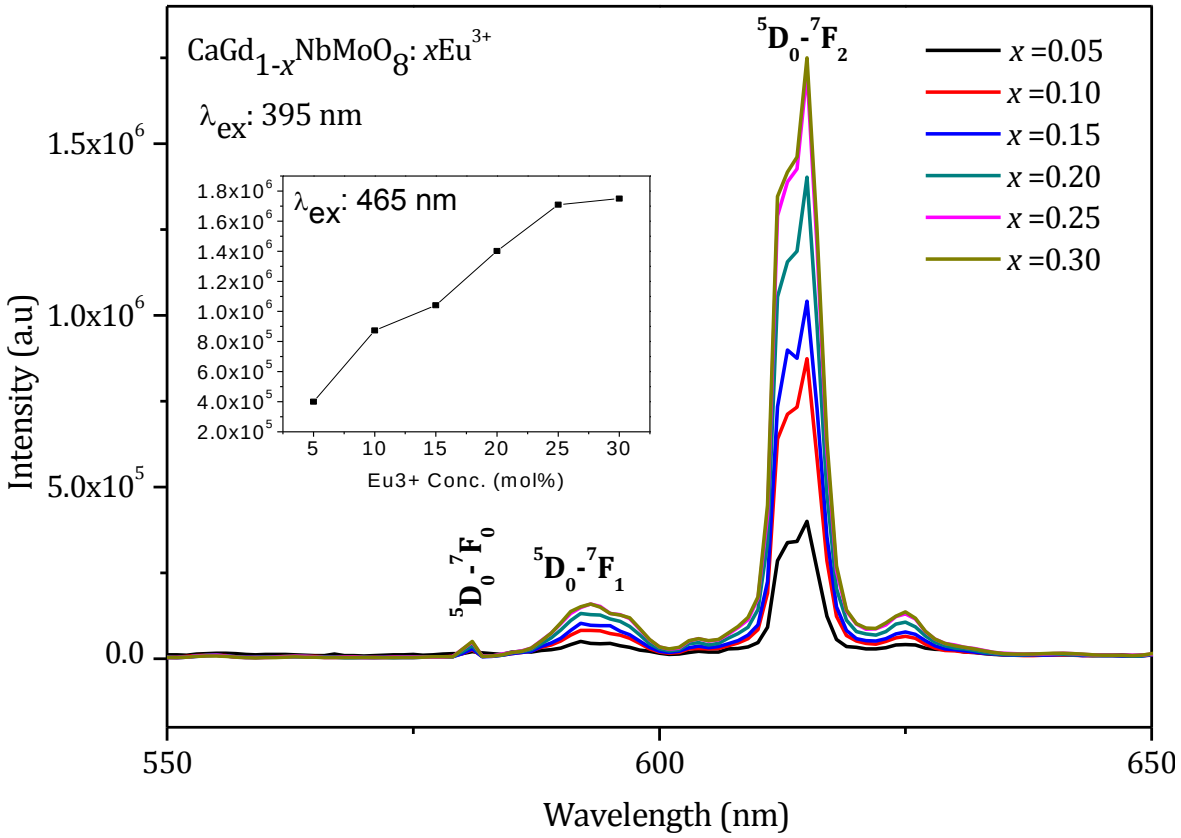

Fig. 3.12 The emission spectra of $CaGd_{1-x}NbMoO_8$: xEu^{3+} under 395 nm excitation (Inset shows the relative intensity of 613 nm peak under 465 nm excitation).

From the emission spectra, it is observed that with the increase of Eu^{3+} concentration, the intensities of all the emission lines are enhanced significantly. For CLNM phosphor, the emission intensity reached a maximum at a concentration of 5 mol% and remains almost same for 10 mol% of Eu^{3+}. In order to understand the optimum Eu^{3+} concentration for maximum intensity, the intermediate compositions of CLNM phosphor between 5 and 10

mol% Eu^{3+} (x = 0.07, 0.08, 0.09) are synthesized and the emission spectra are recorded under both near UV and blue excitations. The variation of red emission intensity under near UV (394 nm) excitation for these intermediate composition is shown in Fig. 3.13. It is observed that at 9 mol% of Eu^{3+} the emission intensity reached the maximum, beyond which the emission intensity is quenched under both near UV and blue excitations. This observation is mainly attributed to the phenomenon of concentration quenching.

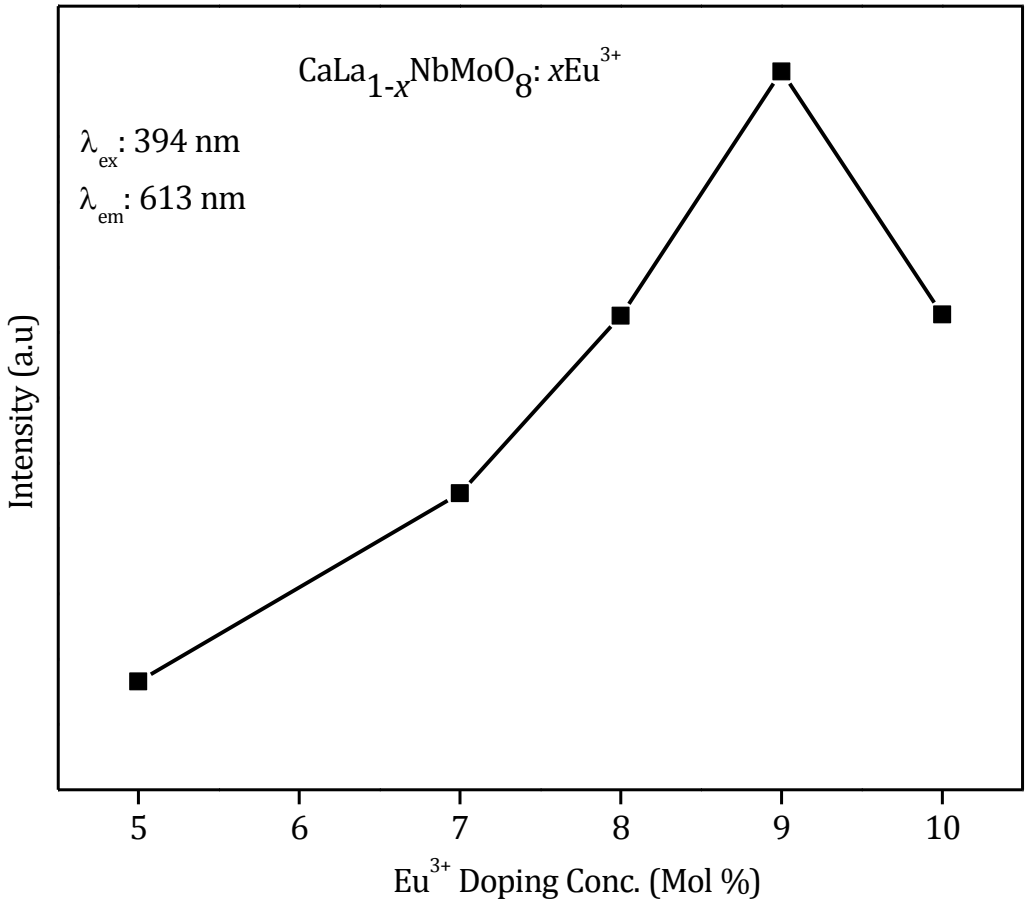

Fig. 3.13 The variation of red emission (613 nm) intensity of $CaLa_{1-x}NbMoO_8$: xEu^{3+} (x = 0.05, 0.07, 0.08, 0.09, 0.10) phosphor under near UV (394 nm) excitation.

It is well known that lower doping concentrations of activator (Eu^{3+}) lead to weak luminescence, while higher doping concentrations cause quenching of the luminescence of Eu^{3+} (Blasse G 1979). When the doping concentration reaches a certain degree, the distance between Eu^{3+} ions become smaller leading to the interactions of Eu^{3+} ions in the excited state resulting in dominant non radiative transitions than radiative transition. This reduces emission intensity and is known as concentration quenching. However no such concentration quenching is observed up to 30 mol% of Eu^{3+} for CGNM phosphors.

How does red emission occur in CLNM and CGNM phosphors? The schematic illustration of the excitation and emission process associated with CLNM and CGNM phosphors are presented in Fig. 3.14. The characteristic energy levels of Eu^{3+} ion are shown and that of host lattice are not included in the diagram. Upon near UV (394/395 nm) and blue (464/465 nm) excitations, the electron in the ground state ($^7F_0$) is excited to $^5L_6$ and $^5D_2$ states respectively. From these levels electrons are cross relaxed non radiatively to the lower excited state ($^5D_0$) and then de excited to the ground state via radiative transition of $^5D_0$- $^7F_2$ resulting in the red emission at 613 nm.

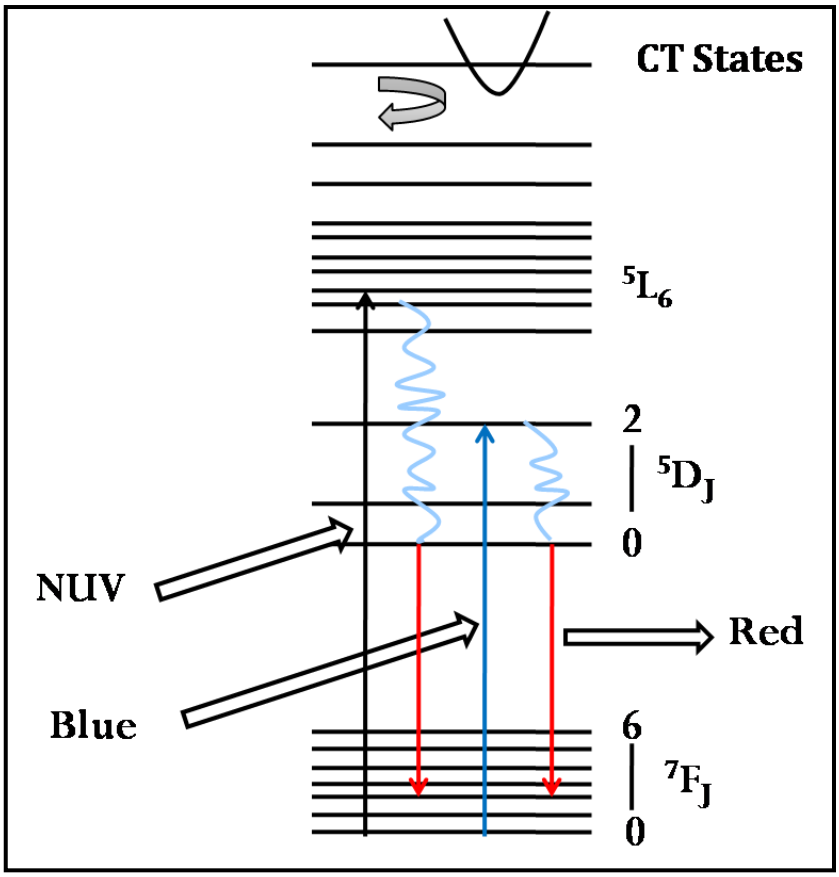

Fig. 3.14 Schematic diagram of excitation and emission process in CL/GNM phosphors.

It is observed that the full width half maximum (FWHM) of the red peak increases with the increase of the doping concentration of Eu^{3+} in both CLNM and CGNM phosphors. The symmetry of the Eu^{3+} site in a host lattice can be clearly determined by calculating the intensity ratio $I(^5D_0–^7F_2)/I(^5D_0–^7F_1)$ (asymmetry ratio) (Liu J *et al* 2007). Table 3.2 enlists asymmetry ratio and FWHM of CLNM and CGNM red phosphors with respect to Eu^{3+} doping concentration under near UV excitation (394/395 nm). Here both phosphors are

characterized by higher values of the asymmetry ratio, which further evidences the non centrosymmetric site occupancy of Eu^{3+} in the host lattice. The red emission peak of CGNM phosphors are sharper with small FWHM than CLNM phosphors. The sharp emission may be due to stiffness of the CGNM lattice compared to CLNM lattice. It is also noted that the asymmetry ratio of CGNM is more, which can contribute to better color purity and red emission intensity for them compared to CLNM phosphors. The asymmetry ratio of a lattice provides information about the activator site symmetry. If asymmetry ratio is more for a particular lattice, then activator site is more asymmetric and the electric dipole transitions become more probable. Thus Eu^{3+} site in CGNM lattice is more asymmetric than that of CLNM lattice. In CGNM lattice, the Eu^{3+} ions (ionic radius, 1.07 Å) are substituting the Gd^{3+} (ionic radius, 1.05 Å) site while in CLNM; the substitution is to La^{3+} (ionic radius, 1.16 Å) site. Thus in CGNM lattice, Eu^{3+} ions face more symmetry distortion than that of CLNM lattice and is contributing to the improvement of the asymmetry ratio in CGNM lattice.

The CIE (Commission Internationale de l'Eclairage) color co ordinates of all compositions are calculated using the software CIE Calculator and are matching with that of standard NTSC (National Television System Committee) red phosphors (0.67, 0.33). Table 3.3 includes the CIE color co ordinates of both CLNM and CGNM phosphors.

Table 3.2 Asymmetry ratio and FWHM of $CaLa_{1-x}NbMoO_8$: xEu^{3+} and $CaGd_{1-x}NbMoO_8$: xEu^{3+} with respect to Eu^{3+} doping concentration under near UV excitation

CLNM *x*	FWHM (nm)	Asymmetry Ratio	CGNM *x*	FWHM (nm)	Asymmetry Ratio
0.01	6.59	6.20	**0.05**	4.69	8.04
0.03	7.66	4.19	**0.10**	4.89	10.11
0.05	8.97	3.09	**0.15**	4.91	10.57
0.10	9.09	3.06	**0.20**	5.02	10.71
			0.25	5.11	10.72
			0.30	5.18	11.0

The purity of red color increases with increasing *x* coordinates. Here, the *x* coordinate is increasing with Eu^{3+} doping concentration. This increment is more prominent in CGNM than CLNM. Thus color co ordinates of CGNM phosphors is closer to the standard red phosphor compared to that of CLNM phosphors as expected.

Table 3.3 CIE color co-ordinates of $CaLa_{1-x}NbMoO_8$: xEu^{3+} and $CaGd_{1-x}NbMoO_8$: xEu^{3+} under near UV excitation

CLNM *x*	Color Co ordinates (*x*, *y*)	CGNM *x*	Color Co ordinates (*x*, *y*)
0.01	(0.56,0.33)	**0.05**	(0.59,0.34)
0.03	(0.56,0.34)	**0.10**	(0.60,0.34)
0.05	(0.56,0.34)	**0.15**	(0.62,0.33)
0.10	(0.59,0.35)	**0.20**	(0.63,0.33)
		0.25	(0.64,0.33)
		0.30	(0.65,0.33)

3.3.4.3 Lifetime and Quantum efficiency calculation

Fig. 3.15 presents the decay curve for $^5D_0$-$^7F_2$ transition of CLNM (x = 0.09) and CGNM (x = 0.25) phosphors under near UV excitation. The decay curves can be fitted well with single exponential function;

$$I = A \exp\left(-x/\tau\right) \tag{3.1}$$

where I, τ and A are intensity, lifetime (decay time) and fitting parameter respectively. The decay times of CLNM and CGNM phosphors are 0.6031 and 0.6051 ms respectively.

On the basis of the emission spectra and lifetimes of the $^5D_0$ emitting level, the emission quantum efficiency of Eu^{3+} ion's excited state ($^5D_0$) in CLNM and CGNM phosphors can be determined. Assuming that only radiative and non radiative processes are essentially involved in the depopulation of $^5D_0$ states of Eu^{3+} ion, the quantum efficiency (η) can be expressed as;

$$\eta = \frac{A_{rad}}{A_{rad} + A_{nrad}} \tag{3.2}$$

where A_{rad} and A_{nrad} are radiative and non radiative transition probabilities respectively (Su Y *et al* 2008). The emission intensity (I) can be taken as integrated intensity (S) of $^5D_0 - {}^7F_{0\text{-}4}$ transitions in the emission curves and can be expressed as ;

$$I_{i-j} = \hbar\omega_{i-j} A_{i-j} N_i \sim S_{i-j} \quad (3.3)$$

where i and j are initial ($^5D_0$) and final ($^7F_{0\text{-}4}$) levels respectively; $\hbar\omega_{i-j}$ is the transition energy, $A_{i\text{-}j}$ is the Einstein's coefficients of spontaneous emission and N_i is the population of the $^5D_0$ emitting level (Su Y *et al* 2008).

As $^5D_0 - ^7F_5$ and $^5D_0$ -$^7F_6$ transitions are not experimentally observed, their contribution to the emission intensity is neglected (Santos P. C. R *et al* 2003; Sa' Ferreira R. A *et al* 2001). The $^5D_0$ -$^7F_1$ magnetic dipole transition is relatively insensitive to the chemical environments around Eu^{3+} ions, and hence can be considered as a reference for the whole spectrum.

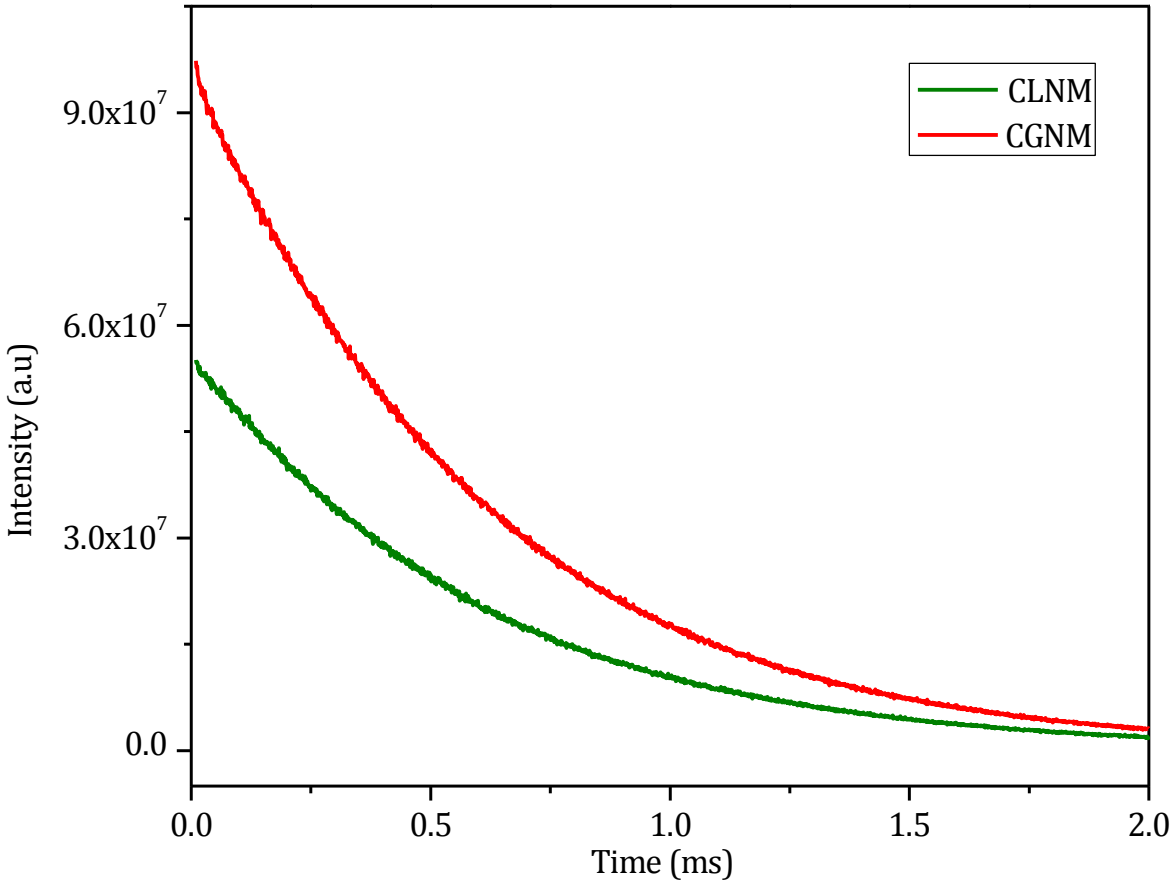

Fig. 3.15 Decay curves of Eu^{3+} emission at 613 nm in $CaLa_{0.91}NbMoO_8$: $0.09Eu^{3+}$ and $CaGd_{0.75}NbMoO_8$: $0.25Eu^{3+}$ phosphors under near UV excitation.

The experimental coefficient of spontaneous emission (A_{0j}) can be calculated based on the relation (Su Y *et al* 2008);

$$A_{0j} = A_{01}\left(\frac{I_{0j}}{I_{01}}\right)\left(\frac{\nu_{01}}{\nu_{0j}}\right) \quad (3.4)$$

where, ν_{01} and ν_{0j} are the energy baricenters of the $^5D_0$ - $^7F_1$ and $^5D_0$ -^7F_j energy levels and can be determined from the emission peaks of Eu^{3+} ion. A_{01} is the Einstein's coefficients of spontaneous emission between $^5D_0$ and $^7F_1$ energy levels.

In vacuum, the average refractive index (n) is 1.506 and $(A_{0\text{-}1})_{vac}$ = 14.65 S^{-1} is considered (Peng C. Y *et al* 2005). Then;

$$A_{0-1} = n^3(A_{0-1})_{vac} \sim 50S^{-1} \quad (3.5)$$

The lifetime (τ) of the $^5D_0$ states, A_{rad}, A_{nrad} are related as (Su Y *et al* 2008);

$$A_{tot} = \frac{1}{\tau} = A_{rad} + A_{nrad} \quad (3.6)$$

where τ is the average lifetime.

$$A_{rad} = A_{01}\left(\frac{\nu_{01}}{I_{01}}\right)\sum_{j=0}^{4}\frac{I_{0j}}{I_{01}} = \sum_j A_{0j} \quad (3.7)$$

When Eqn. (3.2) - (3.7) are applied, the parameters A_{rad} and A_{nrad} and the quantum efficiency values, η, for the $^5D_0$ Eu^{3+} excited state can be calculated. For CLNM and CGNM red phosphors the calculated values of η are 21.03% and 22.90% respectively.

Furthermore, to better understand the effect of chemical environment on the luminescence properties of Eu^{3+}, the Judd - Ofelt (JO) intensity parameters (Ω_2, Ω_4) of Eu^{3+} in CLNM and CGNM phosphors can be calculated directly (Kodaira C. A *et al* 2003). This method takes advantage of the fact that the intensities of the $^5D_0$ - $^7F_2$, and $^5D_0$ - $^7F_4$ transitions are solely dependent on the Ω_2 and Ω_4 parameters respectively. Because the radiative transition rate is proportional to the integrated intensity of the transition band in the emission spectrum (i.e., $A_{0-\lambda} \propto \int \lambda\, I(\lambda)\, d\lambda$), the radiative transition rate of $^5D_0$ - ^7F_J (J = 0, 2, 4) can be estimated according to the ratio of the integrated intensity of $^5D_0$ - $^7F_1$ to these transitions.

From the emission spectra of CLNM and CGNM phosphors we can determine the experimental intensity parameters Ω_2 and Ω_4 using the $^5D_0$-$^7F_2$ and $^5D_0$-$^7F_4$ transitions and they are estimated according to the equation (Malta O. L *et al* 1996; 1997);

$$A_{0-\lambda} = \left(\frac{4e^2\omega^3}{3\hbar c^3}\right)\left(\frac{1}{2J+1}\right)\chi\sum_\lambda \Omega_\lambda \left(\langle 5D0\left|U^{(\lambda)}\right|7FJ\rangle\right)^2 \quad (3.8)$$

where $A_{0\text{-}\lambda}$ is the coefficient of spontaneous emission, e the electronic charge, ω the angular frequency of the transition, ħ Planck's constant over 2π , c the velocity of light, χ the Lorentz local field correction that is given by $\left(\frac{n(n^2+2)^2}{9}\right)$ with the refraction index n = 1.5 (Malta O. L *et al* 1996), and $(\langle 5D0|U^{(\lambda)}|7FJ\rangle)^2$ values are the squared reduced matrix elements whose values are 0.0032 and 0.0023 for J = 2 and 4 (Carnall W. T *et al* 1978), respectively. Since the $^5D_0$-$^7F_6$ transition could not be experimentally detected, the Ω_6 parameter was not determined. The intensity parameters of both CLNM and CGNM are calculated and included in Table 3.4. It is observed that for both the phosphors Ω_2 is more than that of Ω_4, indicating the non centro symmetric site occupancy of Eu^{3+} ion in both phosphors.

The variation of Ω_2, reflected by the hypersensitivity of the $^5D_0$-$^7F_2$ transition, can be related to the variation in the covalency of the Eu-O bond as well as in the structural environment around Eu^{3+} ions (Carnall W. T *et al* 1978). The slightly larger value of Ω_2 parameter of CGNM red phosphor than that of CLNM phosphor suggest shorter bond length between Eu^{3+} and oxide anions due to the stiffness in the lattice and a relatively low site symmetry of Eu^{3+} in CGNM than in CLNM phosphors. An overview of the photoluminescence data of current red phosphors are enlisted in Table 3.4.

Table 3.4 Photoluminescence data of $CaLa_{0.91}NbMoO_8$: $0.09Eu^{3+}$ and $CaGd_{0.75}NbMoO_8$: $0.25Eu^{3+}$ phosphors

PL	**CLNM (*0.09*)**	**CGNM (*0.25*)**
λ_{em}	580, 591, 613, 655, 703	
I_{02}/I_{01}	7.55	10.72
τ (ms)	0.6031	0.6051
$1/\tau$ (s^{-1})	1658	1652
A_{rad} (s^{-1})	348.73	378.44
A_{nrad} (s^{-1})	1309.36	1274.17
η (%)	21.03	22.90
Ω_2 (10^{-20} cm^2)	8.35	9.24
Ω_4 (10^{-20} cm^2)	1.37	1.42

3.4 Conclusions

Molybdate based novel red phosphors, $Ca(La/Gd)_{1-x}NbMoO_8$: xEu^{3+} have been synthesized via solid state reaction route and their structural, microstructural and luminescence properties are studied. Both of these phosphors crystallize in tetragonal powellite type structure. Investigations on their photoluminescence properties reveal that, these phosphors are efficiently excitable under both near UV and blue irradiations corresponding to the two emission lines from near UV and blue LED chips and they emit strong red light under both these excitations. The current molybdate based red phosphors are characterized by good color purity and quantum efficiency. Thus these molybdate based powellite type phosphors could be promising red candidates for pc-WLED applications.

CHAPTER 4

LUMINESCENT PROPERTIES OF SCHEELITE TYPE NOVEL RED EMITTING PHOSPHORS; $Ca(La/Gd)_{1-x}NbWO_8$: xEu^{3+}

Structural, microstructural and luminescent properties of scheelite type novel red phosphors, $Ca(La/Gd)_{1-x}NbWO_8$: xEu^{3+} are presented. The current tungstate based phosphors are also excitable under near UV and blue radiations, which is one of the important prerequisites of a phosphor for pc-WLED applications. These phosphors have shallow CT band of excitation positioned at a high energy realm compared to the molybdate analogues. These phosphors are characterized by sharp red emission with comparable CIE color co-ordinates to that of NTSC standard red phosphor and good quantum efficiency. In addition, they have longer lifetime of milli seconds order. The luminescence process (excitation, emission and energy transfer) associated with both molybdate and tungstate (powellite/ scheelite) based red phosphors are discussed in aid of a schematic illustration.

Phys. Status Solidi A *208[9] (2011) 2170*

4.1 Introduction

The discovery of the InGaN blue light emitting diode (LED) chips opened the exciting and challenging research on pc-WLEDs as a novel generation of solid state lighting (SSL) devices (Nakamura S *et al* 1996; Jüstel T *et al* 1998; Schubert E. F *et al* 2005). The eventual performance of pc-WLED devices strongly depends on the luminescence properties of the phosphors used. The current red emitting phosphor materials used for pc-WLEDs include $Y_2O_2S:Eu^{3+}$ (Shionoya S *et al* 1999), Eu^{2+} activated sulfides (e.g., CaS: Eu^{2+}) (Hu Y *et al* 2005; He X. H *et al* 2008), $Mg_4O_{3.5}FGeO_2$: Mn^{4+} (Shi G 2007), and Eu^{2+} or Ce^{3+} doped (oxy) nitrides (e.g., $CaAlSiN_3$: Eu^{2+}) (Uheda K *et al* 2006) and $CaSiN_2$: Ce^{3+}) (Toquin R. L *et al* 2006). The luminescence efficiency of Y_2O_2S: Eu^{3+} is about eight times lower than that of ZnS: Cu^{2+}, Al^{3+} green and $BaMgAl_{10}O_{17}$: Eu^{2+} blue emitting phosphors (Shionoya S *et al* 1999) and its lifetime is inadequate under extended UV irradiation (Neeraj S *et al* 2004). Eu^{2+} activated sulfides red emitting phosphors are chemically unstable and not desirable in efficiency due to releasing of sulfide gas (Hu Y *et al* 2005; He X. H *et al* 2008). In addition, sulfide based phosphors show luminescence saturation with an increasing applied current when incorporated into pc-WLED devices (Wu H *et al* 2005). $Mg_4O_{3.5}FGeO_2$: Mn^{4+} phosphor has wide absorption band, but its main emission peak is at about 660 nm which is insensitive to the human eye (Shi G 2007). As for (oxy) nitride based red emitting phosphors, high firing temperatures and high nitrogen pressures are required for their synthesis (Uheda K *et al* 2006; Toquin R. L *et al* 2006; Xie R. J *et al* 2007; Piao X *et al* 2006; Duan C. J *et al* 2009), which result in higher production cost. To overcome the aforementioned drawbacks, there are extensive worldwide research efforts to develop new red emitting phosphors for pc-WLED applications as well as to optimize the existing systems (Duan C. J *et al* 2009; Saradhi M. P *et al* 2009; Gundiah G *et al* 2008; Uhlich D *et al* 2008; Won Y *et al* 2008).

An appropriate red emitting phosphor for pc-WLEDs should satisfy some necessary conditions such as; stability of the host lattice, strong and broad absorption to output wavelength of LEDs chips (370 - 470 nm) and strong red emission (Guo C *et al* 1991) under near UV and blue excitations. In addition, the full width at half maximum (FWHM) of the emission band should be as small as possible to achieve high luminous output (Jüstel T *et al* 1998). Eu^{3+} doped tungstates and molybdates are one of the potential classes of red phosphors satisfying these conditions. Calcium tungstate, $CaWO_4$ is a representative example of tungstates with the scheelite structure containing Ca^{2+} ions and $(WO_4)^{2-}$ groups with the coordination number of eight for Ca^{2+} and four for W^{6+}. $CaWO_4$ is considered to be a highly functional material due to its prominent luminescence properties and has received much

attention for their versatile applications in scintillations counter (Yi *et al* 2002), laser host material (Treadaway *et al* 1975), medical devices (Nagirnyi *et al*. 1997) and also employed in detecting the dark matter recently (Petricca *et al*. 2004). Scheelite type $CaWO_4$ is a self activated blue emitting luminescent material via tetrahedral WO_4 groups in the host lattice (Nazarov *et al*. 2004). The luminescence properties of this superior phosphor could be varied by doping with rare earth ions. Tungstates are characterized by broad and intense charge transfer (CT) absorption band in the near UV and hence they are capable of efficiently capturing radiation from a GaN based LED over a range of wavelengths. Powell and co workers studied the luminescent properties and energy transfer of $CaWO_4$: Eu^{3+} systems (Treadaway M. J *et al* 1974; Tyminski J. K *et al* 1982). To obtain a novel red emitting phosphor with proper CIE chromaticity coordinates, it is indisputable that Eu^{3+} activated compound is the preferable choice because Eu^{3+} usually shows red emission via $^5D_0$ - $^7F_2$ transition. An extensive research is going on Eu^{3+} activated tungstate based phosphors and research efforts in line with this is included in the literature review part in Chapter 1.

In line with this background, tungstate based scheelite type Eu^{3+} activated novel red phosphors, $Ca(La/Gd)_{1-x}NbWO_8$ have been synthesized and their luminescent properties are explored. Similar to the molybdates discussed in the previous chapter, these phosphors also exhibit strong red emission under both near UV and blue excitations. These tungstate based phosphors are characterized by sharp red emission with good CIE color co ordinates, pointing the suitability of them as red phosphors for pc-WLED applications. This chapter elaborates structural, microstructural and photoluminescent properties of these novel red phosphors.

4.2 Experimental

Scheelite type red emitting phosphors with the general composition: $CaLa_{1-x}NbWO_8$: xEu^{3+} (x = 0.01, 0.03, 0.05, 0.10, 0.15, 0.20, 0.25) (CLNW) and $CaGd_{1-x}NbWO_8$: xEu^{3+} (x: 0.05, 0.10, 0.15, 0.20, 0.25, 0.30) (CGNW) were prepared by the solid state reaction route. $CaCO_3$, La_2O_3/Gd_2O_3, Nb_2O_5, WO_3, and Eu_2O_3 (Chemicals are from Acros Organics and Sigma Aldrich with 99.99% purity) were used as the starting materials. Stoichiometric amounts of these materials were weighed and then thoroughly wet mixed in an agate mortar with acetone as the wetting medium. The mixing was followed by drying in an air oven. The mixing and drying were repeated thrice to obtain a homogenous mixture and was calcined at 1200°C for 6h in a platinum crucible in an air atmosphere furnace.

The crystal structure as well as the phase purity of the calcined samples were examined by recording the powder XRD patterns using PANalytical X'pert Pro with Ni filtered CuK∝ radiation (λ = 1.54056Å). The structural refinement of all the XRD patterns for

$CaLa/Gd_{1-x}NbWO_8$: xEu^{3+} were further performed by the Rietveld analysis using the X'pert plus program. The Fourier transform infrared spectroscopy (FT-IR) data were recorded on a Thermo Nicolet Magna 560 spectrophotometer in the range of 1200 - 400 cm^{-1} using KBr pellets. The morphological analysis of the powder samples were done by scanning electron microscope (JEOL, JSM-5600LV). The UV–Vis absorption of the samples was recorded by UV-Vis spectrophotometer (Shimadzu UV-2401). Photoluminescence excitation and emission spectra were recorded using a Horiba Yvon Fluorolog® 3 Spectrofluorimeter with a 450W xenon flash lamp as the exciting source (keeping excitation and emission monochromator slit widths at 0.5 and 1 nm respectively). Luminescence lifetime of the phosphors was recorded by the phosphorimeter attached to Fluorolog® 3 Spectrofluorimeter. The CIE chromaticity coordinates of the phosphors were also calculated.

4.3 Results and Discussion

4.3.1 Powder X ray diffraction analysis

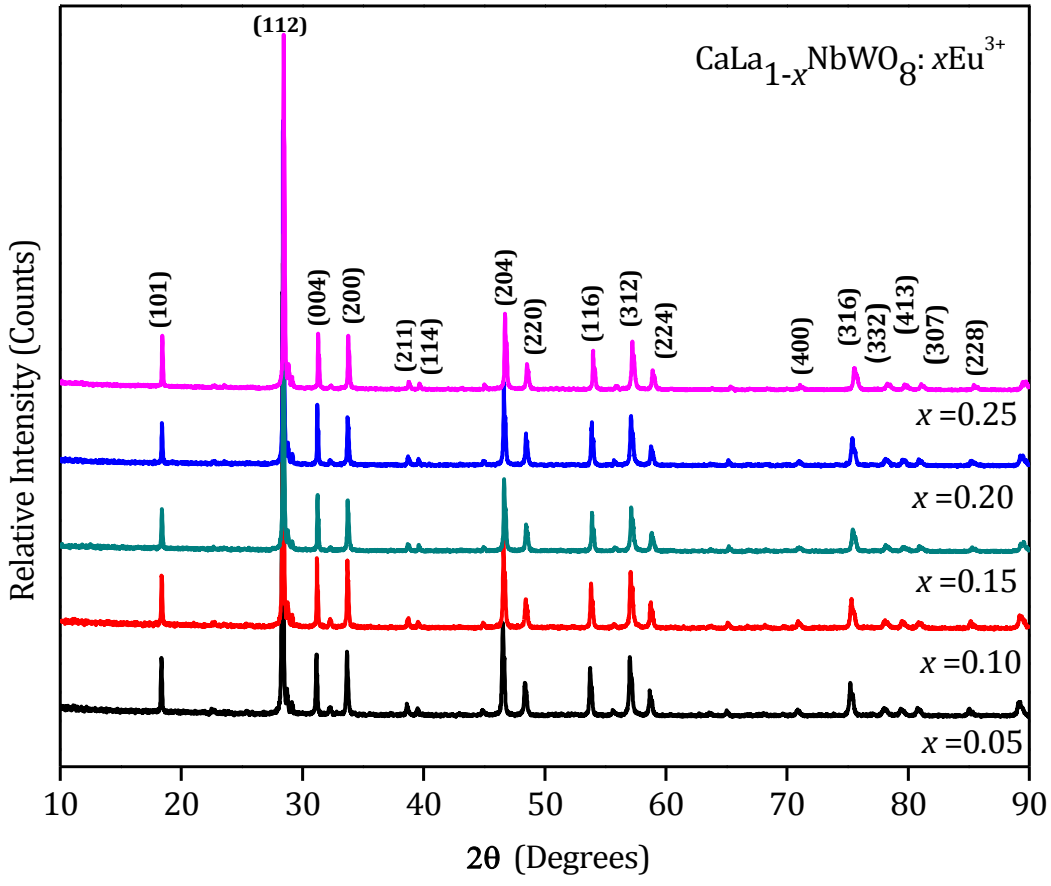

Fig.4.1 Powder X ray diffraction patterns of $CaLa_{1-x}NbWO_8$: xEu^{3+} (x = 0.05, 0.10, 0.15, 0.20, 0.25).

The X ray diffraction (XRD) patterns of selected compositions of CLNW and CGNW phosphors are shown in Fig. 4.1 and Fig. 4.2. The crystalline nature of all samples is revealed by

sharp peaks in XRD patterns. The phase purity of the prepared samples is confirmed by comparing the observed powder XRD pattern with the reported $CaWO_4$ (JCPDS file no. 41-1431) tetragonal scheelite structure with the space group $I4_1/a$ (88) and Z = 4 (Achary S. N *et al* 2006).

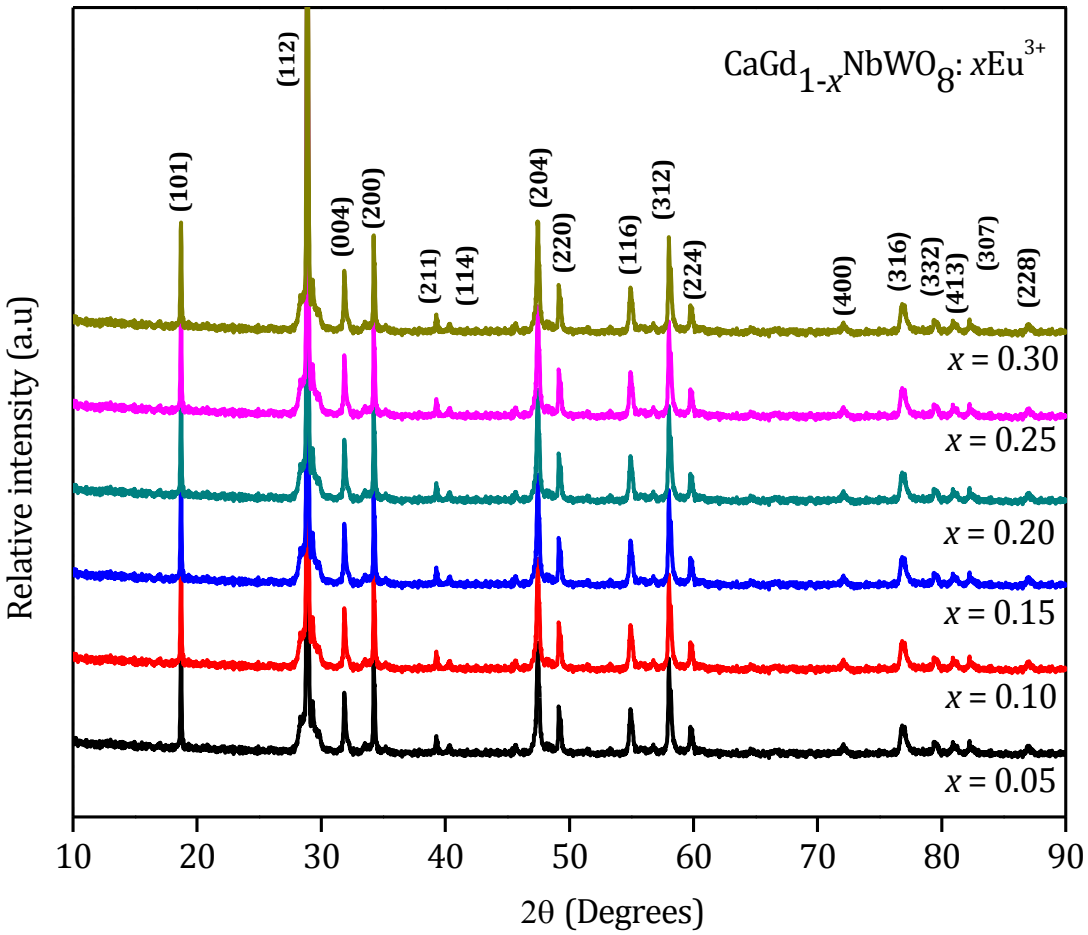

Fig.4.2 Powder X ray diffraction patterns of $CaGd_{1-x}NbWO_8$: xEu^{3+} (x = 0.05, 0.10, 0.15, 0.20, 0.25, 0.30).

The prominent peaks in the XRD patterns correspond to (101), (112), (004), (200), (204), (220), (116), (312) and (316) lattice planes. No traces of additional peaks from other phases are observed in the XRD patterns of both phosphors. Thus, all the samples are single phase forming solid solutions of CLNW and CGNW. Here Ca^{2+}, La^{3+}/Gd^{3+} and Eu^{3+} occupy eight coordinated A site, Nb^{5+} and W^{6+} share four coordinated B site in CLNW and CGNW lattices respectively. Since the ionic radii of Eu^{3+} (r = 1.07Å when coordination number (CN) = 8) is close to that of La^{3+} (r = 1.16Å when CN = 8) and Gd^{3+} (r =1.05 Å when CN = 8), Eu^{3+} ion prefers to occupy in La^{3+}/Gd^{3+} site in CLNW and CGNW respectively. A cubic close packing of Ca^{2+} and NbO_4/WO_4 tetrahedral units in an ordered manner can explain the scheelite structure of both CLNW and CGNW phosphors. On a closer view of the XRD patterns, it is

observed that the peak corresponding to (101) plane in tungstates are more intense than that of molybdates (CL/GNM) discussed in the previous chapter.

The structural refinement of all the XRD patterns for CLNW and CGNW phosphors were performed by the Rietveld analysis using the X'pert plus program. The starting model for the refinement of the phases was taken from the reported crystal structure of $CaWO_4$. For CLNW and CGNW phosphors, Ca and La/Gd/Eu are at (4b: 0, 1/4, 5/8) sites, Nb and W at (4a: 0, 1/4, 1/8) sites and O at (16f: x, y, z), Z = 4 in the space group $I4_1/a$, no.88 (Zhang Z. J *et al* 2007; Achary S. N *et al* 2006). The profile was fitted using Pseudo Voigt profile function.

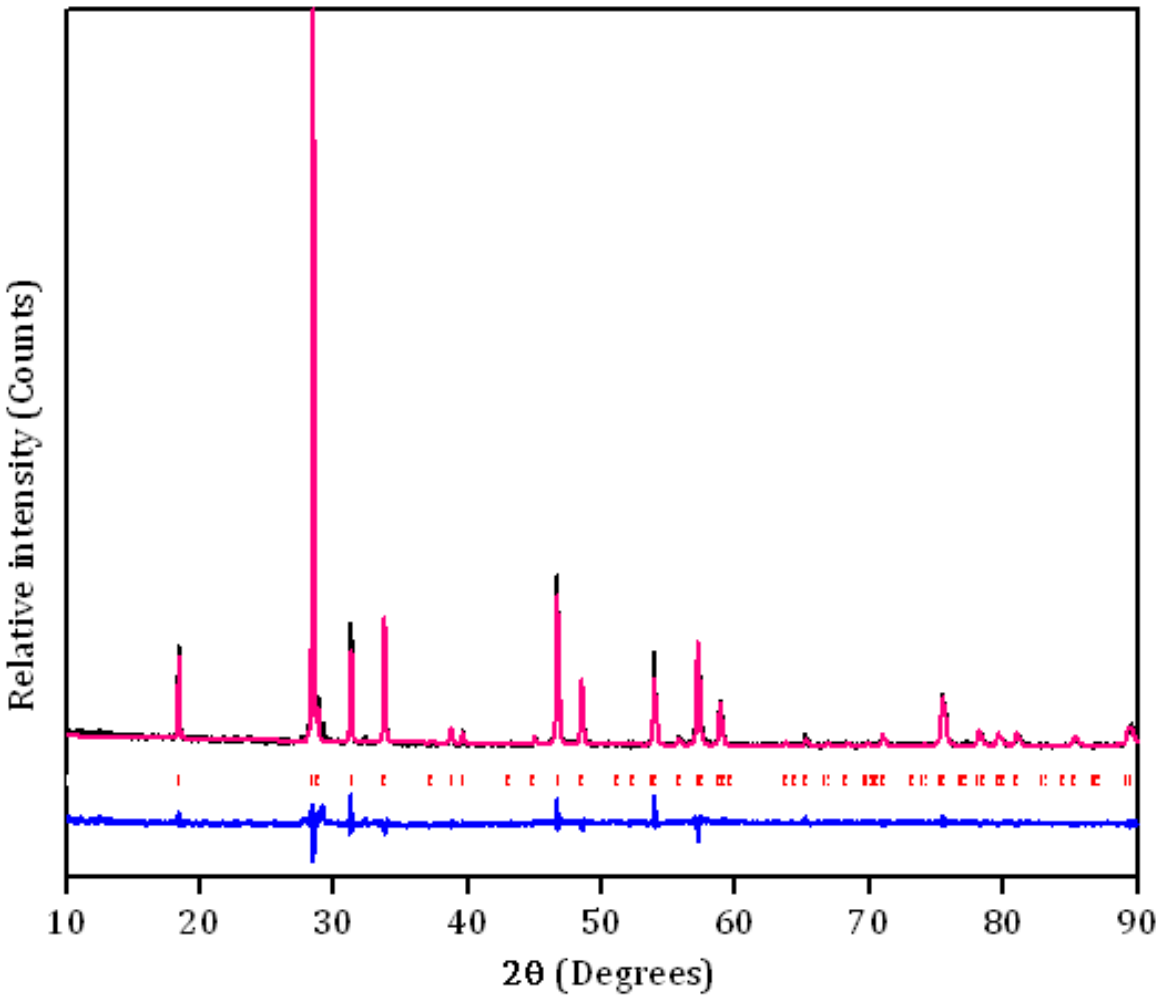

Fig. 4.3 Observed (black), calculated (pink) and difference (blue) X ray diffraction profiles obtained from the Rietveld refinement of XRD data for $CaLa_{0.80}NbWO_8$: $0.20Eu^{3+}$.

Fig. 4.3 and Fig. 4.4 show the typical best fit that was observed, calculated, the difference powder diffraction profiles and the expected Bragg reflections for $CaLa_{0.80}NbWO_8$: $0.20Eu^{3+}$ and $CaGd_{0.80}NbWO_8$: $0.20Eu^{3+}$. The expected Bragg peak positions are marked below the profile fit as vertical bars. The R factors, the refined oxygen coordinates, lattice parameters and other parameters obtained from the Rietveld refinement of the powder diffraction data for some of the compositions of CLNW and CGNW phosphors are given in Table 4.1.

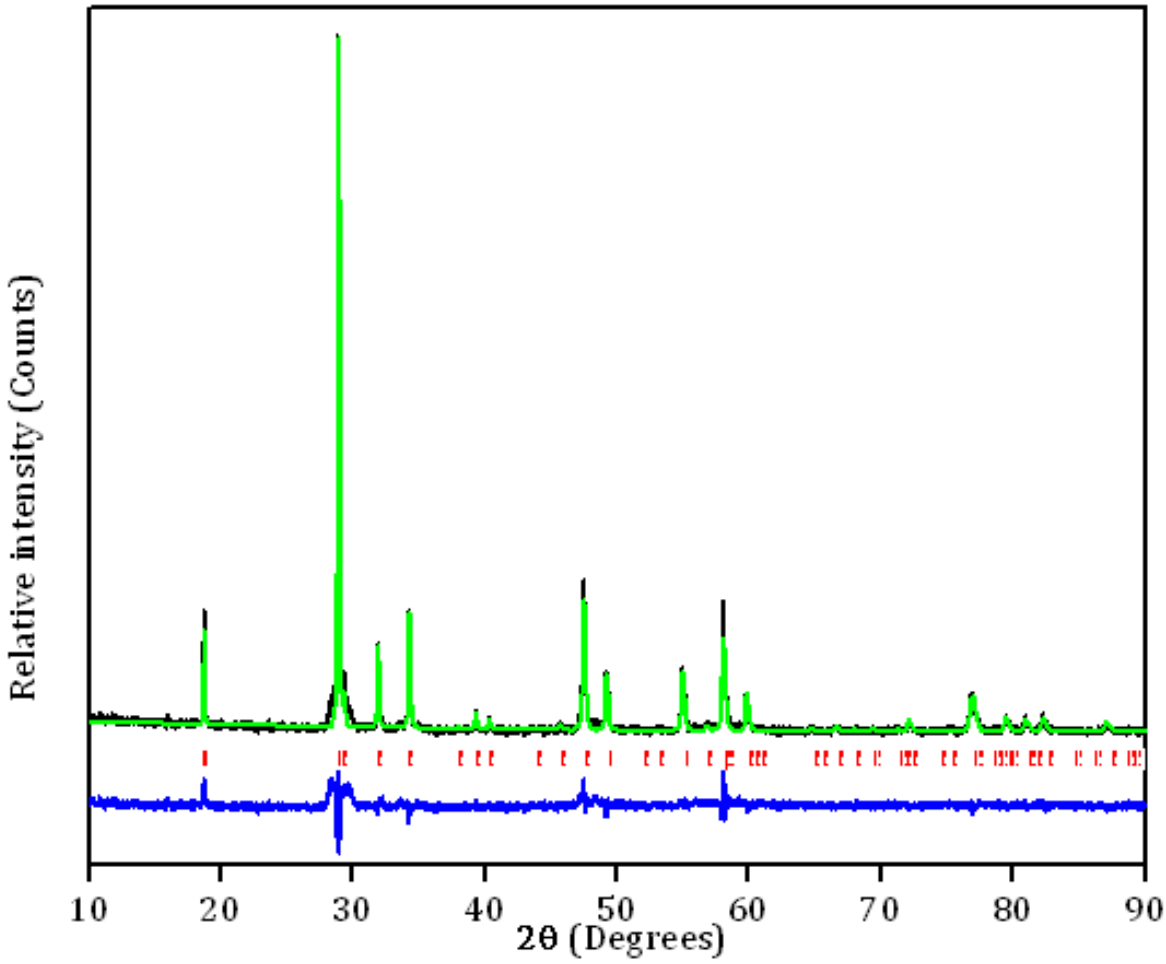

Fig. 4.4 Observed (black), calculated (green) and difference (blue) X ray diffraction profiles obtained from the Rietveld refinement of XRD data for $CaGd_{0.80}NbWO_8$: $0.20Eu^{3+}$.

The refined unit cell parameters and oxygen position co-ordinates of CLNW and CGNW are well matching with scheelite type $CaWO_4$ structure. The variation of lattice parameter and unit cell volume in these phosphors with respect to Eu^{3+} doping further confirms the effective substitution of activator ions in the respective host lattices. In the case

of CLNW phosphors, both lattice parameters and unit cell volume is decreasing with the increase of Eu^{3+} concentration and is due to the lower ionic radius of Eu^{3+} (r = 1.07Å) compared to that of La^{3+} ion (r = 1.16Å). In CGNW phosphors, lattice parameters and unit cell volume is increasing with respect to the increment in the Eu^{3+} doping concentration, the extent of variation of the lattice parameters is less prominent in CGNW compared to that of CLNW phosphors and can be because of the comparable ionic radii of Eu^{3+} and Gd^{3+} ions. Thus similar to the molybdates discussed in the previous chapter, the CGNW lattice is stiffer than that of CLNW lattice. The influence of stiffness of the lattice on luminescence properties will be discussed in later section.

Table 4.1 Variation of lattice parameters, Oxygen coordinates, R factors, and other parameters obtained from Rietveld analysis of $Ca(La/Gd)_{1-x}NbWO_8$: xEu^{3+}

	$CaLa_{1-x}NbWO_8$: xEu^{3+}			**$CaGd_{1-x}NbWO_8$: xEu^{3+}**		
x	0.10	0.15	0.20	0.10	0.15	0.20
Lattice parameters (Å)						
a	5.3095	5.3082	5.3047	5.2377	5.2383	5.2390
c	11.4491	11.4413	11.4301	11.2339	11.2352	11.2322
Unit cell Volume ($Å^3$)	322.76	322.38	321.64	308.19	308.29	308.30
Oxygen position co ordinates						
x	0.152	0.166	0.160	0.1541	0.1546	0.1553
y	0.006	0.001	0.014	0.0104	0.0112	0.0071
z	0.2073	0.2099	0.2096	0.2111	0.2101	0.2109
Residues (%)						
R_{exp}	12.39	12.23	11.93	9.25	9.21	9.52
R_p	11.89	11.12	10.42	10.91	10.74	10.11
R_{wp}	15.18	14.17	13.53	14.88	14.91	13.60
Number of Variables	14	14	14	14	14	14

From the XRD pattern and structural refinement patterns it is clear that both powellite type molybdates and scheelite type tungstates have almost similar crystal structure. It can be mentioned here that the lattice parameter ratio, *c*/*a* is more in molybdates than that of

corresponding tungstates (*c*/*a* for CLNM (*x* = 0.1) and CLNW (*x* = 0.1) are 2.1635 and 2.1563; for CGNM (*x* = 0.1) and CGNW (*x* = 0.1) are 2.1511 and 2.1448 respectively). It is reported that the c/a for $CaMoO_4$ and $CaWO_4$ at ambient temperature is 2.188 and 2.169 respectively (Achary S. N *et al* 2006). The higher *c*/*a* ratio in molybdates can be explained by the higher cation - cation electrostatic repulsion in $CaMoO_4$ than that in $CaWO_4$ (Sleight A. W 1972).

4.3.2 FT-IR spectra

The FT-IR spectra of the CLNW (*x* = 0, 0.1, 0.2) samples are presented in Fig. 4.5. The spectrum of $CaWO_4$ is included in the figure as a reference sample for comparison. For the $CaWO_4$ sample the main absorption peaks are observed at 810, 750 and 438 cm^{-1} (Lei F *et al* 2008). The peaks at 810 and 750 cm^{-1} are assigned to the stretching vibrational modes of O-W-O bond in WO_4 tetrahedron and that at 438 cm^{-1} is due to the stretching vibration of W-O bond. Thus the IR absorption bands of $CaWO_4$ are solely due to the vibrational modes of the WO_4^{2-} group (400-1000 cm^{-1}) (Lei F *et al* 2008).

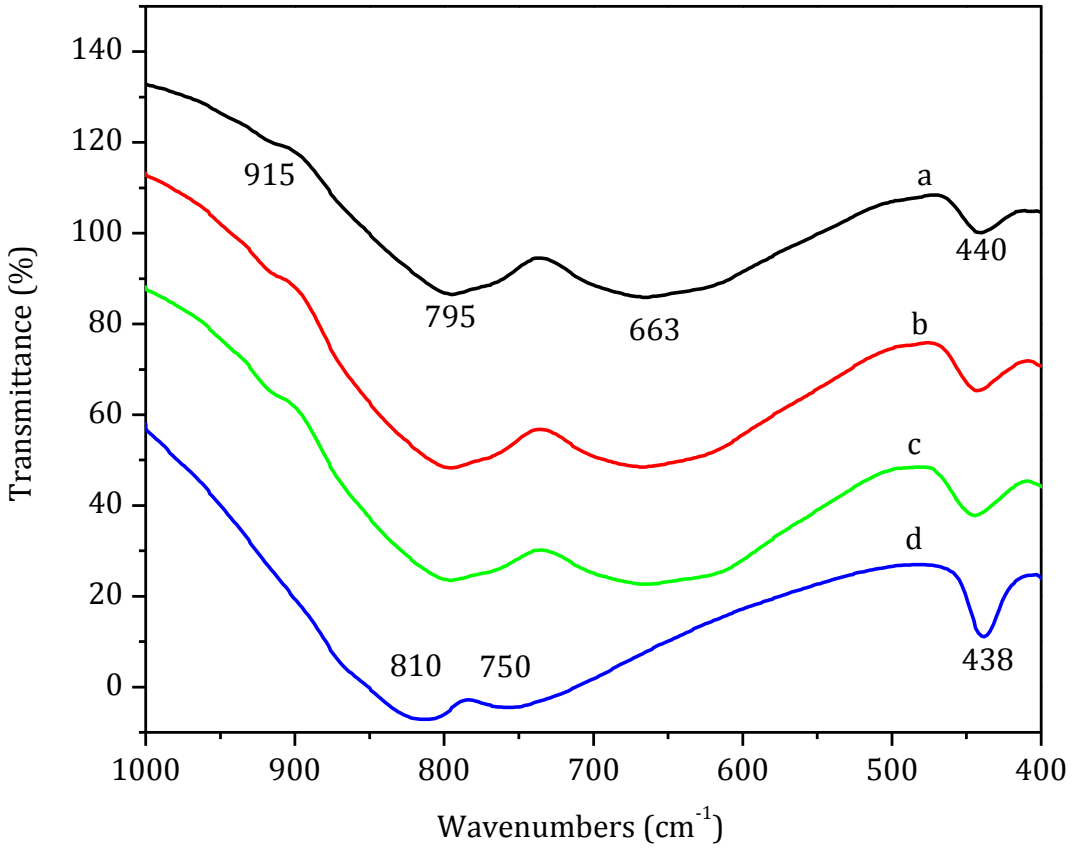

Fig. 4.5 FT-IR spectra of $CaLa_{1-x}NbWO_8$: xEu^{3+} (a) *x* = 0, (b) *x* = 0.1, (c) *x* = 0.2, (d) $CaWO_4$.

The absorption bands of CLNW samples are centered at 915, 795, 663, 440 cm^{-1}. It is already reported that the absorption band around 910 cm^{-1} is related to the O-W-O stretching

vibration of WO_4 tetrahedron (Lei F *et al* 2008) and the absorption peaks corresponding to 650 and 420 cm^{-1} are due to the combinations of the stretching and bending vibrations of Nb-O bond in the NbO_4 group without any distortions (Lei F *et al* 2008). At the same time all these peaks are within the range of 400 -1000 cm^{-1}, which corresponds to the vibrational modes of WO_4 group. The absorption peaks at 429, 805 and 870 cm^{-1} are IR active vibrational modes of WO_4 group (Pode R. B *et al* 1997).

Thus the IR absorption bands of CLNW samples are due to the merged effect of vibrational modes of NbO_4 and WO_4 tetrahedra. Here for CLNW complex oxide, the absorption bands are shifted to a longer wavelength region comparing to that of $CaWO_4$. It is also observed that the absorption bands of the CLNW (0, 0.1, and 0.2) are broader than that of $CaWO_4$ due to the combined vibrational modes of NbO_4 and WO_4 tetrahedra. This further substantiates the change in the local crystallographic environment in the CLNW complex oxide compared to the $CaWO_4$ simple oxide. As expected, similar spectral profile is observed for CGNW samples also. The $CaWO_4$: Eu^{3+} phosphor has approximate vibration modes as the $CaMoO_4$: Eu^{3+} phosphor (Lei F *et al* 2008). Thus molybdate (CL/GNM) and tungstate (CL/GNW) phosphors are characterized by same vibration modes and hence the same FT-IR spectra.

4.3.3 Microstructural characterization

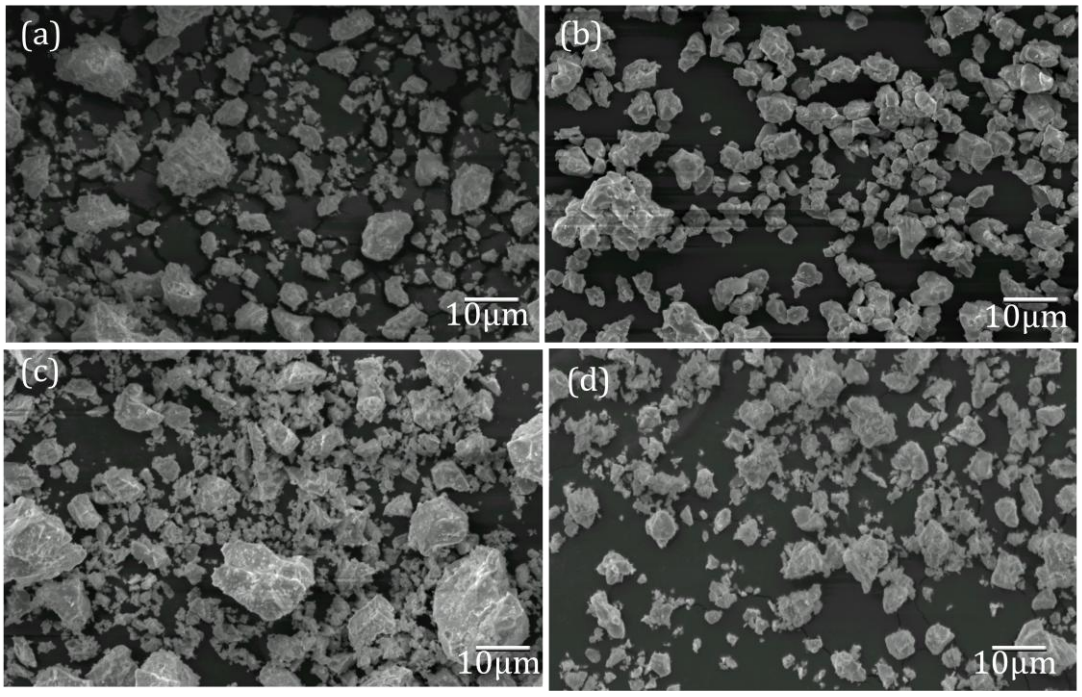

Fig. 4.6 Scanning electron micrographs of $CaLa_{1-x}NbWO_8$: xEu^{3+} with varying Eu^{3+} concentrations: (a) x = 0.10, (b) x = 0.15, (c) x = 0.20, (d) x = 0.25.

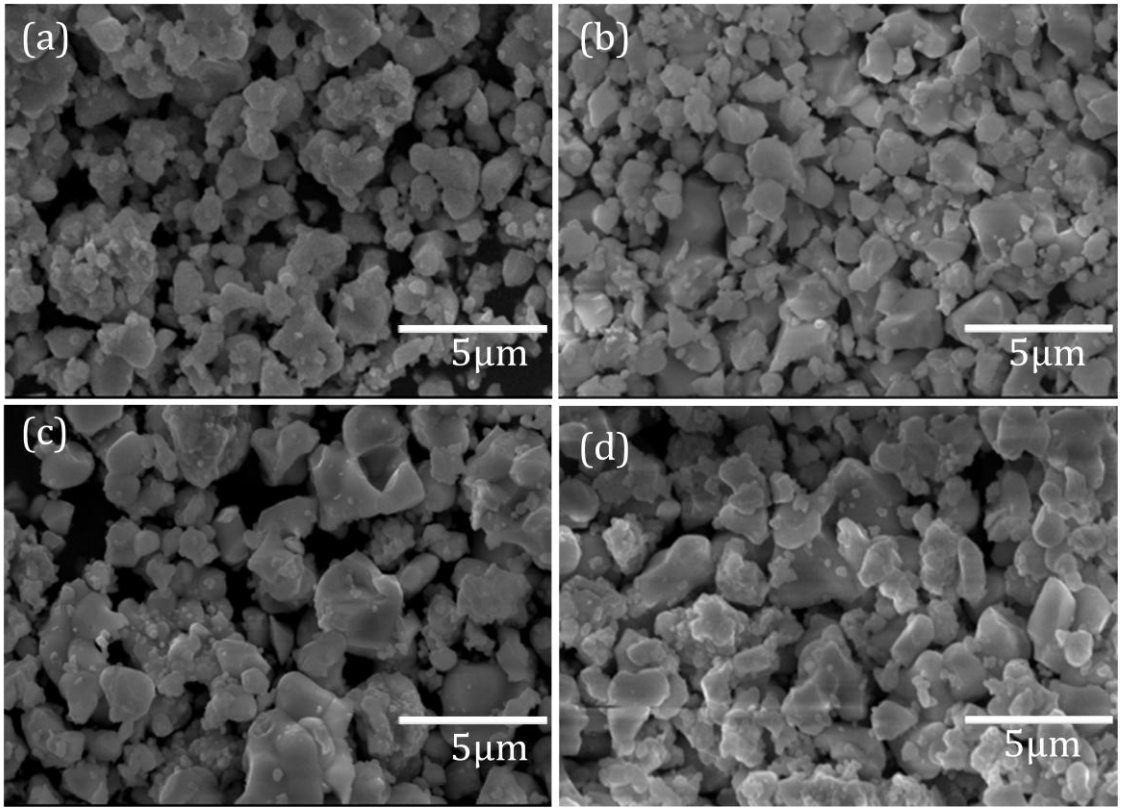

Fig. 4.7 Scanning electron micrographs of $CaGd_{1-x}NbWO_8$: xEu^{3+} with varying Eu^{3+} concentrations: (a) x = 0.10, (b) x = 0.15, (c) x = 0.20, and (d) x = 0.25.

Fig. 4.6 and Fig. 4.7 show the scanning electron micrographs of selected compositions of tungstate based CLNW (magnification: 1,000) and CGNW (magnification: 5,000) phosphors. Powder particles of both phosphors are homogenous, crystalline and agglomerated; the agglomeration is more in CLNW than CGNW phosphors. With respect to Eu^{3+} doping concentration, the extent of agglomeration in both CLNW and CGNW is reducing and can be clearly seen in CGNW phosphors. The average particle size of these phosphors is in the range of 1-5 µm, well suits with the particle size for SSL applications.

4.3.4 UV Visible absorption

UV Visible absorption spectra of CLNW (x = 0, 0.10, 0.25) and CGNW (x = 0.05, 0.15, 0.25) phosphors are presented in Fig. 4.8 and Fig. 4.9 respectively. All spectral profiles are similar with variations in relative absorbance. The spectra include broad and strong absorption in the UV region (200 – 375 nm). For $CaWO_4$:Eu^{3+}, the absorption band is located between 210 and 300 nm and is corresponding to oxygen to tungsten (O-W) ligand to metal charge transfer (LMCT) in the WO_4^{2-} group (Ahmad G *et al* 2006). For CLNW and CGNW phosphors this broad region of absorption corresponds to CT transition from oxygen

ligands to Eu^{3+} ions and to the central W/Nb atoms in WO_4/NbO_4 groups in the host lattice respectively [ligand to metal charge transfer (LMCT)] (Liu X *et al* 2007; Su Y *et al* 2008).

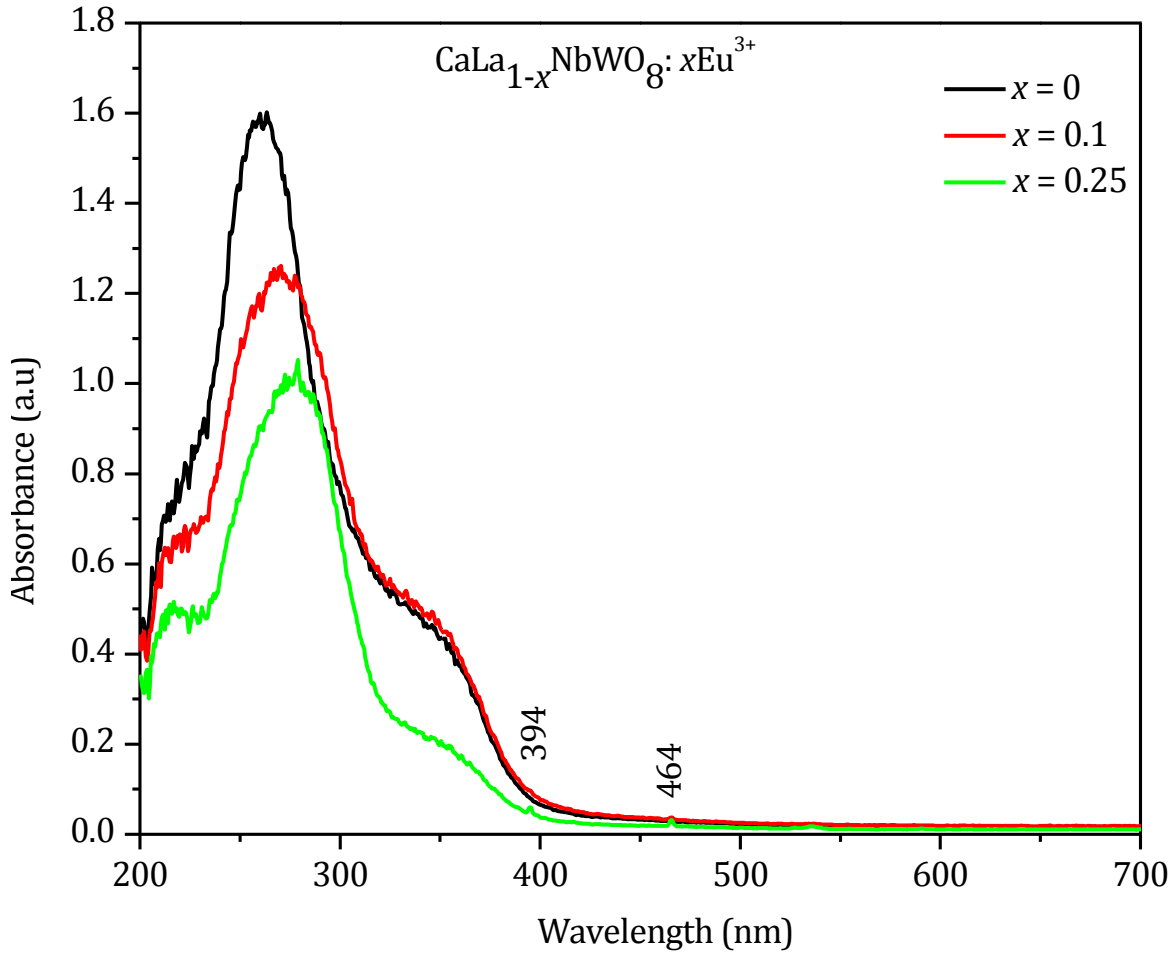

Fig. 4.8 UV-Vis absorption spectra of $CaLa_{1-x}NbWO_8$: xEu^{3+} (x = 0, 0.1, 0.25) phosphor.

In addition to the above mentioned CT band, both Eu^{3+} doped phosphors show absorption peaks arising from the intra configurational 4*f* transitions of Eu^{3+} at 394 nm (near UV) and 464 nm (blue). The degree of absorption of the Eu^{3+} levels is increasing with Eu^{3+} concentration of the samples. Thus it is expected that the phosphors can be effectively excited under both UV and visible region, which is further confirmed from the excitation spectra. Here also efficient energy transfer from host lattice to the activator ions occurs as that of the molybdates. The absorption spectra of molybdates (CL/GNM) discussed in previous chapter is broader than that of corresponding tungstates (CL/GNW). Similar result is reported for Eu^{3+} doped $CaMoO_4$ and $CaWO_4$ samples, where the absorption peak in UV region of $CaMoO_4$: Eu^{3+} is broader than $CaWO_4$: Eu^{3+} (Lei F *et al* 2008).

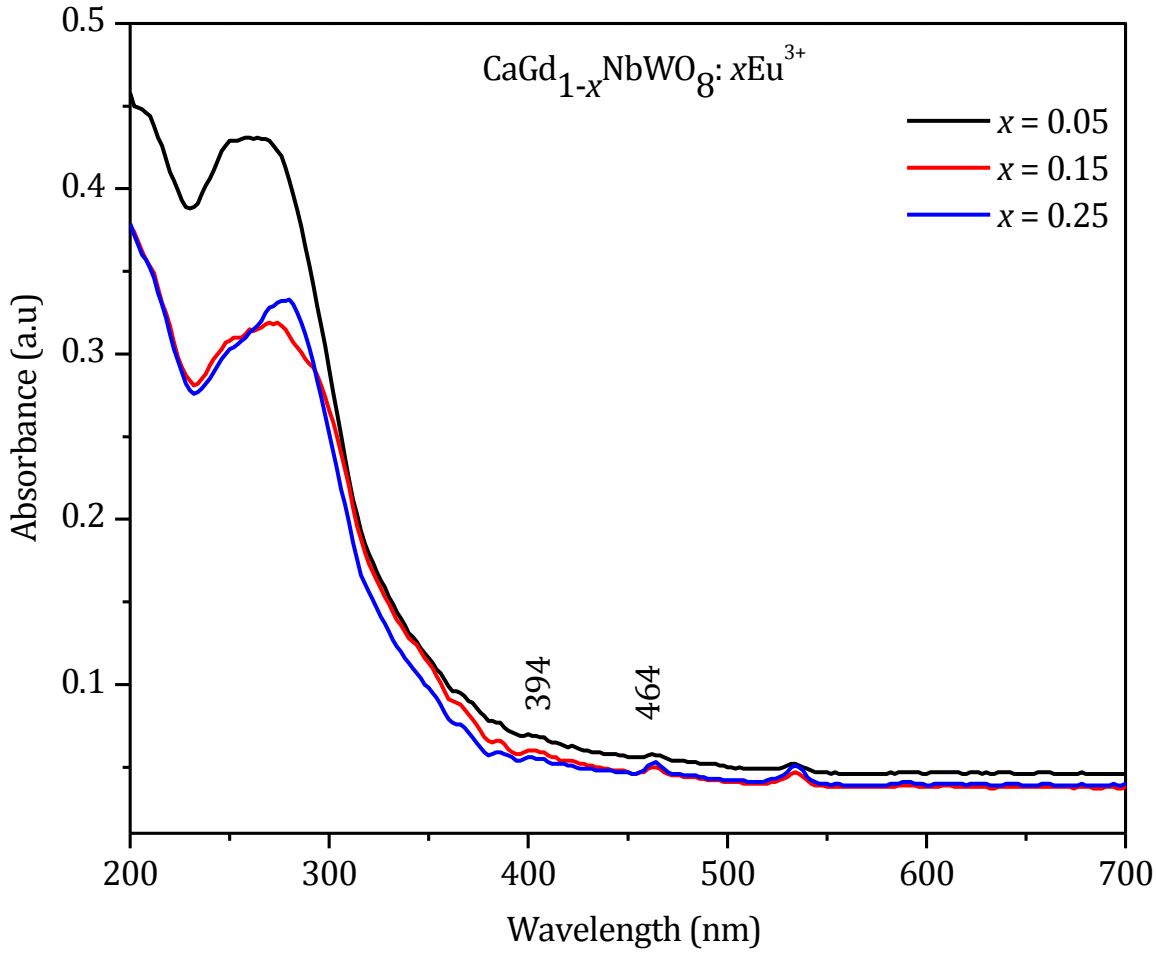

Fig. 4.9 UV-Vis absorption spectra of $CaGd_{1-x}NbWO_8$: xEu^{3+} (x = 0.05, 0.15, 0.25) phosphor.

4.3.5 Photoluminescence properties

4.3.5.1 Excitation spectra

Fig. 4.10 and Fig. 4.11 present the excitation spectra of CLNW and CGNW phosphors for an emission at 613 nm. All the spectra include both broad region (240 – 350 nm) and sharp peaks (beyond 350 nm) of excitation. The broad region of excitation is peaking around 290 nm for CLNW and 303 nm for CGNW phosphors. It is reported that in pure $CaWO_4$, the CT band in the $(WO_4)^{2-}$ group is at 250 nm (Pode R. B *et al* 1997) and $LaNbO_4$ shows strong absorbance at 260 nm corresponding to the CT band in the NbO_4 group (Hsiao Y. J *et al* 2007). Thus the broad band region observed in these tungstate based phosphors can be ascribed to the combinations of the CT transitions of O–W/O–Nb in the WO_4/NbO_4 group and that of Eu^{3+} - O^{2-}.

The sharp peaks beyond 350 nm are due to the intra-configurational (*f–f*) transitions of Eu^{3+} in the host lattice. They are observed at 362, 383, 394/395, 416, 465 nm that are corresponding to the $^7F_0$ - $^5D_4$, $^7F_0$ - $^5G_{2-4}$, $^7F_0$ - $^5L_6$, $^7F_0$ - $^5D_3$, $^7F_0$ - $^5D_2$ transitions respectively

(Blasse G 1979). Of these many peaks beyond 350 nm, the peaks that correspond to the $^7F_0$ - $^5L_6$ and $^7F_0$ - $^5D_2$ transitions are more intense and lying in the near UV and blue wavelength regions (394/395 and 465 nm) respectively. It can be expected that these tungstate based scheelite type phosphors (CL/GNW) can be effectively excited by the radiations in the near UV and blue wavelength regions, which is one of the important pre requisites for a phosphor material for use in generating white light in phosphor converted WLEDs. Also the intensity of intra configurational peaks is more than that of the CT band, which linearly increases with the Eu^{3+} doping concentration. This also evidences the effective incorporation of Eu^{3+} in the CLNW and CGNW host lattices as well as efficient energy transfer from the CT states to the Eu^{3+} levels as that of molybdates discussed in the previous chapter.

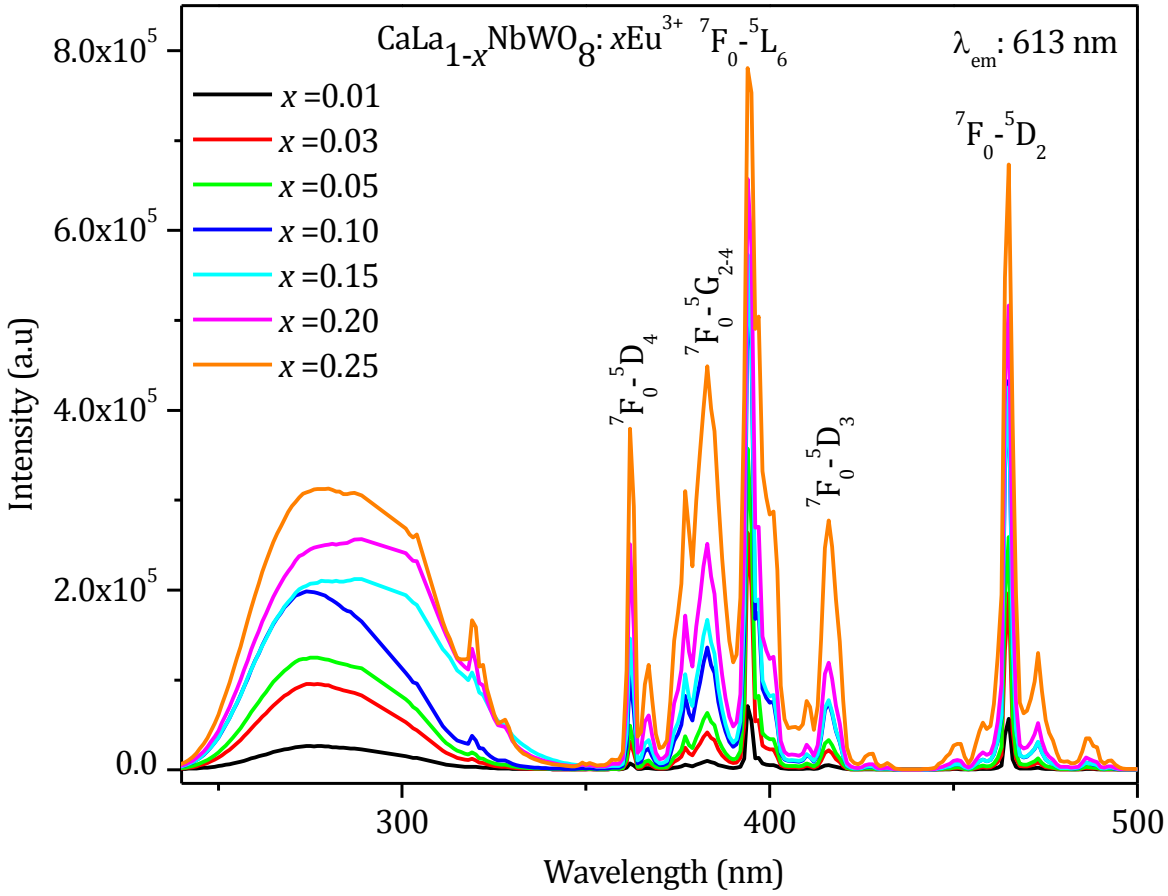

Fig. 4.10 Excitation spectra of $CaLa_{1-x}NbWO_8$: xEu^{3+} for an emission at 613nm.

When comparing the excitation spectra of CLNW and CGNW phosphors, it is observed that the CT band of CGNW phosphors is sharper than that of CLNW phosphors. Analogous observation is found in the molybdates also. The sharpness of the excitation band can be due to the stiffness of the Gd^{3+} substituted lattices (both molybdates and tungstates; CGNM/W).

The broader the absorption band, the larger the value of ΔR (difference in the chemical bond length at excited and ground state) (Blasse G 1979). Thus for Gd^{3+} substituted phosphors, the nature of chemical bonding in the excited and ground state are almost the same.

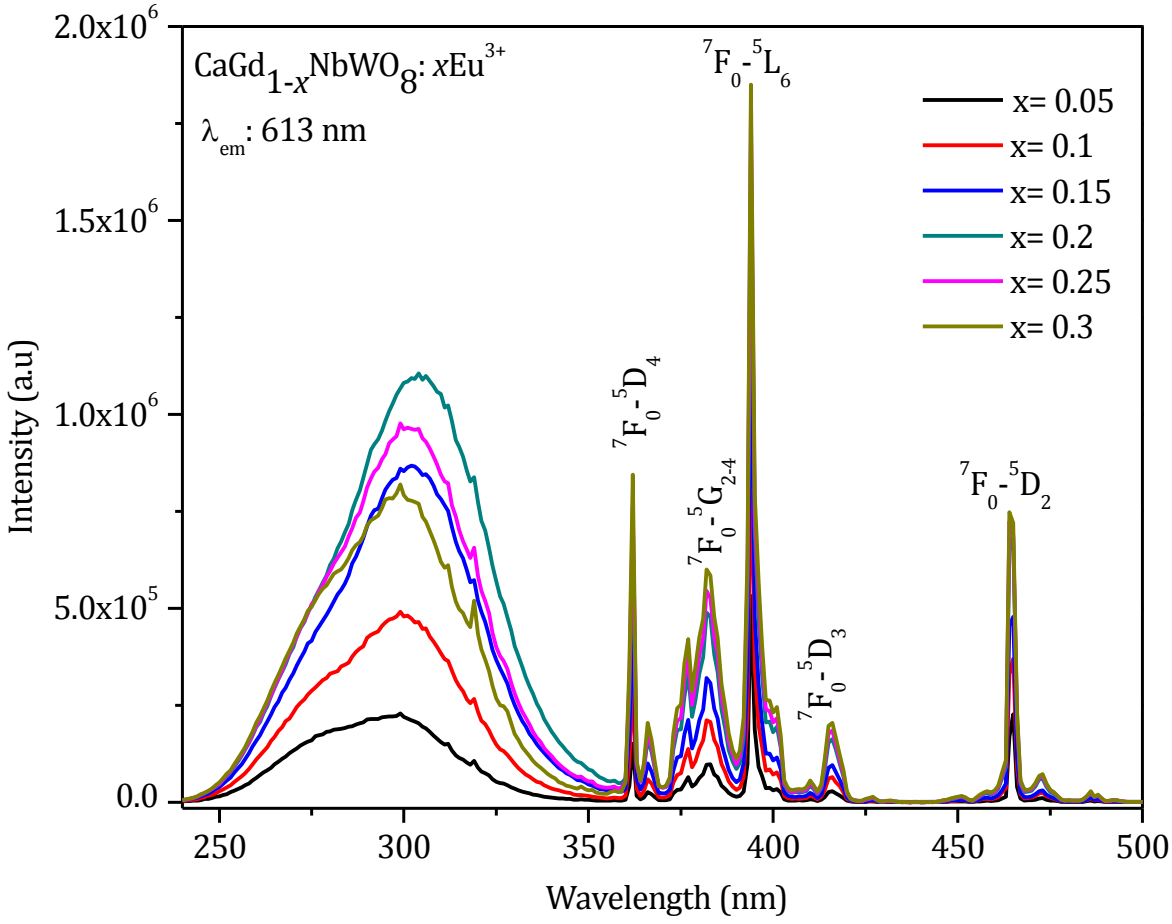

Fig. 4.11 Excitation spectra of $CaGd_{1-x}NbWO_8$: xEu^{3+} for an emission at 613nm.

In the present study, CT band shifts towards shorter wavelength when the molybdate moiety is replaced by the tungstates and is in line with earlier reported observations (Neeraj S *et al* 2004; Sivakumar V *et al* 2005). By introducing tungsten in the host lattice, the CT band is shifted from 313 nm (for CL/GNM) to 290/303 nm (for CL/GNW). This indicates that energy absorption due to Mo–O charge transfer occurs at a longer wavelength than that due to W–O charge transfer. Further, when we compare intensities of CT band of molybdate and tungstate phosphors, the CT band of molybdates have enhanced intensity than the corresponding tungstate based samples. Similar observation is reported in $Li_{4-3x}Eu_x(WO_4)_{2-y}(MoO_4)_y$ and $Na_{4-3x}Eu_x(WO_4)_{2-y}(MoO_4)_y$ phosphors (Lee G.H *et al* 2011). The enhanced CT band in the phosphors containing MoO_4 can be explained by the fact that Mo has a higher sixth ionization potential (70 eV) than W (61 eV). That is, Mo has a greater

tendency to receive an electron from an oxygen ligand and MoO_4 requires a lower energy for ligand - metal charge transfer (LMCT). This reveals that, both the tetrahedral moieties and the other cations present in the host lattices play an important role in determining the position and/or intensity of the CT band. Thus the effective energy transfer from host lattice to activator ions is expected to be more in molybdates than tungstates (Lee G.H *et al* 2011). The excitation process related to these phosphors is schematically illustrated later.

Both the position and intensity of CT band of a phosphor material is a crucial factor that affects its emission properties. On the one hand, the quantum efficiency of Eu^{3+} decreases if the position is at lower energy on the other hand, an intense forced electric dipole $^5D_0$-$^7F_2$ red emission needs its CT band at lower energies because the parity forbidden transitions of Eu^{3+} ion borrow intensity from the lowest strong absorption band (CT) (Su Q *et al* 1995, Blasse G 1979). So it is necessary to understand position of CT band and its influence on luminescence. The details of emission property of these phosphors are discussed in the following section.

4.3.5.2 Emission spectra

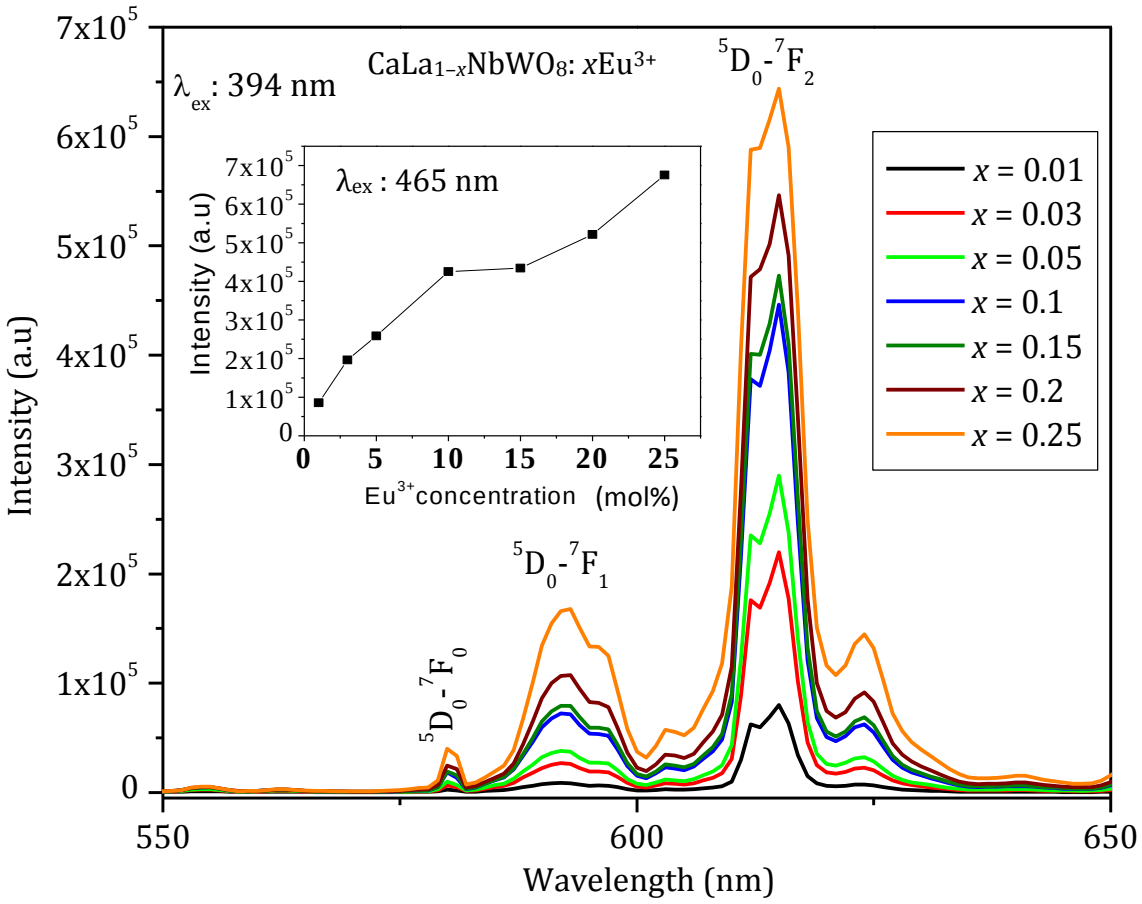

Fig. 4.12 The emission spectra of $CaLa_{1-x}NbWO_8$: xEu^{3+} under 394 nm excitation (Inset: The relative intensity variation of 613 nm peak under 465 nm excitation).

Fig. 4.12 and Fig. 4.13 show the emission spectra of CLNW (x = 0.01, 0.03, 0.05, 0.10, 0.15, 0.20, 0.25) and CGNW (x = 0.05, 0.10, 0.15, 0.20, 0.25, 0.30) phosphors under near UV excitation (394/395 nm). The variation of red emission under blue excitations (465 nm) for both phosphors is shown in the inset. Both phosphors have similar emission profile with some variations in relative emission intensity. The emission spectra include major peaks at 580, 592, 612, 613, 623 nm. All these are characteristic emission peaks of the Eu^{3+} due to $^5D_0$ - ^7F_J (J = 0-2) transitions (Liu X *et al* 2007). Here, emission corresponding to tungstate host lattice is not observed. However, the presence of an absorption band due to a WO_4/NbO_4 group in the excitation spectra clearly reveals that the energy absorbed by the WO_4/NbO_4 group is transferred to Eu^{3+} levels non radiatively. This process is known as ‘‘host sensitized’’ energy transfer (Lou X. M *et al* 2008). The emission lines for both the excitations are similar, but the emission intensity for 394/395 nm excitation is more than that of the 465 nm excitation.

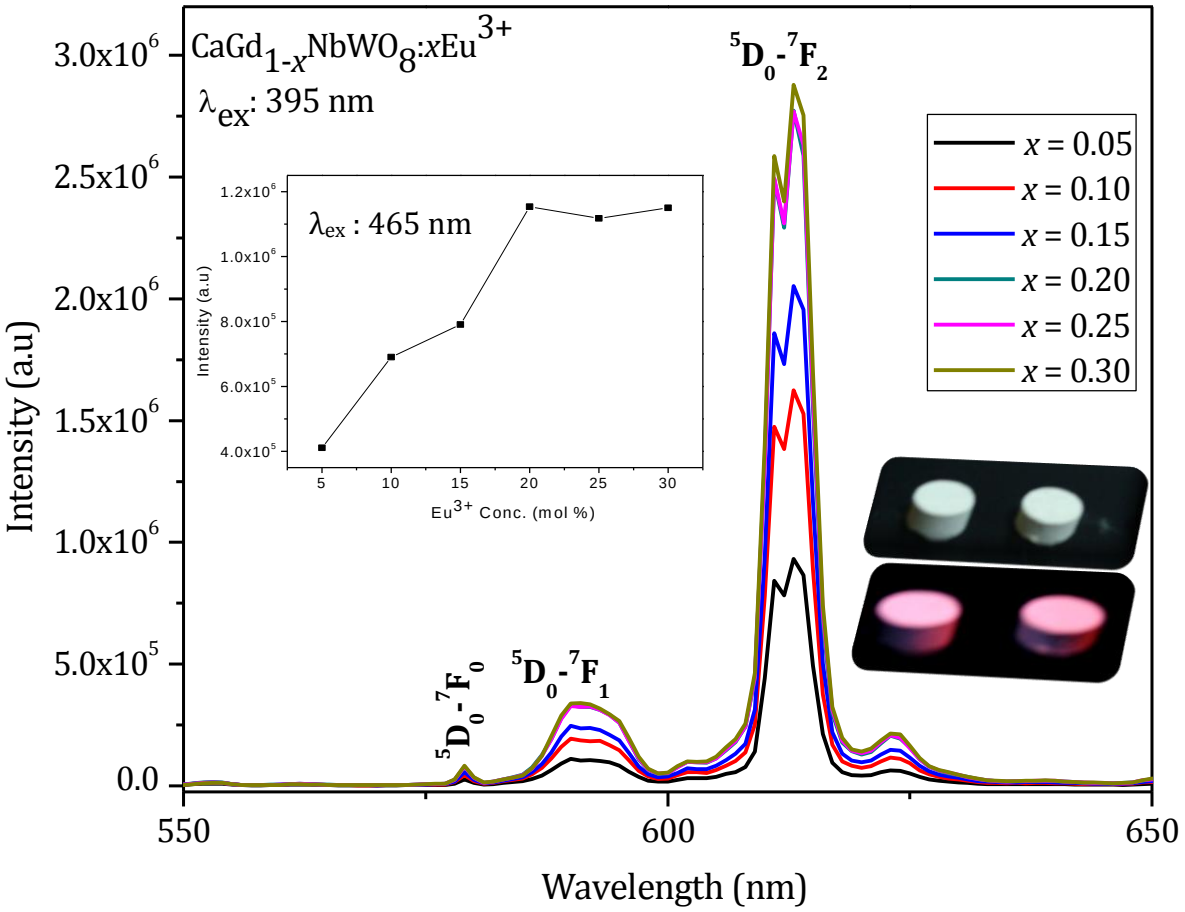

Fig. 4.13 The emission spectra of $CaGd_{1-x}NbWO_8$: xEu^{3+} under 395 nm excitation (Inset: The relative intensity variation of 613 nm peak under 465 nm excitation and phosphors before and after UV irradiations).

Of these emission peaks those peaks at the 613 nm is more intense and is arising because of the electric dipole transitions ($^5D_0$–$^7F_2$). Since the parity does not allow these transitions, they are generally forbidden. The emission peak at 592 nm is due to the parity allowed magnetic dipole transitions ($^5D_0$–$^7F_1$). For the present phosphors these peaks are weak. The symmetry of the Eu^{3+} site can be clearly determined by calculating the intensity ratio I($^5D_0$–$^7F_2$)/I($^5D_0$–$^7F_1$) (asymmetry ratio) (Xie A *et al* 2009) and is included in Table 4.2, which evidences the non centrosymmetric site occupancy of Eu^{3+} in CLNW and CGNW host lattices. It is observed that under 394/395 and 465 nm excitation the emission intensity of the current phosphors is increasing with Eu^{3+} doping concentration and no concentration quenching is observed for both excitations upto 25 mol% for CLNW and 30 mol% for CGNW phosphors.

Table 4.2 Asymmetry ratio and full width at half maximum (FWHM, λ_{em}: 613 nm) of $CaLa_{1-x}NbWO_8$: xEu^{3+} and $CaGd_{1-x}NbWO_8$ red phosphors with respect to Eu^{3+} doping concentration under near UV excitation

CLNW *x*	FWHM (nm)	Asymmetry Ratio	CGNW *x*	FWHM (nm)	Asymmetry Ratio
0.01	5.66	8.11	**0.05**	4.98	8.44
0.03	5.87	6.61	**0.10**	5.01	8.42
0.05	5.99	5.22	**0.15**	5.01	8.34
0.10	6.38	3.89	**0.20**	5.08	8.37
0.15	5.96	3.39	**0.25**	5.09	8.47
0.20	6.76	2.89	**0.30**	5.14	8.52
0.25	7.36	3.08			

The CGNW samples are characterized by sharper red emission (smaller FWHM) and higher asymmetry ratio compared to the CLNW phosphors. The FWHM of red peak (613 nm) of CGNW phosphor remains almost same with respect to the Eu^{3+} doping concentration, while for CLNW significant variation in FWHM with respect to Eu^{3+} concentration is observed. The sharp red emission in CGNW lattice can be due to the stiffness of the CGNW compared to CLNW lattice. This observation is in line with the molybdate analogues. It is also observed that the asymmetry ratio of CGNW phosphors is much better than that of

CLNW. Thus we can consider that the local crystal environment of Eu^{3+} ions in CGNW is more distorted than that of CLNW lattice. The distortion of CGNW lattice is due to the doping of Eu^{3+} at a lower ionic radius site (Gd^{3+}, r = 1.05 Å). Thus better color purity can be achieved for CGNW phosphors.

The luminescence process (excitation, emission and energy transfer) associated with both molybdate and tungstate (powellite/ scheelite) based red phosphors discussed in the present and previous chapters can be schematic as shown in Fig 4.14.

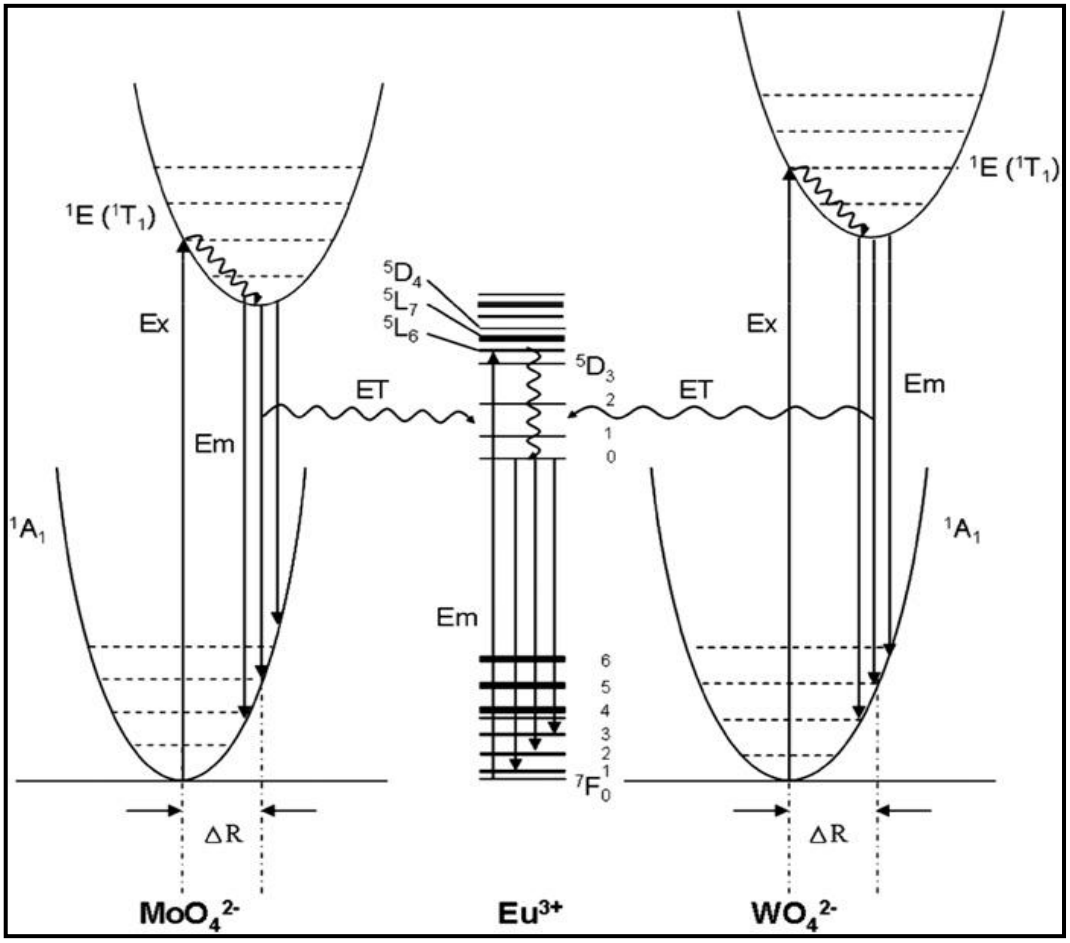

Fig. 4.14 Schematic representation of excitation, energy transfer and emission processes in the molybdate and tungstates based red phosphors.

Here in the diagram, the parabolas at right and left part are corresponding to the energy states (ground and excited) of WO_4 and MoO_4 groups. The energy levels in the central part are that corresponding to Eu^{3+} ions. If a Eu^{3+} ion in the phosphor is excited by near UV or blue irradiations, excitations occurs by the $^7F_0$ - $^5L_6$ or $^7F_0$ - $^5D_2$ transitions of Eu^{3+} and relaxes to the lowest excited energy level ($^5D_0$). Finally, a red emission occurs through a $^5D_0$ - ^7F_J

transition. On the other hand, if the phosphor is excited by wavelengths corresponding to the charge transfer of W–O and Mo–O, the excited energy states of WO_4 and MoO_4 move to the lowest excited energy states through relaxation. The energies are then transferred to the *4f* levels of Eu^{3+}, resulting in a red emission through the $^5D_0$-^7F_J transition of Eu^{3+}. It should be noted here that the energy gap between CT states of molybdates are less compared to that of the tungstates leading to an efficient energy transfer in molybdates (Lee G.H *et al* 2011).

The CIE color co ordinates of all compositions of CLNW and CGNW phosphors are calculated using the software CIE Calculator and is enlisted in Table. 4.3. It is seen that for both phosphors the red color purity (represented by *x* value) is linearly increasing with Eu^{3+} concentration. As expected the color purity of CGNW is better than that of CLNW phosphors and is closer to the color co ordinates (0.67, 0.33) of NTSC standard red phosphors.

Table 4.3 CIE color co-ordinates of $CaLa_{1-x}NbWO_8$: xEu^{3+} and $CaGd_{1-x}NbWO_8$: xEu^{3+} under near UV excitation

CLNW ***X***	**Color co-ordinates** **(*x, y*)**	**CGNW** ***x***	**Color co-ordinates** **(*x, y*)**
0.01	(0.56, 0.31)	**0.05**	(0.60,0.33)
0.03	(0.57, 0.31)	**0.10**	(0.62,0.34)
0.05	(0.59, 0.32)	**0.15**	(0.63,0.34)
0.10	(0.60, 0.31)	**0.20**	(0.63,0.34)
0.15	(0.61, 0.33)	**0.25**	(0.64,0.34)
0.20	(0.62, 0.33)	**0.30**	(0.64,0.34)
0.25	(0.63, 0.34)		

4.3.5.3 Lifetime and Quantum efficiency Calculation

Fig. 4.15 presents the decay curve for $^5D_0$ - $^7F_2$ transition of CLNW (x = 0.25) and CGNW (x = 0.25) phosphors under near UV excitation. The decay curves can be fitted well with single exponential function;

$$I = A \exp\left(-x/\tau\right) \quad (4.1)$$

where I, τ and A are intensity, lifetime (decay time) and fitting parameter respectively. The decay times of CLNW and CGNW phosphors are almost same and are 0.7609 and 0.7103 ms respectively (Su Y *et al* 2008). Thus the tungstate based red phosphors have relatively longer lifetime compared to that of the molybdates (CL/GNM) discussed in the previous chapter.

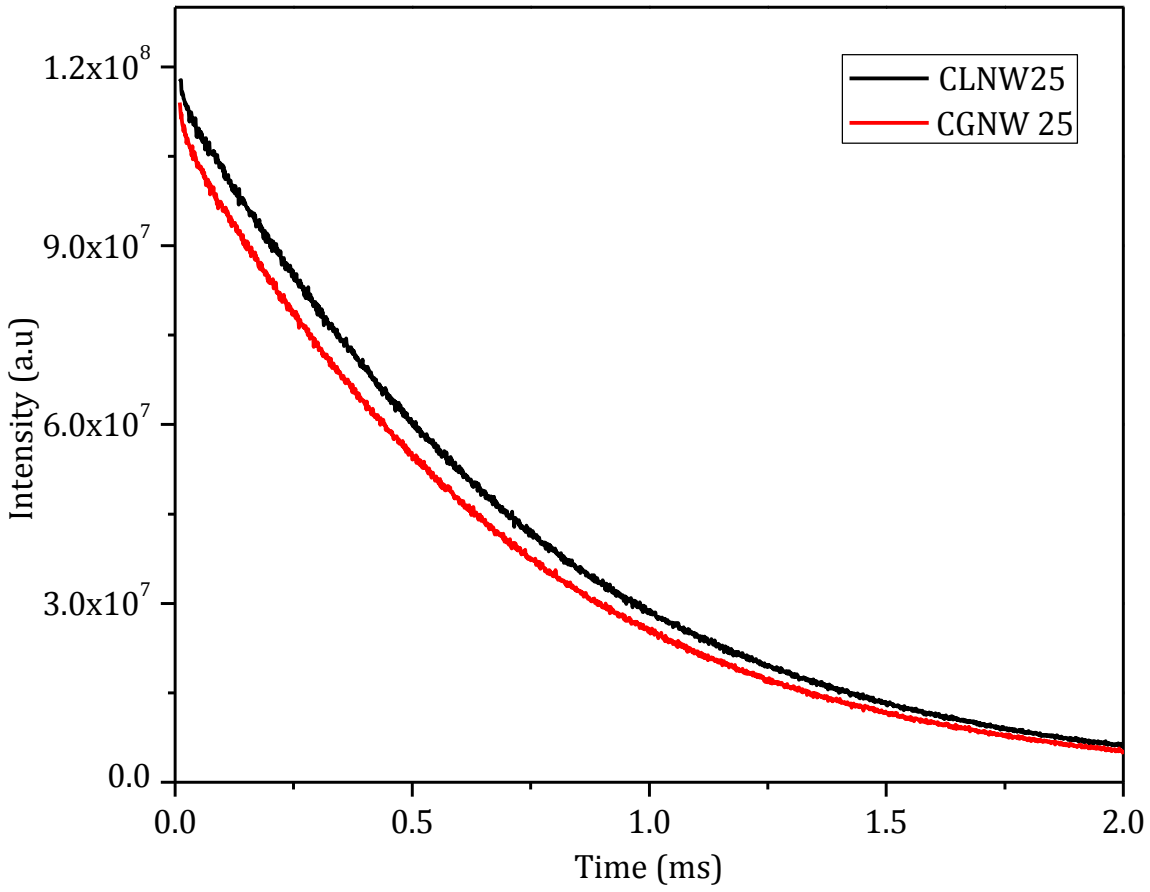

Fig. 4.15 Decay curves of Eu^{3+} emission at 613 nm in $CaLa_{0.75}NbWO_8$: $0.25Eu^{3+}$ and $CaGd_{0.75}NbWO_8$:$0.25Eu^{3+}$ phosphors under near UV excitation.

The quantum efficiency of Eu^{3+} ($^5D_0$) excited state and Judd- Ofelt intensity parameters of CLNW and CGNW phosphors under near UV excitation are calculated. The detailed principle and method of calculation of quantum efficiency and intensity parameters were the same as given in chapter 3. The calculated quantum efficiencies of CLNW and CGNW red phosphors are 26.36% and 25.03% respectively. The details of the photoluminescence data of both tungstate phosphors (CLNW and CGNW) are included in Table. 4.4. For both CLNW and CGNW phosphors the Ω_2 is more than Ω_4, indicating the non centro symmetric site occupancy of Eu^{3+} in both the lattices (Su Y *et al* 2008). Ω_2 value is slightly more for CGNW

than that of CLNW, implying the more polarizable environment in CGNW lattice for Eu^{3+} ions. This can be due to the stiffness and symmetry distortion in CGNW lattice.

The quantum efficiency of both tungstates is better than that of molybdate (CL/GNM) phosphors. This can be due to the blue shift of CT band position in tungstates compared to the molybdates. Also the intensity parameters of both the molybdate and tungstates are almost the same, pointing the fact that chemical environment of both lattices are the same and have comparable red emission intensity. In the present study, we modified the $CaMoO_4$ and $CaWO_4$ lattices by introducing $LaNbO_4$ and generated novel red phosphors. By this modification we could able to synthesize red phosphors with good quantum efficiency, color purity and red emission intensity. The quantum efficiency of both tungstates and molybdates (discussed in chapter 3) are better than the reported values of quantum efficiency of Eu^{3+} activated $CaMoO_4$ and $CaWO_4$ phosphors (12.18% and 17.13% respectively) synthesized by solid state reaction route (Lei F *et al* 2008). Also both the molybdates and tungstate phosphors have comparable emission intensity with Eu^{3+} doped $CaMoO_4$ phosphors.

Table 4.4 Photoluminescence data of $CaLa_{0.75}NbWO_8$: $0.25Eu^{3+}$ and $CaGd_{0.75}NbWO_8$:$0.25Eu^{3+}$ phosphors

PL	CLNW (0.25)	CGNW (0.25)
λ_{em}	580, 592, 613, 655, 703	
I_{02}/I_{01}	3.08	8.47
τ (ms)	0.7609	0.7103
$1/\tau$ (s^{-1})	1314	1408
A_{rad} (s^{-1})	346.48	352.42
A_{nrad} (s^{-1})	967.74	1055.43
η (%)	26.36	25.03
Ω_2 ($10^{-20}cm^2$)	8.28	8.50
Ω_4 (10^{-20} cm^2)	1.40	1.35

4.4 Conclusions

Tungstate based scheelite type novel red phosphors, $Ca(La/Gd)_{1-x}NbWO_8$: xEu^{3+} have been synthesized by solid state reaction route and its photoluminescence properties are investigated in detail. The photoluminescence properties reveal that these phosphors are effectively excitable under near UV and blue irradiations and show strong red emission under both these excitations. By the introduction of tungsten in the host lattice, the position of CT band is shifted to higher energy and the quantum efficiency of the phosphor is improved. The developed phosphors exhibit sharp red emission with good color purity, quantum efficiency and lifetime in milli seconds order. These characteristic features of tungstate based red phosphors point to the suitability of them for pc-WLED applications.

CHAPTER 5

EFFECT OF Bi^{3+} CODOPING ON LUMINESCENT PROPERTIES OF $Ca(La/Gd)_{1-x}NbMo/WO_8$: xEu^{3+} PHOSPHORS

The position and intensity of CT band of phosphors play an important role in determining their luminescence behavior. An improvement in the red emission of phosphors is possible by red shifting the CT band position. For this purpose, a suitable codopant (Bi^{3+}) is incorporated in typical compositions of both molybdate and tungstate based optimized red phosphors. Effect of Bi^{3+} codoping in the luminescence performance is investigated. Red shift as well as intensification of the CT band is resulted via Bi^{3+} codoping. Luminescence enhancement of both phosphors is achieved and the role of Bi^{3+} in line with this is discussed. Various attributes such as lifetime, asymmetry ratio, energy transfer, absorption strength, CT band position and its intensity are analyzed in detail. Bi^{3+} codoping is more prominent in the luminescence improvement of tungstate based red phosphors than that of the molybdates.

Phys. Status Solidi A *208 [9](2011) 2170.*

CHAPTER 5A

EFFECT OF Bi^{3+} CODOPING ON LUMINESCENT PROPERTIES OF $Ca(La/Gd)_{1-x}NbMoO_8$: xEu^{3+} PHOSPHORS

5A.1 Introduction

Superior luminescence behavior of red phosphors is a prior requisite for the advancement of pc-WLEDs as a source for indoor and outdoor lighting applications. In this regard, development of novel and stable red phosphors or improvement of current red phosphors is an urgent goal to be fulfilled. For this a better understanding of the basic dependent factors on the luminescence properties of phosphor materials is essential. As already stated, molybdates/tungstates with powellite/scheelite type structure are considered to be good host lattices because of the presence of broad - intense CT band at near UV region and the effective energy transfer to the localized energy states of activator ions (Eu^{3+} in the present case) (Gundiah G *et al* 2008). The luminescence performance of such Eu^{3+} activated molybdate/ tungstate based red phosphors can be improved by enhancing the absorption strength of parity forbidden $4f - 4f$ transitions of Eu^{3+} ions. This can be achieved mainly by lowering the site symmetries of Eu^{3+} through chemical modification of host such as introducing lattice distortions (Ying Z *et al* 2009). Broadening of CT bands of the corresponding phosphors is another way to improve the absorption efficiency of $4f - 4f$ transitions via energy transfer process (Ye S *et al* 2009).

The absorption edge of (MoO_4) group in molybdates usually appears at short wavelength (about 350 nm for $CaMoO_4$: Eu^{3+}, Li^+) (Wang J. G *et al* 2005) although these materials normally exhibit effective red emission. Whereas the absorption edge of MoO_6 in materials such as Eu doped perovskite type molybdates, $(Ba,Sr)_2CaMoO_6$ is located at relatively long wavelengths normally at 450 nm, it is rare for these materials to show effective red emission at the same time (Sivakumar V *et al* 2007; Ye S *et al* 2008; Blasse G *et al* 1966). Therefore, broadening the absorption band of the MoO_4 contained materials would be a possible way to improve the properties of the Eu^{3+} doped molybdate red phosphors for white light UV LED applications. The position of CT band has vital role to determine the luminescence performance of Eu^{3+} activated phosphors (Su Q *et al* 1995). An intense red emission of Eu^{3+} via parity forbidden electric dipole transitions ($^5D_0$ - $^7F_2$) prefers lower energy position of its CT band, as they can borrow intensity from the lowest strong absorption band (i.e., CT band) (Su Q *et al* 1995). It has been reported that incorporation of codopants in various host lattices can lead to a great improvement of their luminescent efficiency (Junli H *et al* 2010; Pode R. B *et al* 1997; Shi S et al 2008; Wang Z et al 2006). These codopants can enhance luminescence intensity by acting as a flux or sensitizer and

sometimes create oxygen vacancies in the host lattices or alter the crystal field surrounding the activator (Liu X *et al* 2007).

The selection of codopant ions (coactivators) is very important and should satisfy certain prerequisites. The codopants should have proper valence state which can easily establish in its crystalline environment and should stabilize that valence state within the crystalline host lattice. To improve the absorption efficiency in the near UV region, Sm^{3+} is codoped with Eu^{3+} in different phosphors (Cao F. B *et al* 2009; Okamoto S *et al* 2007; Wang Z. L *et al* 2008; Wang X. X *et al* 2007). To broaden the excitation bands at the near UV region, Bi^{3+} is also used as codopant ion in phosphors such as Y_2O_3: Eu^{3+} (Chi L. S *et al* 2005), $CaMoO_4$: Eu^{3+} (Xie A *et al* 2009), YVO_4: Eu^{3+} (Neeraj S *et al* 2004), $LiEuMo_2O_8$: Eu^{3+} (Ye S *et al* 2009), etc. It was found that both the polarization effect of Bi^{3+} on the charge transfer state (CTS) of MoO_4 and the $6s \rightarrow 6p$ transition of Bi^{3+} play roles in the red shift of the absorption band at UV region. Moreover, the incorporation of Bi^{3+} could also enhance the red emission intensity of Eu^{3+} efficiently upon near UV excitation.

We had seen that $Ca(La/Gd)_{1-x}NbMo/WO_8$: xEu^{3+} phosphors exhibit intense red emission under near UV and blue excitations (Chapters 3 and 4) and the CT bands of these phosphors are observed in the wavelength range of 240 – 360/350 nm. It may be possible to extend the absorption edge of these phosphors to longer wavelength and improve their emission intensities. In the present study, an effort has been taken to broaden the CT band of developed molybdate and tungstate based red phosphors through Bi^{3+} codoping. For this, optimized compositions of both molybdate and tungstate red phosphors are selected and different concentrations of Bi^{3+} ions are incorporated. Detailed investigation on structural, microstructural and photoluminescent properties of these phosphors with codopant incorporation are carried out. Further, the role of Bi^{3+} codoping and CT band position on the luminescence behavior of the developed red phosphors is studied. First part (Chapter 5A) of this chapter elucidates results of Bi^{3+} coactivated molybdate based red phosphors and that of tungstate based red phosphors are included in the second part (Chapter 5B).

5A.2 Experimental

Selected compositions of $CaLa_{0.91-y}NbMoO_8$: $0.09Eu^{3+}$, yBi^{3+}(y = 0.07, 0.08, 0.09, 0.10, 0.15) (CLNMB) and $CaGd_{0.75-y}NbMoO_8$: $0.25Eu^{3+}$, yBi^{3+}(y = 0.01, 0.03, 0.05, 0.07) (CGNMB) were synthesized by solid state reaction route. Stoichiometric amount of starting materials such as $CaCO_3$, La_2O_3/Gd_2O_3, Bi_2O_3, Nb_2O_5, MoO_3, and Eu_2O_3 (Chemicals are from Acros Organics and Sigma Aldrich with 99.99% purity) were weighed and thoroughly wet mixed in an agate mortar with acetone as the wetting medium. The mixing was followed

by drying in an air oven. The mixing and drying were repeated thrice to obtain a homogenous mixture and was calcined at 1200°C for 6 h in a platinum crucible in an air atmosphere furnace.

The crystal structure as well as the phase purity of the calcined samples were examined by recording the powder X ray diffraction patterns using a PANalytical X'pert Pro diffractometer with Ni filtered CuKα radiation (λ= 1.54056Å). The morphological analysis of the powder samples were done by a scanning electron microscope (JEOL, JSM- 5600LV). The UV Visible absorption spectra of the samples were recorded by UV–Vis Spectrophotometer (Shimadzu UV-2401). Photoluminescence excitation and emission spectra were recorded using a Horiba Yvon Fluorolog® 3 Spectrofluorimeter with a 450W xenon flash lamp as the exciting source. To record the emission spectra, the excitation wavelength is fixed at 394/395 and 465 nm and the emitted light intensity is measured at the wavelength range of 500 - 750 nm. For recording excitation spectra, the emission monochromator is fixed at 613 nm emission wavelength and the excitation wavelength is scanned in 200 - 500 nm spectral range. Both the excitation and emission spectra are recorded by fixing the excitation and emission monochromator slit widths at 0.5 and 1 nm respectively. The CIE chromaticity coordinates of the phosphors were also calculated. Luminescence lifetime of the phosphors was recorded by the phosphorimeter attached to Fluorolog® 3 Spectrofluorimeter.

5A.3 Results and Discussion

5A.3.1 Powder X ray diffraction analysis

The powder XRD patterns of CLNMB (y = 0.07, 0.08, 0.09, 0.10, 0.15) and CGNMB (y = 0.01, 0.03, 0.05, 0.07) samples are shown in Fig. 5A.1 and Fig. 5A.2 respectively. All the peaks in the XRD patterns are indexed with the $CaMoO_4$ (JCPDS file no. 29-0351) powellite structure with the space group $I4_1/a$ and are similar to the patterns of uncodoped (y = 0; CL/GNM) samples (Ravindran Nair K *et al* 2008). The sharp peaks indicate the crystalline nature of the samples. There are no traces of impure peaks in the XRD pattern. Thus these samples form solid solutions with a tetragonal crystal structure.

In the CLNMB and CGNMB crystal structure, the A site is shared by Ca^{2+}, La^{3+}/Gd^{3+}, Eu^{3+} and Bi^{3+} ions and Nb^{5+} and Mo^{6+} ions are occupied at the B site. As the ionic radius of Bi^{3+} (r = 1.17 Å when CN = 8) are close to that of La^{3+} (r = 1.16 Å when CN = 8) and Gd^{3+} (r = 1.05 Å when CN = 8), Bi^{3+} ion prefer to occupy the La^{3+}/Gd^{3+} sites in CLNMB and CGNMB lattices. It should be mentioned here that the phosphors were synthesized without any charge compensation approach as required in the case of $CaMoO_4$: Eu^{3+} (Liu J *et al* 2007).

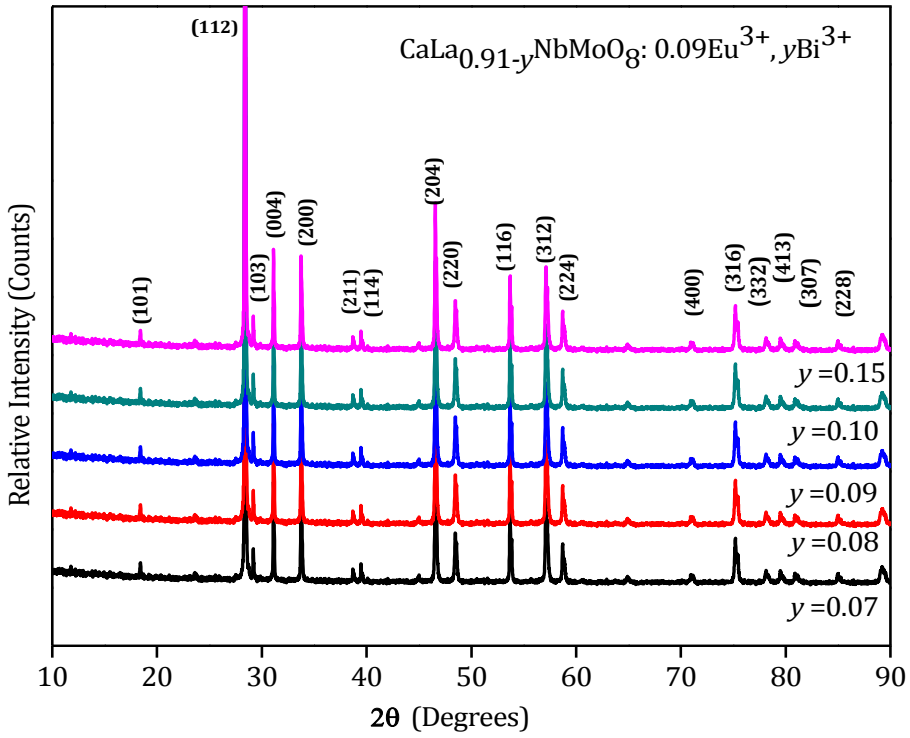

Fig. 5A.1 Powder X ray diffraction patterns of $CaLa_{0.91-y}NbMoO_8$: $0.09Eu^{3+}$, yBi^{3+} (y = 0.07, 0.08, 0.09, 0.10, 0.15).

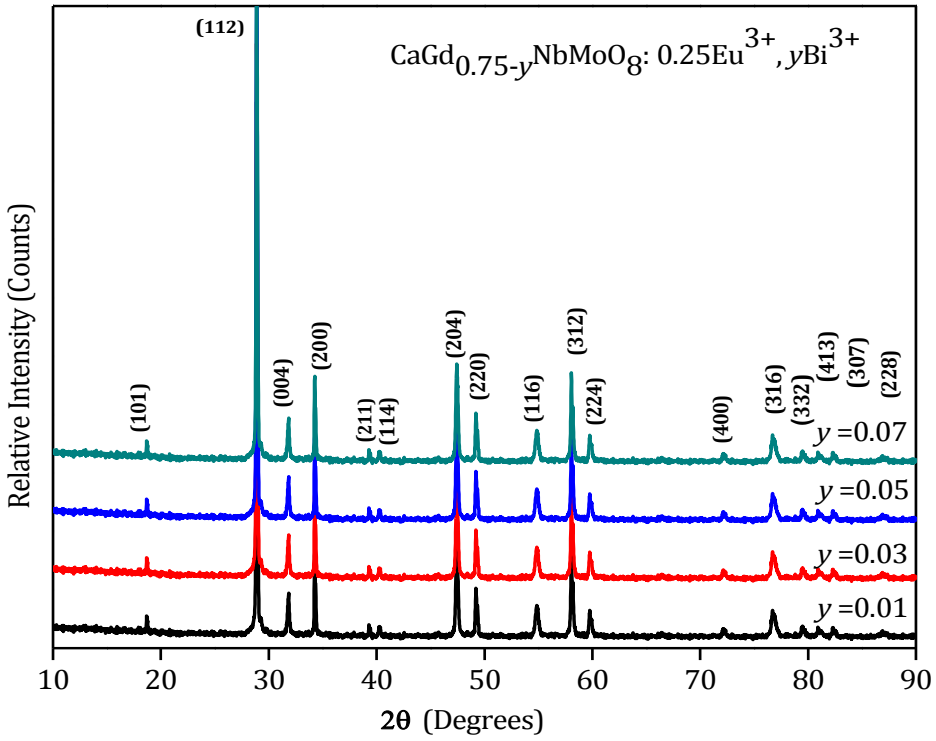

Fig. 5A.2 Powder X ray diffraction patterns of $CaGd_{0.75-y}NbMoO_8$: $0.25Eu^{3+}$, yBi^{3+} (y = 0.01, 0.03, 0.05, 0.07).

5A.3.2 Microstructural characterization

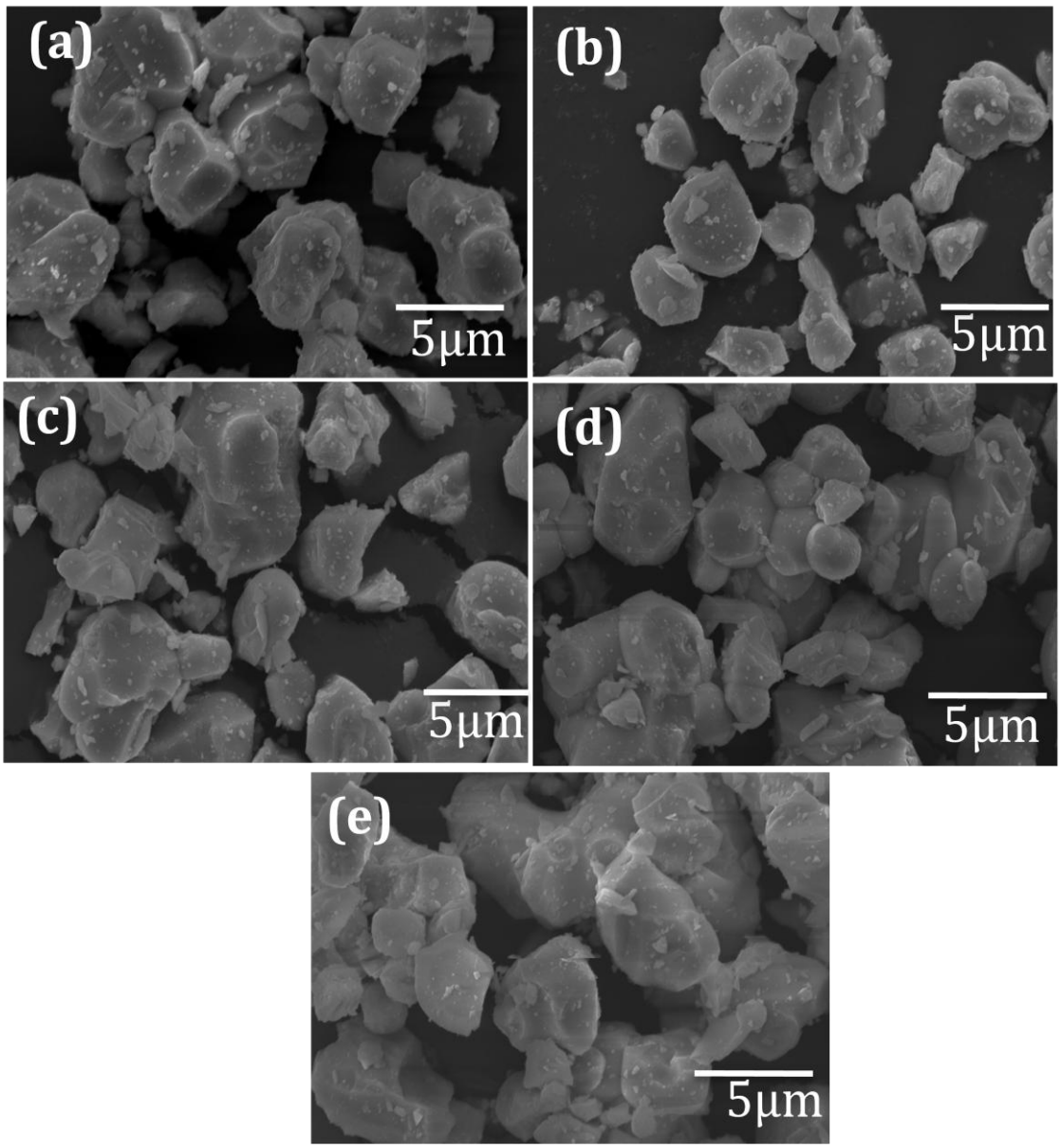

Fig. 5A.3 Scanning electron micrographs of $CaLa_{0.91-y}NbMoO_8$: $0.09Eu^{3+}$, yBi^{3+} with varying Bi^{3+} concentrations: (a) $y = 0.07$, (b) $y = 0.08$, (c) $y = 0.09$, (d) $y = 0.1$, (e) $y = 0.15$ (x 5, 000 magnification).

Fig. 5A.3 and Fig. 5A.4 present the SEM images of CLNMB and CGNMB samples with varying Bi^{3+} ion concentrations. For the CLNMB samples, slightly spherical particle morphology have been achieved. Particle surfaces have become smoother with the introduction of Bi^{3+} ions and it can reduce the scattering loss or improve the absorption strength of the samples. All the samples are homogenous in nature and are highly crystalline with an average particle size of ~1-5 µm.

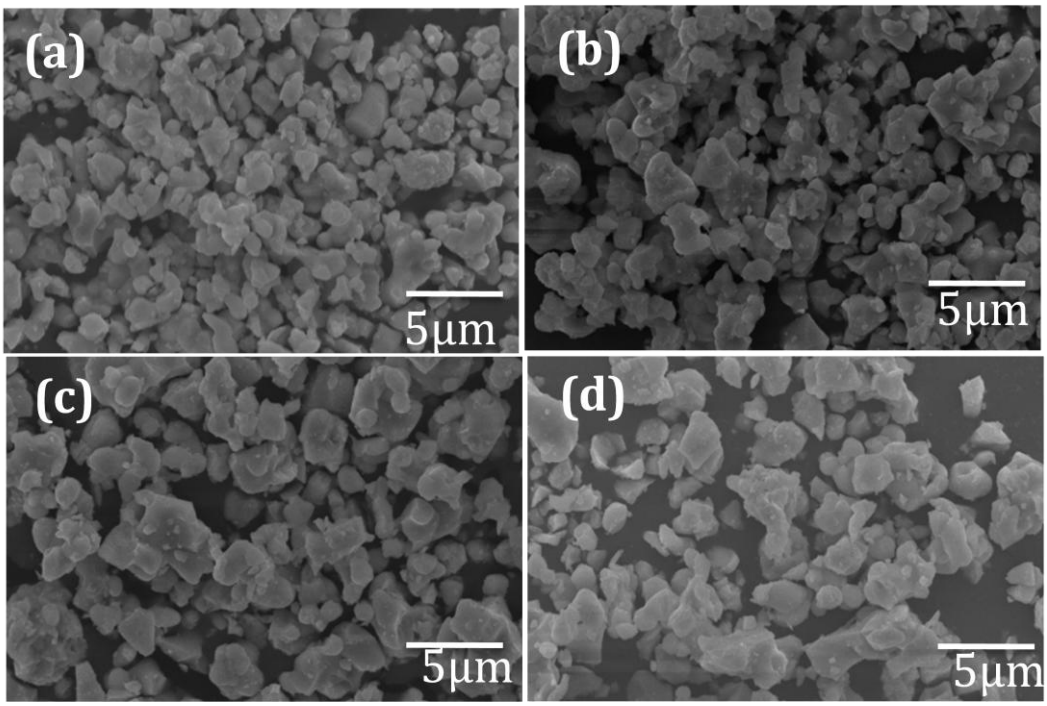

Fig. 5A.4 Scanning electron micrographs of $CaGd_{0.75-y}NbMoO_8$: $0.25Eu^{3+}$, $yBi^{3+}$with varying Bi^{3+} concentrations: (a) y = 0.01, (b) y = 0.03, (c) y = 0.05, and (d) y = 0.07 (x 5, 000 magnification).

The degree of agglomeration of both CLNMB and CGNMB samples is getting reduced compared to the uncodoped samples discussed in chapter 3. But with the increase in Bi^{3+} concentration the extent of agglomeration is increasing. For CLNMB samples at 10 and 15 mol% Bi^{3+} codoping, the particles are highly agglomerated and for CGNMB samples only at lower concentration of Bi^{3+} (1 mol%) the particles are less agglomerated. We can see that there is an increase in the average particle size of both CLNMB and CGNMB samples at higher concentrations of Bi^{3+}. To sum up, Bi^{3+} incorporation in the molybdate based Eu^{3+} activated samples improved the morphology to some extent which may have an influence in controlling their luminescent performance.

5A.3.3 UV Visible absorption

UV Visible absorption spectra of both CLNMB (y = 0, 0.08, 0.10) and CGNMB (y = 0, 0.03, 0.07) samples are shown in Fig. 5A.5 and Fig. 5A.6. For Bi^{3+} uncodoped samples, the spectra consist of an absorption band in the range of 200 – 375 nm (centered at ~ 217 nm). But with Bi^{3+} codoping, this absorption band is broadened and is extended to 400 nm with an additional band of absorption peaking at ~ 325 nm for CLNMB and ~ 330 nm for CGNMB samples.

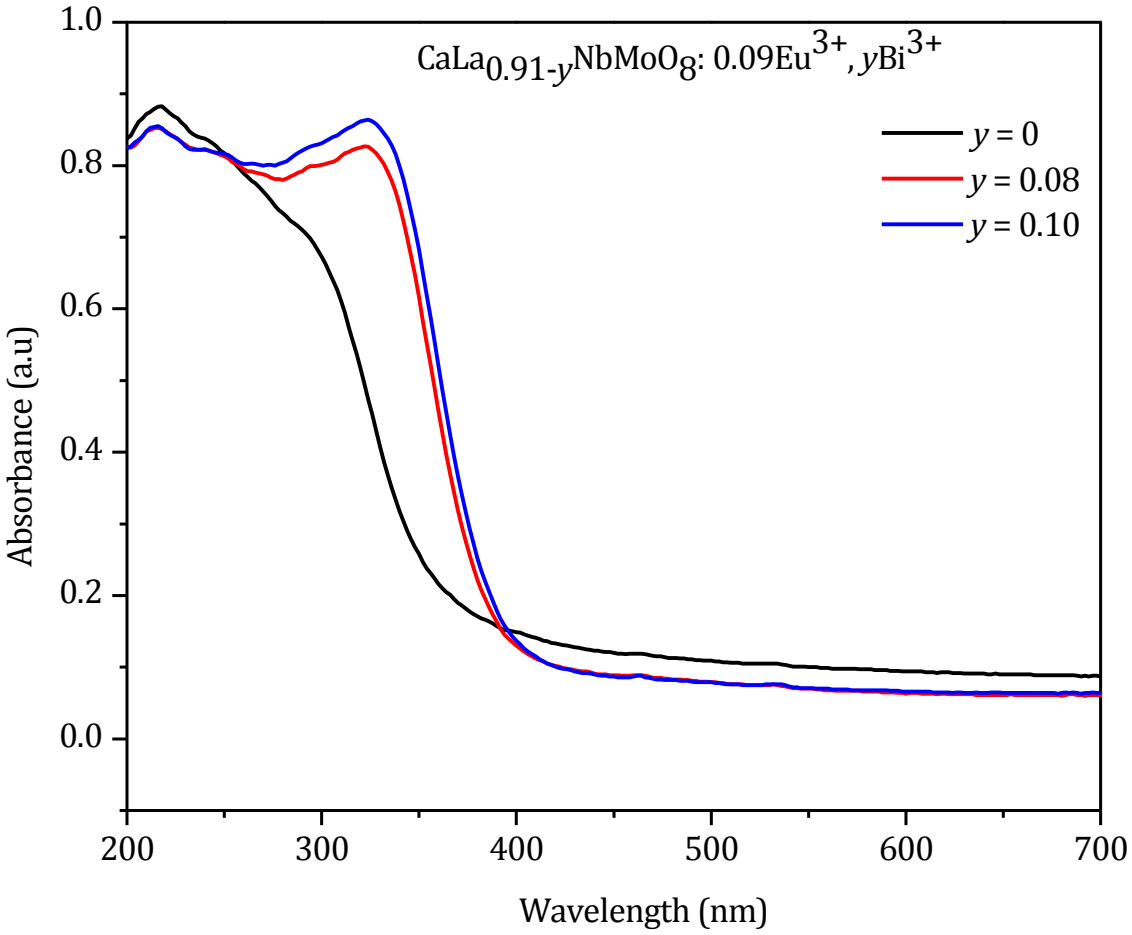

Fig. 5A.5 UV Vis absorption spectra of $CaLa_{0.91-y}NbMoO_8$: $0.09Eu^{3+}$, yBi^{3+} (y = 0, 0.08, 0.10).

The absorption band observed for both Bi^{3+} uncodoped and codoped samples are ascribed to the CT transitions (LMCT) of MoO_4/ NbO_4 and O^{2-} - Eu^{3+} groups in the host lattice (i.e., charge transfer from O^{2-} to Mo^{6+}/Nb^{5+} atoms in the MoO_4/ NbO_4 groups respectively) (Thomas M *et al* 2009). The additional band of absorption observed for Bi^{3+} codoped samples can be due to the overlapped transition from Bi^{3+} ground state to its excited states corresponding to $^0S_1 \rightarrow {}^3P_1$ and $^0S_1 \rightarrow {}^1P_1$ transitions (Xie A *et al* 2009) and this observation is in line with that of the Bi^{3+} codoping in Eu^{3+} activated $CaMoO_4$ host lattice. The absorption peaks caused by the intra configurational transitions of Eu^{3+} is not much observable in the absorption spectra, which can be well resolved in their excitation spectra and is included in the coming section. Thus broadening of CT band and red shift of the absorption edge has been achieved by Bi^{3+} codoping in Eu^{3+} activated molybdate based red phosphors which may influence the luminescence behavior of the samples.

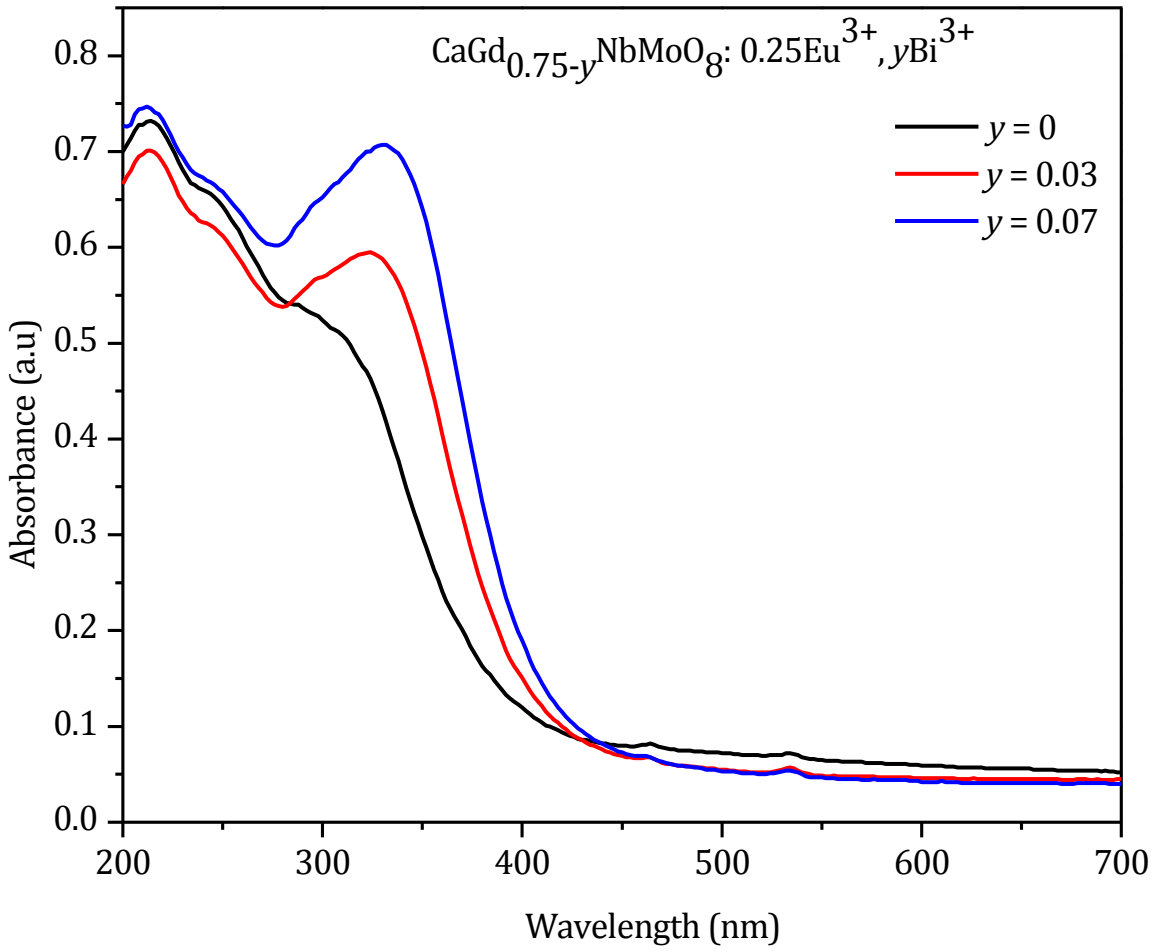

Fig. 5A.6 UV-Vis absorption spectra of $CaGd_{0.75-y}NbMoO_8$: $0.25Eu^{3+}$, yBi^{3+} (y = 0, 0.03, 0.07).

5A.3.4 Photoluminescence properties

5A.3.4.1 Excitation spectra

The photoluminescence excitation spectra of both CLNMB (y = 0, 0.07, 0.08, 0.09, 0.10, 0.15) and CGNMB (y = 0, 0.01, 0.03, 0.05, 0.07) samples for an emission at 613 nm are presented in Fig. 5A.7 and Fig. 5A.8. The spectra include broad band (240 – 350 nm) of absorption in the UV region and sharp peaks of absorption in the near UV and visible region (beyond 350 nm). The absorption band (peaking at ~313 nm) in the Bi^{3+} uncodoped samples of CLNMB and CGNMB are due to the combined LMCT transitions of Eu^{3+}- O^{2-}, MoO_4 and NbO_4 groups in the host lattices (Hu Y *et al* 2005; Hsiao Y. J *et al* 2007). The sharp peaks of excitation at 362, 384, 394/395, 412, 464/465 nm are due to the intra configurational *f-f* transitions of Eu^{3+} such as $^7F_0$ - $^5D_4$, $^7F_0$ - $^5G_{2,4}$, $^7F_0$ - $^5L_6$, $^7F_0$ - $^5D_3$, $^7F_0$ - $^5D_2$ respectively (Thomas S. M *et al* 2008; Wang J *et al* 2005).

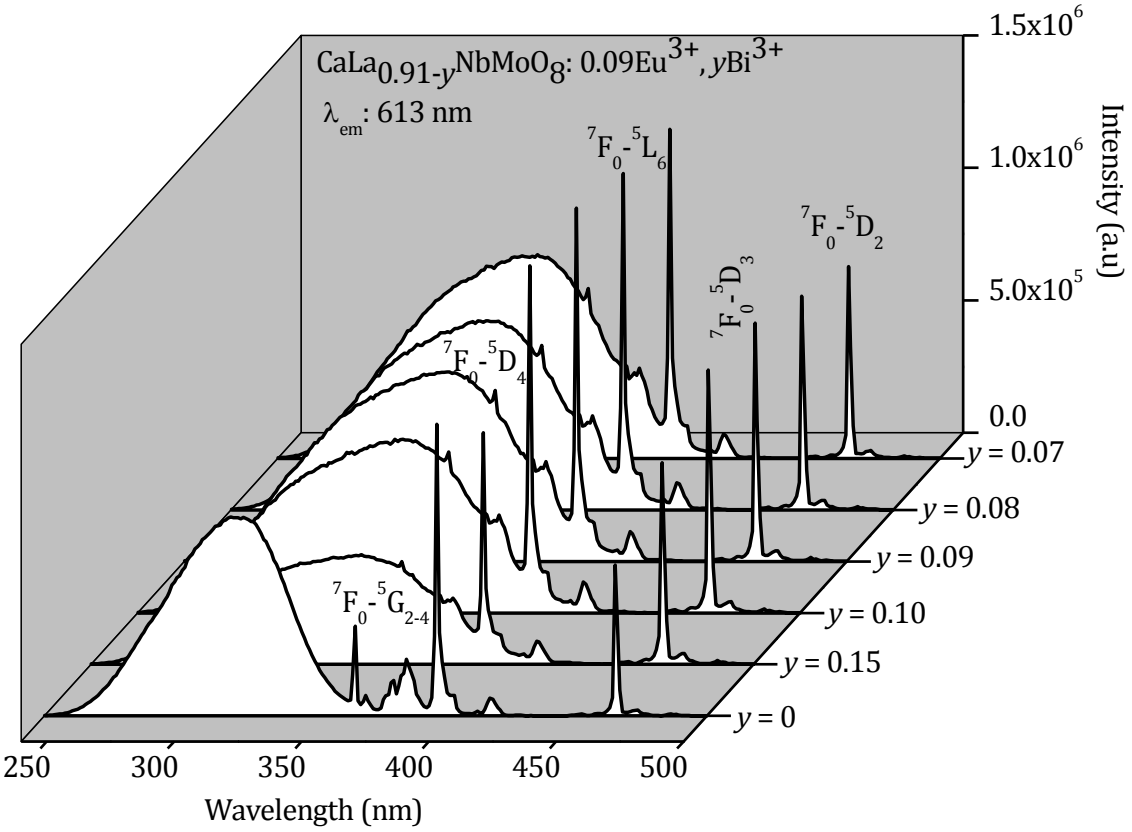

Fig. 5A.7 Excitation spectra of $CaLa_{0.91-y}NbMoO_8$: $0.09Eu^{3+}$, yBi^{3+} (y = 0, 0.07, 0.08, 0.09, 0.10, 0.15) for an emission at 613 nm.

With Bi^{3+} codoping, the CT band is broadened (240 - 390 nm) and the band edge is extended to 390 nm for both CLNMB and CGNMB samples. Accordingly, the CT band center is also red shifted from ~313 nm to ~330 nm with Bi^{3+} codoping. However, the intensity of CT band remains almost the same as that of the Bi^{3+} uncodoped sample and it starts decreasing at higher concentrations of Bi^{3+}. It is clear from the excitation spectra that for Bi^{3+} codoped samples, the CT band of excitation is overlapped with *f-f* excitation peaks to some extent. But the positions of *f-f* excitation peaks beyond 350 nm remains unaltered with Bi^{3+} incorporation.

Why the CT band broadened with Bi^{3+} codoping in CLNMB and CGNMB samples? Bi^{3+} ion is mercury like ion with a $6s^2$ configuration and its luminescence properties depends strongly on the composition and crystal structure of the host lattice. The electronic configuration of Bi^{3+} is composed of the ground state $6s^2$ and the first excited state 6*s*6*p* (Shin S. H *et al* 2001). In $CaMoO_4$ host lattice, Bi^{3+} emits blue light at 480 nm. The excitation spectrum of $CaMoO_4$ for 480 nm emission of Bi^{3+} exhibits a band centered at ~330 nm, which is consistent with the present observation of red shifting of the CT band position with Bi^{3+} codoping in CLNMB and CGNMB samples. This observation suggests the occurrence of

energy transfer process from Bi^{3+} to Eu^{3+} in the UV region (Blasse G *et al* 1967; Neeraj S *et al* 2004). Thus the broadening of CT band with respect to Bi^{3+} codoping in CLNMB and CGNMB phosphors can be mainly attributed to Bi^{3+} absorption via transition from $^1S_0$ to $^3P_1$ and $^1P_1$ levels.

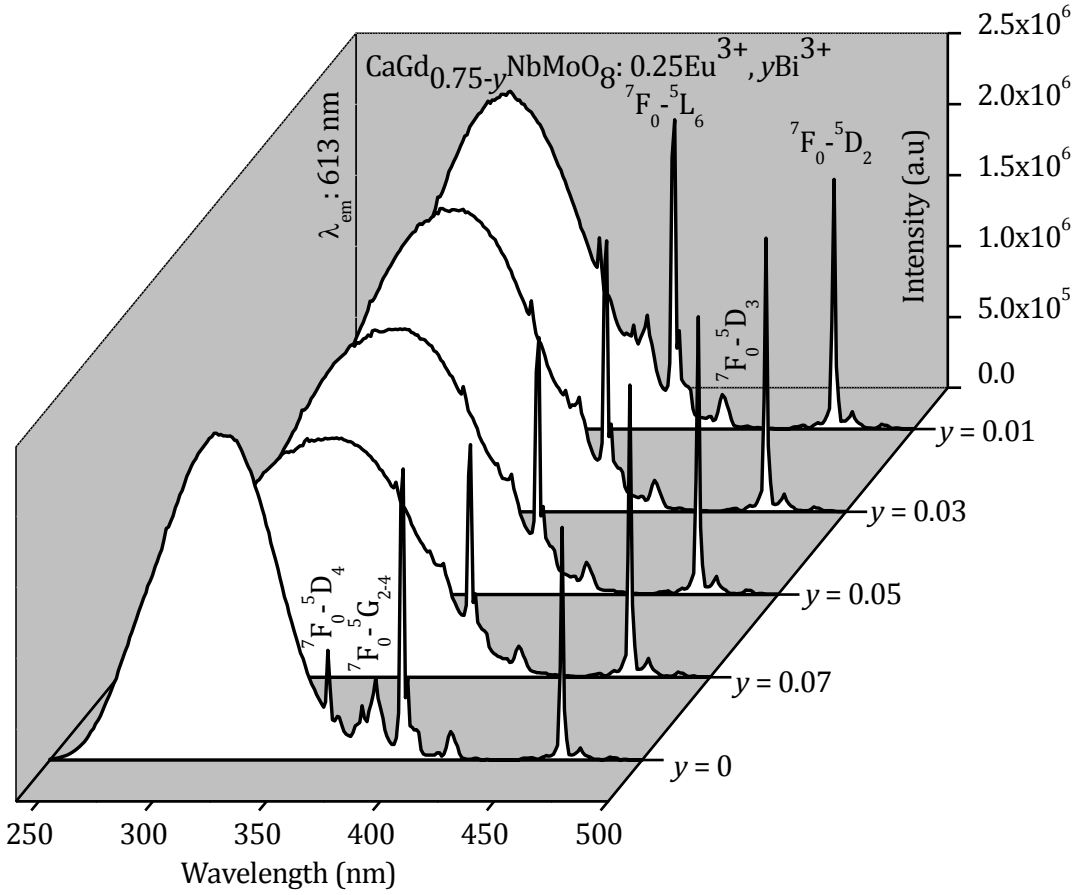

Fig. 5A.8 Excitation spectra of $CaGd_{0.75-y}NbMoO_8$: $0.25Eu^{3+}$, yBi^{3+} (y = 0, 0.01, 0.03, 0.05, 0.07) for an emission at 613 nm.

In general for molybdate (MoO_4) based Eu^{3+} activated phosphors; the CT band is strong enough and is located at a higher wavelength region. Without Bi^{3+} codoping itself, we had seen the presence of strong CT band centered at relatively high wavelength region (313 nm). The Bi^{3+} codoping in the present Eu^{3+} activated molybdate based phosphors has more contribution on red shifting the CT band position by Bi^{3+} absorption process than to intensify the CT band. Consequently for both CLNMB and CGNMB phosphors even though the CT band is red shifted, its intensity is not enhanced with Bi^{3+} codoping.

Similar to that of Bi^{3+} uncodoped molybdate based (CL/GNM) samples, the Bi^{3+} codoped samples have strong excitation peaks at both 394/395 nm and 465 nm. Thus the current phosphor samples are also well excitable under both near UV and blue irradiations.

With Bi^{3+} codoping, the relative intensity of intra configurational *f-f* transitions is improving for CLNMB phosphors upto 9 mol% of Bi^{3+} and then onwards the intensity is decreasing. But in the case of CGNMB phosphors only at a lower concentration of Bi^{3+} (1 mol%) the intensity of *f-f* transitions is improved. The improvement of excitation intensity of intra configurational peaks of Eu^{3+} with Bi^{3+} codoping is attributed to several factors. Both morphological improvement and the crystallinity help to enhance the absorption strength of the phosphor samples with Bi^{3+} codoping. We know that the intraconfigurational *f-f* transitions of Eu^{3+} are parity forbidden and these transitions of Eu^{3+} ion borrow intensity from the lowest strong absorption band (CT band) (Su Q *et al* 1995). Thus the red shift of CT band can improve *f-f* excitation intensity, by non radiative energy transfer process and can be visualized from the energy level diagram of the samples (included in next part).

5A.3.4.2 Emission spectra

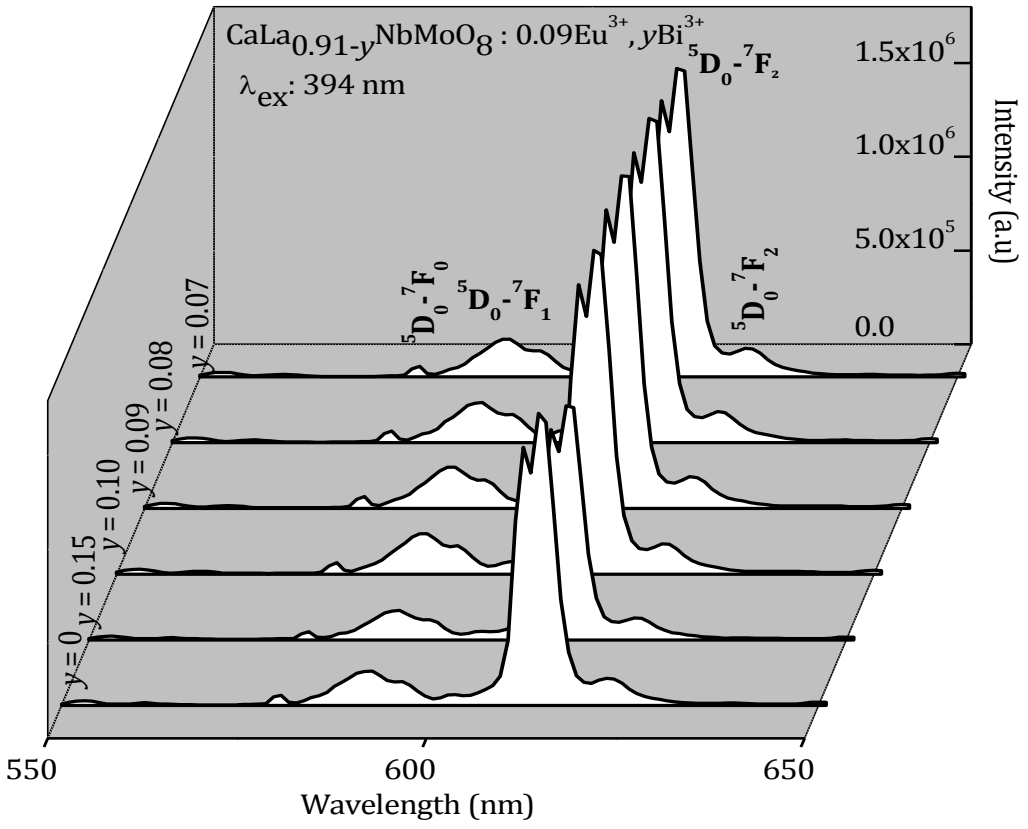

Fig. 5A.9 Emission spectra of $CaLa_{0.91-y}NbMoO_8$:0.09Eu^{3+}, *y*Bi^{3+} (*y* = 0, 0.07, 0.08, 0.09, 0.10, 0.15) under 394 nm excitation.

Fig. 5A.9 and Fig. 5A.10 present the emission spectra of CLNMB (*y* = 0, 0.07, 0.08, 0.09, 0.10, 0.15) and CGNMB (*y* = 0, 0.01, 0.03, 0.05, 0.07) samples under near UV excitation (394/395 nm). The spectra include emission peaks corresponding to intra configurational *f-f* transitions ($^5D_0$ - ^7F_J, J = 0, 1, 2) of Eu^{3+} (Zhang Z. J *et al* 2007). Similar

emission spectra are observed under blue (465 nm) irradiation also. The dominant red emission peak observed at 613 nm is due to parity forbidden $^5D_0$ – $^7F_2$ electric dipole transition, implying the fact that Eu^{3+} is occupying in a non centrosymmetric site in the Bi^{3+} codoped samples also (Blasse G 1979). i.e., in CLNMB and CGNMB samples, Eu^{3+} is located at the non centrosymmetric A site shared by Ca^{2+}, La^{3+}/ Gd^{3+} and Bi^{3+} ions.

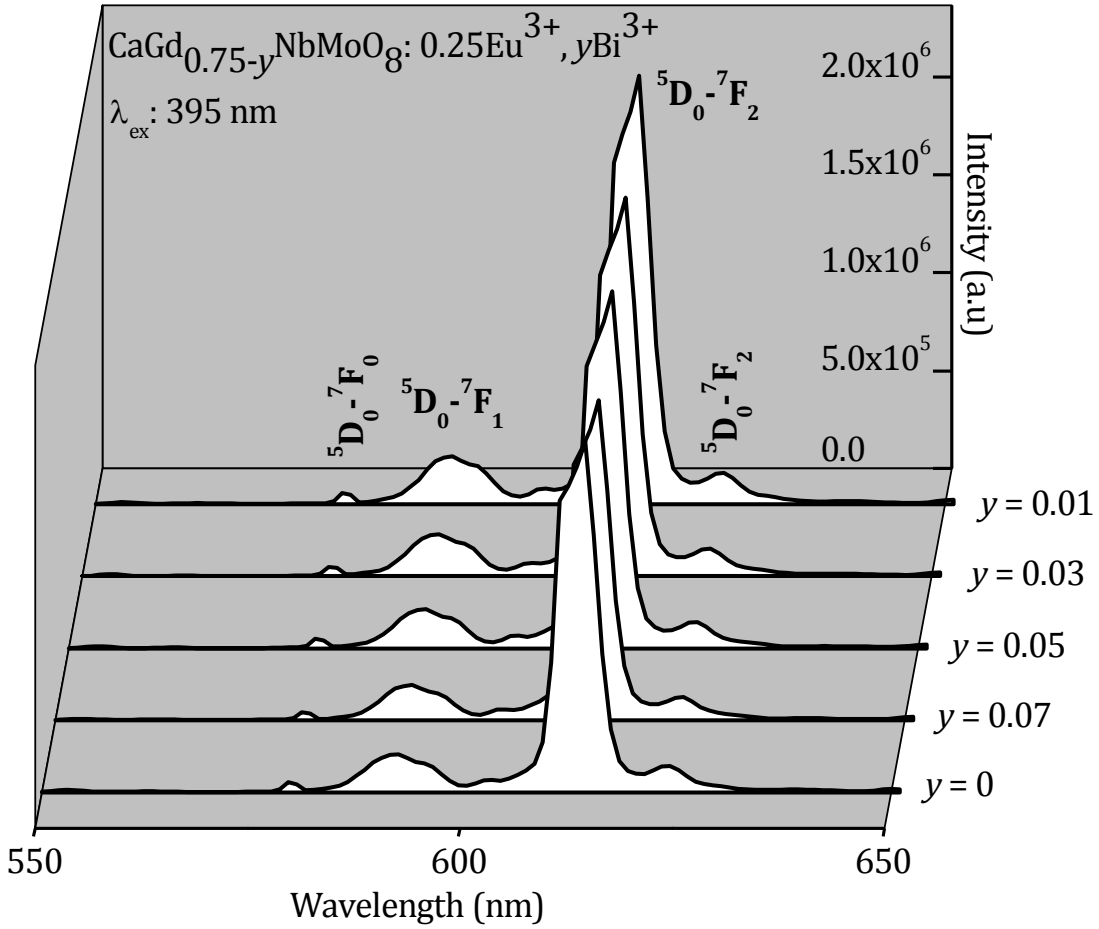

Fig. 5A.10 Emission spectra of $CaGd_{0.75-y}NbMoO_8$: $0.25Eu^{3+}$, yBi^{3+} (y = 0, 0.01, 0.03, 0.05, 0.07) under 395 nm excitation.

For CLNMB phosphors, it is observed that the red emission intensity is increasing with Bi^{3+} concentration upto 9 mol% and it starts decreasing beyond that. However in the case of CGNMB samples, the red emission intensity is at its maximum value at 1 mol% of Bi^{3+} and the intensity is decreasing further with Bi^{3+} codoping. When compared with Bi^{3+} uncodoped samples (y = 0, CLNM9 & CGNM25) the red emission intensity of CLNMB and CGNMB samples is improved by a factor of 1.14 and 1.2 respectively.

In general, either the increase of quantum efficiency of $^5D_0$ - $^7F_2$ transition (613 nm) of Eu^{3+} or the increase of absorption strengths of $^7F_0$ - $^5L_6$ (near UV) and $^7F_0$ - $^5D_2$ (blue)

transitions are considered to be the key attributes to luminescence enhancement of Eu^{3+} activated phosphors (Yan S *et al* 2007).

To make this clear in the case of present Bi^{3+} codoped molybdate based red phosphors, lifetimes of $^5D_0$ state of Eu^{3+} in CL/GNMB phosphors were measured. Fig. 5A.11 (a) and (b) show the decay curves of CLNMB and CGNMB red phosphors under near UV excitation. All the decay curves can be fitted well with a single exponential function; $I = A \exp(-x/\tau)$ where I, τ and A are intensity, decay time and fitting parameter respectively.

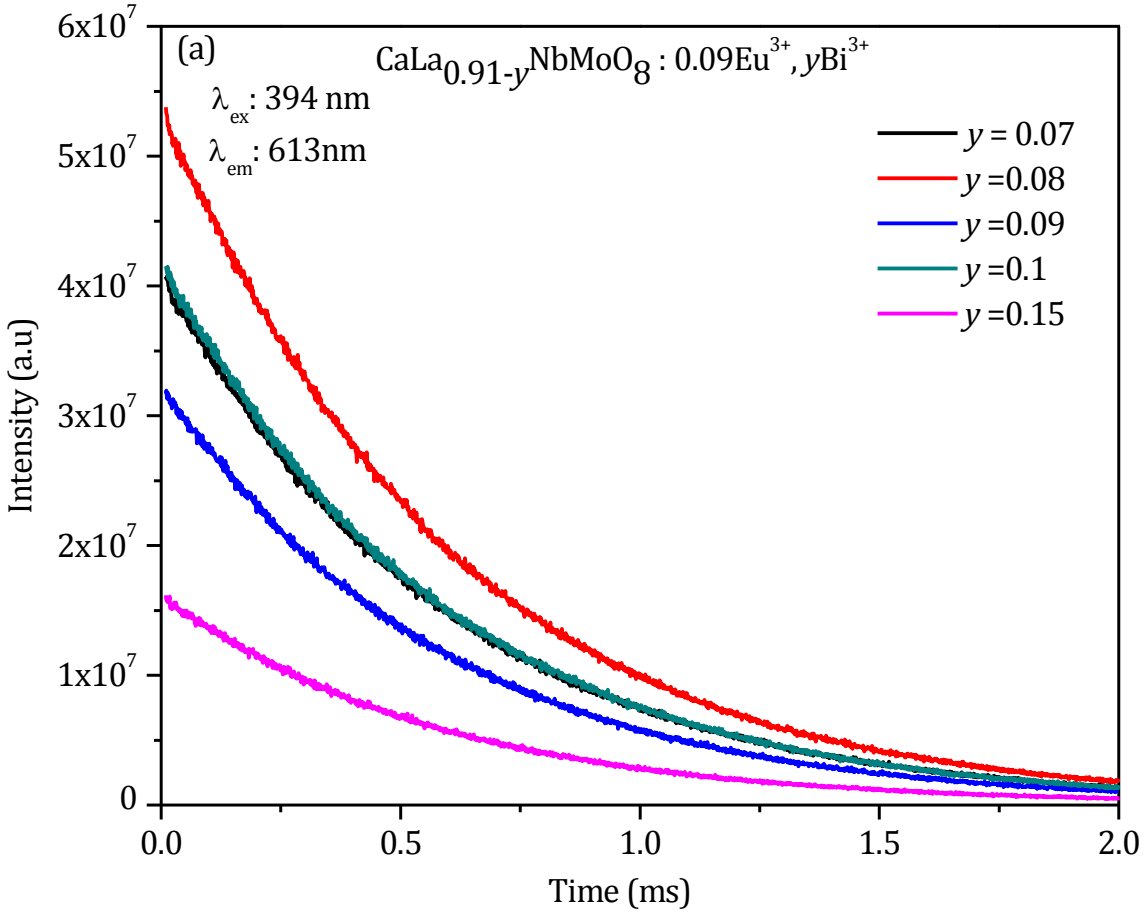

Fig. 5A.11 Decay curves of Eu^{3+} (λ_{em}: 613 nm) in (a) $CaLa_{0.91-y}NbMoO_8$: $0.09Eu^{3+}$, yBi^{3+} (b) $CaGd_{0.75-y}NbMoO_8$: $0.25Eu^{3+}$, yBi^{3+} under near UV excitation.

The dependence of lifetime of $^5D_0$ state of Eu^{3+} in both CLNMB and CGNMB phosphors on Bi^{3+} concentrations is plotted (shown in Fig. 5A.12). It is observed that with respect to Bi^{3+} concentration the lifetime is varying within the range of 0.55 – 0.60 ms. No regular variation in lifetime is observed, which hints the fact that the quantum efficiency of $^5D_0$ - $^7F_2$ transition is hardly affected by the Bi^{3+} codoping in CL/GNMB phosphors. Similar observation is reported in the case of Bi^{3+} codoped $CaMoO_4$: Eu^{3+} samples also (Yan S *et al* 2007).

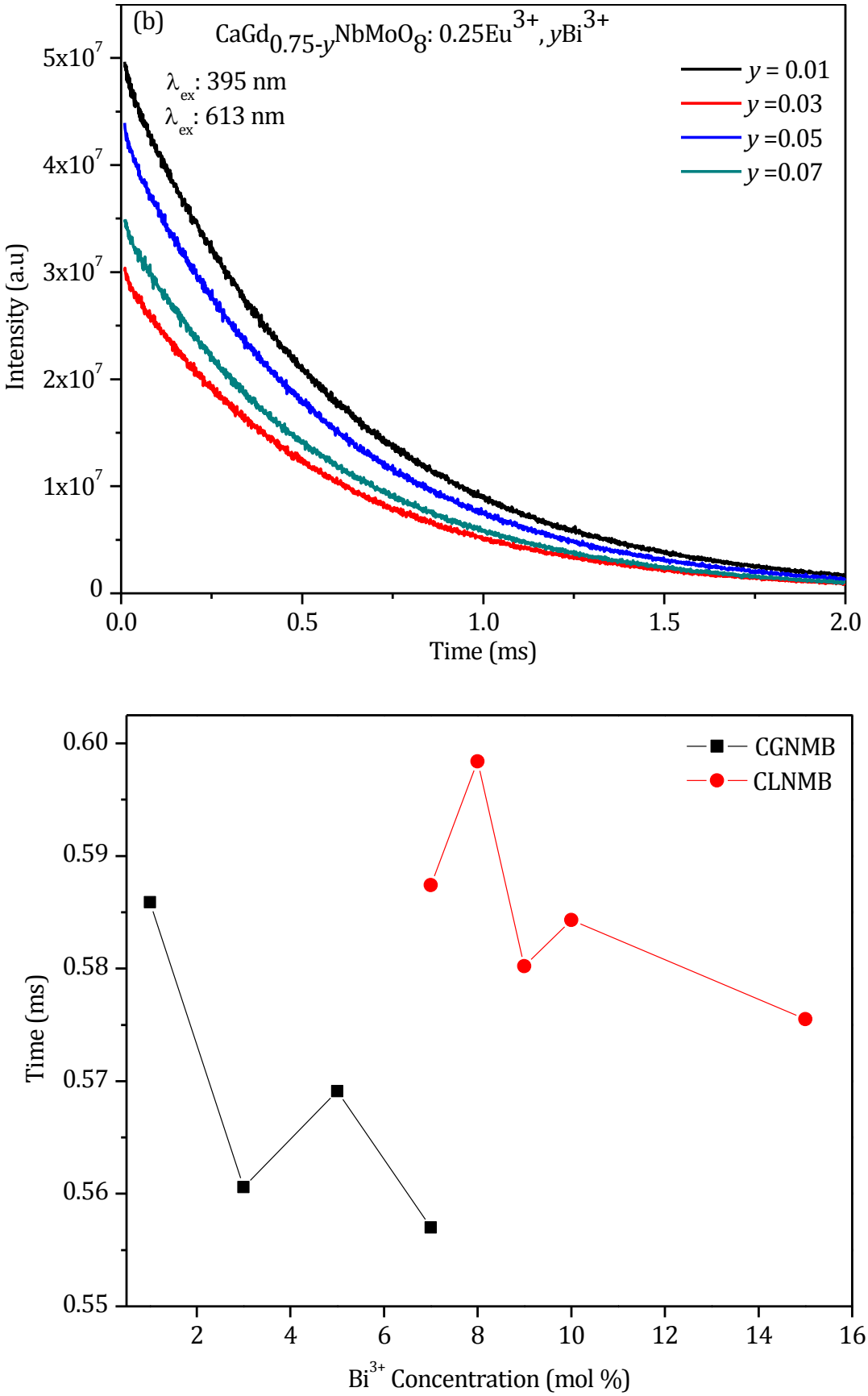

Fig. 5A.12 Dependence of Bi^{3+} concentration and Eu^{3+} lifetimes of $CaLa_{0.91-y}NbMoO_8$: 0.09Eu^{3+}, yBi^{3+} (y = 0.07, 0.08, 0.09, 0.10, 0.15) and $CaGd_{0.75-y}NbMoO_8$: 0.25 Eu^{3+}, yBi^{3+} (y = 0.01, 0.03, 0.05, 0.07) under near UV excitation.

Another factor taken into consideration is the absorption strength of the phosphor with respect to Bi^{3+} codoping. The excitation intensity of $^7F_0$ - $^5L_6$ (near UV) and $^7F_0$ - $^5D_2$ (blue) transitions in CL/GNMB phosphors with respect to Bi^{3+} codoping is plotted in the Fig. 5A.13 and Fig. 5A.14. It could be observed that for CLNMB samples the excitation intensity of both $^7F_0$ -$^5L_6$ (near UV) and $^7F_0$ - $^5D_2$ (blue) transitions is increasing with Bi^{3+} codoping and is getting reduced after 9 mol% of Bi^{3+}. However for CGNMB phosphors, the excitation intensity improvement of $^7F_0$ - $^5L_6$ (near UV) transition is only observed at 1 mol% and the intensity of $^7F_0$ - $^5D_2$ (blue) transition improved to some more extent up to 7 mol% of Bi^{3+}. The reduction of excitation intensity after a specific concentration of codopant ion may be due to the formation of Bi^{3+} aggregates. Thus the increase of absorption strength of the *f-f* transition is the key factor behind the luminescence improvement in the CL/GNMB phosphors.

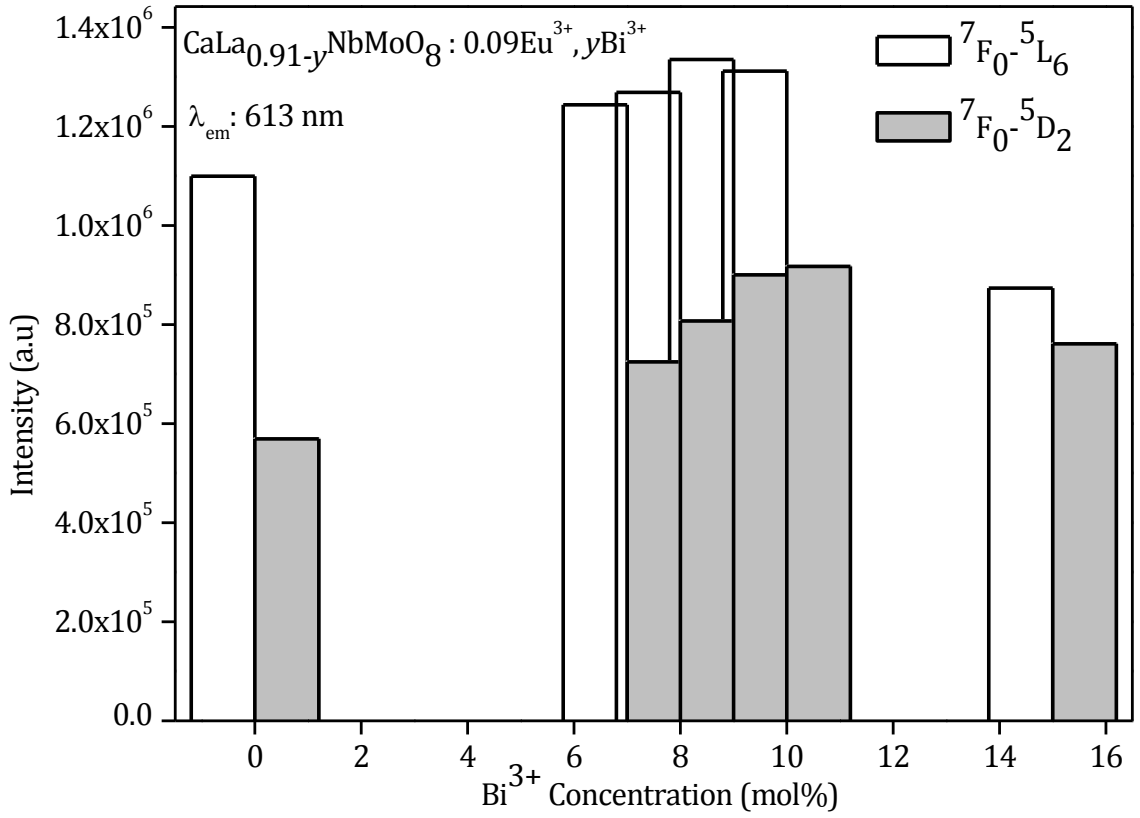

Fig. 5A.13 The excitation intensity of $^7F_0$ - $^5L_6$ (near UV) and $^7F_0$ - $^5D_2$ (blue) transitions of $CaLa_{0.91-y}NbMoO_8$: $0.09Eu^{3+}$, yBi^{3+} (y = 0, 0.07, 0.08, 0.09, 0.10, 0.15) (λ_{em}: 613 nm).

How does Bi^{3+} codoping affect the absorption strength of $^7F_0$ - $^5L_6$ (near UV) and $^7F_0$ - $^5D_2$ (blue) transitions or what is the role of Bi^{3+} in determining the luminescence property of the current red phosphors? By parity selection rule, the intra configurational *f-f* transitions of

Eu^{3+} such as $^7F_0$ - $^5L_6$ and $^7F_0$ - $^5D_2$ are parity forbidden and weak (Hu Y *et al* 2005). These transitions will be allowed/enhanced under certain conditions such as; (1) if there is a distortion in the symmetry of Eu^{3+} site (2) if the position of CT band is at a lower energy (3) if the phosphor has a superior morphology and high crystallinity (Blasse G 1979; Su Q *et al* 1995).

Thus it is necessary to understand aforementioned three conditions in the case of CL/GNMB phosphors. In general, asymmetry ratio of Eu^{3+} activated phosphor hints the extent of symmetry distortion to the crystalline environment of Eu^{3+} site. Table 5A.1 presents the variation of asymmetry ratio of both CLNMB and CGNMB phosphors with Bi^{3+} concentration under near UV excitation. Both for CLNMB and CGNMB phosphors the asymmetry ratio is slightly varying with respect to Bi^{3+} codoping.

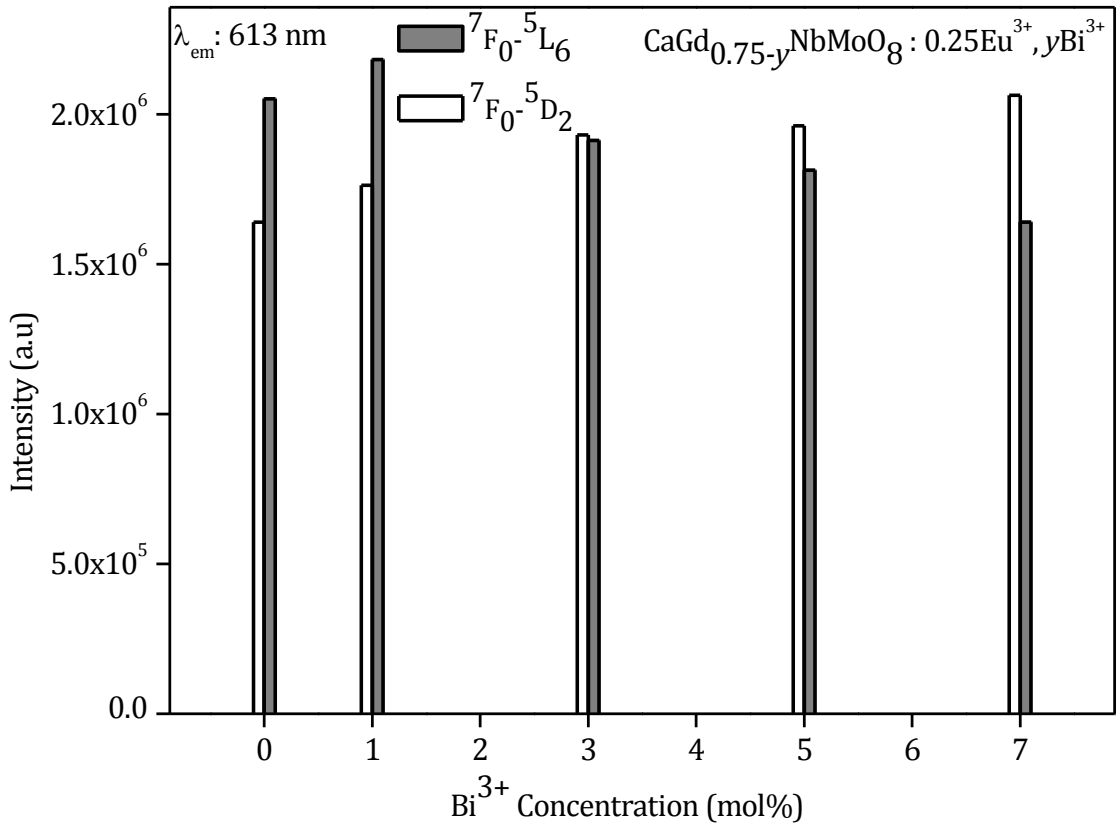

Fig. 5A.14 The excitation intensity of $^7F_0$ - $^5L_6$ (near UV) and $^7F_0$-$^5D_2$ (blue) transitions of $CaGd_{0.75-y}NbMoO_8$: $0.25Eu^{3+}$, yBi^{3+} (y = 0, 0.01, 0.03, 0.05, 0.07) for an emission at 613 nm.

With respect to Bi^{3+} uncodoped samples, the degree of increase of asymmetry ratio of CGNMB is more compared to CLNMB. In CL/GNMB lattice Bi^{3+} (ionic radius: 1.17) is occupying at A site shared by both La^{3+}/Gd^{3+} and Eu^{3+} with ionic radii 1.16/1.05 and 1.07 nm

respectively. Moreover, the oxidation state of host cations and the codopant ion is the same. Thus the incorporation of Bi^{3+} in CL/GNMB lattice may make only a minor symmetry distortion. But in the case of $CaMoO_4$: Eu^{3+}, Bi^{3+} phosphor, the incorporation of Bi^{3+} ions destroys the crystal symmetry of Eu^{3+} ion in two ways. One due to the bigger ionic radius of Bi^{3+} and the other due to the charge compensation of Bi^{3+} on substituting for Ca^{2+} ions which leads to the generation of Ca^{2+} vacancies and point defects (Yan S *et al* 2007).

Another aspect related to enhancement of parity forbidden *f-f* transitions is the position of CT band in the CL/GNMB phosphors. The CT band position of both CLNMB and CGNMB phosphors is shifted from 313 nm (Bi^{3+} uncodoped) to ~342 nm (CLNMB) and ~323 nm (CGNMB). This red shift of CT band is mainly attributed to the Bi^{3+} absorption (discussed earlier). The parity forbidden intra configurational *f-f* transitions of Eu^{3+} can borrow intensity from the lowest strong absorption band (CT) leading to the improvement of *f-f* excitation intensity by non radiative energy transfer process. Thus Bi^{3+} addition in the current phosphors enhanced the absorption strength of the material by red shifting their CT band position.

Table 5A.1 Variation of asymmetry ratio of $CaLa_{0.91-y}NbMoO_8$:$0.09Eu^{3+}$, yBi^{3+} (y = 0, 0.07, 0.08, 0.09, 0.10, 0.15) and $CaGd_{0.75-y}NbMoO_8$: $0.25Eu^{3+}$, yBi^{3+} (y = 0, 0.01, 0.03, 0.05, 0.07) under near UV excitation

CLNMB y **(Bi^{3+} mol %)**	**Asymmetry Ratio** ($I_{5D0-7F2}$/ $I_{5D0-7F1}$)	**CGNMB** y **(Bi^{3+} mol %)**	**Asymmetry Ratio** ($I_{5D0-7F2}$/ $I_{5D0-7F1}$)
0	8.15	0	9
0.07	8.16	0.01	10
0.08	8.22	0.03	10.2
0.09	8.23	0.05	10.4
0.10	8.02	0.07	10.1
0.15	8.09		

The morphology and crystallinity of the phosphors are the concluding attributes taken into consideration for the absorption enhancement of the CL/GNMB phosphors. From SEM analysis, it is observed that the morphology of both phosphors has been improved compared to their Bi^{3+} uncodoped analogues. The X ray diffraction peaks of the Bi^{3+} codoped samples

are very sharp and are relatively high intense indicating the extent of crystallinity of the samples. The improved morphology as well as crystallinity of Bi^{3+} lead to efficient absorption of light incident on the samples. Precisely, the luminescence enhancement of the molybdate based red phosphors (CL/GNM) is mainly because of the increase of the absorption strength of intra configurational *f-f* transitions arising from the CT band red shift, improvement of morphology and crystallinity via Bi^{3+} codoping.

The color purity of both CL/GNMB samples is checked by calculating CIE color co ordinates. All these samples are characterized by color co ordinates that are matching well with that of NTSC standard red phosphor (0.67, 0.33). The color co-ordinates of CLNMB samples are (0.61, 0.34) (for y = 0.07) and (0.62, 0.35) (for y = 0.08, 0.09, 0.10, 0.15). CGNMB samples have the color co ordinates of (0.65, 0.35) for all Bi^{3+} concentrations. The color co ordinates of CLNM9 and CGNM25 (Bi^{3+} uncodoped samples) are (0.59, 0.34) and (0.64, 0.33) respectively. Thus it is clear that Bi^{3+} codoping improved the color purity of the molybdate based red phosphors to some extent.

5A.4 Conclusions

Bi^{3+} codoped molybdate based red phosphors, $CaLa_{0.91-y}NbMoO_8$:$0.09Eu^{3+}$, yBi^{3+} and $CaGd_{0.75-y}NbMoO_8$: $0.25Eu^{3+}$, yBi^{3+} were synthesized via solid state reaction route. The influence of Bi^{3+} introduction on structural, microstructural and optical properties is investigated in detail. It is observed that Bi^{3+} incorporation improved the crystallinity as well as morphology leading to increased absorption strength of the samples. Another notable observation is the red shift of CT band of the samples and enhancement in the red emission intensity under both near UV and blue excitations. The intensity of red emission is improved by a factor of 1.14 and 1.2 for $CaLa_{0.91-y}NbMoO_8$: $0.09Eu^{3+}$, yBi^{3+} and $CaGd_{0.75-y}NbMoO_8$: $0.25Eu^{3+}$, yBi^{3+} respectively. The mechanism of luminescence enhancement by Bi^{3+} codoping is investigated and these phosphors are characterized by longer lifetime and good color purity pointing to the suitability of them for pc-WLED applications.

CHAPTER 5B

EFFECT OF Bi^{3+} CODOPING ON LUMINESCENT PROPERTIES OF $Ca(La/Gd)_{1-x}NbWO_8$: xEu^{3+} PHOSPHORS

5B.1 Introduction

Metal tungstates and molybdates are two important families of inorganic materials that have potential applications in various fields such as phosphors, optical fibers, scintillators, magnets and catalysts (Wang H *et al* 1992; Geng J *et al* 2005; Moszyn´ ski M *et al* 2005; Kato A *et al* 2005; Nazarov M. V *et al* 2004; Zhang G. X *et al* 2006). Tungstates doped with rare earth ions have shown incredible optical characteristics and hence considered as important optical materials. As mentioned in the previous chapters, red phosphors based on Eu^{3+} activated scheelite type tungstates are appropriate for pc-WLED applications because of the presence of broad - intense CT band arising from WO_4 tetrahedron unit, chemical stability and high average refractive index (Gundiah G *et al* 2008; Minami T *et al* 2003; Dai Q *et al* 2007). These red phosphors are utilizing the peculiarities of energy levels of both host lattice and activator ions for the efficient energy transfer process and luminescence performance. The red emission from Eu^{3+} activated phosphors under near UV or blue excitations are primarily due to forced electric dipole transition ($^5D_0$ - $^7F_2$) of Eu^{3+} and these transitions are hypersensitive to the site symmetry of the activator ion and its crystalline environment. Materials research in this regard has got more technological importance nowadays.

It would be much beneficial to improve the luminescence intensity of phosphor materials for practical applications. Specifically for the current red phosphors, the brightness is still a limitation (~8 times less than that of the green and blue phosphors). Thus various ways to achieve enhanced luminescence behavior and good color purity of the current red phosphors is to be understood. The codopant incorporation in various host lattices can improve their luminescence performance. The codopants can enhance luminescence intensity by acting as a flux or sensitizer and sometimes create oxygen vacancies in the host lattices or alter the crystal field surrounding the activator ions (Liu X *et al* 2007). In this regard, codoping of rare earth ions to tungstate based phosphor materials are studied by various research groups. Powell and co-workers studied the luminescent properties and energy transfer of $CaWO_4$: Eu^{3+} phosphors (Treadaway M. J *et al* 1974; Tyminski J. K *et al* 1982). However, these materials need a high doping concentration of activator (24 mol% Eu^{3+}) for the strong red emission (Yan S *et al* 2007) and the substitution of Eu^{3+} for Ca^{2+} site is non equivalent. To overcome some of these problems, many authors adopted charge compensation approach using Li^+, Na^+ or K^+ as a charge compensator (Shi S *et al* 2008). Co substitution of Sm^{3+}, Bi^{3+} has also been considered for improving the emission intensity of

Eu^{3+} (Wang Z *et al* 2006). The enhanced luminescence property of $CaWO_4$: Eu^{3+}, Bi^{3+} under UV excitation (277 nm) is studied by Pode et al and the energy transfer mechanism is also reported (Pode R. B *et al* 1997).

In Chapter 4 we had seen the optimum luminescence behavior of tungstate based scheelite type red phosphors, CL/GNW with respect to activator (Eu^{3+}) concentration. It is observed that the CT band position of these phosphors is located at a higher energy position (~290/303 nm) compared to that of the corresponding molybdate red phosphors (~313 nm). More over the CT band of tungstates is relatively shallower than the molybdates, due to the higher sixth ionization potential of Mo^{6+}. Thus there is an easy charge transfer transition in MoO_4 group than WO_4 group. In line with this, an attempt has been made to strengthen and shift the CT band of the aforementioned tungstate phosphors to a lower energy position. For this purpose, suitable codopant (Bi^{3+}) is introduced into the lattice and its effect on the structural, microstructural and luminescent properties is investigated in detail. The present part of this chapter elucidates the results regarding Bi^{3+} codoping in the CL/GNW phosphors. Role of Bi^{3+} in the luminescence mechanism is also incorporated.

5B.2 Experimental

Selected compositions of $CaLa_{0.80-y}NbWO_8$: $0.20Eu^{3+}$, yBi^{3+} (y = 0.10, 0.15, 0.20) (CLNWB) and $CaGd_{0.75-y}NbWO_8$: $0.25Eu^{3+}$, yBi^{3+} (y = 0.10, 0.15, 0.20, 0.25) (CGNWB) were synthesized by solid state reaction route. Stoichiometric amount of starting materials such as $CaCO_3$, La_2O_3/Gd_2O_3, Bi_2O_3, Nb_2O_5, WO_3, and Eu_2O_3 (Chemicals are from Acros Organics and Sigma Aldrich with 99.99% purity) were weighed and thoroughly wet mixed in an agate mortar with acetone as the wetting medium. The mixing was followed by drying in an air oven. The mixing and drying were repeated thrice to obtain a homogenous mixture and was calcined at 1200°C for 6 h in a platinum crucible in an air atmosphere furnace.

The crystal structure as well as the phase purity of the calcined samples were examined by recording the powder X ray diffraction patterns using a PANalytical X'pert Pro diffractometer with Ni filtered CuKα radiation (λ= 1.54056Å). The morphological analysis of the powder samples was done by a scanning electron microscope (JEOL, JSM- 5600LV). The UV Visible absorption spectra of the samples were recorded by UV–Vis Spectrophotometer (Shimadzu UV-2401). Photoluminescence excitation spectra and emission spectra were recorded using a Horiba Yvon Fluorolog® 3 Spectrofluorimeter with a 450W xenon flash lamp as the exciting source. To record the emission spectra, the excitation wavelength is fixed at 394/395 and 465 nm respectively and the emitted light intensity is measured at the wavelength range of 500 - 750 nm. For recording excitation spectra, the emission

monochromator is fixed at 613 nm emission wavelength and the excitation wavelength is scanned in 200 - 500 nm spectral range. Both the excitation and emission spectra were recorded by fixing the excitation and emission monochromator slit width at 0.5 and 1 nm respectively. The CIE chromaticity coordinates of the phosphors were also calculated. Luminescence lifetime of the phosphors was recorded by the phosphorimeter attached to Fluorolog® 3 Spectrofluorimeter.

5B.3 Results and Discussion

5B.3.1 Powder X ray diffraction analysis

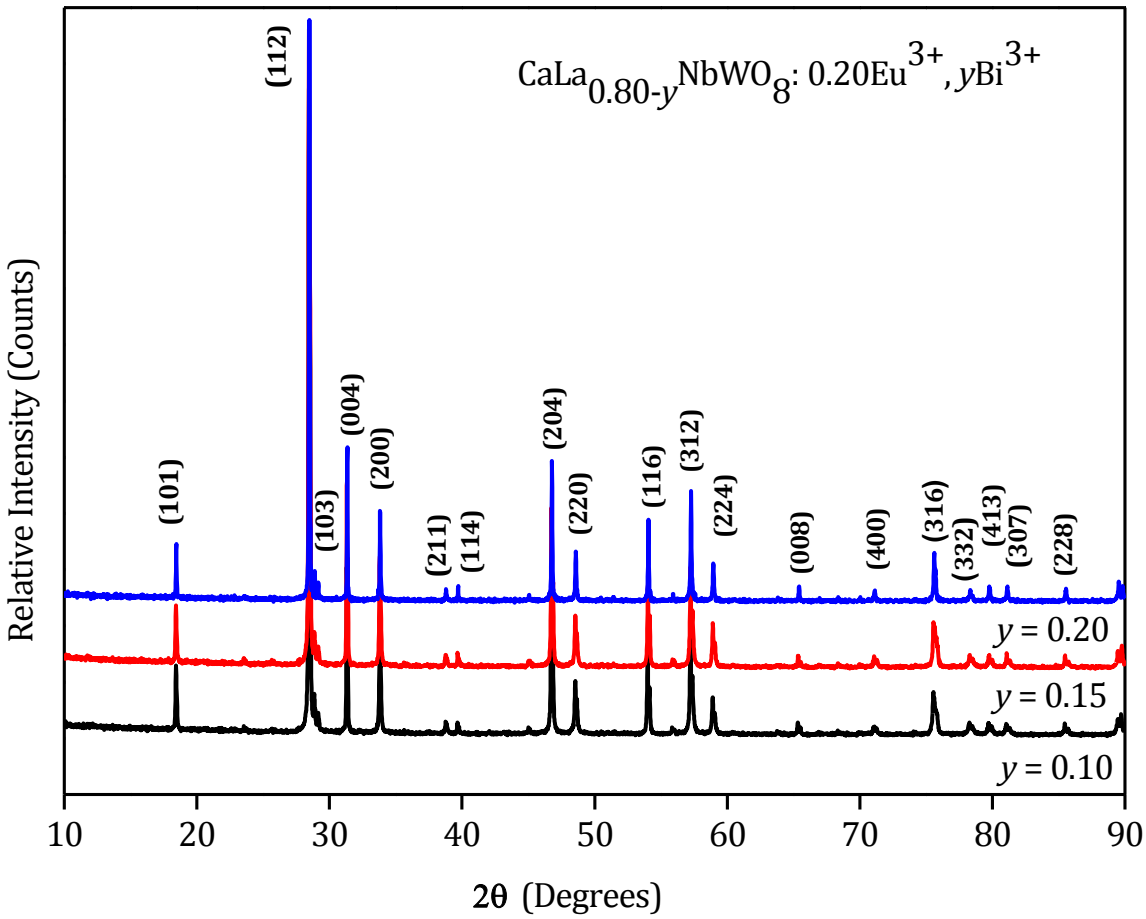

Fig. 5B.1 Powder X ray diffraction patterns of $CaLa_{0.80-y}NbWO_8$: $0.20Eu^{3+}$, yBi^{3+} (y = 0.10, 0.15, 0.20).

The X ray diffraction patterns of $CaLa_{0.80-y}NbWO_8$: $0.20Eu^{3+}$, yBi^{3+} (y = 0.10, 0.15, 0.20) (CLNWB) and $CaGd_{0.75-y}NbWO_8$: $0.25Eu^{3+}$, yBi^{3+} (y = 0.10, 0.15, 0.20, 0.25) (CGNWB) are shown in Fig. 5B.1 and Fig. 5B.2 respectively. All the peaks in the XRD patterns are very sharp, which indicate the crystalline nature of the samples. The phase purity of the prepared samples were confirmed by comparing the observed powder XRD pattern with the reported $CaWO_4$ (JCPDS file no.41-1431) tetragonal scheelite structure with the

space group $I4_1/a$ (88) and Z= 4 (Achary S. N *et al* 2006). The prominent peaks in the XRD patterns correspond to (101), (112), (004), (200), (204), (220), (116), (312) and (316) lattice planes. No traces of additional peaks from other phases are observed in Eu^{3+}, Bi^{3+} coactivated systems.

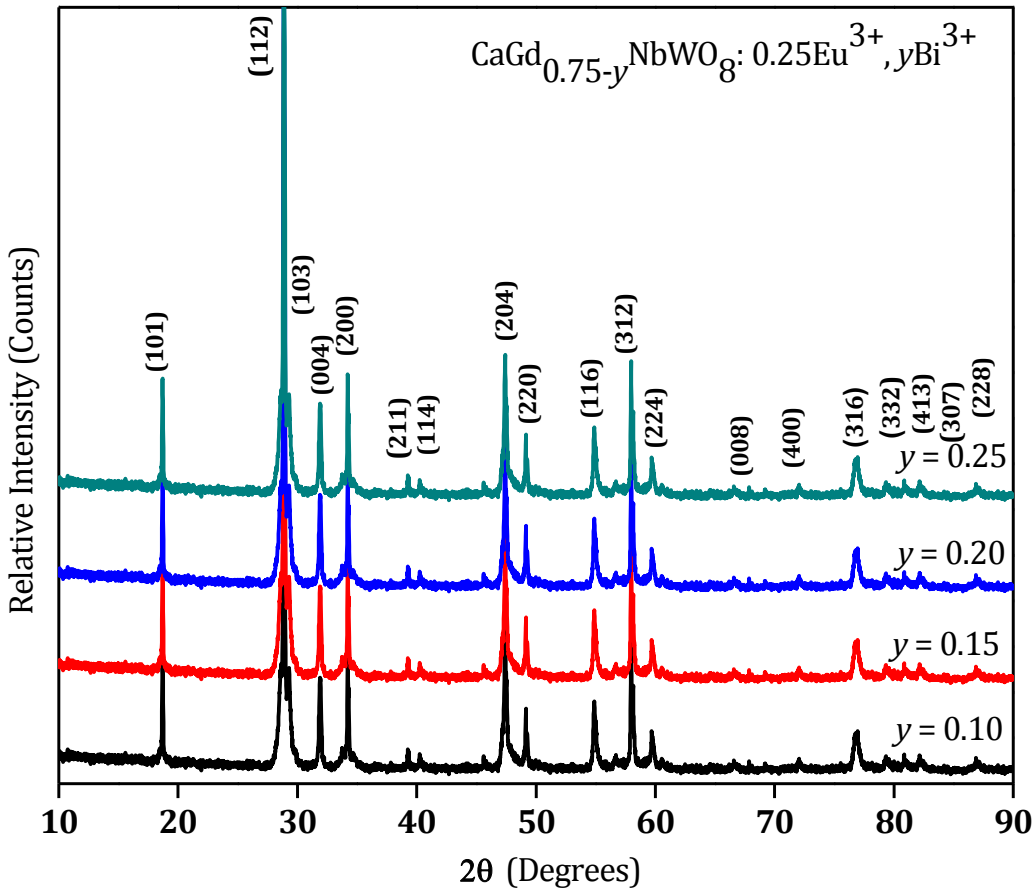

Fig. 5B.2 Powder X ray diffraction patterns of $CaGd_{0.75-y}NbWO_8$: $0.25Eu^{3+}$, yBi^{3+} (y = 0.10, 0.15, 0.20, 0.25).

Thus all the samples are single phase, forming solid solutions of $CaLa_{0.80-y}NbWO_8$: $0.20Eu^{3+}$, yBi^{3+} and $CaGd_{0.75-y}NbWO_8$: $0.25Eu^{3+}$, yBi^{3+}. Looking closer to the crystal structure, the host cations such as Ca^{2+}, La^{3+}/Gd^{3+}, and activator/coactivator ions such as Eu^{3+}/Bi^{3+} occupy eight coordinated sites, Nb^{5+} and W^{6+} share four coordinated sites. Since the ionic radii of Eu^{3+} [r = 1.07 Å when coordination number (CN) = 8] and Bi^{3+} (r = 1.17 Å when CN = 8) are close to that of La^{3+} (r = 1.16 Å when CN = 8) and Gd^{3+}(r = 1.05 Å when CN = 8), both $Eu^{3+}$and Bi^{3+} ions prefer the La^{3+} sites to occupy. It should be mentioned here that the phosphors were synthesized without any charge compensation approach as required in the case of $CaWO_4$: Eu^{3+}.

5B.3.2 Microstructural characterization

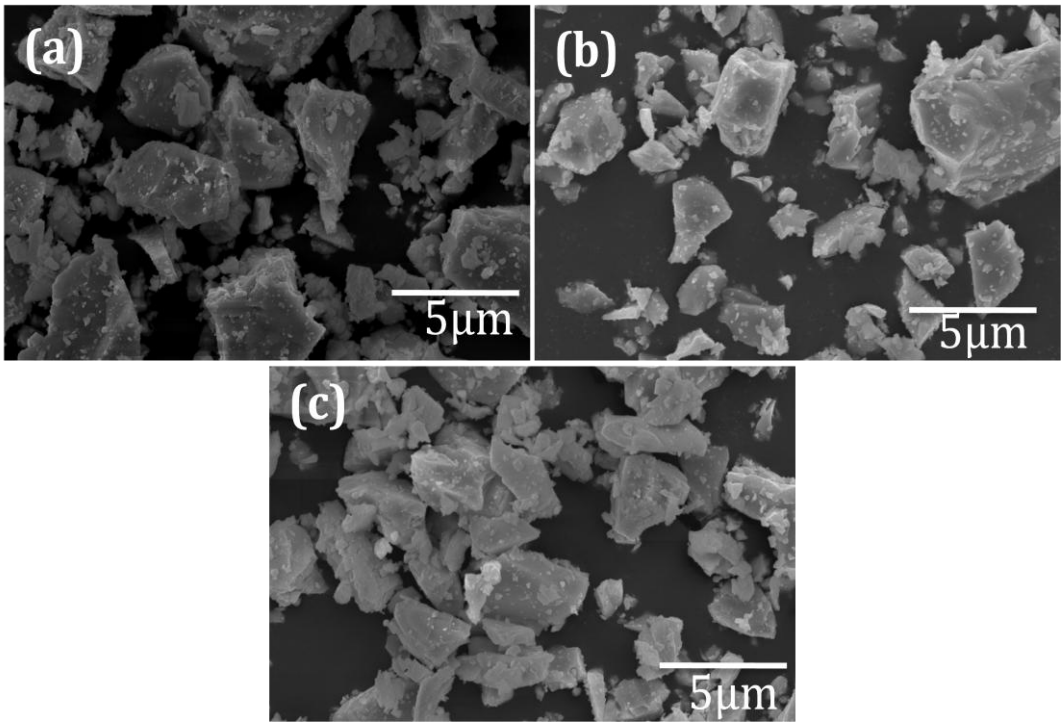

Fig. 5B.3 Scanning electron micrographs of $CaLa_{0.80-y}NbWO_8$: $0.20Eu^{3+}$, yBi^{3+} with varying Bi^{3+} concentrations: (a) y = 0.10, (b) y = 0.15, (c) y = 0.20 (x5, 000 magnification).

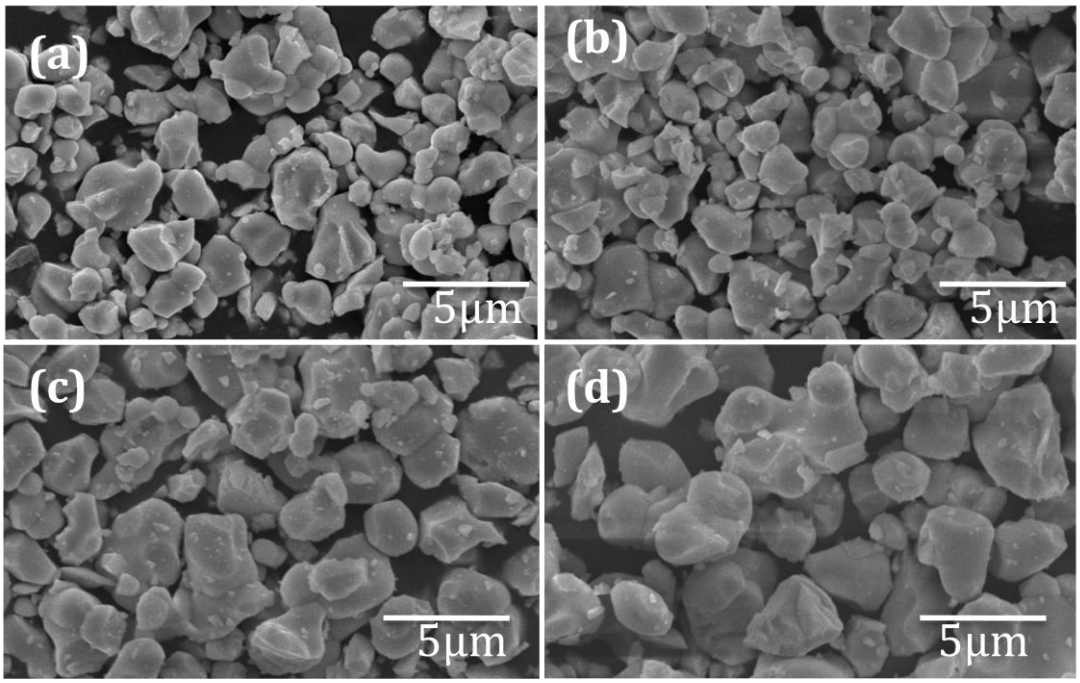

Fig. 5B.4 Scanning electron micrographs of $CaGd_{0.75-y}NbWO_8$: $0.25Eu^{3+}$, yBi^{3+} with (a) y = 0.10, (b) y = 0.15, (c) y = 0.20, (d) y = 0.25 (x 5, 000 magnification).

The scanning electron micrographs of CLNWB and CGNMB with varying Bi^{3+} concentration are presented in Fig. 5B.3 and Fig. 5B.4 (x5,000 magnification). The micrographs of the Bi^{3+} coactivated phosphors reveal their crystalline nature. The CLNWB samples are more agglomerated compared to that of CGNWB samples and they are characterized by sharp edges also. The morphology of CGNWB is improved to a great extent by Bi^{3+} codoping. Notable observations with respect to Bi^{3+} codoping are the reduction of particle agglomeration, relatively spherical nature of the particles, uniform shape and size distributions. Moreover on a closer look into the micrographs of CGNWB phosphors, it is seen that the particle size is increasing with Bi^{3+} concentration and becoming more homogenous. The smooth edges of the particles reduce the scattering loss. The morphological improvement of the tungstate based red phosphors is achieved with Bi^{3+} codoping and hence Bi^{3+} is acting as a flux in the present case. The average particle size of CL/GNWB is ~5µm. This notable improvement in the morphology of present samples can contribute strongly to their luminescence performance and is discussed in the succeeding sections.

5B.3.3 UV Visible absorption

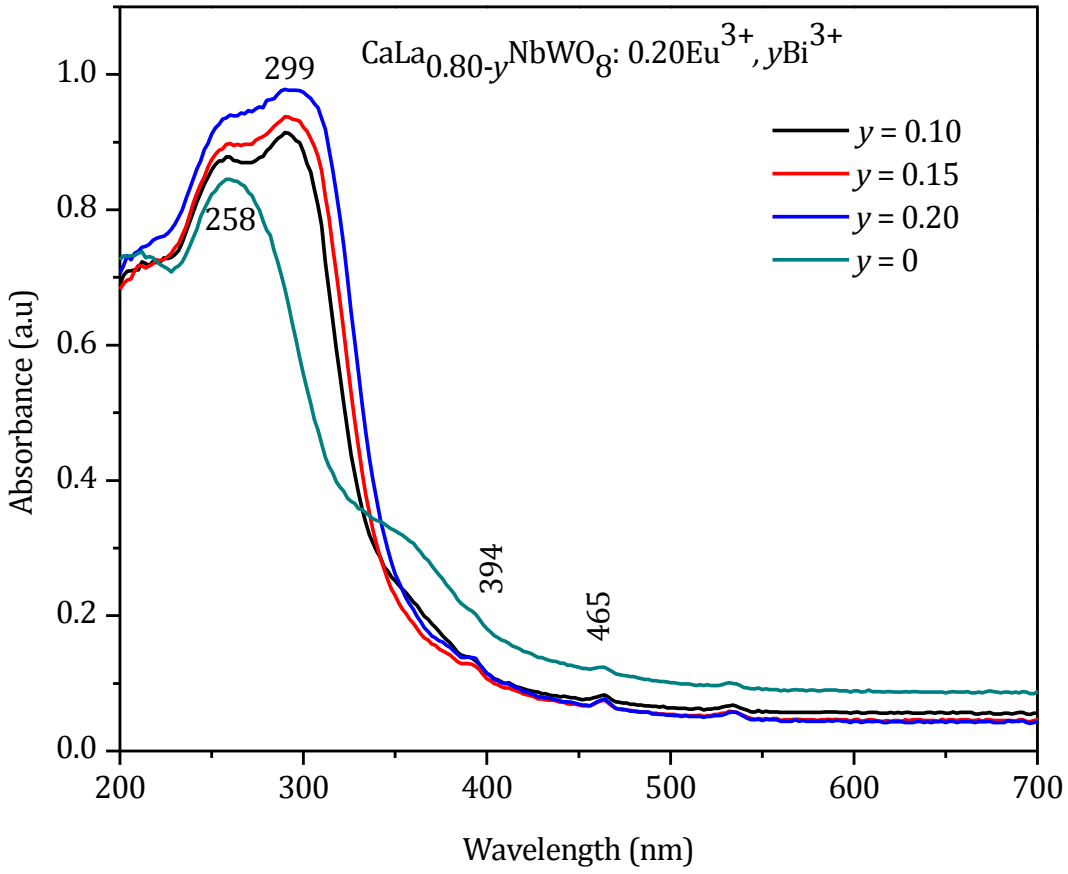

Fig. 5B.5 UV-Vis absorption spectra of $CaLa_{0.80-y}NbWO_8$: $0.20Eu^{3+}$, yBi^{3+} (y = 0, 0.10, 0.15, 0.20).

UV Visible absorption spectra of CL/GNWB with different Bi^{3+} codopant concentrations are shown in Fig. 5B.5 and Fig. 5B.6. The spectra of Bi^{3+} uncodoped (y = 0) sample are also included. It is observed that Bi^{3+} codoped samples also have almost same absorption spectral profile with a band of absorption in the UV region and sharp lines of absorption in the visible region.

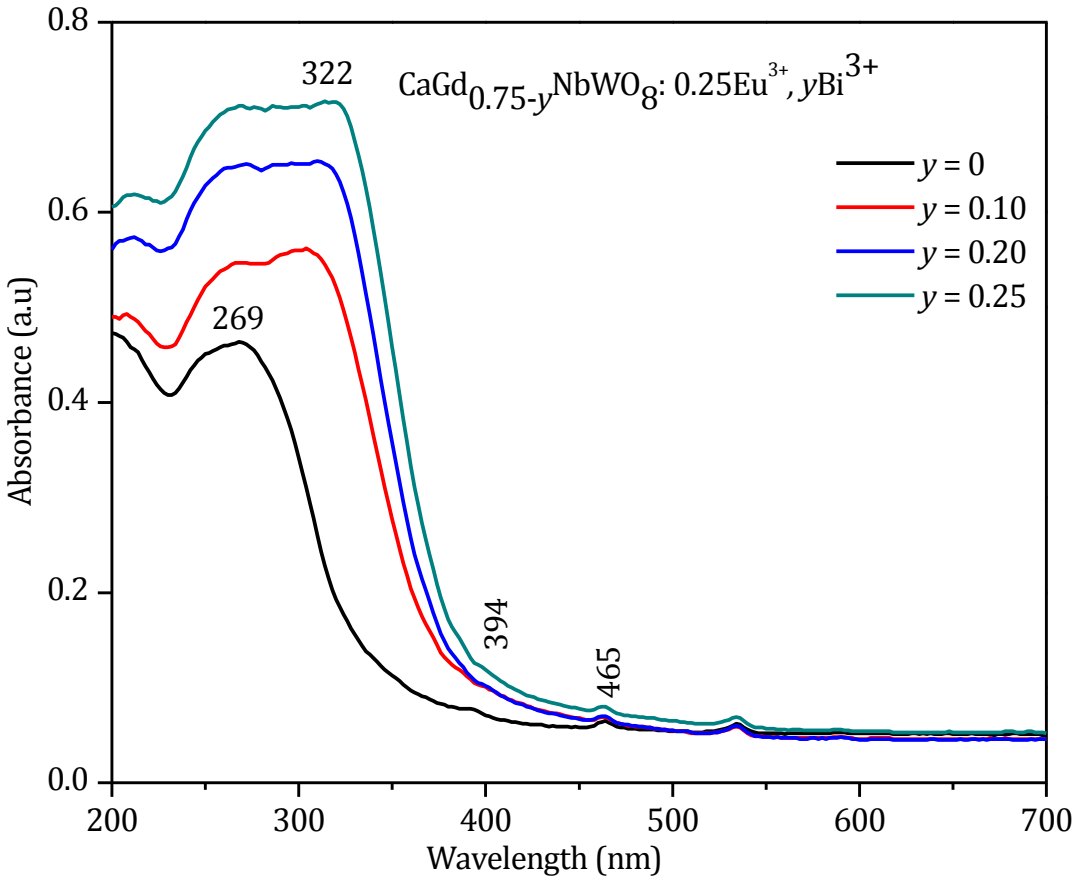

Fig. 5B.6 UV-Vis absorption spectra of $CaGd_{0.75-y}NbWO_8$: $0.25Eu^{3+}$, yBi^{3+} (y = 0, 0.10, 0.20, 0.25).

The notable variation observed for the Bi^{3+} codoped samples from uncodoped sample is the presence of an additional absorption band in the UV region. The first band of absorption centering at ~258 nm (CLNWB) and 269 nm (CGNWB) corresponds to the CT transitions arising from WO_4/ NbO_4 and O^{2-} - Eu^{3+} groups (Ahmad G *et al* 2006; Liu X *et al* 2007; Su Y *et al* 2008). The second band in the UV region is owing to the Bi^{3+} absorption via the electronic transition from ground state ($^0S_1$) to its excited states ($^1P_1$) (Xie A *et al* 2009). The absorption band for the Bi^{3+} codoped samples is extended to lower energy position compared to that of the Bi^{3+} uncodoped samples. The absorption lines due to intra configurational *f-f* transitions (394 and 465 nm) of Eu^{3+} are clearly observable in the present case unlike the Bi^{3+} codoped molybdate (CL/GNMB) samples. Also the intensity of these two absorption peaks is

increasing with Bi^{3+} concentration. The increase in the absorption strengths of the peaks at 394 and 465 nm positions lead to an increase in their excitation intensity and the corresponding emission. Thus Bi^{3+} codoping in the tungstate based samples broadened their absorption band in the UV region and consequently a red shift of the absorption edge, which is a prior requisite for a phosphor for pc-WLED application.

5B.3.4 Photoluminescence properties

5B.3.4.1 Excitation spectra

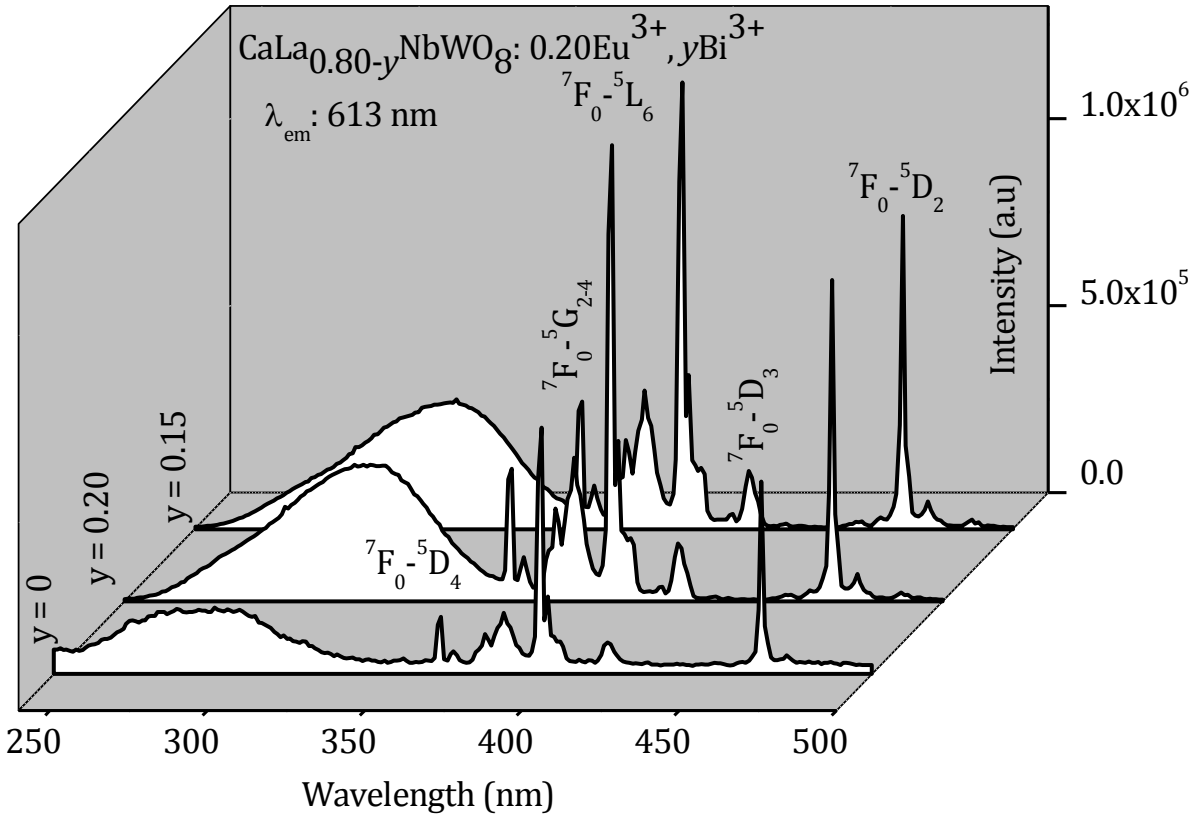

Fig. 5B.7 Excitation spectra of $CaLa_{0.80-y}NbWO_8$: $0.20Eu^{3+}$, yBi^{3+} (y = 0, 0.15, 0.20) for an emission at 613 nm.

The photoluminescence excitation spectra of CL/GNWB phosphors for an emission at 613 nm with different Bi^{3+} concentration are shown in Fig. 5B.7 and Fig. 5B.8. The spectra of Bi^{3+} uncodoped samples (y = 0) are also shown. The spectra of both Bi^{3+} codoped and uncodoped samples show broad band of excitation at UV region and sharp peaks from near UV to visible region. The broad band of excitation is due to the CT transitions of O - W/O - Nb in the WO_4/NbO_4 group, and that of Eu^{3+} - O^{2-} (Pode R. B *et al* 1997; Hsiao Y. J *et al* 2007). The CT band of Bi^{3+} uncodoped samples is in the range of 240 - 350 nm, and is

centered at ~290 nm (CLNW) and ~303 nm (CGNW). With the introduction of Bi^{3+} in CLNW and CGNW lattices, the CT band is extended to a longer wavelength of ~360 nm. Consequently, the CT band is red shifted from 290 to 324 nm (CLNWB) and 303 to 327 nm (CGNWB). A remarkable increase in the relative intensity of CT band is also observed with Bi^{3+} codoping. Thus, with Bi^{3+} codoping in the tungstate based samples, the CT band becomes broader and stronger. The sharp peaks of both CL/GNWB samples are observed at 362, 383, 394/395, 416, 465 nm and are corresponding to the $^7F_0$–$^5D_4$, $^7F_0$–$^5G_{2,4}$, $^7F_0$–$^5L_6$, $^7F_0$–$^5D_3$, $^7F_0$–$^5D_2$ transitions respectively (Blasse G 1979), which have no significant variation in the energy position.

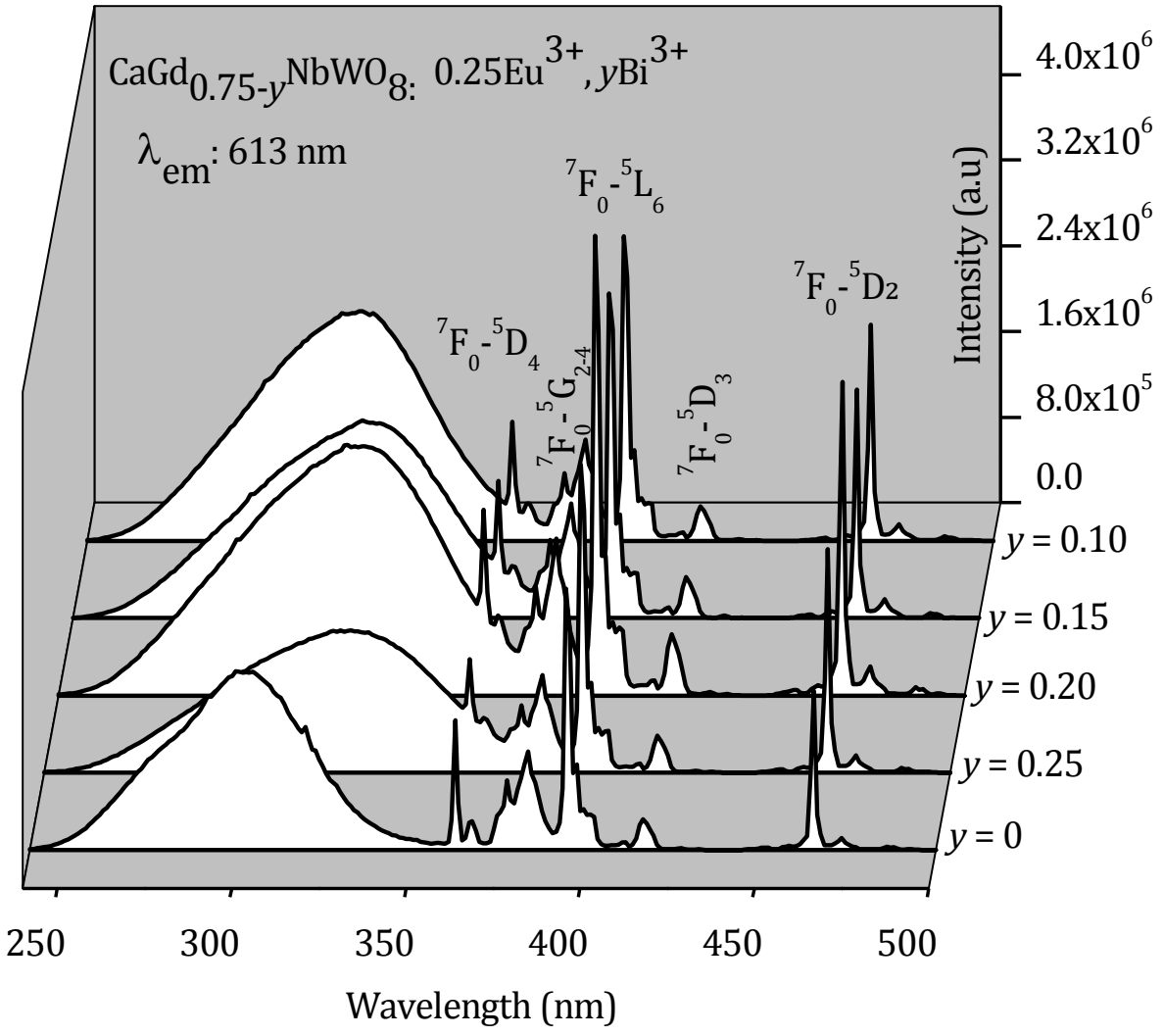

Fig. 5B.8 Excitation spectra of $CaGd_{0.75-y}NbWO_8$: $0.25Eu^{3+}$, yBi^{3+} (y = 0, 0.10, 0.15 0.20, 0.25) for an emission at 613 nm.

The red shift of CT band observed in the case of Bi^{3+} codoped tungstates, CL/GNWB is mainly due to Bi^{3+} absorption. Bi^{3+} ion has an outer $6s^2$ configuration with a ground state of $^1S_0$. The excited states have a 6*s*6*p* configuration and are splitting into $^3P_0$, $^3P_1$, $^3P_2$ and $^1P_1$ levels in the sequence of energy increase. If no other configurations are taken into account, the transitions from $^1S_0$ to $^3P_0$ and $^3P_2$ are completely spin forbidden. The other two excited levels $^3P_1$ and $^1P_1$ are mixed by spin–orbit coupling. Thus, the broad absorption from 300 to 360 nm is an overlap of the transition from $^1S_0$ to $^3P_1$ and $^1P_1$ levels (Shin S. H *et al* 2001).

In the first part of this chapter we had seen that, Bi^{3+} codoping in molybdate based red phosphors red shifted the CT band position with no significant improvement in its intensity. But in the present case of tungstate based samples, it is clearly observed that both red shift and intensification of CT band happened with Bi^{3+} codoping. As mentioned in the earlier chapters, (MoO_4) groups in molybdates are in general having strong CT band while tungstates are characterized by shallow CT band positioned at comparatively higher energy region. The enhanced CT band in the solid solution phosphors (CL/GNM) containing MoO_4 can be explained by the fact that Mo has a higher sixth ionization potential (70 eV) than W (61eV) (Lee G. H et al 2011). That is, Mo has a greater tendency to receive an electron from an oxygen ligand and MoO_4 requires a lower energy for ligand - metal charge transfer (LMCT). By the introduction of Bi^{3+} in the current tungstate based red phosphors, the absorption process between Bi^{3+} energy levels (from $^1S_0$ to $^3P_1$ and $^1P_1$) prominently contributed to the intensification of the CT band. In other words, Bi^{3+} codoping in tungstate based samples enhanced the probability of CT from WO_4 group. In line with the Bi^{3+} absorption process the red shift of the CT band is also observed.

The dependence of excitation intensity of intra configurational transitions such as $^7F_0$–$^5L_6$ (394 nm) and $^7F_0$–$^5D_2$ (465 nm) of CL/GNWB phosphors with respect to Bi^{3+} concentrations is presented in Fig. 5B.9(a) and Fig. 5B.9(b) respectively. It is observed that all the Bi^{3+} codoped samples have more excitation intensity compared to that of uncodoped analogues. For CLNWB samples, the excitation intensity is linearly increasing upto 20 mol% of Bi^{3+} but for CGNWB samples, the intensity of excitation is reducing beyond 20 mol% of Bi^{3+}. This may be due to the formation of aggregates in the samples at higher concentrations of codopant ions which are acting as killers or quenchers of luminescence performance of the phosphor.

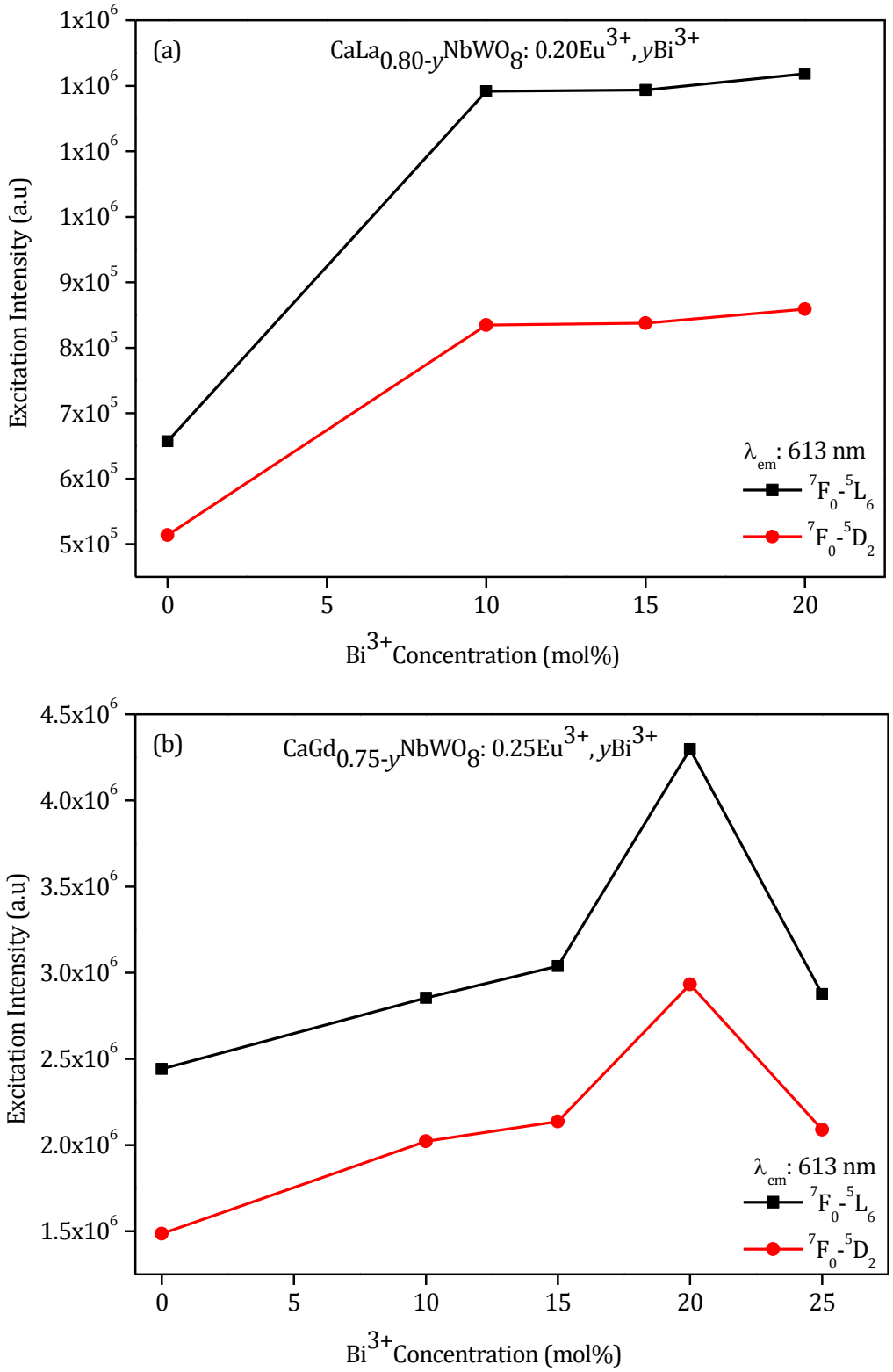

Fig. 5B.9 Dependence of excitation intensity (λ_{em}: 613 nm) of $^7F_0$-$^5L_6$ and $^7F_0$-$^5D_2$ transitions of (a) $CaLa_{0.80-y}NbWO_8$: $0.20Eu^{3+}$, yBi^{3+} (y = 0, 0.10,0.15, 0.20) and (b) $CaGd_{0.75-y}NbWO_8$: $0.25Eu^{3+}$, yBi^{3+} (y = 0, 0.10,0.15, 0.20, 0.25).

The improvement in these excitation intensity or absorption strength of the samples directly increases the luminescence emission intensity under the same excitation. Major

motive for the enhancement in the intra configurational excitation intensity with Bi^{3+} codoping is the red shift of CT band, better morphology and crystallinity of the samples. This red shift in the CT band can contribute indirectly to the enhancement of excitation intensity of parity forbidden intra configurational *f-f* transitions of Eu^{3+}. The detailed discussion on these aspects is included in the coming section.

In the earlier chapter, we have seen a marginal improvement in the luminescence emission intensity for CL/GNMB phosphors compared to the uncodoped samples (CL/GNM). However, it is expected that the enhancement in the CT band intensity and intra configurational *f–f* transition intensity and red shift of CT band by Bi^{3+} codoping will enhance the luminescence emission intensity of CL/GNWB samples to a great extent.

5B.3.4.2 Emission spectra

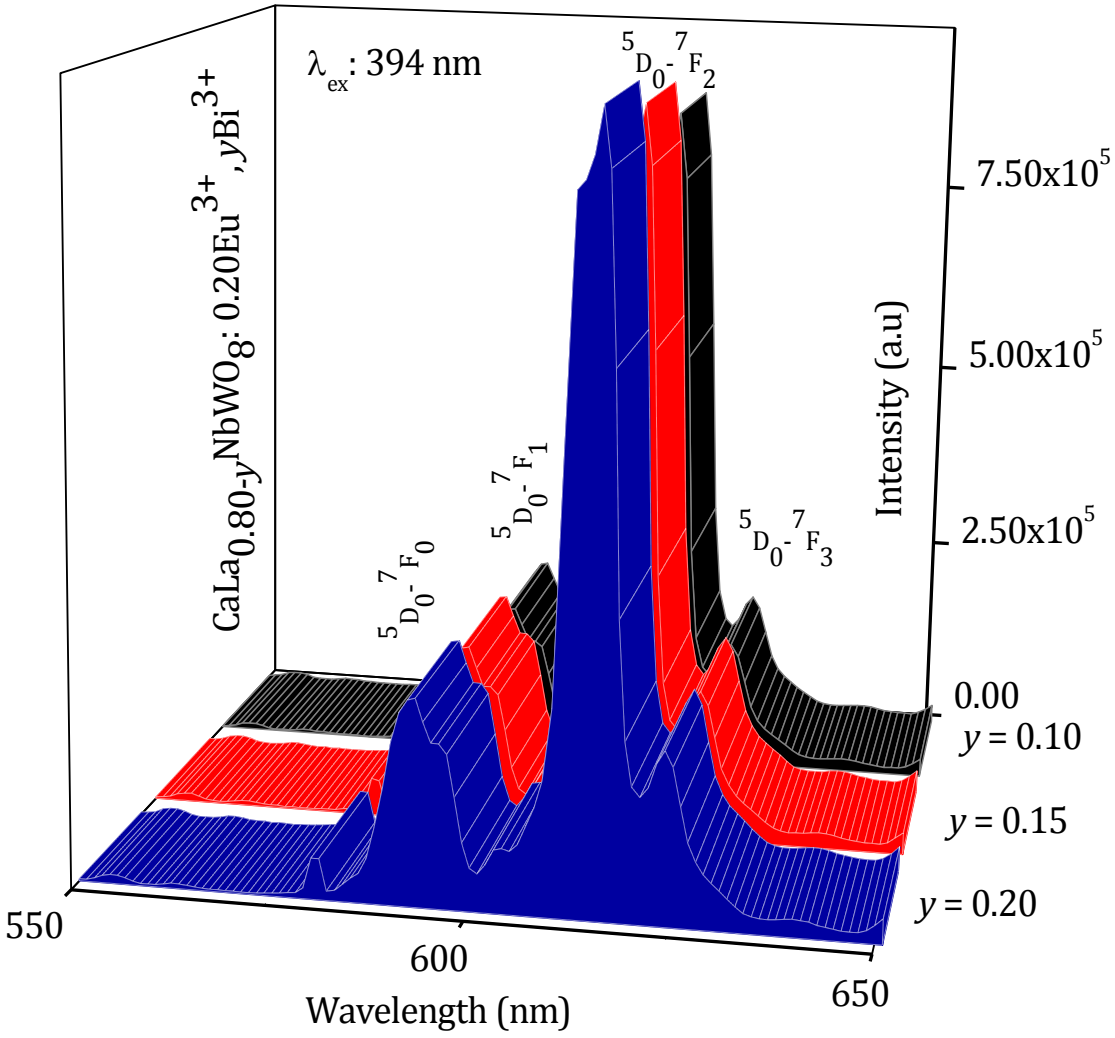

Fig. 5B.10 Emission spectra of $CaLa_{0.80-y}NbWO_8$: $0.20Eu^{3+}$, yBi^{3+} (y = 0.10, 0.15, 0.20) under 394 nm excitation.

The emission spectra of CLNWB (y = 0.10, 0.15, 0.20) and CLNWB (y = 0, 0.10, 0.15, 0.20, 0.25) samples under near UV excitation are shown in Fig. 5B.10 and Fig. 5B.11 respectively. The spectral profile of Bi^{3+} codoped samples are same as that of the uncodoped samples. The spectra include emission peaks corresponding to intra configurational *f-f* transitions ($^5D_0 - {}^7F_J$, J = 0, 1, 2) of Eu^{3+} (Liu X *et al* 2007). Similar emission spectra are observed under blue (465 nm) excitation also. The dominant red emission peak observed at 613 nm is due to parity forbidden $^5D_0 - {}^7F_2$ electric dipole transition which hints that Eu^{3+} is also occupying in a non centrosymmetric site in the Bi^{3+} codoped samples (Xie A *et al* 2009).

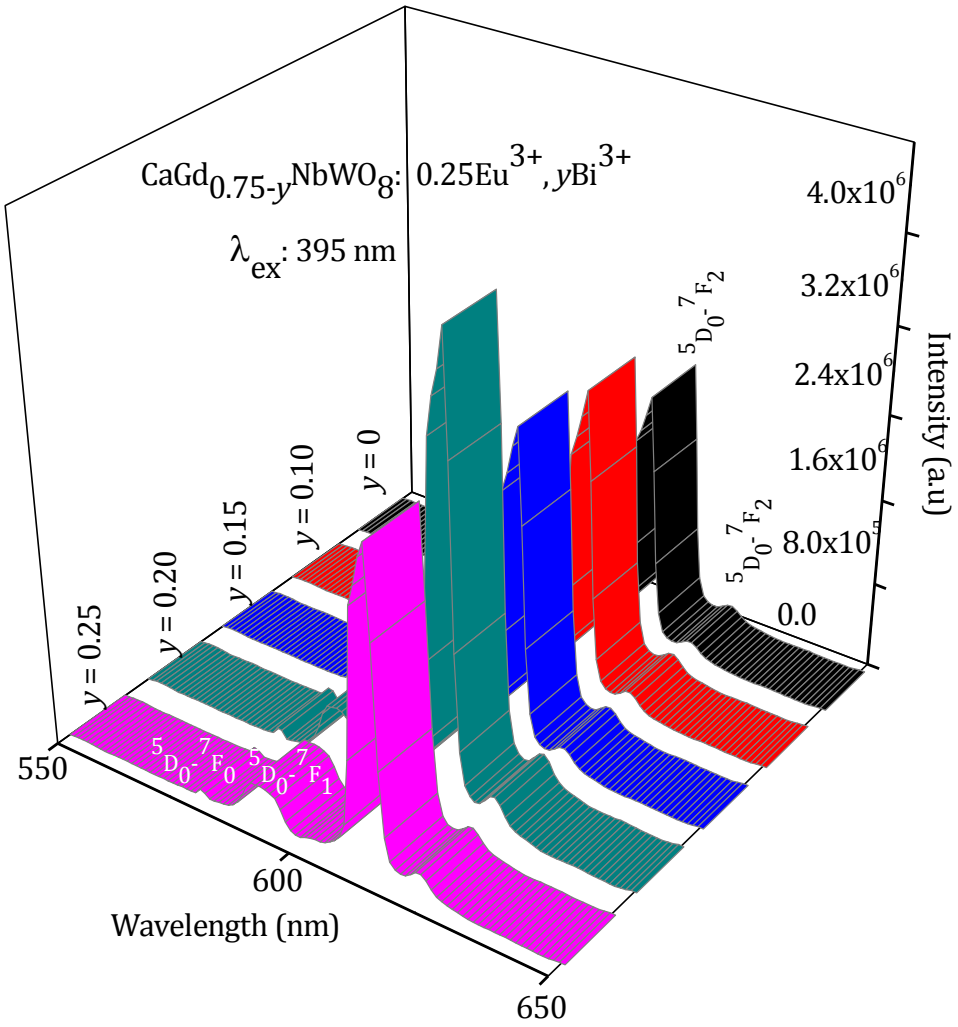

Fig. 5B.11 Emission spectra of $CaGd_{0.75-y}NbWO_8$: $0.25Eu^{3+}$, yBi^{3+} (y = 0, 0.10, 0.15, 0.20, 0.25) under 395 nm excitation.

In the present samples, Eu^{3+} is occupying the non centrosymmetric A site shared by Ca^{2+}, La^{3+}/ Gd^{3+} and Bi^{3+} ions. It is observed that the emission intensity of the CLNWB is increasing with respect to Bi^{3+} concentration and for CGNMB phosphors; it is observed that

the red emission intensity is increasing with Bi^{3+} concentration upto 20 mol% and it starts decreasing beyond that. This observation is in line with that of the excitation spectra. When compared with Bi^{3+} uncodoped samples (y = 0, CLNW20 & CGNW25) the red emission intensity of CLNWB and CGNWB samples is doubled.

Considering the factors such as lifetimes and absorption strengths of CL/GNWB phosphors, their luminescence mechanism can be well understood. For this, a closer look into the decay curves and absorption or excitation spectra of CL/GNWB with different codopant (Bi^{3+}) concentration is essential.

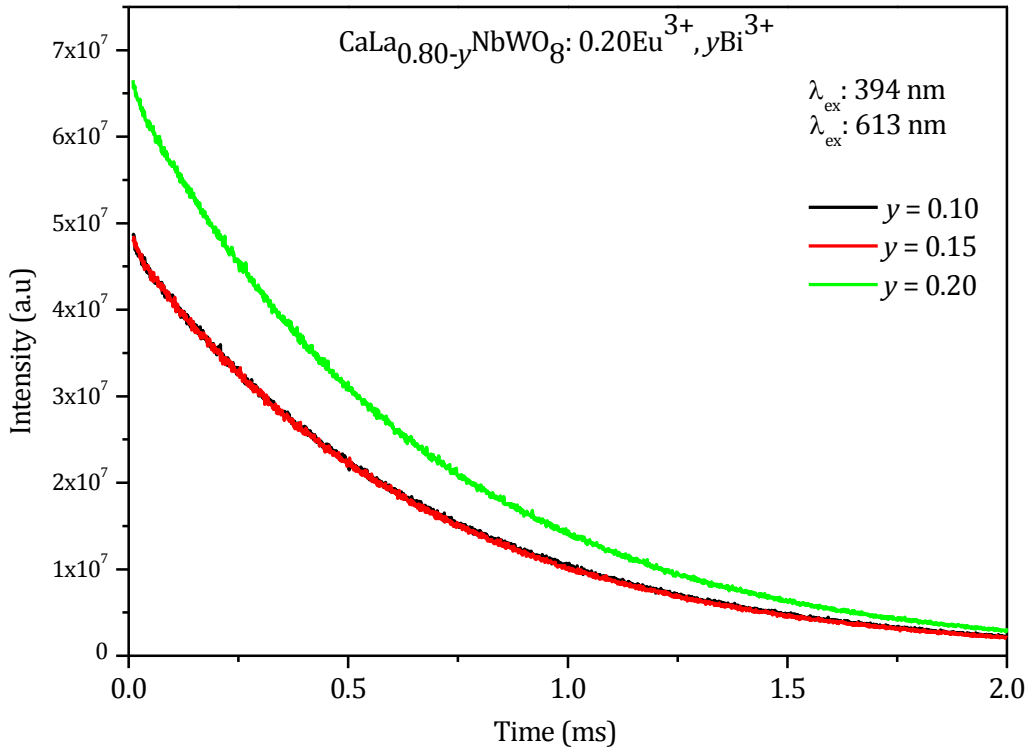

Fig. 5A.12 Decay curves of $CaLa_{0.80-y}NbWO_8$: $0.20Eu^{3+}$, yBi^{3+} (y = 0, 0.10, 0.15, 0.20) under near UV excitation.

Table 5B.1 Lifetimes of $CaLa_{0.80-y}NbWO_8$:$0.20Eu^{3+}$, yBi^{3+} and $CaGd_{0.75-y}NbWO_8$: $0.25Eu^{3+}$, yBi^{3+} phosphors under near UV excitation

Sample	**$CaLa_{0.80-y}NbWO_8$:$0.20Eu^{3+}$, yBi^{3+}**			**$CaGd_{0.75-y}NbWO_8$:$0.25Eu^{3+}$, yBi^{3+}**			
y	0.01	0.15	0.20	0.01	0.15	0.20	0.25
Lifetime (ms)	0.6593	0.6512	0.6629	0.7118	0.7202	0.6765	0.6277

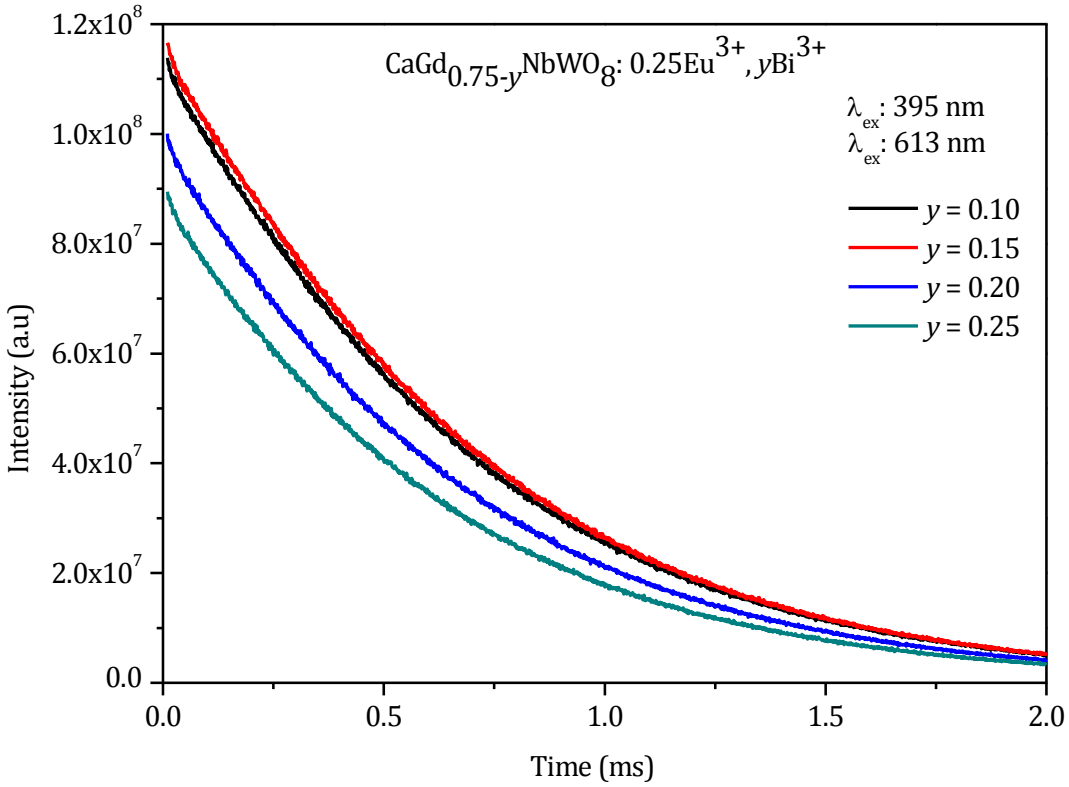

Fig. 5A.13 Decay curves of $CaGd_{0.75-y}NbWO_8$: $0.25Eu^{3+}$, yBi^{3+} (y = 0, 0.10, 0.15, 0.20, 0.25) under near UV excitation.

The decay curves of the samples under near UV excitation with different Bi^{3+} concentrations are shown in Fig. 5B.12 and Fig. 5B.13. The decay curves for $^5D_0$ excited state (emission level in CL/GNWB) of Eu^{3+} for both samples show single exponential behavior and is well fitted with the function I = A exp (-x/τ) where I, τ and A are intensity, decay time and fitting parameter respectively and the corresponding lifetimes of phosphors are enlisted in Table 5B.1. It is observed that the lifetime of tungstate based phosphors are not showing any notable regular variation with Bi^{3+} codoping. Consequently, quantum efficiency of the phosphors is hardly affected by Bi^{3+} codoping similar to that of CL/GNMB.

The absorption strength of the samples is the other factor to be considered with the Bi^{3+} codopant incorporation in tungstate based phosphors. From the excitation spectra and absorption spectra of the samples, it is clearly observed that the absorption strength of both CL/GNWB phosphors is increased compared to that of their uncodoped samples. Specifically, the intensity of $^7F_0$–$^5L_6$ (394/395 nm) and $^7F_0$–$^5D_2$ (465 nm) transitions (excitation wavelengths of phosphors) are increasing linearly upto 20 mol% of Bi^{3+}in CL/GNWB phosphors (Fig. 5B.9). The observation of increase of absorption strength of phosphors with Bi^{3+} is similar to that of corresponding molybdates discussed in the earlier part of this chapter.

The different factors that might contribute to the increase of absorption strength of phosphors such as symmetry distortions, morphology, crystallinity, CT band position and intensity are to be checked in the present case of tungstate based red phosphors also (Blasse G 1979; Su Q *et al* 1995). In CL/GNWB phosphors, the Bi^{3+} and Eu^{3+} are respectively sharing the site occupied by La^{3+} and Gd^{3+} and all are having the same oxidation state and matching ionic radii. In other words, no significant symmetry distortion to the Eu^{3+} crystalline environment is expected in the CL/GNWB lattice similar to that of CL/GNMB. The asymmetry ratio (I_{590}/I_{613}) of CL/GNWB is in the range of ~ 9 – 8 with Bi^{3+} concentration. Thus in the present case also there is only a minor contribution of symmetry variations to the improvement of parity forbidden *f-f* transition. From XRD and SEM analysis, it is observed that Bi^{3+} has improved the crystallinity as well as morphology of the phosphors. The presence of relatively spherical particles lead to efficient absorption of light irradiated on the phosphor surface and thereby better excitation process. The scattering loss is also reduced to some extent.

Looking closer into the aspect of the position and intensity of CT band of CL/GNWB phosphors with Bi^{3+} codoping, we had seen a red shift of ~34 nm (CLNWB) and ~24 nm (CGNWB) with respect to Bi^{3+} codoping in comparison with the uncodoped samples. The amount of red shift of tungstate based phosphors is more than that of the corresponding molybdates, CL/GNMB (~17 nm). This makes an easier CT process in the tungstates with Bi^{3+} codoping. In addition to the red shift in the CT band position, a remarkable increase in the intensity of CT band is observed in both CL/GNWB phosphors and is in contrast to that of CL/GNMB phosphors. The red shift in the CT band position and increase of its intensity act as a channel for enhancing the probability of intra configurational transitions in CL/GNWB phosphors and their luminescence performance. i.e., the parity forbidden will achieve intensity via non radiative energy transfer from the lowest strong absorption band which is the CT band (Su Q *et al* 1995).

Another aspect responsible for the enhancement of luminescence is the energy transfer from Bi^{3+} to Eu^{3+} and it can be of radiative or non radiative nature. The excitation spectra (λ_{em}: 490 nm) of $CaLa_{0.8}NbWO_8$: $0.2Bi^{3+}$ sample exhibits a band centered around 313 nm (shown in the inset of Fig. 5B.14) and is consistent with the excitation spectrum of $CaLa_{0.6}NbWO_8$: $0.2Bi^{3+}$, $0.2Eu^{3+}$. It is also clear from Fig. 5B.13 that there is a considerable spectral overlap between the Eu^{3+} excitation transitions and the emission band of Bi^{3+}, $^3P_1$ - $^1S_0$ centered at 490 nm, suggesting the occurrence of resonance radiative energy transfer from Bi^{3+} to Eu^{3+} (similar for CGNWB also).

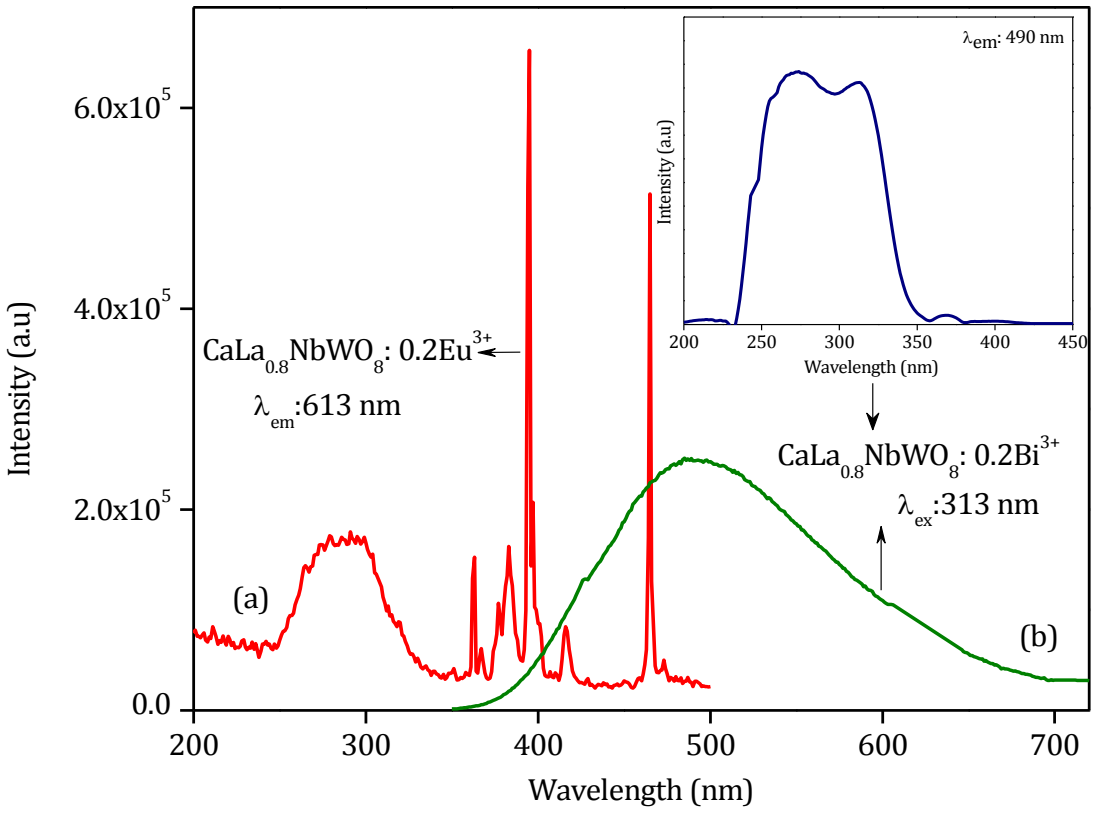

Fig. 5B.14 Spectral overlap between the excitation spectrum of (a) $CaLa_{0.80}NbWO_8$: $0.20Eu^{3+}$ (λ_{em}: 613 nm) and emission spectrum of (b) $CaLa_{0.80}NbWO_8$: $0.20Bi^{3+}$ (λ_{ex}:313 nm).

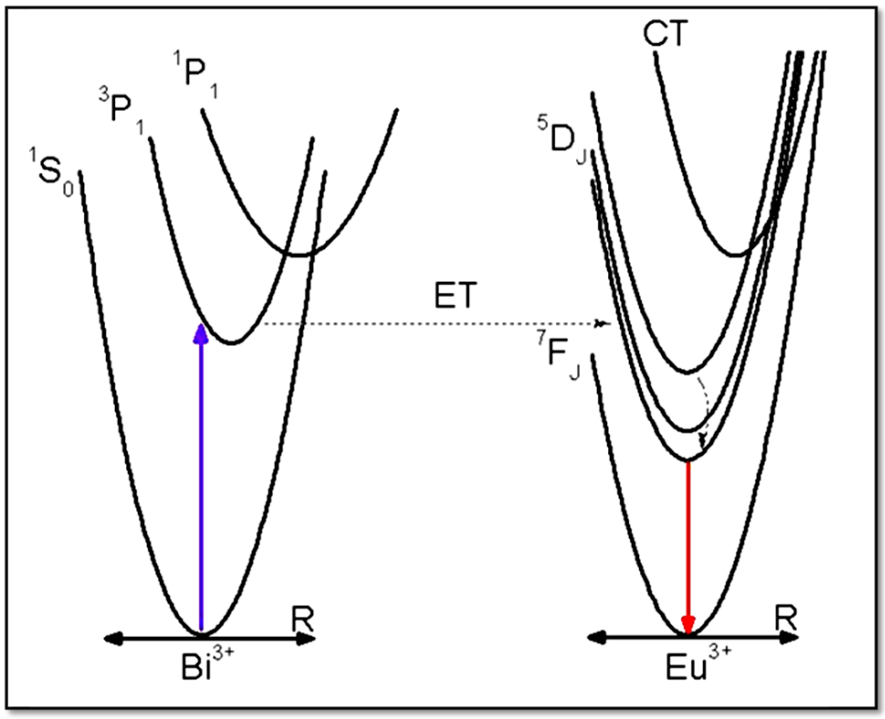

Fig. 5B.15 Schematic configurational coordinate diagram for Bi^{3+} and Eu^{3+} and the possible energy transfer process from Bi^{3+} to Eu^{3+} under the excitation of 313 nm.

However, this effectively occurs in the UV region (under an excitation of 313 nm). i.e., when the phosphor is excited by wavelength corresponding to the Bi^{3+} excitation wavelength of 313 nm, the excited energy state of Bi^{3+} ($^3P_1$) relaxes to its ground state ($^1S_0$) and the corresponding energy is transferred to the 4*f* levels of Eu^{3+} resulting in a red emission through the $^5D_0$-^7F_J transition of Eu^{3+}.

Schematic representation of this process is shown in Fig. 5B.15. However this type of resonance radiative energy transfer process is not utilized in the current phosphors, since they are excited by near UV (395 nm) and blue irradiations (465 nm) corresponding to Eu^{3+} intra configurational transition wavelengths. The same ET process happens when the samples are excited to CT states (under an excitation of 324 or 327 nm), where the CT states will transfer energy to Eu^{3+} excited state instead of Bi^{3+} energy levels.

Another ET process is the non radiative process and it occurs from the CT states of the CL/GNWB phosphors to excited levels of Eu^{3+} and is schematically illustrated in Fig. 5B.16.

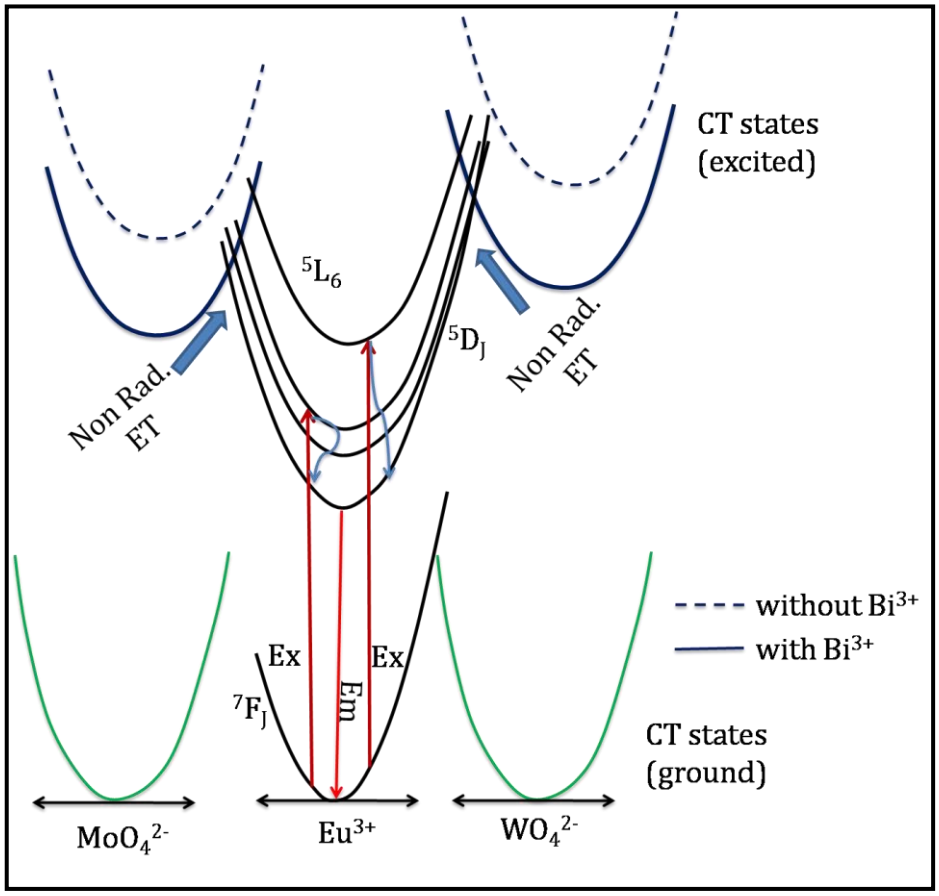

Fig. 5B.16 Configurational co-ordinate diagram of the possible non radiative energy transfer process from CT states to Eu^{3+} level under near UV or blue excitations.

We had already seen that the CT states of Bi^{3+} uncodoped tungstates (CL/GNW) are positioned at a higher energy region (290 and 303 nm) and is shifted to a lower energy position (324 and 327 nm) via Bi^{3+} codoping. Thus there is more possibility for the overlap between the CT states and *f-f* levels of Eu^{3+}; leading to a non radiative ET from the CT states to excited levels ($^5L_6$ and $^5D_2$) of Eu^{3+} and attaining more intensity for *f-f* transitions (Blasse G 1979; Struck *et al* 1970) Lifetime variation of the phosphors (both tungstates and molybdates) can also be related to this. This process happens in molybdate based phosphors (CL/GNMB) also and is more effective in the current tungstate based red phosphors (CL/GNWB).

These phosphors are also characterized by good color purity and its CIE chromaticity co ordinates are (0.64, 0.35), which are comparable to that of NTSC standards. Thus in the Bi^{3+} codoped tungstates also, the increase of absorption strength via CT band red shift, morphological improvement and crystallinity played key role in luminescence enhancement.

5B.4 Conclusions

In conclusion, scheelite type tungstate based red emitting phosphors, $CaLa_{0.80-y}NbWO_8$: $0.20Eu^{3+}$, yBi^{3+} and $CaGd_{0.75-y}NbWO_8$: $0.25Eu^{3+}$, yBi^{3+} have been synthesized by solid state reaction route and its structural, microstructural and photoluminescent properties are investigated in detail. It is observed that Bi^{3+} codoping improved the crystallinity as well as morphology of the samples. Notable observations in the luminescence properties with Bi^{3+} coping are the red shift and intensification of CT band of excitation (unlike to the corresponding molybdates) leading to an increment in the absorption strength of the phosphors. The photoluminescent properties of $CaLa_{0.80-y}NbWO_8$: $0.20Eu^{3+}$, yBi^{3+} points out that the samples exhibit enhanced (~2 times) red emission of Eu^{3+} (615 nm) under the excitation of near UV and blue light that correspond to the emission lines from near UV and blue LED, The possible mechanism behind luminescence enhancement is explored. With the incorporation of Eu^{3+} and Bi^{3+} in the host lattice, host sensitized non radiative energy transfer is effectively occurred in the current phosphor samples. The phosphors also exhibit sharp red emission peaks with good color purity having matching color co ordinates of standard red phosphors.

CHAPTER 6

MORPHOLOGICAL IMPROVEMENT AND LUMINESCENT PROPERTIES OF $Ca(La/Gd)_{1-x}NbMo/WO_8$: xEu^{3+} PHOSPHORS

In addition to the position and intensity of CT band, the physical properties of powellite/ scheelite type molybdate/ tungstate phosphors such as crystallinity, surface area, morphology and distribution of activator etc. have crucial roles in determining their luminescence properties. These properties can be controlled by variation in the synthesis method and heat treatment process. The optimized red phosphors are synthesized via citrate gel route and the effect of heat treatment process on their luminescence properties is also investigated. Particle morphology of the phosphors prepared by the CG route has been improved. The red phosphors prepared via CG route were characterized by sharper red emission with longer lifetime compared to that of phosphors synthesized via SSR route. The variation of lifetime with respect to heat treatment process revealed the possibility of overlap of CT states of phosphor with f-f levels and hence non radiative energy transfer process. The mechanism of luminescence enhancement with respect to variation in the synthesis method and heat treatment process is discussed in detail.

J. Am. Ceram. Soc. *95[7] (2012) 2260.*

CHAPTER 6A

MORPHOLOGICAL IMPROVEMENT AND LUMINESCENT PROPERTIES OF $Ca(La/Gd)_{1-x}NbMoO_8$: xEu^{3+} PHOSPHORS

6A.1 Introduction

Phosphor materials play a key role in making SSL based on White Light Emitting Diodes (WLEDs) as a source of general illumination. Thus better performance of phosphor materials is essential. For effective photoluminescence emission, the activator should absorb large amount of excitation energy and simultaneously the excited electrons return to the ground state by the radiative process. If the host material and the activator concentration are optimized, their luminescence efficiency strongly depends on the physical properties. The major physical properties of a phosphor material include surface area, crystallinity, phase purity and the distribution of activator in the host matrix (Bosze E. J *et al* 2003; Sun Y *et al* 2004; Lenggoro I. W *et al* 2004; Pang M. L *et al* 2004). Such properties can be influenced by the method of synthesis and the preparation temperature. The preparation temperature strongly influences the luminescence intensity of phosphor since it directly changes the crystallinity, crystal phase, surface area of host materials and the distribution of activator ions. For the same phosphor these properties are variable if the synthesis process changes.

Most of today's phosphor materials are synthesized via solid state reaction route (SSR) using powdered raw materials as the starting materials. This approach usually requires high temperatures and subsequent grinding to obtain phosphors with designed compositions and desired performances (Ye S *et al* 2010). The grinding process damages the phosphor surfaces resulting in the loss of emission intensity (Boyer D *et al* 1999; Jung M. K *et al* 2007). In addition, the aggregation and the inhomogeneous shape are also unavoidable, which inhibit the absorption of the excitation energy and therefore reduce the emission intensity (Pang M. L *et al* 2004). Therefore a simple and economical method for making high quality phosphors is desirable. There are various synthesis methods such as sol gel, citrate gel, co precipitation and combustion methods that ensure easy mixing of precursor solutions at the molecular level, providing a high degree of homogeneity at low processing temperatures, and making doping of activators, coactivators or sensitizers straightforward and effective (Rao R. P 1996; Wang S. F *et al* 2009; Guo C *et al* 2009; Kumar A *et al* 2011). Citrate gel (CG) method is one of the most important techniques for the synthesis of various functional materials because it offers many advantages over conventional solid state method in the synthesis of fine powders and particularly phosphor materials, such as higher uniformity in particle size distribution, non agglomeration and higher photoluminescent intensity.

Ample research efforts have been there to develop molybdate based red phosphors via various synthesis routes other than SSR method to achieve better luminescence properties. Nano sized $CaMoO_4$ powders were successfully synthesized at low temperatures by a modified citrate complex method using microwave irradiation. The variation of their luminescence property with respect to heat treatment process from 400 to 700°C is reported and it is observed that heat treatment process improved the luminescence emission intensity of $CaMoO_4$ phosphor (Ryu H. J *et al* 2005). Guo et al synthesized $Gd_{2-x}Eu_x(MoO_4)_3$ red phosphors via sol gel method and improved the morphology and red emission compared to that synthesized by SSR route (Guo C *et al* 2008). In addition, the effects of annealing temperature, time and Eu^{3+} doping concentration on the luminescence intensities were also investigated in detail. Microassemblies of $CaMoO_4$: Eu^{3+} red phosphors were synthesized by hydrothermal method by Yu (Yu F *et al* 2011). A potential red phosphor, $NaGd(MoO_4)_2$: Eu^{3+} has been prepared by sol gel method and the luminescence properties are studied in detail by Liao (Liao J *et al* 2010).

In this regard, we made an attempt to synthesize molybdate and tungstate based red phosphors (discussed in chapters 3&4) via citrate gel route. It is observed that phosphors developed by the citrate gel method are formed at a lower temperature and its luminescence emission intensity is better than that of the phosphors synthesized by the SSR method. Effect of heat treatment on the luminescent properties of the phosphors developed by the citrate gel method was also explored. Heat treatment has improved the average particle size, crystallinity and effective red emission. Experimental details and results of molybdate based red phosphors are presented in the first part of this chapter (6A) and that of tungstate based red phosphors are included in the next part (Part 6B) of this chapter.

6A.2 Experimental

Typical compositions $CaLa_{0.91}NbMoO_8$: $0.09Eu^{3+}$ (CLNM9) and $CaGd_{0.75}NbMoO_8$: $0.25Eu^{3+}$ (CGNM25) were synthesized by the citrate gel method (CG). $CaCl_2.2H_2O$, $La/Gd(NO_3)_3.6H_2O$, $NbCl_5$, $(NH_4)_6Mo_7O_{24}.4H_2O$, $Eu(NO_3)_3.5H_2O$ (Sigma Aldrich,99.9% purity) were used as starting materials. Distilled water and citric acid (Sigma Aldrich, 99.9% purity) were used as solvent and chelating agent for the process. The citrate solution was prepared by dissolving appropriate amount of citric acid in distilled water. After complete homogenization of citrate solution, all the cationic solutions were dissolved in the citrate solution (1:5). The solution was kept for constant stirring for 1 h for homogenous mixing and concentrated by keeping it in the water bath (maintained at 100°C) for 3h and the solution became viscous gel. The gel was dried to form a brown colored product and then powdered

by grinding in an agate mortar which is the precursor. Heat treatment of the precursor was then carried out at various temperatures from 700 to 1000°C.

The crystal structure as well as the phase purity of the samples were examined by recording the powder XRD patterns using a PANalytical X'pert Pro diffractometer with a Ni filtered CuKα radiation (λ = 1.54056Å). The morphological analysis of the powder samples were recorded by a scanning electron microscope (JEOL, JSM-5600LV). Photoluminescence excitation spectra, emission spectra and decay time curves were recorded using a Horiba Yvon Fluorolog® 3 spectrofluorimeter with a 450W xenon flash lamp as the exciting source. CIE chromaticity coordinates of the phosphors were also calculated.

6A.3 Results and Discussion

6A.3.1 Powder X ray diffraction analysis

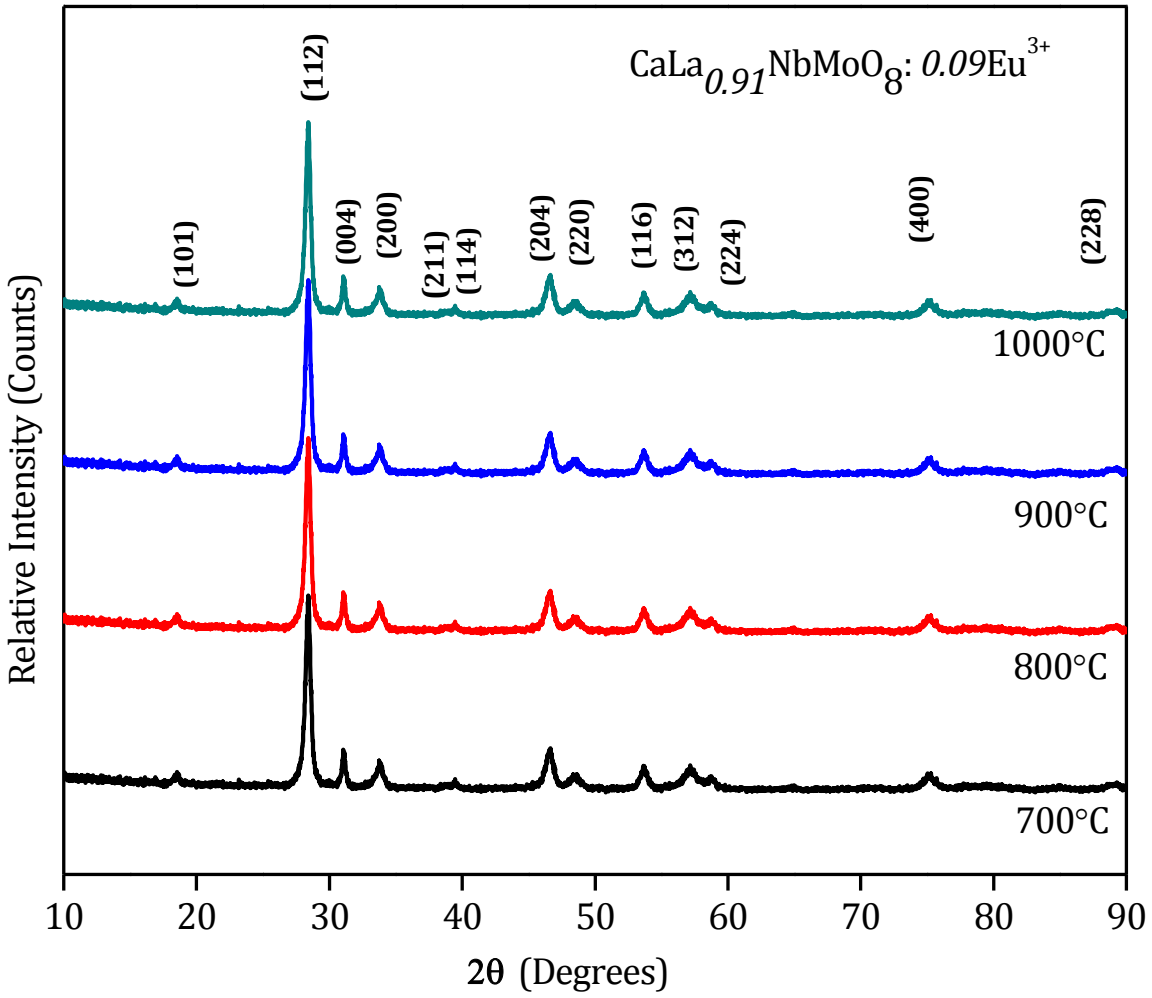

Fig. 6A.1 Powder X ray diffraction patterns of $CaLa_{0.91}NbMoO_8$: $0.09Eu^{3+}$ phosphors heat treated at different temperatures from 700 to 1000°C.

The powder X ray diffraction pattern of $CaLa_{0.91}NbMoO_8$: $0.09Eu^{3+}$ (CLNM9) and $CaGd_{0.75}NbMoO_8$: $0.25Eu^{3+}$ (CGNM25) synthesized via CG route and heat treated at different temperatures from 700 to 1000°C is presented in Fig. 6A.1 and Fig. 6A.2.

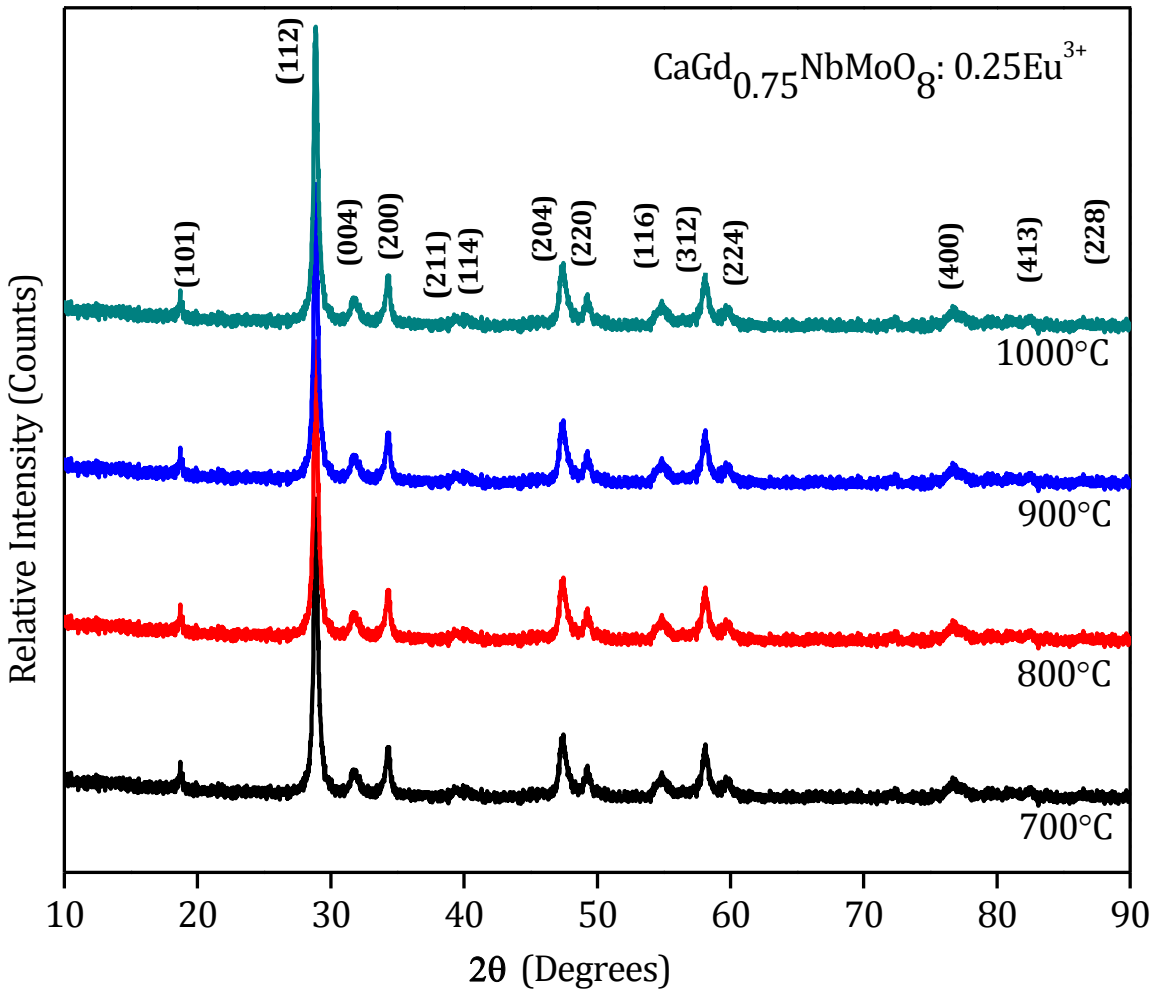

Fig. 6A.2 Powder X ray diffraction patterns of $CaGd_{0.75}NbMoO_8$: $0.25Eu^{3+}$ phosphors heat treated at different temperatures from 700 to 1000°C.

Sharp peaks in the X ray diffraction patterns indicate the crystalline nature of the samples. All the peaks in the X ray diffraction patterns are matching well with that of $CaMoO_4$ (JCPDS file no. 29-0351) with a space group $I4_1/a$ (88) (Ravindran Nair K *et al* 2008). The prominent peaks in the XRD patterns correspond to (101), (112), (004), (200), (204), (220), (116), (312), and (400) lattice planes. There are no traces of extra peaks from impurities in the pattern. It is observed that phase formation of both phosphors takes place at 700°C, which is a lower calcination temperature compared to that of the samples prepared by SSR route. The diffraction peaks of the sample prepared by CG method are broader than that

prepared by SSR route, which hints the reduction of average crystallite size of the phosphor material. With respect to heat treatment process, the relative intensity and sharpness of all the peaks are increasing. This implies the extent of improvement of crystallinity and crystallite size with heat treatment process from 700 to 1000°C.

The average crystallite size of the phosphors is calculated using Scherrer formula (Chen G Y *et al* 2007),

$$D_{av} = 0.91\lambda / \beta\cos\theta \qquad (6A.1)$$

where,

D_{av} - Average crystallite size

λ - Wavelength of Cu K$\propto$ radiation (1.54056 Å)

β - Full Width at Half Maximum (FWHM)

θ - Bragg angle (Glancing angle).

The variation of average crystallite size of both phosphors with respect to heat treatment process is included in Table 6A.1.

Table 6A.1 The variation of average crystallite size with respect to heat treatment process

Temperature (°C)		700	800	900	1000
Av. Crystallite Size (nm)	**CLNM 9**	25.47	45.26	58.20	67.90
	CGNM 25	23.90	40.78	50.98	58.26

6A.3.2 Microstructural characterization

The scanning electron micrographs of $CaLa_{0.91}NbMoO_8$: $0.09Eu^{3+}$ (CLNM9) (x40,000) and $CaGd_{0.75}NbMoO_8$: $0.25Eu^{3+}$ (CGNM25) (x30,000) synthesized via CG route and heat treated at different temperatures from 700 to 1000°C are presented in Fig. 6A.3 and Fig. 6A.4.

For both CLNM9 and CGNM25 samples, particles are less agglomerated and the particle size is reduced. Particles have uniform size and shape compared to the morphology of SSR samples. Moreover the particles are relatively spherically shaped and have smooth edges. With respect to heat treatment from 700-1000°C the average particle size is increasing. The average size is about 100 nm to 0.5 μm, which fits to fabricate solid state lighting devices. In addition, the surface of the samples prepared by SSR route is coarser than that of samples prepared by CG route also SSR route samples are irregular in shape. Thus an improvement in morphology as well as average particle size of molybdate red phosphors is achieved by variation in the synthesis method.

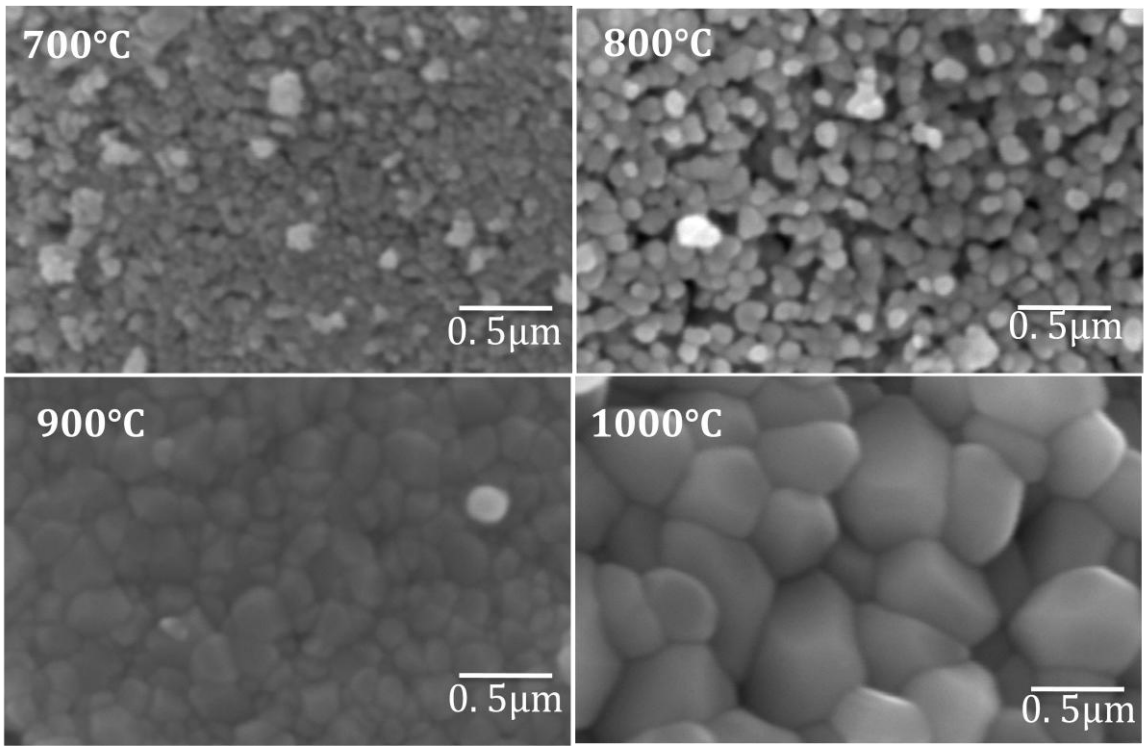

Fig. 6A.3 Scanning electron micrographs (x 40,000) of phosphor powders of $CaLa_{0.91}NbMoO_8$: $0.09Eu^{3+}$ heat treated from 700 to 1000°C.

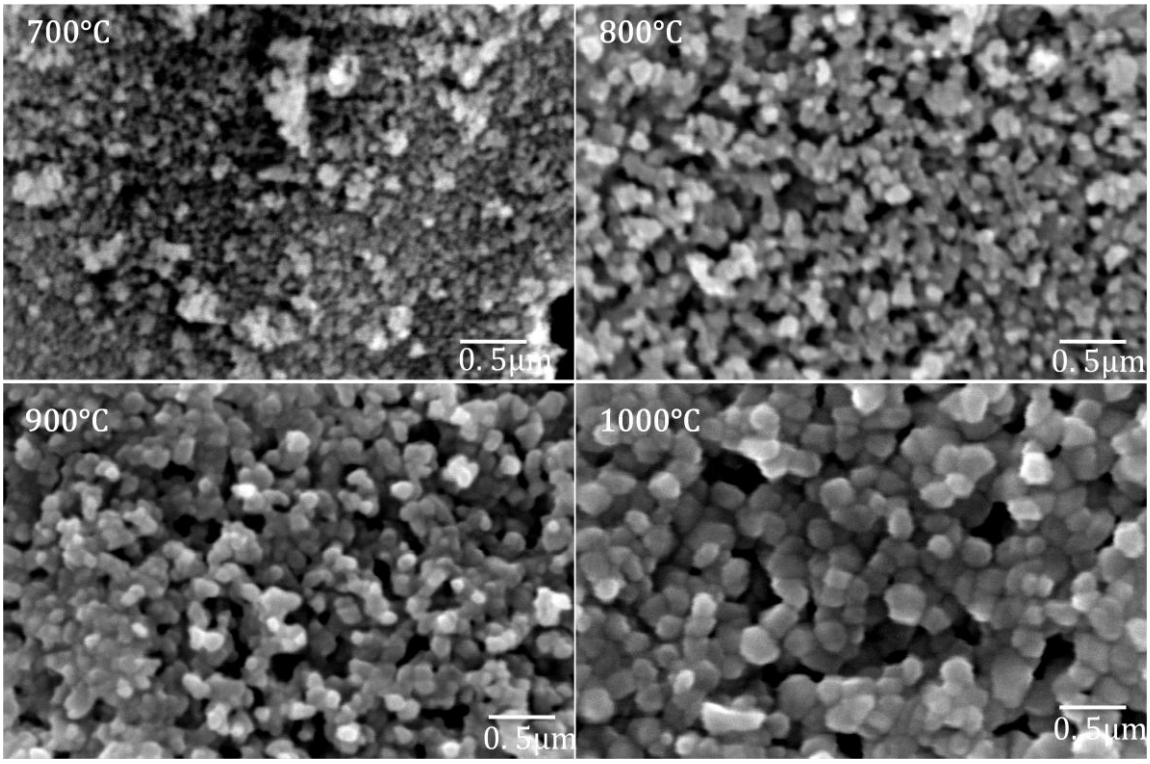

Fig. 6A.4 Scanning electron micrographs (x 30,000) of phosphor powders of $CaGd_{0.75}NbMoO_8$: $0.25Eu^{3+}$ heat treated from 700 to 1000°C.

This improvement in the morphology with respect to synthesis method has improved the red emission of the phosphors and the morphological effect on luminescence enhancement is discussed in the later section.

6A.3.3 Photoluminescence properties

6A.3.3.1 Excitation spectra

Fig. 6A.5 and Fig. 6A.6 show the excitation spectra of CLNM9 and CGNM25 phosphors synthesized via CG route and heat treated at different temperatures from 700 to 1000°C for an emission at 613 nm. (The excitation spectra of SSR route analogues are also included in the figures).

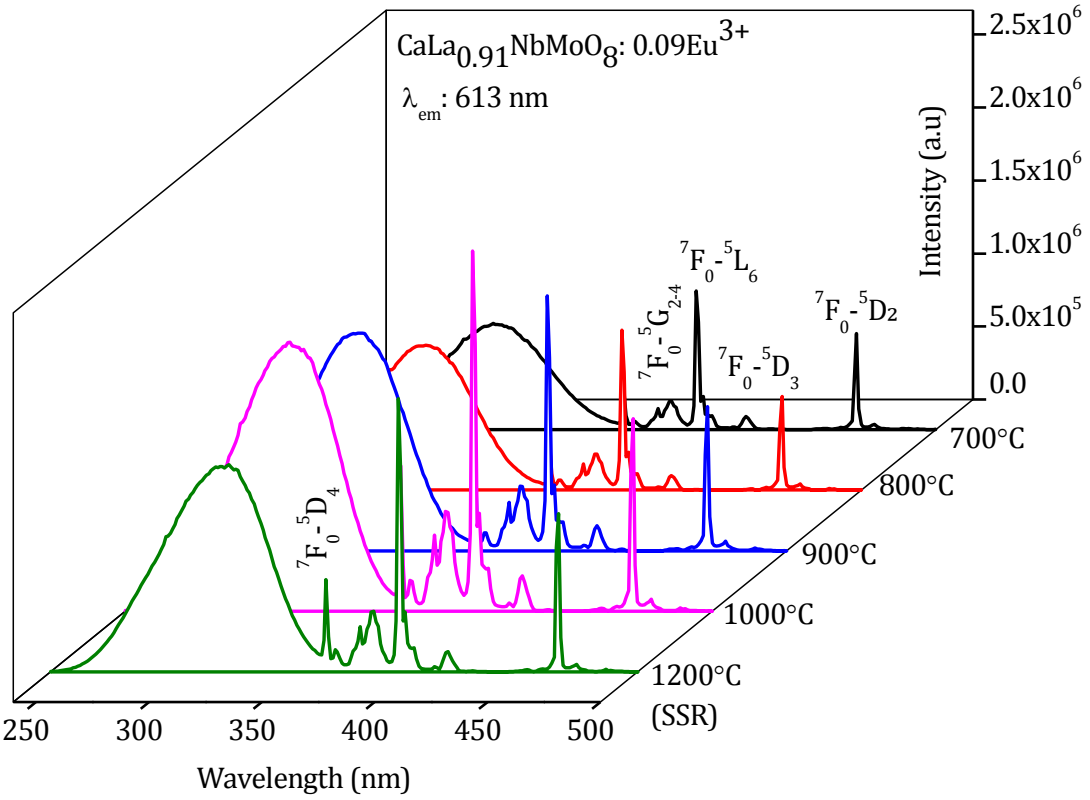

Fig. 6A.5 Excitation spectra of $CaLa_{0.91}NbMoO_8$: $0.09Eu^{3+}$ heat treated from 700 to 1000°C for an emission at 613nm.

Similar to that of the SSR route samples, the excitation spectra of both CLNM9 and CGNM25 phosphors include broad band (240-360 nm, peaking around 313 nm) and sharp peaks (beyond 360 nm) of excitation corresponding to the charge transfer (CT) transitions from Eu^{3+} - O^{2-}, MoO_4 and NbO_4 groups and Eu^{3+} intra configurational *f-f* transitions respectively (Hu Y *et al* 2005; Hsiao Y. J *et al* 2007).

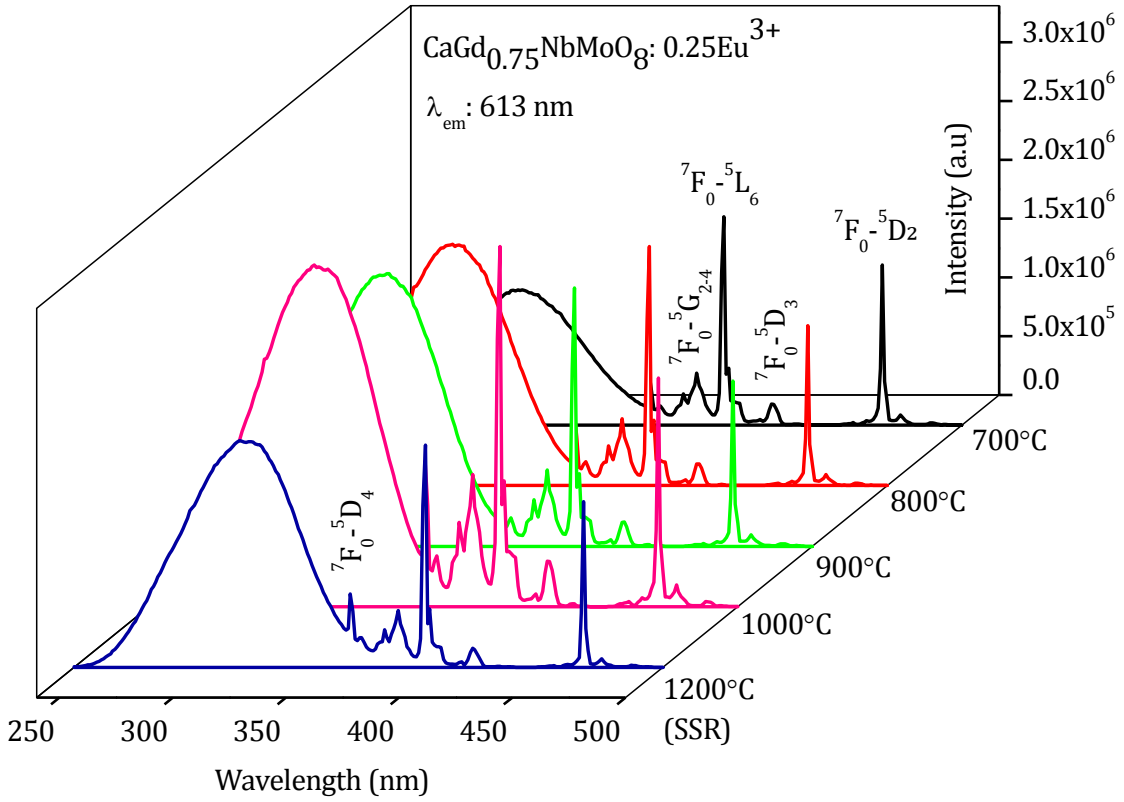

Fig. 6A.6 Excitation spectra of $CaGd_{0.75}NbMoO_8$: $0.25Eu^{3+}$ heat treated from 700 to 1000°C for an emission at 613nm.

Of the many *f-f* peaks of excitation, those at 394/395 nm and 465 nm corresponding to $^7F_0$– $^5L_6$ and $^7F_0$– $^5D_2$ transitions are more intense (Thomas S. M *et al* 2008). Thus all these phosphors are well excitable under both near UV and blue irradiations. With respect to heat treatment from 700 to 1000°C, the CT band in the excitation spectra of both CLNM9 and CGNM25 samples show significant variations in the relative intensity and energy position. However, *f-f* transitions peaks beyond 360 nm show variation only in their relative intensity with respect to the heat treatment process. It is observed that for CG route samples both CT and *f-f* transitions become stronger compared to the SSR route sample. The enhancement in the intensity of both CT band and *f-f* transitions can be due to the effective mixing of starting materials including activator at the molecular level, improvement of crystallinity and morphology of the phosphors synthesized by the CG route than the SSR route. In addition, with respect to heat treatment the position of CT band is red shifted from 304 to 313 nm (700 to 1000°C). The variation of CT band position and intensity with respect to heat treatment process is presented in Table 6A.2.

Table 6A.2 The Variation of CT band position and intensity of $CaLa_{0.91}NbMoO_8$: $0.09Eu^{3+}$ and $CaGd_{0.75}NbMoO_8$: $0.25Eu^{3+}$ phosphors with heat treatment process

Temperature (°C)	CT band position (nm)		Intensity (a.u)	
	CLNM 9	**CGNM 25**	**CLNM 9**	**CGNM 25**
700	304	304	$7.28x10^5$	$1.15x10^6$
800	307	308	$9.94x10^5$	$2.05x10^6$
900	311	312	$1.49x10^6$	$2.32x10^6$
1000	313	313	$1.84x10^6$	$2.90x10^6$
1200 (SSR)	313	313	$1.40x10^6$	$1.92x10^6$

The position of CT band plays an important role in determining the luminescence properties. On the one hand, the quantum efficiency of Eu^{3+} decreases if the position is at a lower energy on the other hand, an intense forced electric dipole $^5D_0$-$^7F_2$ (613 nm) red emission needs its CT band at lower energies because the parity forbidden transitions of Eu^{3+} ion borrow intensity from the lowest strong absorption band (CT) (Su Q *et al* 1995; Blasse G *et al* 1979). Thus by red shifting CT band position, we can improve the red emission intensity, but a reduction in the decay time and quantum efficiency of phosphors occur at the same time. Why is this happening? It is because when we shift the CT band to a lower energy position, the probability of non radiative transition through CT states is increasing, leading to faster decay and reduction in the quantum efficiency. So it is necessary to understand position of CT band and its influence on luminescence (Lee E. Y et al 2009). Further explanation of this observation with the aid of energy level diagram is included in later session.

In Eu^{3+} doped phosphors, the CT band corresponds to the electronic transitions from the 2*p* orbital of O^{2-} to the 4*f* orbital of Eu^{3+} and is closely related to the covalency between O^{2-} and Eu^{3+} and the coordination environment around Eu^{3+} (Blasse G *et al* 1966). In the other way CT band is related to the stability of electron cloud of the surrounding O^{2-} ion, i.e. the CT transition is sensitive to a ligand environment (the bonding energy between the central ion and the ligand ions). Thus the position of CT band divulges the extent of interaction between the ligand ion and the central metal ion. This interaction is influenced by two

factors: (i) covalency between O^{2-} and Eu^{3+} (ii) crystal field of the ion under consideration due to surroundings. The first factor, covalency is estimated based on the bond distance and electronegativity difference between the ions. As the bond distance increases, the electron interaction is reduced as they spread out wider orbitals, consequently the electronic transition energy shift to a lower energy (red shift) and vice versa for the blue shift. The other factor is the crystal field at the anion site (O^{2-}) due to surrounding ions. If the potential energy increases, the energy required for transferring an electron from O^{2-} ion to the cation (Eu^{3+}) increases and the charge transfer band energy moves to a higher energy side (blue shift). Many researchers observed a blue shift of CT band in nano scale regime of the phosphors transforming from defect nanostructures to perfect nanostructures which is attributed to the reduction in Eu-O bond distance and disorder of the nanostructures.

The red shift of CT band with heat treatment in the present study of both CLNM9 and CGNM25 phosphors is mainly attributed to formation of Eu^{3+} - Eu^{3+} pairs or clusters due to improvement of crystallinity of the phosphor powders accompanied by increase in particle size (Fu Z *et al* 2006; Rao B. V *et al* 2012; Singh N. S *et al* 2010; Raju G. S. R *et al* 2010). As observed from SEM micrographs, the heat treatment of the phosphor powders from 700 - 1000 °C increases particle size from 100 nm to 0.5 μm. The large particles reduce the average bond distance between Eu^{3+} ions. Similar results are observed in $Ca_2Gd_8Si_6O_{26}$: Eu^{3+} nanophosphors (Raju G. S. R *et al* 2010). Fu et al. also observed a similar result in Eu^{3+}: Y_2O_3 for nano crystals to bulk (Fu Z *et al* 2007). This has been ascribed to lowering the centroid shift of the 5*d* energy due to change in band gap of material from nano size to bulk. In addition, it is considered that the energy level of f^n configuration is unchanged in bulk and nanocrystals since f^n are shielded from the surrounding electronic shell. It is also interpreted as, when the particle size diminishes the environmental change around rare earth ions has great influence on the *d* energy level of rare earth ions but has weak influence on the *f* energy level of rare earths. The present results are also agreeing to both the explanations.

6A.3.3.2 Emission spectra

The emission spectra of CLNM9 and CGNM25 phosphors under near UV (394/395 nm) excitation are shown in Fig. 6A.7 and Fig. 6A.8 (The variation of red emission intensity with respect to heat treatment under 465 nm excitation is shown in the inset). CLNM9 and CGNM25 synthesized via CG route have major emission peaks at 579, 592, 613, 624 nm and are corresponding to $^5D_0$-^7F_J (J = 0, 1, 2) transitions of Eu^{3+} ion similar to that of their SSR analogues (Thomas M *et al* 2009).

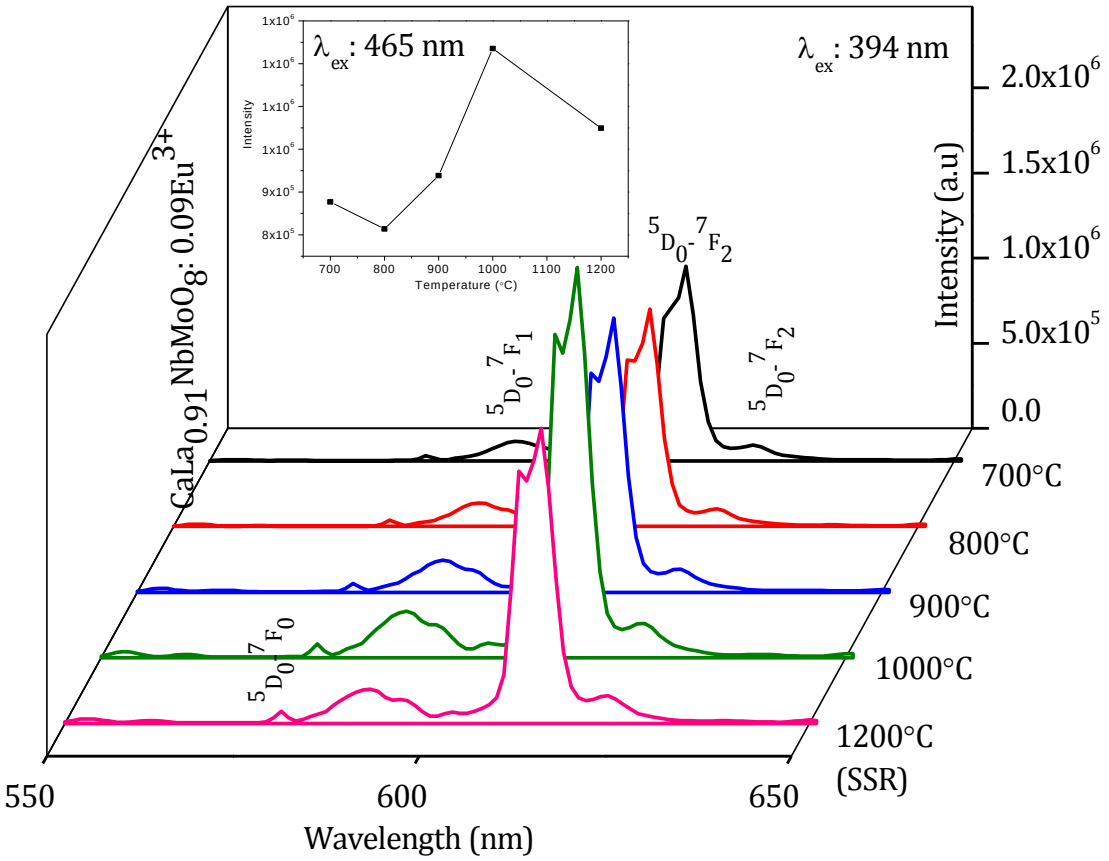

Fig. 6A.7 Emission spectra of $CaLa_{0.91}NbMoO_8$: $0.09Eu^{3+}$ heat treated from 700 to 1000°C under 394 nm excitation.

The samples show dominant red emission (613 nm) under near UV and blue excitations due to the parity forbidden electric dipole ($^5D_0$ - $^7F_2$) transition and weak emission peak at 592 nm due to parity allowed magnetic dipole ($^5D_0$ - $^7F_1$) transition (Hu Y *et al* 2005). It is observed that for both phosphors, the intensity of red emission is increasing with heat treatment from 700 to 1000°C and has maximum red emission at 1000°C. The emission intensity is improved by a factor of ~1.7 with respect to variation in the synthesis method from SSR to CG route. The emission peaks of CG route phosphors are sharper with smaller full width at half maximum (FWHM) compared to their SSR analogues (Included in Table 6A.3).Thus better color purity of the phosphors comparable to that of NTSC standard red phosphors can be achieved via CG route compared to SSR route.

The luminescence enhancement of both CLNM9 and CGNM25 samples with respect to variation in the synthesis method and heat treatment is owing to many factors. Generally, photoluminescent intensity of phosphors depends strongly on particle shape, size distribution and doping concentration (Guo C *et al* 2008).

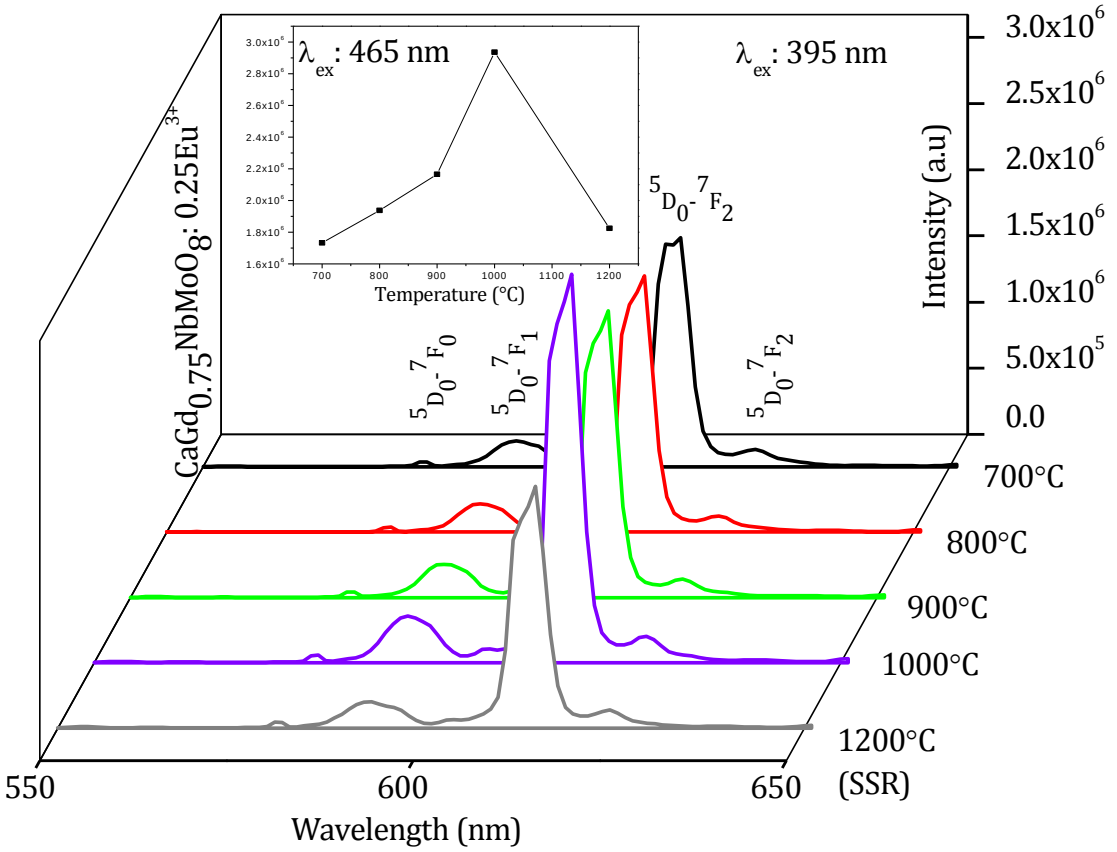

Fig. 6A.8 Emission spectra of $CaGd_{0.75}NbMoO_8$: $0.25Eu^{3+}$ heat treated from 700 to 1000°C under 395 nm excitation.

Table 6A.3 The variation of FWHM, asymmetry ratio and color co ordinates of $CaLa_{0.91}NbMoO_8$: $0.09Eu^{3+}$ and $CaGd_{0.75}NbMoO_8$: $0.25Eu^{3+}$ synthesized via CG route with heat treatment process

°C	FWHM (nm)		Asymmetry Ratio		Color Co ordinates (x, y)	
	CLNM9	CGNM25	CLNM9	CGNM25	CLNM9	CGNM25
700	5.16	4.65	9.93	9.07	(0.64, 0.34)	(0.65, 0.35)
800	5.24	4.67	9.28	8.84	(0.64, 0.34)	(0.65, 0.34)
900	5.35	4.69	8.54	8.64	(0.65, 0.34)	(0.65, 0.34)
1000	5.5	4.76	8.40	8.30	(0.65, 0.34)	(0.65, 0.34)
1200 (SSR)	5.7	5	8.59	9.09	(0.59, 0.35)	(0.64, 0.33)

From the SEM images, it is clear that both phosphors have uniform particle size distribution and homogenous particles compared to their SSR analogues. These factors are favorable to luminescent characteristics because of less contamination or fewer inactive layers on the surface of the phosphor (Yang H. K *et al* 2010). Moreover, both molybdate based phosphors synthesized via CG route have slightly spherical morphology and particles have smooth edges which reduces the scattering of light. Effective mixing of starting materials including the activator at molecular level by CG route can also lead to the improvement in luminescent intensity (Guo C *et al* 2008).

It is known that symmetry distortion can improve the red emission intensity of Eu^{3+} activated phosphors by making $^5D_0$-$^7F_2$ parity forbidden electric dipole transition more probable. Here it is observed that with respect to heat treatment process the asymmetry ratio of both phosphors is reducing. This implies that the lattice of both phosphors is attaining more order with respect to heat treatment. i.e., the symmetry of local environment of the Eu^{3+} is increasing. Thus the symmetry factor is not a major cause for the improvement of red emission intensity in the present work. Here the red emission enhancement with respect to heat treatment from 700 to 1000°C can be mainly due to the improved absorption strengths of $^7F_0$ - $^5L_6$ and $^7F_0$ - $^5D_2$ transitions by improvement of crystallinity, average particle size, and red shift in the CT band position. Since electric dipole transition $^5D_0$ - $^7F_2$ is parity forbidden, it can borrow intensity from lowest strong absorption band making $^5D_0$ -$^7F_2$ (613 nm) electric dipole transition more probable and hence an improvement in luminescence intensity (Su Q *et al* 1995).

6A.3.3.3 Lifetime measurement

The decay curves for $^5D_0$-$^7F_2$ transition (613 nm) of CLNM9 and CGNM25 phosphors under near UV excitation are shown in Fig 6A.9 and Fig 6A.10. All the decay curves can be fitted well with a single exponential function given as;

$$I = A \exp(-x/\tau) \qquad (6A.2)$$

where, I, τ and A are intensity, decay time and fitting parameter respectively.

The variation of decay time of red emission with respect to heat treatment from 700 to 1000°C is presented in Table 6A.4.

Here it is observed that the luminescence decay time of red emission of both CLNM9 and CGNM25 phosphors is decreasing with respect to heat treatment from 700 to 1000°C. The observation is that the lifetime of $^5D_0$ decreases whereas the intensity of $^5D_0$-$^7F_2$ transition increases with the improvement of particle size (by heat treatment process). It is also to be noted that the absorption strength of CT band and intra configurational *f-f*

transitions are enhanced at the same time with the heat treatment of phosphor powders. Regarding the luminescence lifetime of Eu^{3+} ($^5D_0$) contradicting results are reported in the literature.

Table 6A.4 The variation of decay time of red emission of $CaLa_{0.91}NbMoO_8$: $0.09Eu^{3+}$ and $CaGd_{0.75}NbMoO_8$: $0.25Eu^{3+}$ phosphors with heat treatment from 700 to 1000°C

Temperature (°C)	τ(ms) CLNM9	τ(ms) CGNM25
700	1.0144	0.9299
800	0.7851	0.7786
900	0.7036	0.7237
1000	0.6639	0.7082
1200 (SSR)	0.6031	0.6051

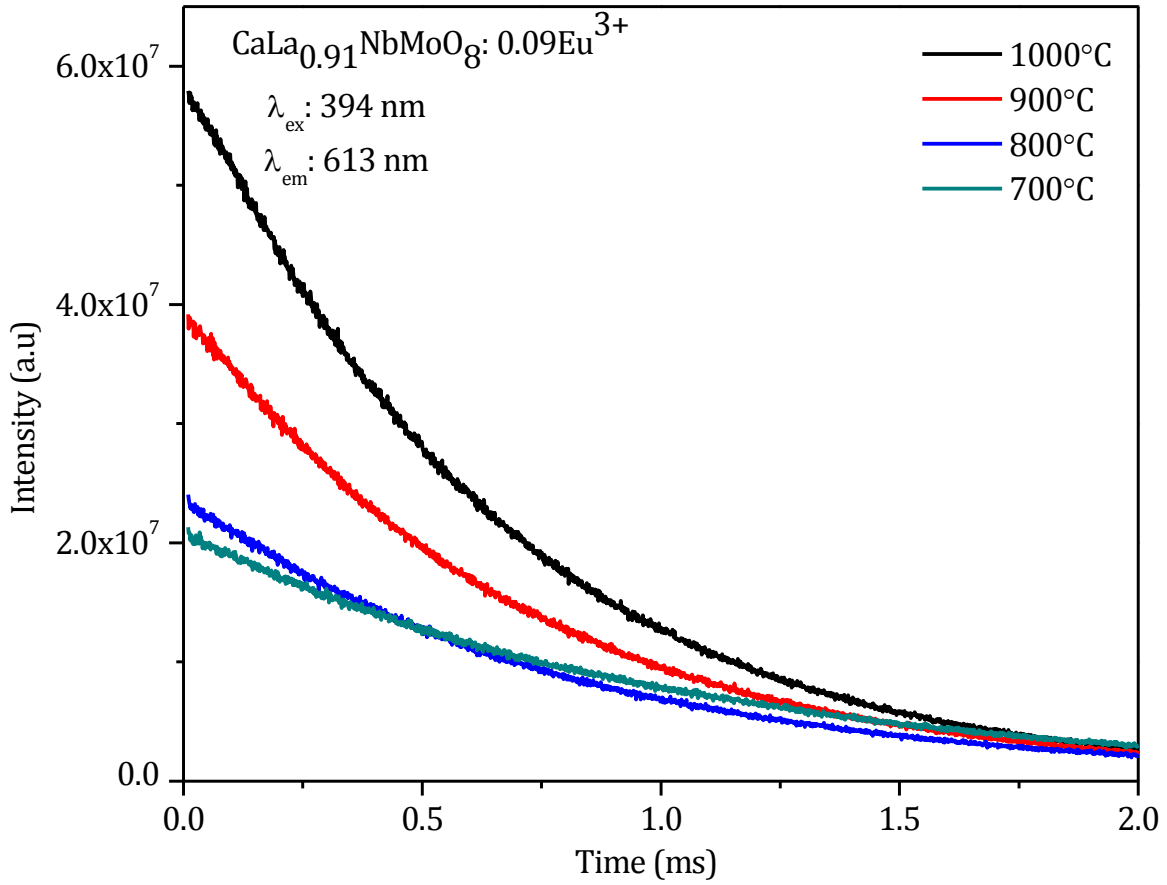

Fig. 6A.9 Decay curves of Eu^{3+} emission at 613 nm in $CaLa_{0.91}NbMoO_8$: $0.09Eu^{3+}$ phosphors under an excitation of 394 nm.

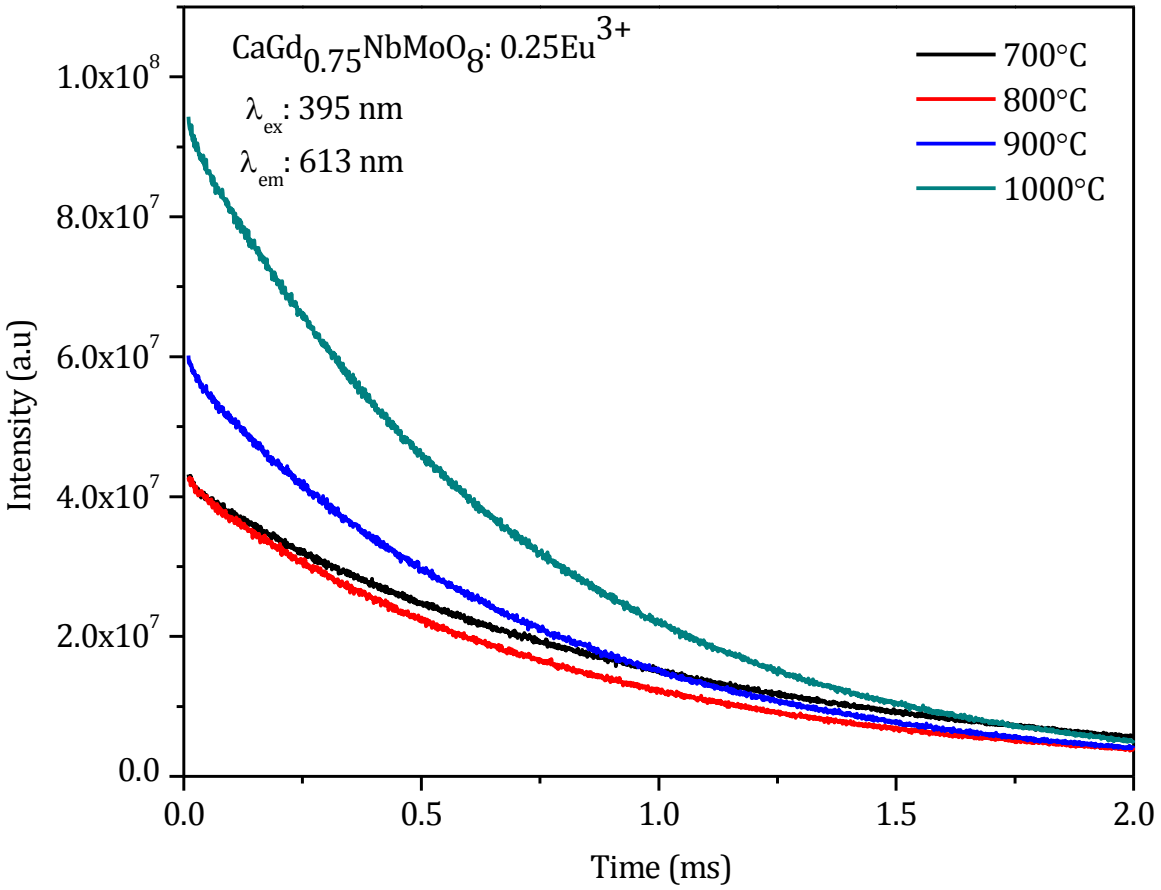

Fig. 6A.10 Decay curves of Eu^{3+} emission at 613 nm in $CaGd_{0.75}NbMoO_8$: $0.25Eu^{3+}$ phosphors under an excitation of 395 nm.

The luminescence lifetime for Eu^{3+} decreased with particle size, (Peng H. S *et al* 2003; Song H. W *et al* 2003). On the contrary, in other literatures (Parchur A. K *et al* 2011; Williams D. K *et al* 1999) the lifetime increased which depends on various factors such as the host and the preparation methods.

The lifetime of $^5D_0$ excited state is mainly contributed by the radiative and non-radiative decay rates.

i.e.,

$$\frac{1}{\tau} = A_{rad} + A_{nrad} \qquad (6A.3)$$

where A_{rad} and A_{nrad} are radiative and non radiative transition probabilities respectively.

Thus the decrease in the lifetime (τ) of $^5D_0$ energy level can be explained on the basis of the variation of radiative (A_{rad}) and non radiative (A_{nrad}) decay rates. In the present study, the decrease in lifetime with respect to heat treatment can be attributed to two main factors. First,

the red shift of CT band position and second, the chance of formation Eu^{3+} - Eu^{3+} pairs or clusters with heat treatment process.

The effect of red shift of CT band on lifetime can be better understood with the help of configurational coordinate diagram shown in Fig. 6A.11.

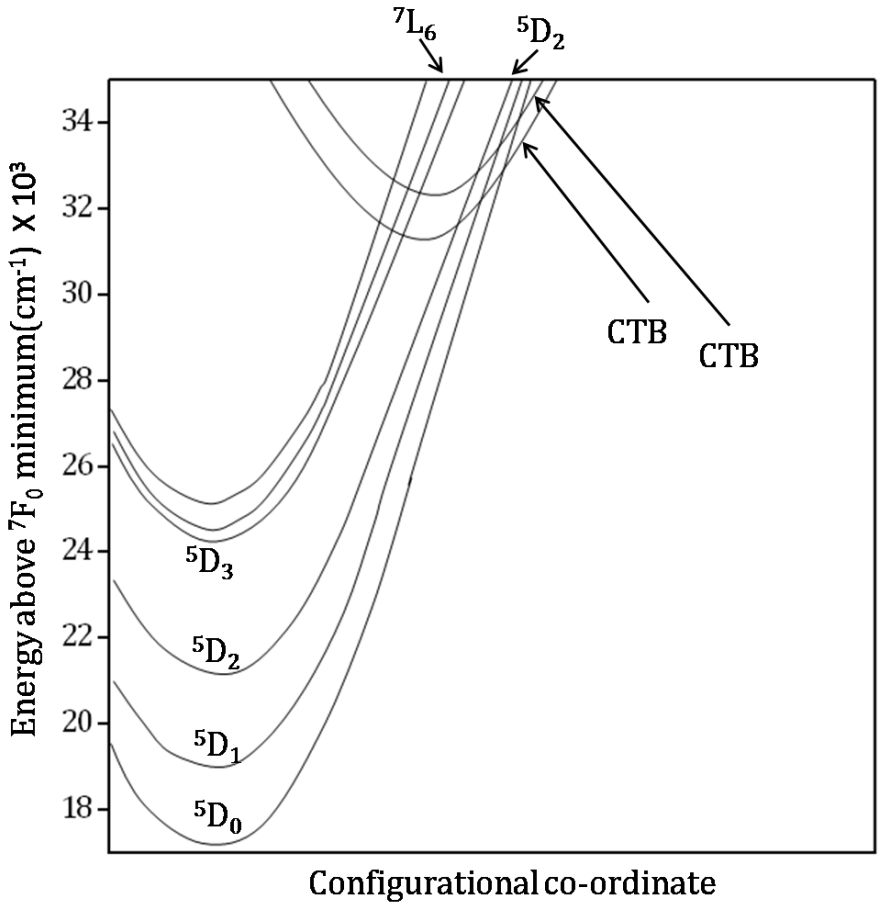

Fig. 6A.11 Configurational coordinate diagram for $CaLa_{0.91}NbMoO_8$: $0.09Eu^{3+}$ and $CaGd_{0.75}NbMoO_8$: $0.25Eu^{3+}$ phosphors.

In many oxide host lattices, the CT band lie at a higher energy position so that the extent of overlapping of Eu^{3+} intraconfigurational levels and CT band in oxide lattices is very small compared to other host lattices such as oxy sulfides, sulfides etc (Struck C. W *et al* 1970). Here for the molybdate based phosphors (CLNM9 and CGNM 25) the CT band position is red shifting (from 304 nm (32,894 cm^{-1}) to 313 nm (31,948 cm^{-1}). i.e., the energy gap between CT states of host lattice and Eu^{3+} intra configurational *f-f* levels is reducing with heat treatment. This red shift of CT band can lead to crossing of CT states with $^5D_0$ level to some extent (Struck C. W *et al* 1970). Thus $^5D_0$ states can de-excite non radiatively through CT states. This can increase the non radiative transition rate than the radiative transition rate

which leads to the faster decay and reduction in $^5D_0$ lifetime with respect to heat treatment. Similar observation of increment of luminescence emission intensity and reduction of lifetime with heat treatment is reported in YAG: Eu^{3+} phosphors synthesized by high energy ball milling (Yang H. K *et al* 2010).

In addition to the red shift of CT band, Eu^{3+} - Eu^{3+} pair formation as a result of heat treatment process also lead to reduction in lifetime. This results in a strong interaction between Eu^{3+} ions via non radiative interaction leading to reduction in lifetime. Here in the case of CLNM9 and CGNM25 phosphors, the contribution of red shift of CT band is more pronouncing than that of Eu^{3+} - Eu^{3+} pair formation. It is also observed that the SSR analogues of both CLNM9 and CGNM25 phosphors decay much faster. This is mainly due to the presence of more defects or inactive layers on particle surface formed during intermediate grinding process in SSR, which can act as quenching centers (Yang H. K *et al* 2010).

6A.4 Conclusions

Typical compositions of molybdate based red phosphors, $CaLa_{0.91}NbMoO_8$: $0.09Eu^{3+}$ and $CaGd_{0.75}NbMoO_8$: $0.25Eu^{3+}$ have been synthesized by citrate gel route. The effects of variation of the synthesis method and heat treatment process on their luminescence properties were investigated. Compared to the solid state reaction route, phase pure samples were formed at a lower temperature (700°C) by citrate gel route. They are also characterized with better morphology with more homogeneity and less agglomeration. By variation in the synthesis method and heat treatment process from 700 to 1000°C, we could improve the luminescence emission intensity of phosphors. They exhibited sharper red emission with longer lifetime under the excitation of near UV (394/395 nm) and blue (465 nm) light that corresponding to the emission lines from near UV and blue LED chips. The factors such as improved crystallinity, average particle size, absorption strengths of $^7F_0$ - $^5L_6$ and $^7F_0$ - $^5D_2$ transitions and red shift in the CT band position were the crucial factors for luminescence emission enhancement.

CHAPTER 6B

MORPHOLOGICAL IMPROVEMENT AND LUMINESCENT PROPERTIES OF $Ca(La/Gd)_{1-x}NbWO_8$: xEu^{3+} PHOSPHORS

6B.1 Introduction

The specific luminescence behavior of inorganic materials is highly sensitive to the initial composition of the host material, dopant or substitutant concentration and processing conditions (Žalga A *et al* 2009). Particularly as a good host lattice for the luminescence property, scheelite type tungstates hold a superior position. However, the luminescence properties of this superior phosphor could be varied by doping with rare earth ions, and the phosphor nanolization may also alter their physical properties (Wang W *et al* 2010). The physical properties of a phosphor material such as morphology, particle size and shape, homogeneity etc. are very important concerning their luminescence performance. Many approaches such as charge compensation, variation in the synthesis method, codopant incorporation etc. may improve the luminescence emission intensity of current tungstate based phosphors. For good luminescent characteristics, phosphor materials must have a narrow size distribution, non agglomeration properties and spherical morphology (Kang H. S *et al* 2005). To achieve such better kind of physical and luminescence properties, the synthesis method and subsequent heating process play a key role as we discussed in the earlier part of this chapter. The methods such as sol gel, citrate gel, chemical co precipitation etc. are some of the important solution based synthesis methods which usually do not require normal mixing, calcinations and grinding process. Homogenous distribution of activator ions in the host lattice is a must for better luminescence property and is effectively takes place via the aforementioned synthesis methods.

To date, few efforts are there to explore the luminescence behavior of tungstate based phosphors via different synthesis methods other than conventional solid state reaction (SSR) route. Scheelite $CaWO_4$ doped with rare earth ions (Eu^{3+}, Sm^{3+}, Dy^{3+}) were fabricated via a facile solvothermal process without further heat treatment and their luminescence properties were reported by Wang et al (Wang W *et al* 2010). Optimum luminescence of $CaWO_4$ based red phosphors with codoping of Eu^{3+} and Na^{+} synthesized via hydrothermal method is also reported (Su Y *et al* 2008). Žalga et al synthesized a series of red emitting phosphors $CaWO_4$: RE (RE = Tb^{3+}, Eu^{3+}, Sm^{3+}) by aqueous sol gel method and they can be effectively excited under photoexcitation at 280, 360 and 460 nm and exhibited red emission in the vicinity of 620 nm (Žalga A *et al* 2009).

In chapter 4, we had seen the optimum luminescence property of tungstate based novel red phosphors, $Ca(La/Gd)_{1-x}$ $NbWO_8$: xEu^{3+} synthesized via SSR route. In the present study,

an attempt has been made to study the effect of variation of the synthesis method and subsequent heat treatment process on the luminescence emission property of typical compositions of $CaLa_{0.80}NbWO_8$: $0.20Eu^{3+}$ and $CaGd_{0.75}NbWO_8$: $0.25Eu^{3+}$. Here the phosphor samples are synthesized via citrate gel (CG) route and are heat treated at different temperatures from 700 to 1200°C. The variation of structural, microstructural and optical properties with respect to variation in the synthesis method and heat treatment process is also investigated. It is observed that by the variation in the synthesis method, an efficient control over the crystallite size and morphology is possible which are crucial for high luminescence performance. The red emission intensity of current phosphors is enhanced by means of many contributing factors. The experimental details and the factors that contributed for the luminescence improvement of tungstate based red phosphors are discussed and presented in this chapter.

6B.2 Experimental

Typical compositions of $CaLa_{0.80}NbWO_8$: $0.20Eu^{3+}$ (CLNW20) and $CaGd_{0.75}NbWO_8$: $0.25Eu^{3+}$ (CGNW25) were synthesized by the citrate gel method (CG). The starting materials were $CaCl_2.2H_2O$, $La/Gd(NO_3)_3.6H_2O$, $NbCl_5$, WCl_6, $Eu(NO_3)_3.5H_2O$ (Sigma Aldrich,99.9% purity). Distilled water and citric acid (Sigma Aldrich, 99.9% purity) were used as solvent and chelating agent for the process. The citrate solution was prepared by dissolving appropriate amount of citric acid in distilled water. After complete homogenization of citrate solution, all the cationic solutions were dissolved in the citrate solution (1:5). The solution was kept for constant stirring for 1 h for homogenous mixing and concentrated by keeping it in the water bath (maintained at 100°C) for 3h and the solution became viscous gel. The gel was dried to form a brown colored product and then powdered by grinding in an agate mortar, which is the precursor. Then heat treatment of the precursor was carried out at various temperatures from 700 to 1200°C.

The crystal structure as well as the phase purity of the samples were examined by recording the powder X ray diffraction patterns using a PANalytical X'pert Pro diffractometer with a Ni filtered CuKα radiation ($\lambda = 1.54056$Å). The morphological analysis of the powder samples heat treated at various temperatures from 700 to 1200°C were done by a scanning electron microscope (JEOL, JSM-5600LV). Photoluminescence excitation, emission spectra, and decay time curves were recorded using a Horiba Yvon Fluorolog 3 spectrofluorimeter with a 450W xenon flash lamp as the exciting source. CIE chromaticity coordinates of the phosphors were also calculated.

6B.3 Results and Discussion

6B.3.1 Powder X ray diffraction analysis

Fig. 6B.1 and Fig. 6B.2 show the powder XRD pattern of $CaLa_{0.80}NbWO_8$: $0.20Eu^{3+}$ (CLNW20) and $CaGd_{0.75}NbWO_8$: $0.25Eu^{3+}$ (CGNW25) synthesized via CG route and heat treated at different temperatures from 700 to 1200°C.

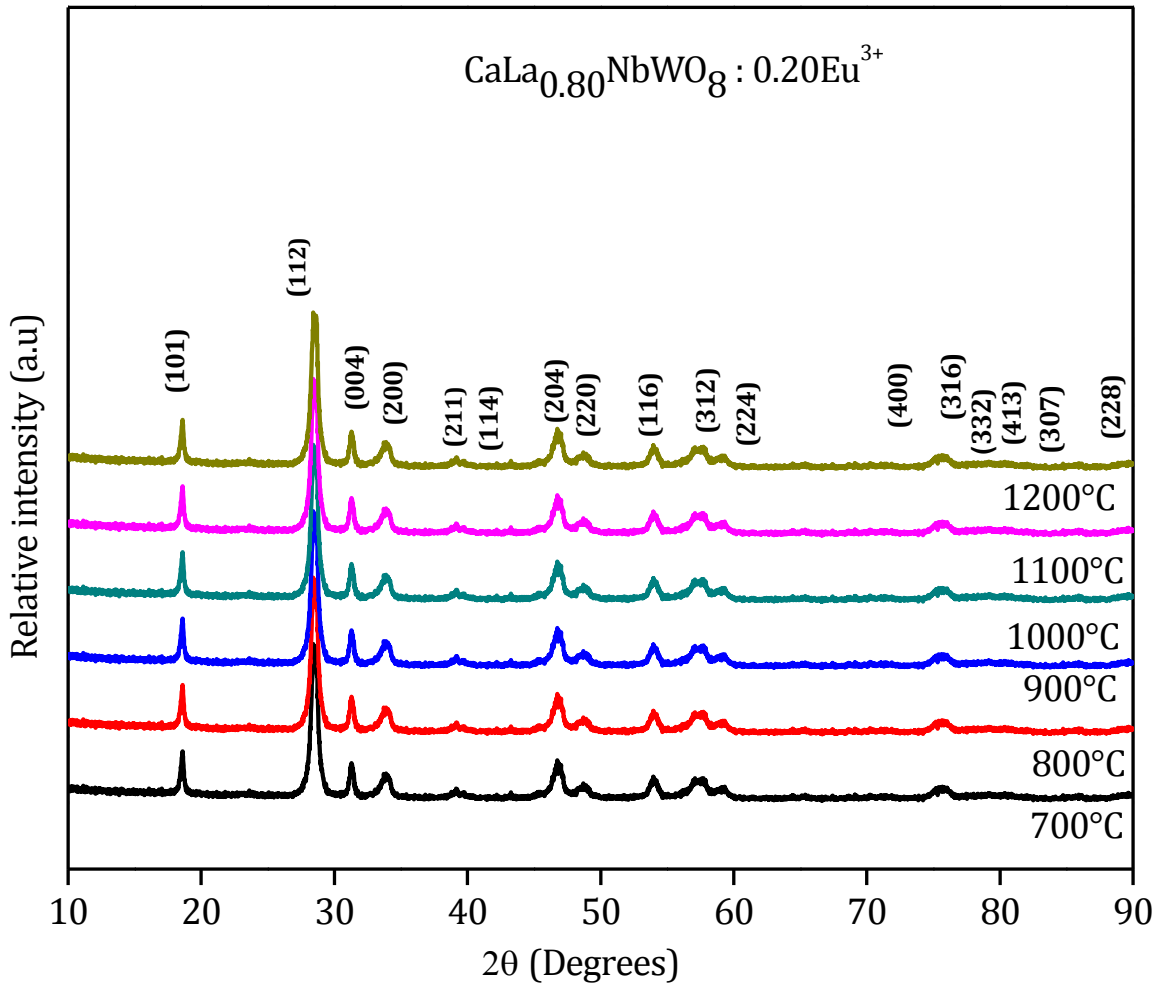

Fig. 6B.1 Powder X ray diffraction patterns of $CaLa_{0.80}NbWO_8$: $0.20Eu^{3+}$ phosphors heat treated at different temperatures from 700 to 1200°C.

All the peaks in the XRD patterns are matching well with that of scheelite type $CaWO_4$ (JCPDS file no. 41-1431) with a space group $I4_1/a$ (88) (Achary S. N *et al* 2006). The prominent peaks in the XRD patterns correspond to (101), (112), (004), (200), (204), (220), (116), (312), and (316) lattice planes. There are no traces of extra peaks from impurities in the pattern. Similar to the molybdate phosphors, the phase formation of tungstate phosphors synthesized by CG route also takes place at a lower calcination temperature of 700°C compared to that of the samples prepared by SSR route. Sharp peaks in the XRD pattern

reveal the crystalline nature of the samples and the intensity of all the peaks are increasing linearly with heat treatment process.

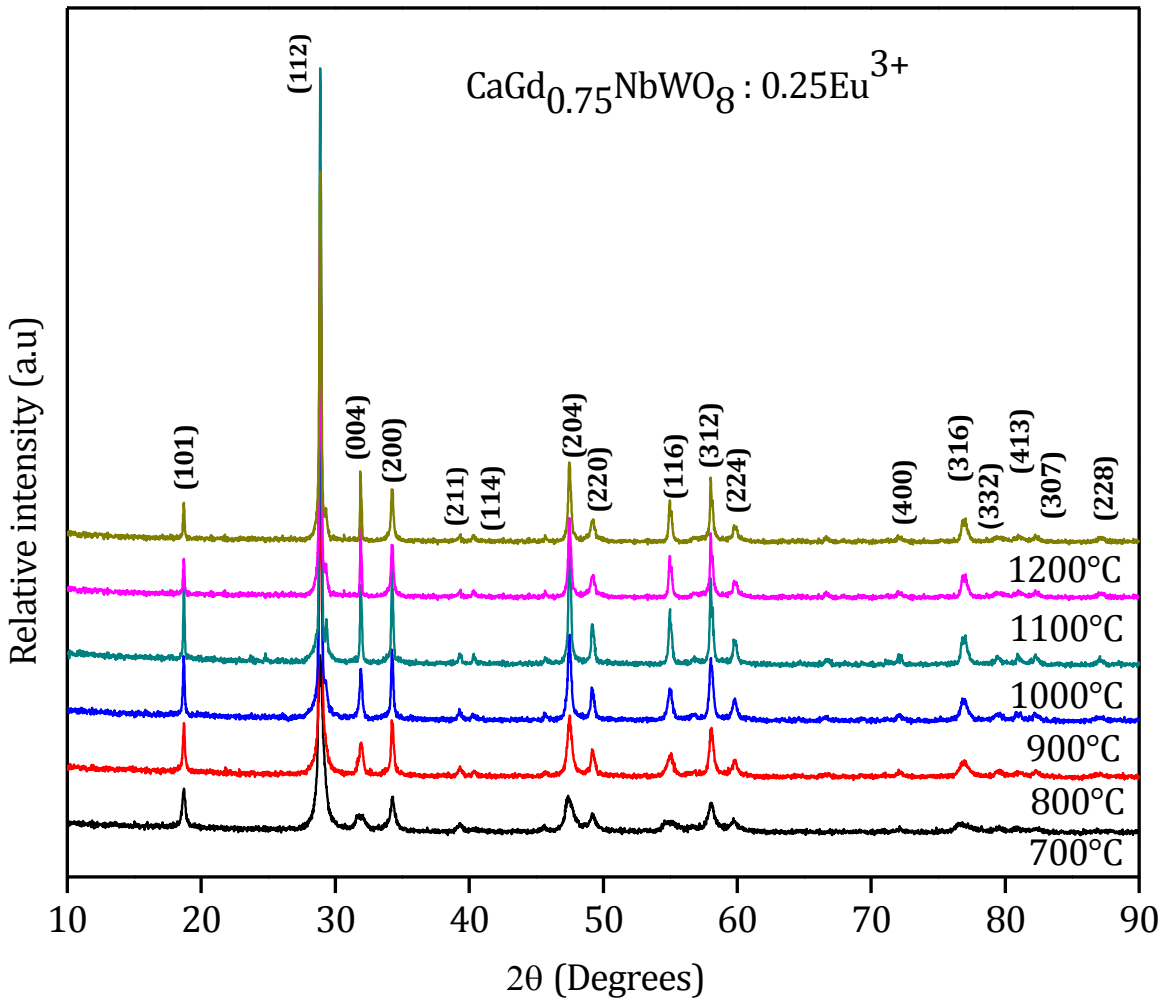

Fig. 6B.2 Powder X ray diffraction patterns of $CaGd_{0.75}NbWO_8$: $0.25Eu^{3+}$ phosphors heat treated at different temperatures from 700 to 1200°C.

The diffraction peaks of the sample synthesized by CG method are broader than that prepared by SSR route, which hints the reduction of average crystallite size of the phosphor material. With respect to heat treatment process from 700 to 1200°C, the sharpness of all the peaks is increasing. Thus the extent of crystallinity and crystallite size of the phosphor samples are increasing with heat treatment process.

The average crystallite size of the phosphors with respect to heat treatment process is calculated using Scherrer formula (Chen G Y *et al* 2007),

$$D_{av} = 0.91\lambda / \beta\cos\theta \qquad (6B.1)$$

where,

D_{av} - Average crystallite size,

λ - Wavelength of Cu K∝ radiation (1.54056 Å)

β - Full Width at Half Maximum (FWHM)

θ - Bragg angle (Glancing angle).

The crystallite size at various temperatures is calculated by taking into account of the FWHM and Bragg angle of maximum intense peak (112) at ~ 28°. The variation of average crystallite size of both CLNW20 and CGNW 25 phosphors is shown in Fig. 6B.3.

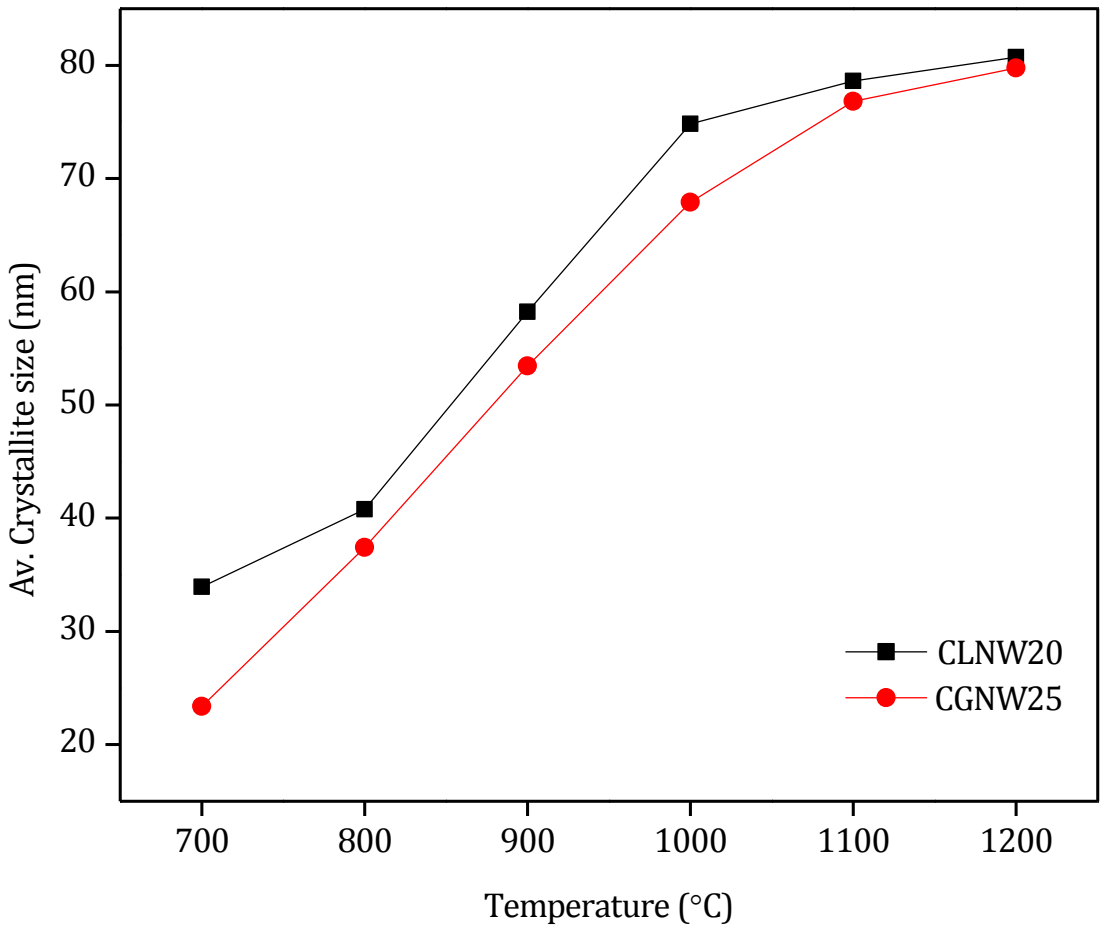

Fig. 6B.3 The variation of average crystallite size of $CaLa_{0.80}NbWO_8$: $0.20Eu^{3+}$ and $CaGd_{0.75}NbWO_8$: $0.25Eu^{3+}$ phosphors with heat treatment process.

From the figure it is clearly observed that the crystallite size of CGNW 25 is smaller than that of CLNW20 phosphor. This observation is in line with the variation of ionic radii of Gd^{3+} and La^{3+} ions. The ionic radius of Gd^{3+} ion when occupying a site with coordination number 8 is 1.053Å and that of La^{3+} is 1.16Å. Similar variation is observed in the molybdate based samples also (CL/GNM).

6B.3.2 Microstructural characterization

Fig. 6B.4 and Fig. 6B.5 show the scanning electron micrographs of CLNW20 and CGNW25 phosphors synthesized via CG route and heat treated at different temperatures from 700 to 1200°C.

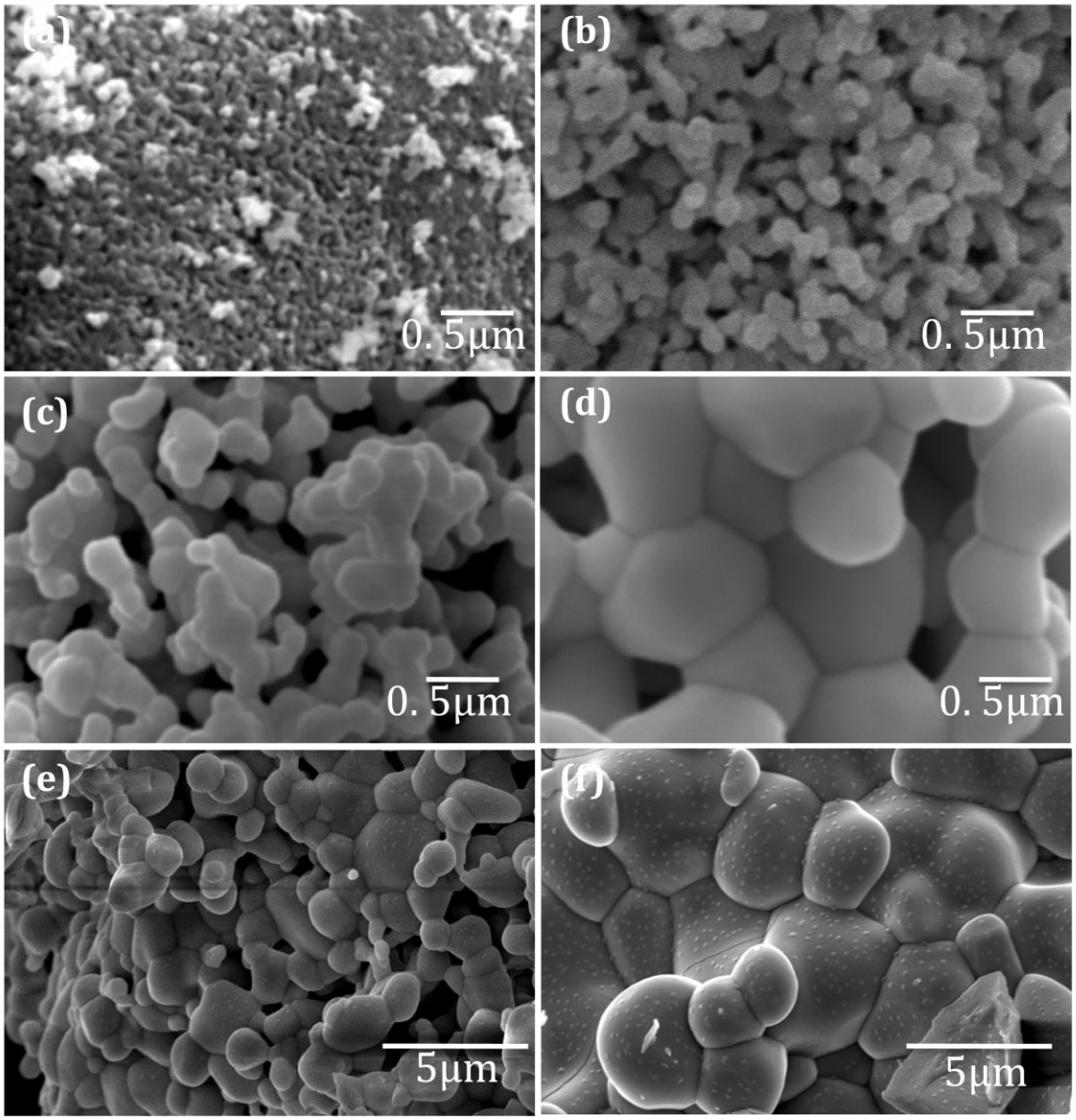

Fig. 6B.4 Scanning electron micrographs of $CaLa_{0.80}NbWO_8$: 0.20 Eu^{3+} phosphors heat treated at (a) 700°C, (b) 800°C, (c) 900°C, (d) 1000°C, (e) 1100°C, (f) 1200°C [Magnification: x30, 000 for (a) to (d) and x10, 000 for (e), (f)].

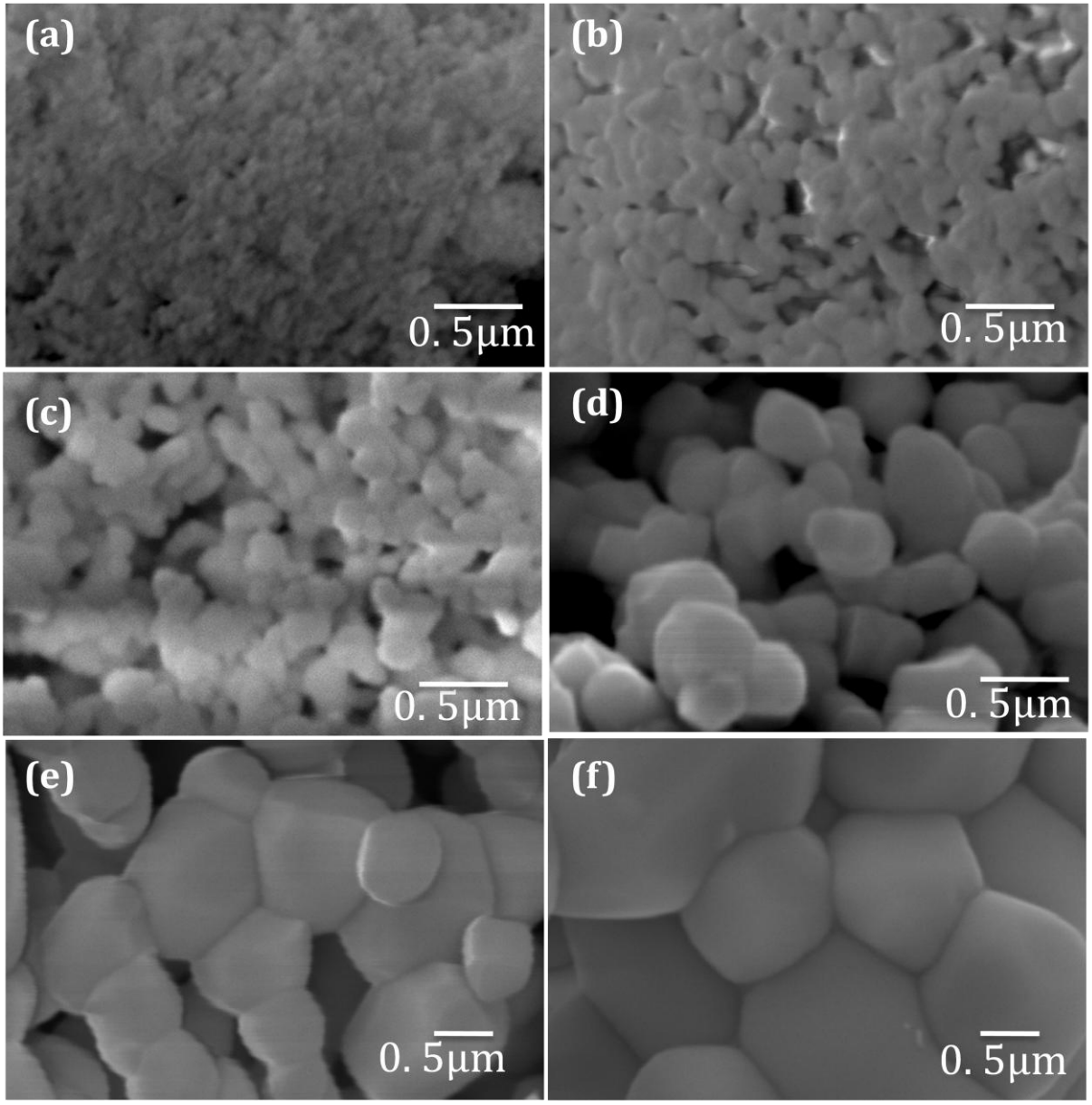

Fig. 6B.5 Scanning electron micrographs of $CaGd_{0.75}NbWO_8$: $0.25Eu^{3+}$ phosphors heat treated at (a) 700°C, (b) 800°C, (c) 900°C, (d) 1000°C, (e) 1100°C, (f) 1200°C [Magnification: x40, 000 for (a) to (f)].

The micrographs reveal that both the tungstate phosphors have uniform particle shape and narrow particle size distribution. It is observed that with respect to heat treatment process the average particle size is increasing and the variation is in the range of 100 nm to 2 µm (700 to 1200°C). From XRD analysis, we had seen that simultaneous increments of average crystallite size of both phosphors are occurring with heat treatment process. This particle size range fits well to SSL applications. The extent of agglomeration of the phosphor particles is very less compared to that synthesized via SSR route. Also the amount of light scattering is reduced for the phosphor particle synthesized via CG route because of their smooth edges

with relatively spherical morphology and this may help to improve the absorption strength of the phosphor samples and hence the emission intensity. The particle homogeneity is also achieved by the CG route. Thus better morphology of the tungstate phosphors are realized by the variation in the synthesis route from SSR to CG and the heat treatment process. The effect of morphological variation of the phosphor samples on their photoluminescence excitation and emission spectra will be discussed in the coming part.

6B.3.3 Photoluminescence properties

6B.3.3.1 Excitation spectra

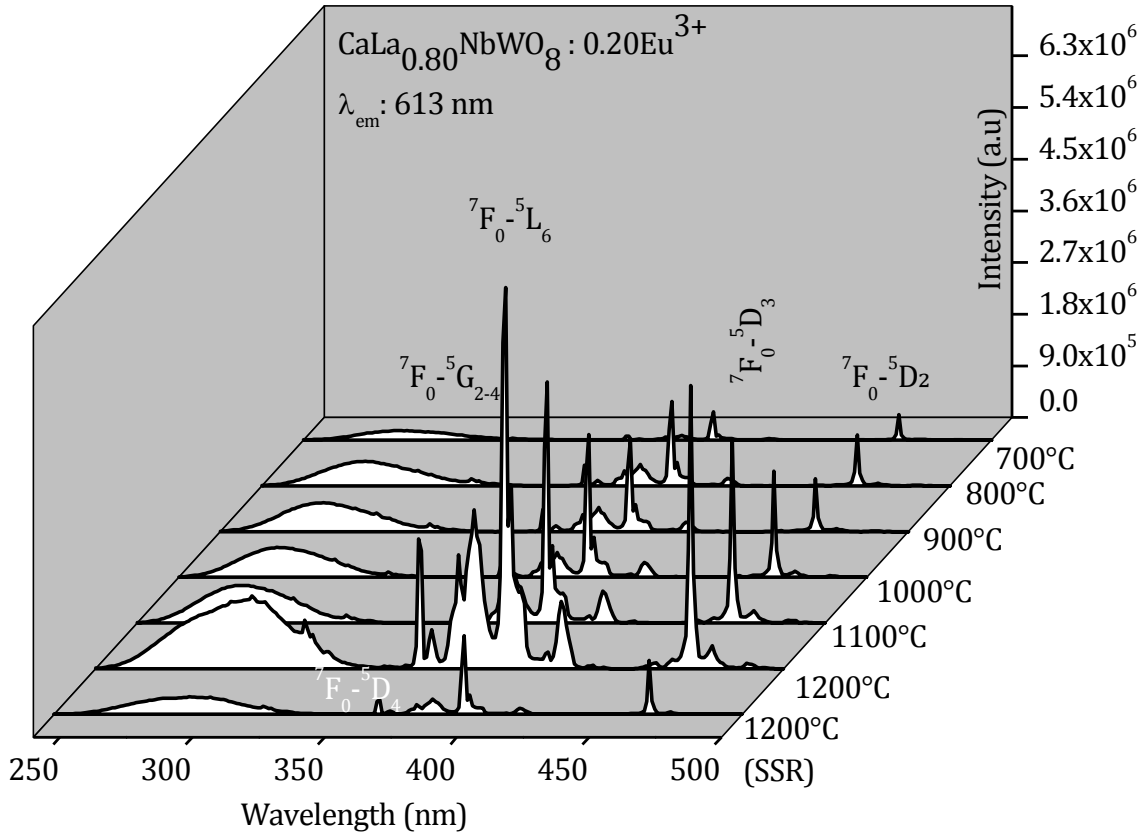

Fig. 6B.6 Excitation spectra of $CaLa_{0.80}NbWO_8$: $0.20Eu^{3+}$ heat treated from 700 to 1200°C for an emission at 613nm.

The photoluminescence excitation spectra (for an emission at 613 nm) of CLNW20 and CGNW25 phosphors synthesized via CG route and heat treated at different temperatures from 700 to 1200°C is presented in Fig. 6B.6 and Fig. 6B.7 respectively (Excitation spectrum of the corresponding SSR tungstate phosphor is also included). All the spectra include CT transition band (240- 340 nm) of Eu^{3+}- O^{2-}, WO_4 and NbO_4 groups and Eu^{3+} intra configurational *f-f* transitions (beyond 360 nm) (Pode R. B *et al* 1997; Hsiao Y. J *et al* 2007), similar to excitation spectra of Eu^{3+} activated tungstate phosphors synthesized via SSR route. Both

CLNW20 and CGNW25 phosphors are well excitable under near UV and blue excitations, since they are characterized by strong and intense $^7F_0$ - $^5L_6$ (394/395 nm) and $^7F_0$ - $^5D_2$ (464/465 nm) transitions.

It can be observed that with heat treatment process from 700 to 1200°C, the excitation intensity of both CT and *f-f* transitions is increasing and the position of CT band is shifting to higher wavelength region (red shift). The absorption strength of both $^7F_0$-$^5L_6$ (394/395 nm) and $^7F_0$-$^5D_2$ (464/465 nm) transitions is increasing steadily, which can enhance the emission strength of the phosphor. This improvement in the excitation intensity can be mainly due to the effective mixing of the activator ions, good crystallinity and improved morphology of the phosphors.

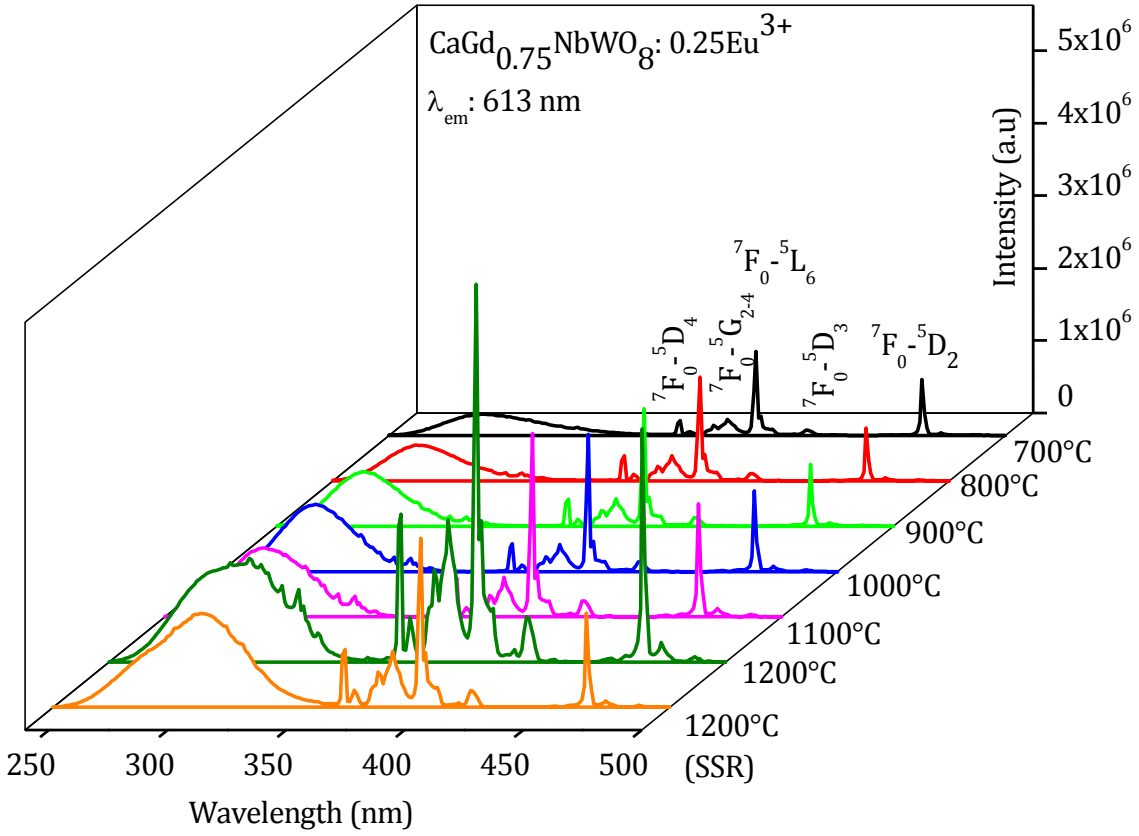

Fig. 6B.7 Excitation spectra of $CaGd_{0.75}NbWO_8$: $0.25Eu^{3+}$ heat treated from 700 to 1200°C for an emission at 613nm.

The variation of CT band position and intensity of both CLNW20 and CGNW25 phosphors with respect to heat treatment process is enlisted in Table 6B.1.

Table. 6B.1 The variation of CT band position and intensity of $CaLa_{0.80}NbWO_8$: $0.20Eu^{3+}$ and $CaGd_{0.75}NbWO_8$: $0.25Eu^{3+}$ phosphors with heat treatment process

Temperature (°C)	CT band position (nm)		Intensity (a.u)	
	CLNW 20	**CGNW 25**	**CLNW 20**	**CGNW 25**
700	276	279	$1.65x10^5$	$2.95x10^5$
800	279	279	$4.29x10^5$	$4.89x10^5$
900	279	280	$5.01x10^5$	$7.80x10^5$
1000	279	280	$5.12x10^5$	$9.26x10^5$
1100	280	283	$6.56x10^5$	$9.45x10^5$
1200	299	299	$1.26x10^6$	$1.43x10^6$
1200 (SSR)	290	303	$2.96x10^5$	$1.29x10^6$

The red shift of CT band with heat treatment of $CaGd_{0.75}NbWO_8$: $0.25Eu^{3+}$ phosphor is attributed mainly to formation of Eu^{3+}- Eu^{3+} pairs or clusters due to improvement of crystallinity of the phosphor powders accompanied by increase in particle size (Singh N. S *et al* 2010; Raju G. S. R *et al* 2010). The particle size increment (100 nm to 1 µm) of the current phosphors is clear from the SEM micrographs. The large particles reduce the average bond distance between Eu^{3+} ions. Similar results are observed in $Ca_2Gd_8Si_6O_{26}$:Eu^{3+} nanophosphors (Raju G. S. R *et al* 2010). Fu et al. also observed a similar result in Eu^{3+}: Y_2O_3 for nano-crystals to bulk (Fu Z *et al* 2007). This has been ascribed to lowering the centroid shift of the 5d energy due to change in band gap of material from nano to bulk. In addition, it is considered that the energy level of f^n configuration is unchanged in bulk and nanocrystals since f^n are shielded from the surrounding electronic shell. It is also interpreted as when the particle size diminishes; the environmental change around rare earth ions has great influence on the *d* energy level of rare earth ions but has weak influence on the *f* energy level of rare earths. The present results are also agreeing to both the explanations. The same observation is found in the molybdate phosphors discussed in the earlier part of this chapter.

It can be seen that the extent of red shift at lower temperature is very small. The CT band position of CLNW20 heat treated at 1200°C (CG route) is located at more higher wavelength of 299 nm compared to that of its SSR analogue (CT band at 290 nm). But the CT band position of CGNW25 heat treated at 1200°C (CG route) is located at still higher energy (299 nm) corresponding to its SSR analogue (303 nm). Thus more luminescence

improvement for CLNW20 is expected compared to its SSR sample and is discussed in the coming session.

6B.3.3.2 Emission spectra

Fig. 6B.8 and Fig. 6B.9 present the emission spectra of CLNW20 and CGNW25 phosphors under near UV (394/395 nm) excitation. CLNW20 and CGNW25 synthesized via CG route have major emission peaks at 579, 592, 613, 624 nm and are corresponding to $^5D_0$-^7F_J (J = 0, 1, 2) transitions of Eu^{3+} ion similar to that of their SSR analogues (Liu X *et al* 2007). The spectral profile is same under blue excitation (464/465 nm) with some variations in their emission intensities. These phosphors show dominant red emission at 613 nm under both near UV and blue excitations indicating the non centrosymmetric site occupancy of Eu^{3+} (Xie A *et al* 2009).

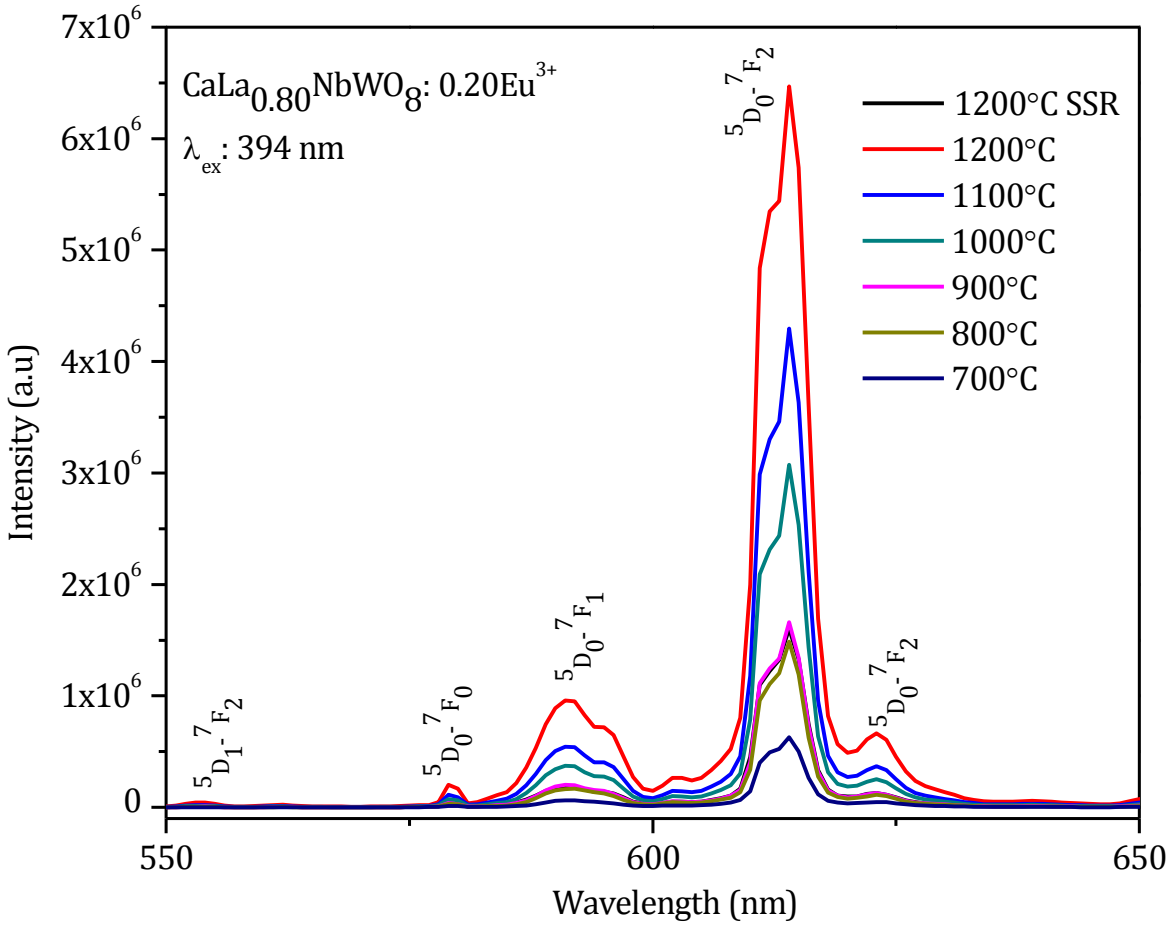

Fig. 6B.8 Emission spectra of $CaLa_{0.80}NbWO_8$: $0.20Eu^{3+}$ heat treated from 700 to 1200°C under 394 nm excitation.

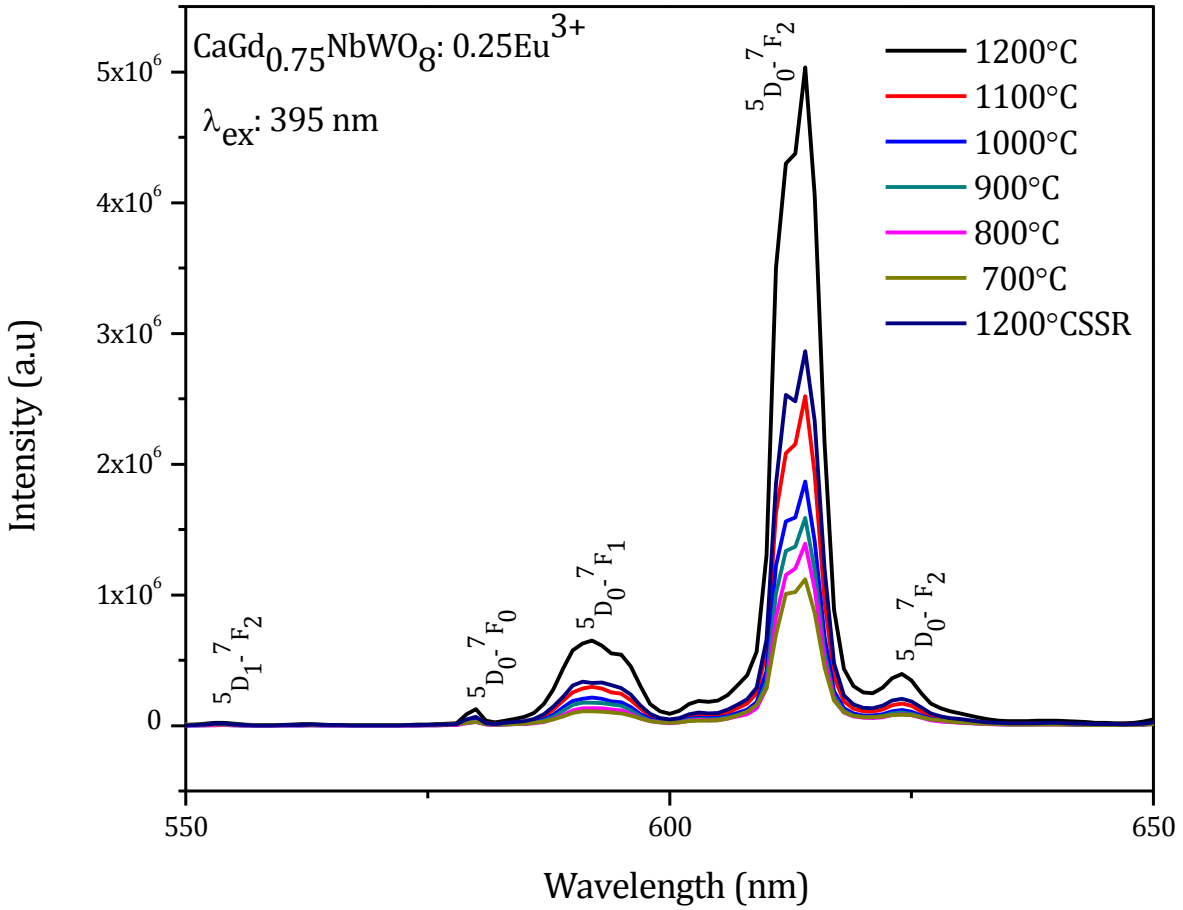

Fig. 6B.9 Emission spectra of $CaGd_{0.75}NbWO_8$: $0.25Eu^{3+}$ heat treated from 700 to 1200°C under 395 nm excitation.

It is observed that the emission intensity of both phosphors is increasing with respect to the heat treatment process from 700 to 1200°C. The variation of red emission intensity of CLNW20 and CGNW25 phosphors under near UV excitations and its comparison with the corresponding SSR sample is shown in Fig. 6B.10. The CLNW20 phosphor synthesized via CG route and heat treated at temperatures of 1000, 1100 and 1200°C show better red emission than the equivalent SSR sample calcined at 1200°C; while CGNW25 phosphor synthesized via CG route and heat treated at a temperature of 1200°C show improved red emission than SSR counterpart calcined at 1200°C. The red emission intensity of CLNW20 and CGNW25 phosphors (CG route, 1200°C) under near UV (394/395 nm) excitation improved by a factor of ~4 and ~2 respectively compared to their SSR equivalent sample.

Why the emission intensity improved with variation in the synthesis method and heat treatment process? Different attributing factors are there for the luminescence enhancement of the current red phosphors. As we know the red emission is due to the parity forbidden electric dipole intra configurational transition ($^5D_0$-$^7F_2$) of Eu^{3+} ion and its transition intensity increases with reduction in the Eu^{3+} site symmetry. Eu^{3+} site symmetry can be well

understood from the asymmetry ratio ($I_{5D0-7F2}/I_{5D0-7F1}$), and it is observed that the asymmetry ratio of both CLNW20 and CGNW25 phosphors are slightly decreasing with the heat treatment process (Table 6B.2). i.e., in the current red phosphors, Eu^{3+} is not facing any symmetry distortion with heat treatment process. Thus the site symmetry of Eu^{3+} is not an important attributing factor to the luminescence enhancement of current red phosphors.

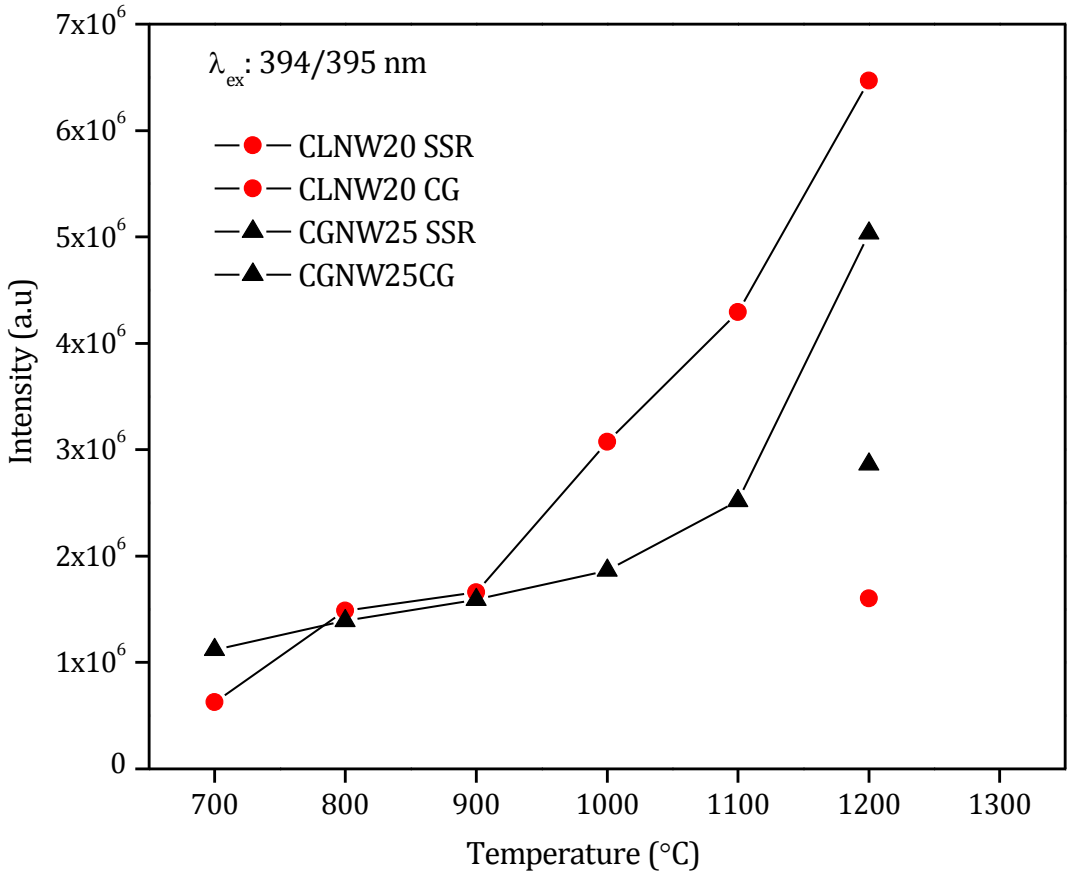

Fig. 6B.10 The variation of red emission intensity under near UV excitation of $CaLa_{0.80}NbWO_8$: $0.20Eu^{3+}$ and $CaGd_{0.75}NbWO_8$: $0.25Eu^{3+}$ (SSR & CG) heat treated at different temperatures from 700 to 1200°C.

Looking into other factors responsible for the luminescence enhancement, morphological variation of the phosphor samples is more prominent. From the SEM images of the phosphors (Figs. 6B.4 and 6B.5), they have uniform particle size, shape and less agglomeration. The particle surfaces are smoother, which can reduce the scattering loss and hence more absorption (Rao R. P *et al* 1996). Also with variation in the synthesis route from SSR to CG, an effective mixing of the activator ions (Eu^{3+}) in the host lattice at the molecular level is possible and this can help more number of electrons to participate in the absorption and luminescence process. There is a reduction in the average crystallite size and increment

in the crystallinity of the current red phosphors with respect to the heat treatment process from 700 to 1200°C (clear from XRD patterns Figs. 6B.1 and 6B.2). These all factors are favorable for the effective absorption of the incident light and excitation process (Guo C *et al* 2008) (Yang H. K *et al* 2010). Excitation spectra reveal such increase in the intensity of excitation with heat treatment process.

Table 6B.2 The asymmetry ratio, FWHM and color co ordinates of $CaLa_{0.80}NbWO_8$: $0.20Eu^{3+}$ and $CaGd_{0.75}NbWO_8$: $0.25Eu^{3+}$ with heat treatment process

°C	FWHM (nm)		Asymmetry Ratio		Color Co ordinates (x, y)	
	CLNW20	CGNW25	CLNW20	CGNW25	CLNW20	CGNW25
700	4.93	4.71	10.64	10.5	(0.64, 0.34)	(0.65, 0.35)
800	4.96	4.59	9.32	10.5	(0.64, 0.34)	(0.65, 0.34)
900	5.07	4.69	9.01	9.1	(0.65, 0.34)	(0.65, 0.34)
1000	5.19	4.73	8.54	8.67	(0.65, 0.34)	(0.65, 0.34)
1200	5.29	4.75	8.26	8.53	(0.65, 0.34)	(0.64, 0.33)
1100	5.51	4.96	7.83	7.74	(0.65, 0.34)	(0.65,0.34)
1200 (SSR)	5.20	5.09	8.81	8.47	(0.62, 0.33)	(0.64,0.34)

One notable observation from the excitation spectra is the red shift of the CT band of phosphor samples with respect to the heat treatment process which can contribute to the luminescence enhancement to some extent. Since electric dipole transition $^5D_0$-$^7F_2$ is parity forbidden, it can borrow intensity from lowest strong absorption band making the $^5D_0$-$^7F_2$ transition more probable and hence an improvement in luminescence intensity. For CLNW20 and CGNW25 samples, CT band is red shifted from 276/279 nm to 299 nm with heat

treatment from 700 to 1200°C and for corresponding SSR samples, the CT band is positioned at 290 and 303 nm respectively. This red shift associated with heat treatment process can improve the absorption strength of the intra configurational transitions of Eu^{3+}, specifically $^7F_0$– $^5L_6$ (394/395 nm) and $^7F_0$– $^5D_2$ (465 nm) transitions through process of energy transfer. However the position of CT band for SSR analogue of CGNW25 sample is still at a lower energy and hence more luminescence enhancement (~4 times) of CLNW20 (CG) sample compared to its SSR analogue is obvious. Further it is necessary to understand the variation of lifetime of $^5D_0$ levels of Eu^{3+} in these phosphors with respect to heat treatment process. This can help us to realize the contributing factors (whether absorption strength variation or lifetime variation) to the luminescence enhancement and is included in the next session.

6B.3.3.3 Lifetime measurement

The decay curves of $^5D_0$ emitting levels of Eu^{3+} in CLNW20 and CGNW25 phosphors are recorded under near UV (394/395 nm) excitations. All the decay curves are well fitted with the single exponential function $I = A \exp(-x/\tau)$ where I, τ and A are intensity, decay time and fitting parameter respectively. The variation of decay time of red emission with respect to heat treatment from 700 to 1200°C is presented in Table 6B.3.

Table 6B.3. The variation of decay time of red emission of $CaLa_{0.80}NbWO_8$: $0.20Eu^{3+}$ and $CaGd_{0.75}NbWO_8$: $0.25Eu^{3+}$ with respect to heat treatment from 700 to 1200°C

Temperature (°C)	τ(ms) CLNW20	τ(ms) CGNW25
700	1.1142	1.1659
800	1.0196	1.157
900	0.8138	0.9864
1000	0.7016	0.8847
1200(SSR)	0.7609	0.7103

The lifetime value is steadily decreasing with heat treatment process from 700 to 1200°C, similar to that for the molybdate red phosphors discussed in the earlier part of this chapter.

From the decay curve measurement we are getting the total lifetime of Eu^{3+}, which includes both radiative lifetime (τ_R) and non radiative lifetime (τ_{NR}) , such that;

$$\tau = \tau_R + \tau_{NR} \quad (6B.2)$$

and

$$\frac{1}{\tau} = A_{rad} + A_{nrad} \quad (6B.3)$$

where A_{rad} and A_{nrad} are radiative and non radiative transition probabilities respectively. Thus the variation of lifetime is well related to the variation of both radiative and non radiative components of lifetime. Similar to the molybdate red phosphors, in the present phosphors also there is a trend of increasing the absorption strength and emission intensity with the heat treatment process.

What may be the factors responsible for the lifetime variation of the tungstate red phosphors with respect to heat treatment process? From XRD patterns and scanning electron micrographs we got the information that the average crystallite size and particle size is increasing with heat treatment. However, contrary results are reported with the variation of lifetime with respect to particle size as mentioned in the earlier part. Here in the present study the correlation of particle size and lifetime looks to be not very significant.

Another aspect is the red shift of CT band position of phosphors with heat treatment process. From the excitation spectra it is very clear that the CT band is shifting to lower energy regime especially at higher temperature of 1200°C. As the heat treatment from 700°C to 1200°C occurs, the CT band for CLNW20 and CGNW25 phosphors is shifted from 276/279 nm (36,231/35,842 cm^{-1}) to 299 nm (33,444 cm^{-1}). Red shifting of CT band implies the reduction of energy gap between CT states of the phosphor host lattice and intra configurational *f -f* levels of activator ion (Eu^{3+}). However, in the present case CT band is still at a higher energy (lower wavelength) region compared to that of the molybdates (31,948 cm^{-1}). Thus the extent of overlapping of CT states of host lattice and *f -f* levels is minimum for both CLNW20 and CGNW25 red phosphors (shown in Fig. 6B.11) and a less chance for the non radiative transition through CT states. Consequently the red shifting of CT states of CLNW20 and CGNW25 red phosphors with heat treatment may have a less prominent role for their lifetime reduction.

It is also noted that with heat treatment process the extent of crystallinity of the current phosphors is improved and this can lead to the formation of Eu^{3+} clusters or Eu^{3+} - Eu^{3+} pairs.

This in turn will cause strong interaction between the activator ions leading to non radiative transitions and a reduction in the lifetime. This is a more prominent factor for the lifetime reduction of the current red phosphors. Both in the molybdates which are discussed earlier and in current tungstates synthesized via CG route and heat treated at different temperature are characterized by the similar observation of reduction in lifetime with heat treatment process. But for the present case, Eu^{3+} cluster formation is the major reason for lifetime reduction than red shifting of CT states with heat treatment process. The lifetime of the SSR analogues of CLNW20 and CGNW25 phosphors are still lower. This can be due to the presence of inactive layers on their particle surface through intermittent grinding during the SSR process.

In nut shell, the variation of the synthesis method and heat treatment process for both CLNW20 and CGNW25 red phosphors resulted in their luminescence enhancement. This luminescence enhancement can be mainly due to the improved absorption strength of the phosphors and is achieved by the improvement in the morphology, crystallinity, CT red shift etc. The degree of luminescence improvement of tungstate based red phosphors is more with respect to their SSR analogues than that of the molybdate phosphors.

6B.4 Conclusions

Tungstate based red phosphors $CaLa_{0.80}NbWO_8$: $0.20Eu^{3+}$ and $CaLa_{0.75}NbWO_8$: $0.25Eu^{3+}$ were successfully synthesized via citrate gel route. The influence of variation of synthesis method and heat treatment process on the luminescence behavior is investigated in detail. Morphological improvement as well as the effective mixing of Eu^{3+} ions at the molecular level was possible by citrate gel method and heat treatment. The absorption strength of the phosphors was increased by improvement of crystallinity and red shift of the CT band during the heat treatment. These phosphors are characterized by longer lifetime and better red emission intensity compared to that of their SSR and molybdate analogue samples.

CHAPTER 7

CONCLUSIONS AND FUTURE SCOPE OF THE WORK

CONCLUSIONS

A series of Eu^{3+} activated molybdate/ tungstate based powellite/ scheelite type novel red phosphors have been synthesized via both solid state reaction and citrate gel route. During the present research work efforts have been taken to study the luminescence properties of these red phosphors and the factors affecting their luminescence performance. Major conclusions drawn from the results and discussions presented in the previous chapters covering the three parts of the present research work are included in this chapter.

- The photoluminescence properties of powellite/scheelite type Eu^{3+} activated phosphors: $Ca(La/Gd)_{1-x}NbMoO_8$ and $Ca(La/Gd)_{1-x}NbWO_8$ are reported for the first time.

- All the aforementioned phosphors are well excitable under near UV and blue irradiations via intra configurational *f-f* transitions of Eu^{3+}.

- The CT band of molybdates are positioned at a lower energy region; making a more probable energy transfer from its CT states to Eu^{3+} levels compared to their tungstate analogues.

- The activator ions (Eu^{3+}) are distributed in the non centrosymmetric sites in the lattice of both phosphors leading to a sharp red emission via $^5D_0$ - $^7F_2$ transitions.

- The lifetimes of Eu^{3+} states in the current molybdate and tungstate based red phosphors are in the order of milli seconds.

- Bi^{3+} incorporation in the optimized (activator concentration) samples improved their morphology as well as crystallinity.

- The red shifting of CT band position of both molybdates (313 nm to 330 nm) and tungstates (290 to 324/327 nm) is accomplished by Bi^{3+} codoping and is owing to Bi^{3+} absorption process.

- The position and intensity of CT band of the phosphors played a key role in controlling the luminescence behavior of current red phosphors.

- In the case of tungstate based red phosphors, the Bi^{3+} codoping not only red shifted the CT band position but also intensified its CT transitions.

- An enhancement in the red emission intensity of both phosphors is achieved (~2 times) via Bi^{3+} codoping.

- Bi^{3+} codoping influenced the microstructure of both phosphors progressively. The extent of agglomeration of both phosphors reduced to a great extent which also had a direct contribution to their luminescence enhancement.

- Synthesis method and heat treatment process influenced the luminescence performance of current red phosphors to a great extent.

- The phase formation of the phosphor samples is occurred at a lower temperature of 700°C via citrate gel method compared to the solid state reaction method.

- The phosphor particles attained uniform particle shape, more homogeneity as well as narrow size distribution via the CG route. The average particle size of the particle is reduced from 5 µm to 100 nm - 1 µm.

- An enhanced red emission (~4 times) is achieved by the variation in the synthesis method and heat treatment process.

- The lifetime reduction of the phosphors with respect to heat treatment process revealed the possibility of overlapping of CT states of the host lattice with *f-f* levels of Eu^{3+} and hence the non radiative energy transfer process.

- All these phosphors are characterized by good color purity with CIE color co ordinates comparable to that of NTSC standard red phosphors and quantum efficiency.

- The current red phosphors could be good red candidates for pc-WLED applications.

FUTURE SCOPE

The present research work on luminescence properties of molybdate and tungstate based red phosphors work can open up ways to different areas of study. Major scope of the present research work for future studies includes the following points.

- Thermal stability of luminescence behavior of developed red phosphors and its optimization.
- Structural variation and luminescence property correlation.
- Broadening the excitation wavelength region via cationic variations in the host lattice.
- Synthesis of phosphors via different methods to achieve a more spherical morphology to improve its absorption strength.
- Variation of luminescence emission intensity with respect to particle size.
- Influence of position and intensity of charge transfer band on luminescence emission intensity and quantum efficiency of phosphors.
- Incorporation of developed red phosphors on suitable near UV/ Blue LED chips.
- The output characteristics of aforementioned LED chip - Phosphor combination.

LIST OF PUBLICATIONS

SCI Journals

1. Novel powellite based red emitting phosphors: $CaLa_{1-x}NbMoO_8$: xEu^{3+} for white light emitting diodes, **Mariyam Thomas**, P. Prabhakar Rao, M. Deepa, M.R. Chandran, Peter Koshy, J. Solid State Chem. 182 (2009) 203-207.

2. Luminescent properties of Eu^{3+}, Bi^{3+} co activated $CaLaNbWO_8$ red phosphors under near UV and Blue excitations, **Mariyam Thomas**, P. Prabhakar Rao, S.K. Mahesh, Sandhya Kumari L, Peter Koshy, Phys. Status Solidi A, 208 (2011) 2170-2175.

3. Improvement of Morphology and Luminescence properties of Powellite type Red phosphors $CaGd_{1-x}NbMoO_8$: xEu^{3+} synthesized via Citrate gel route, **Mariyam Thomas**, P. Prabhakar Rao, S. K. Mahesh, V. R. Reshmi, T. Linda Francis, Peter Koshy, J. Am. Ceram. Soc. 95 (2012) 2260-2265.

4. New orange red emitting phosphor La_3NbO_7: Eu^{3+} under blue excitation, Linda Francis T, Prabhakar Rao P, **Mariyam Thomas**, Mahesh S K, Reshmi V R, Mat. Lett. 81 (2012) 142-144.

5. Photoluminescence characteristics of new stannate pyrochlore based red phosphors: $CaLaSnNbO_7$: Eu^{3+} , S. K. Mahesh P. Prabhakar Rao, **Mariyam Thomas**, A. N. Radhakrishnan, Peter Koshy , J Mater Sci: Mater Electron 23 (2012) 1605-1609.

6. Multiband Orange Red Emitting Phosphors $SrY_3SiP_5O_{20}$: Eu^{3+} under Near-UV Irradiation, L. Sandhya Kumari, P. Prabhakar Rao, **Mariyam Thomas**, Peter Koshy, J. Electrochem. Soc., 156 (8) (2009) P127-P131.

International/ National Conferences Poster presentations

1. Synthesis and luminescent properties of novel red phosphors $CaGd_{1-x}NbMoO_8$: xEu^{3+} for White Light Emitting Diodes, *23rd Kerala Science Congress*, Thiruvananthapuram, Kerala, January 29-31, 2011 **Mariyam Thomas**, Prabhakar Rao P, S.K. Mahesh, V.R. Reshmi, Linda Francis T, Peter Koshy.

2. Luminescent Properties of Bi^{3+} Coactivated Novel Red Phosphors $CaGd_{0.75-y}NbWO_8$: $0.25Eu^{3+}$,yBi^{3+} for White Light Emitting Diodes, *National Conference on Science, Technology and Applications of Rare earths (STAR),*Munnar, Kerala, August 19-20, 2011 **Mariyam Thomas**, Prabhakar Rao P, Mahesh S K, Reshmi V R, Linda Francis T, Peter Koshy.

3. New Molybdenum based Pyrochlore type red phosphors $KGd_{1-x}SnMoO_7$: xEu^{3+}, International Conference on Luminescence and its Applications (*ICLA)*, Hyderabad, February 7-12, 2012 Reshmi V. R, Prabhakar Rao P, **Mariyam Thomas**, Mahesh S. K, Linda Francis T.

4. Intense Orange Red emitting phosphor La_3NbO_7: Eu^{3+} under Blue excitation, International Conference on Luminescence and its Applications (*ICLA)*, Hyderabad, February 7-12, 2012 Linda Francis T, Prabhakar Rao P, **Mariyam Thomas**, Mahesh S K, Reshmi V. R.

5. Photoluminescence Properties in New Pyrochlore Type Oxides $Gd_{3-x}Y_xMO_7$: yEu^{3+} [M=Nb, Ta, Sb] *National Conference on Science, Technology and Applications of Rare earths (STAR),*Munnar, Kerala, August 19-20, 2011 Linda Francis T, Prabhakar Rao P, **Mariyam Thomas**, Mahesh S K, Reshmi V R

6. New Powellite based Red phosphors $CaLa_{1-x}SbMo/WO_8$: xEu^{3+} for WLED applications, *National Conference on Science, Technology and Applications of Rare earths (STAR),*Munnar, Kerala, August 19-20, 2011 Reshmi V R, Prabhakar Rao P, **Mariyam Thomas**, Mahesh S K, Linda Francis T

7. Red luminescence in Stannate Based Pyrochlore Type Phosphors: $CaYSnNbO_7$: Eu^{3+} *7th National Symposium and Conference on Solid state Chemistry and Allied areas (ISCAS),* Thiruvananthapuram, Kerala, November 24-26, 2011 S.K. Mahesh, P. Prabhakar Rao, Mariyam Thomas, Linda Francis T, Reshmi V R Peter Koshy.

8. Forbidden electric dipole transition ($^5D_0$-$^7F_2$) dominant red luminescence in new quaternary stannate pyrochlores: $CaLaSnNbO_7$: Eu^{3+} , International Conference on Advanced Functional Materials (*ICAFM)*Thiruvananthapuram, Kerala, December 9-10, 2009 S.K. Mahesh, P. Prabhakar Rao, **Mariyam Thomas,** Peter Koshy.

9. Structure, microstructure and luminescent properties of rare earth phosphors for WLED application, *Indian Analytical Science Congress* (*IASC),* Lonavala, Maharashtra, November 12-13, 2009 Sandhya Kumari L, **Mariyam Thomas**, S.K. Mahesh, P. Prabhakar Rao, Peter Koshy.

10. Synthesis and Luminescent Properties of Powellite type Red phosphors $CaLa_{1-x}NbMoO_8$: xEu^{3+} (x = 0.01, 0.03, 0.05, 0.1) *National Conference on Electron Microscopy and Allied fields (EMSI NC),* Jhansi, Delhi January 17-19, 2009 (Oral Presentation).

Awards / Achievements

- Selected the paper entitled 'Novel powellite based red emitting phosphors: $CaLa_{1-x}NbMoO_8$: xEu^{3+} for white light emitting diodes' as **Top 25 Hottest Articles** list in Science Direct (Materials Science - Journal Solid state Chemistry) January – March 2009.

- The research work on Red phosphors based on powellite $CaLa_{1-x}NbMoO_8$: xEu^{3+} has got special mention in **Dataweek** Tech News Magazine in the article '*Phosphors based LEDs*' (Issue: 15 April 2009).

- **Best Poster Award** in 23rd Kerala Science Congress for the poster entitled 'Synthesis and luminescent properties of novel red phosphors $CaGd_{1-x}NbMoO_8$: xEu^{3+} for White Light Emitting Diodes'

- The research work on Red phosphors based on Scheelite $CaLa_{1-x}NbWO_8$: xEu^{3+}, Bi^{3+} has got special mention in **Vertical News** in the article entitled '*New findings from NIIST describe advances in Materials Science'* (Issue: 6 November 2011).

REFERENCES

Aanegola S, Petroski J, Radkov E, "Let there be light" *Proc. SPIE Int. Soc. Opt. Eng.* **10** (2003) 16.

Achary S. N, Patwe S. J, Mathews M. D, Tyagi A. K, "High temperature crystal chemistry and thermal expansion of synthetic powellite ($CaMoO_4$): A high temperature X ray diffraction (HT-XRD) study" *J. Phys. Chem. Solids* **67** (2006) 774.

Ahmad G, Dickerson M. B, Church B. C, "Room Temperature Formation of Crystalline Calcium Molybdate Phosphor Microparticles via Peptide Induced Precipitation" *Adv. Mater.* **18** (2006) 1759.

Bachmann V, Justel T, Meijerink A, Ronda C. J, Schmidt P, "Luminescence properties of $SrSi_2O_2N_2$ doped with divalent rare earth ions" *J. Lumin.* **121** (2006) 441.

Bando K, Sakano K, Noguchi Y, Shimizu Y, "Development of high bright and pure white LED lamps", *J. Light Vis.* Environ, **22**, (1998) 2.

Barbosa L. B, Reyes Ardila D, Cusatis C, Andreeta J. P, "Growth and characterization of crack-free scheelite calcium molybdate single crystal fiber" *J. Cryst. Growth* **235** (2002) 327.

Blasse G, "Hand book on Physics and chemistry of Rare earths" *North Holland Publishing company*, Netherlands (1979).

Blasse G, "On the Eu^{3+} Fluorescence of Mixed Metal Oxides (IV): The Photoluminescent Efficiency of Eu^{3+} Activated Oxides" *J. Chem. Phys.* **45** (1966) 2356.

Blasse G, Bril A, "Characteristic Luminescence" *Philips Tech. Rev.* **31** (1970) 314.

Blasse G, Bril A, "Study of Energy Transfer from Sb^{3+}, Bi^{3+}, Ce^{3+} to Sm^{3+}, Eu^{3+}, Tb^{3+}, Dy^{3+}," *J. Chem. Phys.* **47** (1967)1920.

Blasse G, Grambier B. C, "Luminescent Materials" *Springer Verlag*, Heidelberg (1994).

Bosze E. J, McKittrick J, Hirata G. A, "Investigation of the physical properties of a blue-emitting phosphor produced using a rapid exothermic reaction" *Mater. Sci. Eng. B.* **97** (2003) 265.

Boyer D, Chadeyron B. G, Mahiou R, Caperaa C, Cousseins J. C, "Synthesis dependent luminescence efficiency inEu^{3+} doped polycrystalline YBO_3" *J. Mater. Chem.* **9** (1999) 211.

Bozzola J. J, Russell L. D, "Electron Microscopy" *Jones and Bartlett Publishers Inc*, Boston (1992).

Cao F, Tian Y, Chen Y, Xiao L, Wu Q, "Novel red phosphors for solid state lighting: $Ca_{0.54}Sr_{0.34-1.5x}Eu_{0.08}La_x(MoO_4)_y(WO_4)_{1-y}$" *J. Alloys Compd.* **475** (2009) 387.

Cao F. B, Tian Y. W, Chen Y. J, Xiao L. J, Wu Q, "Luminescence investigation of red phosphors $Ca_{0.54}Sr_{0.34-1.5x}Eu_{0.08}Sm_x(MoO_4)_y\ (WO_4)_{1-y}$ for UV white LED device" *J. Lumin.* **129** (2009) 585.

Carnall W. T, Crosswhite H, Crosswhite H. M, "Energy level structure and transition probabilities of Trivalent Lanthanides in LaF_3" *Argonne National Laboratory Report* **ANL-78-XX-95** (1978).

Chen G. Y, Somesfalean G, Liu Y, Zhang Z. G, Sun Q, Wang F. P, "Upconversion mechanism for two color emission in rare earth ion doped ZrO_2 nanocrystals" *Phys. Rev. B* **75** (2007) 195204.

Chi L. S, Liu R. S, Lee B. J, "Synthesis of Y_2O_3: Eu, Bi red phosphors by homogeneous co-precipitation and their photoluminescence behaviors" *J. Electrochem. Soc.* **152** (2005) 93.

Chiu C. H, Wang M. F, Lee C. S, Chen T. M, "Structural, spectroscopic and photoluminescence studies of $LiEu(WO_4)_{2-x}(MoO_4)_x$ as a near UV convertible phosphor" *J. Solid State Chem.* **180** (2007) 619.

Ci Z. P, Wang Y. H, Zhang J. C, "$Ca_{1-x}Mo_{1-y}Si_yO_4$: Eu_x^{3+}: A novel red phosphor for white light emitting diodes" *Physica* B **403** (2008) 670.

Cullity B. D, "Elements of X-ray Diffraction" 2nd Ed, *Addison Wesley Publishing Company*, Massachusetts (1978).

Dai Q, Song H, Bai X, Pan G, Lu S, Wang T, Ren X, Zhao H, "Photoluminescence Properties of $ZnWO_4$: Eu^{3+} Nanocrystals Prepared by a Hydrothermal Method" *J. Phys. Chem. C.* **111** (2007) 7586.

Dhage S. R, Gaikwad S. P, Muthukumar P, Ravi V, "Synthesis of $Ce_{0.75}Zr_{0.25}O_2$ by citrate gel method" *Mater. Lett*. **58** (2004) 2704 (a).

Dhage S. R, Khollam Y, Deshpande S. B, Potdar H. S, Ravi V, "Synthesis of bismuth titanate by citrate method" *Mater. Res. Bull*. **39** (2004) 1993 (b).

Do Y. R, Huh Y. D, "Optical properties of potassium europium tungstate phosphors" *J. Electrochem. Soc*. **147** (2000) 4385.

Duan C. J, Delsing A, Hintzen H. T, "Photoluminescence Properties of Novel Red-Emitting Mn^{2+}-Activated MZnOS (M = Ca, Ba) Phosphors" *Chem. Mater.* **21** (2009) 1010.

Duan C. J, Wang X. J, Otten W. M, Delsing A. C. A, Zhao J. T, Hintzen H. T, "Preparation, Electronic Structure, and Photoluminescence Properties of Eu^{2+}- and Ce^{3+}/Li^{+}Activated Alkaline Earth Silicon Nitride $MSiN_2$ (M = Sr, Ba)" *Chem. Mater.* **20** (2008) 1597.

Dubrovskii G. P, Zykov A. M, Chernovets B. V, "Luminescence of Rare Earth Activated $MgSiN_2$" *Inorganic Materials* **17** (1981) 1059 (translated from *Izv. Akad. Nauk. SSSR, Neorg. Mater.* **17** (1981) 1421).

Feldmann C, Justel T, Ronda C. R, Schmidt P. J, "Inorganic Luminescent Materials - 100 Years of Research and Application" *Adv. Funct. Mater.* **13** (2003) 511.

Fergus J. W, Chen H. P, "Structure and Conductivity of Tetragonal and Rhombohedral Lanthanum Oxyfluoride Compounds" *J. Electrochem. Soc.* **147** (2000) 4696.

Flegler S. L, Heckman Jr J. W, Klomparens K. L, "Scanning and Transmission Electron Microscopy" *W. H. Freeman and Company*, New York (1993).

Fu Z, Zhou S, Pan T, Zhang S, "Preparation and Luminescent Properties of Cubic Eu^{3+}: Y_2O_3 Nanocrystals and Comparison to Bulk Eu^{3+}: Y_2O_3*" J. Lumin.* **124** (2007) 213.

Fu Z, Zhou S, Zhang S, "Preparation and Optical Properties of Trivalent Europium Doped Bulk and Nanocrystalline SrY_2O_4" J. Opt. Soc. Am. B **23** (2006) 1852.

Fujihara S, Kato T, Kimura T, "Sol-gel synthesis and luminescent properties of oxyfluoride LaOF:Eu^{3+} thin films" *J. Mater. Sci. Lett.* **20** (2001) 687.

Gaido G. K, Dubrovskii G. P, Zykov A. M, "Photoluminescence of Europium Activated $MgSiN_2$" *Inorganic Materials* **10** (1974) 485 (translated from *Izv. Akad. Nauk. SSSR, Neorg. Mater.* **10** (1974) 564).

Geng J, Zhang J. R, Hong J. M, Zhu J. J, "Sonochemical synthesis of $PbWO_4$ nanoparticles" *Int. J. Mod. Phys. B* **19** (2005) 2734.

Goldstein J. I, Newbery D. E, Echlin P, Joy D. C, Fiori C, Lifshin E, "Scanning electron microscopy and X-ray microanalysis", *Plenum press,* New York, (1981).

GonHzalez A. H. M, Simoes A. Z, Zaghete M. A Varela J. A, "Effect of preannealing on the morphology of $LiTaO_3$ thin films prepared from the polymeric precursor method" *Mater. Charact.* **50** (2003) 233.

Graser R, Pitt Et al, Scharmann A, Zimmerer G, "Optical properties of $CaWO_4$ and $CaMoO_4$ crystals in the 4 to 25 eV region" *Phys. Status Solidi B* **69** (1975) 359.

Gundiah G, Shimomura Y, Kijima N, Cheetham A. K, "Novel red phosphors based on vanadate garnets for solid state lighting applications" *Chem.Phys. Lett.* **455** (2008) 279.

Guo C, Li B, Jin F, "Synthesis luminescence properties of host luminescent materials $Na_5Eu(MoO_4)_4$ and $NaEu(MoO_4)_2$" *Chin. J. Lumin.* **12** (1991) 118.

Guo C, Zhang W, Luan L, Chen T, Cheng H, Huang D, "A promising red emitting phosphor for white light emitting diodes prepared by sol gel method" *Sens. Actuators, B* **133** (2008) 33.

Guo C. F, Gao F, Xu Y, Liang L. F, Shi F. G, Yan B. H, "Efficient red phosphors $Na_5Ln(MoO_4)_4 : Eu^{3+}$ (Ln = La, Gd and Y) for white LEDs" *J. Phys. D* **42** (2009) 095407 (a).

Guo C. F, Yang H. K, Fu Z, Li L, Choi B. C, Jeong J. H, "A Potential Red Emitting Phosphor $BaGd_2(MoO_4)_4: Eu^{3+}$ for Near UV White LED" *J. Am. Ceram. Soc.* **92** (2009) 1713 (b).

H.J. Borchardt , "Rare earth phosphors" *J. Chem. Phys.* **38** (1963) 1251.

He X. H, Zhu Y, "Improvement of morphology and luminescence of CaS: Eu^{2+} red-emitting phosphor particles via carbon-containing additive strategy" *J. Mater. Sci*. **43** (2008)1515.

Heath J. P, "Dictionary of Microscopy" *John Wiley and Sons Ltd.* England (2005).

Henderson B,.Imbusch G. F, "Optical Spectroscopy of Inorganic Solids" *Clarendon Press*, Oxford (1989).

Hill C. G. A, "CRT Phosphors" *SID Seminar Lecture Notes*, S-6.2 (1984).

Hirosaki N, X ie R. J, Kimoto K, Sekiguchi T, Yamamoto Y, Suehiro T, Mitomo M, "Characterization and properties of green emitting β-SiAlON:Eu^{2+} powder phosphors for white light emitting diodes" *Appl. Phys. Lett.* **86** (2005) 211905.

Hoppe H. A, Lutz H, Morys P, Schnick W, Seilmeier A, "Luminescence in Eu^{2+}-doped $Ba_2Si_5N_8$: fluorescence, thermoluminescence, and upconversion", *J. Phys. Chem. Solids* **61** (2000) 2001.

Hsiao Y. J, Fang T. H, Chang Y. S, Chang Y. H, Liu C. H, "Structure and luminescent properties of $LaNbO_4$ synthesized by sol–gel process" *J. Lumin.* **126** (2007) 866.

Hu Y, Zhuang W, Ye H. Q, Zhang S. S, Fang Y, Huang X. W, "Preparation and Luminescent Properties of $(Ca_{1-x}Sr)S$: Eu^{2+} Red-Emitting Phosphor for White LED" *J. Lumin.* **111** (2005) 139.

Hu Y. S, Zhuang W. D, Ye H. Q, Wang D. H, Zhang S. S, Huang X: W, "A novel red phosphor for white light emitting diodes" *J. Alloys Compd.* **390** (2005) 226.

Huh Y. D, Park J. Y, Kweon S. S, Kim J. H, Kim J. G, Do Y. R, "Phosphor Converted Three Band White LED" *Bull. Korean Chem. Soc.* **25** (2004) 1585.

Huh Y. D, Shim J. H, Kim Y, Do Y. R, "Optical properties of three band white light emitting diodes," *J. Electrochem. Soc.* **150** (2003) H57.

J Wang J. G, Jing X. P, Yan C. H, Lin J. H, Liao F. H, "Influence of fluoride on f–f transitions of Eu^{3+} in $LiEuM_2O_8$ (*M*=Mo, W)" *J. Lumin.* **121** (2006) 57.

Jin Y, Zhang J, Lu S, Zhao H, Zhang X, Wang X, "Fabrication of Eu^{3+} and Sm^{3+} Codoped Micro/Nanosized $MMoO_4$ (M = Ca, Ba, and Sr) via Facile Hydrothermal Method and Their Photoluminescence Properties through Energy Transfer" *J. Phys. Chem. C* **112** (2008) 5860.

Jin Y, Hao Z, Zhang X, Luo Y, Wang X, Zhang J, "Dynamical processes of energy transfer in red emitting phosphor $CaMoO_4$: Sm^{3+}, Eu^{3+}"*Opt. Mater.* **33** (2011) 1591.

Johnson L. F, Boyd G. D, Nassau K, Soden R. R, "Continuous operation of a solid state optical maser" *Phys. Re*V. **126** (1962) 1406.

Jung M. K, Park W. J, Yoon D. H, "Photoluminescence characteristics of red phosphor Eu^{3+}, Sm^{3+} co-doped Y_2O_3 for white light emitting diodes" *Sens. Actuators,* B **126** (2007) 328.

Junli H, Liya Z, Zhaoping L, Fuzhong G, Jianpeng H, Rongfang W, "Promising red phosphors $LaNbO_4$:Eu^{3+}, Bi^{3+} for LED solid-state lighting application" *J. Rare Earth.* **28** (2010) 356.

Jüstel T, Nikel H, Ronda C, "New Developments in the Field of Luminescent Materials for Lighting and Displays" *Angew Chem.* **37** (1998) 3084.

Kang H. S, Kang Y. C, Jung K.Y, Park S. B, "Eu doped barium strontium silicate phosphor particles prepared from spray solution containing NH_4Cl flux by spray pyrolysis" *Mater. Sci. Eng. B* **121** (2005) 81.

Kato A, Oishi S, Shishido T, Yamazaki M, Iida S, "Evaluation of stoichiometric rare- earth molybdate and tungstate compounds as laser materials" *J. Phys. Chem. Solids* **66** (2005) 2079.

Kato K, Okamoto F, "Preparation and Cathodoluminescence of CaS: Eu and $Ca_{1-x}Sr_xS$: Eu Phosphors" *Jpn. J. Appl. Phys.* **22** (1983) 76.

Kaufman J. E, Christensen J. F, "Lighting Handbook" *Waverly Press,* Maryland (1972).

Kim J. S, Jeon P. E, Park Y. H, Choi J. C, Park H. L, "White-light generation through ultraviolet-emitting diode and white-emitting phosphor" *Applied Physics Letters* **85** (2004), 3696.

Kim K, Moon Y. M, Choi S, Jung H. K, Nahm S, "Luminescent properties of a novel green-emitting gallium borate phosphor under vacuum ultraviolet excitation" *Mater. Lett.* **62**(2008) 3925.

Kim T, Kang S, "Potential red phosphor for UV-white LED device" J. Lumin. **122-123 (**2007) 964.

Kodaira C. A, Brito H. F, Claudia M, Felinto F. C, "Luminescence investigation of Eu^{3+} ion in the $RE_2(WO_4)_3$ matrix (*RE* = La and Gd) produced using the Pechini method" *J. Solid State Chem.* **171** (2003) 401.

Kong L. B, Zhang T. S, Ma J, Boey F, "Progress in synthesis of ferroelectric ceramic materials via high-energy mechanochemical technique" *Prog. Mater. Sci*. **53** (2008) 207.

Kramer K. W, Biner D, Frei G, Gudel H. U, Hehlen M. P, Luthi S. R, "Hexagonal sodium yttrium fluoride based green and blue emitting upconversion phosphors" *Chem. Mater.* **16** (2004) 1244.

Krames M. R, Shchekin O. B, Mueller Mach R, Mueller G. O, Zhou L, Harbers G, Craford M. G, "Status and Future of High Power Light Emitting Diodes for Solid-State Lighting" *J. Display Technol.* **3** (2007) 160.

Kuleshov N. V, Lagatsky A. A, Podlipensky A. V, Mikhailov V. P, Huber G, "Pulsed laser operation of Yb doped $KY(WO_4)_2$ and $KGd(WO_4)_2$ *Opt. Lett.* **22** (1997) 1317.

Kumar A, Kumar J, "Perspective on Europium Activated Fine Grained Metal Molybdate Phosphors for Solid State Illumination" *J. Mater. Chem.* **21** (2011) 3788.

Le T. R, Cheetham A. K, "Red emitting cerium based phosphor materials for solid state lighting applications" *Chem. Phys. Lett.* **423** (2006) 352.

Lee E. Y, Kim Y. J, "Optical Excitation and Emission Spectra of $YNbO_4$: Eu^{3+}" *J. Korean Electrochem. Soc.* **12** (2009) 243.

Lee G. H, Kang S, "Solid-solution red phosphors for white LEDs" *J. Lumin.* **131** (2011) 2582 (a).

Lee G. H, Kang S, "Studies in crystal structure and luminescence properties of Eu^{3+} doped metal tungstate phosphors for white LEDs" *J. Lumin.* **131** (2011) 2606 (b).

Lee, S. Lim, S. S. Sun, J. F. Wager, "Photoluminescence and electroluminescence characteristics of $CaSiN_2$: Eu phosphor" *Proc. SPIE-Int. Soc. Opt. Eng.* **3241** (1997) 75.

Lei F, Yan B, "Hydrothermal synthesis and luminescence of $CaMO_4$: RE^{3+} (M = W, Mo; RE = Eu, Tb) submicro phosphors" *J. Solid State Chem.* **181** (2008) 855.

Lei F, Yan B, Chen H. H, "Solid state synthesis, characterization and luminescent properties of Eu^{3+} doped gadolinium tungstate and molybdate phosphors: $Gd_{(2-x)}MO_6:Eu_x^{3+}$ (M = W, Mo)" *J. Solid State Chem.* **181** (2008) 2845.

Lei S, Zhang X, Li Z, Yu T, Zou Z, "Enhancement in Photoluminescence of $CaMoO_4:Eu^{3+}$ Through Introducing MVO_4 (M = Y or Bi)" *J. Electro. Chem. Soc.* **156** (2009) J367.

Lenggoro I.W, Panatarani C, Okuyama K, "One-step synthesis and photoluminescence of doped strontium titanate particles with controlled morphology" *Mater. Sci. Eng. B* **113** (2004) 60.

Li P, Wang Z, Yang Z, Guo Q, Li X, "Emission features of $LiBaBO_3:Sm^{3+}$ red phosphor for white LED**"** *Mater. Lett.* **63** (2009) 751.

Li P. L, Yang Z. P, Wang Z. J, Guo Q. L, "White light emitting diodes of UV based $Sr_3Y_2(BO_3)_4:Dy^{3+}$ and luminescent properties" *Mater. Lett.* **62**(2008) 1455.

Li X, Yang Z. P, Guan L, "Luminescent properties of alkali metal ion and trivalent europium ion co activated alkaline earth molybdate phosphors" *J. Synth. Cryst.* **36** (2007) 1192.

Li Y. Q, Fang C. M, With G, Hintzen H. T, "Preparation, structure and photoluminescence properties of Eu^{2+} and Ce^{3+}-doped $SrYSi_4N_7$" *J. Solid State Chem.* **177** (2004) 4687 (a).

Li Y. Q, Fang C. M, With G, Hintzen H. T, "Synthesis, structure, and luminescence properties of Eu^{2+} and Ce^{3+} activated $BaYSi_4N_7$" *J. Alloys. Compd.* **385** (2004) 1 (b).

Li Y. Q, With G, Hintzen H. T, "Luminescence of a new class of UV – blue emitting phosphors $MSi_2O_{2-\delta}N_{2+2/3\delta}$: Ce^{3+} (M = Ca, Sr, Ba)" *J. Mater. Chem.* **15** (2005) 4492.

Li Z. H, Zheng L. Z, Zhang L. N, Xiong L. Y, "Synthesis, characterization and upconversion emission properties of the nanocrystals of Yb^{3+}/Er^{3+}codoped YF_3 – YOF -Y_2O_3 system" *J. Lumin.* **126** (2007) 481.

Lia H, Zhou S, Zhang S, "The relationship between the thermal expansions and structures of ABO_4 oxides", *J. Solid State Chem.* **180** (2007) 589.

Liao J, Huang H, You H, Qiu X, Li Y, Qiu B, Wen H. R, "Photoluminescence properties of $NaGd(MoO_4)_2$: Eu^{3+} nanophosphors prepared by sol-gel method" *Mater. Res. Bull.* **45** (2010) 1145.

Linga Y. Y, Minga L. X, Lin F. W, Lin L. W, Yia T. C, "Co-precipitation synthesis and photoluminescence properties of $(Ca_{1-x-y,}Ln_y)MoO_4$: xEu^{3+} (Ln = Y, Gd) red phosphors" *J. Alloys Compd.* **505** (2010) 239.

Liu J, Lian H. Z, Shi C. S "Improved optical photoluminescence by charge compensation in the phosphor system $CaMoO_4$:Eu^{3+}" *Opt. Mater.* **29 (**2007) 1591.

Liu X, Han K, Gu M, Xiao L, Ni C, Huang S, Liu B, "Effect of codopants on enhanced luminescence of $GdTaO_4$: Eu^{3+} phosphors" *Solid State Commun.* **142** (2007) 680.

Llanos J, Cortes R, "Preparation, characterization and luminescence of La_2TeO_6 phosphor doped with Eu^{3+}" *Mater. Res. Bull.* **43** (2008) 2763.

Llanos J, Cortes R, "Synthesis and luminescent properties of a new red-emitting phosphor for solid-state lighting: $Eu_{0.1}Gd_xLa_{1.9-x}TeO_6$ ($0.02 \leq x \leq 0.1$)" *J. Lumin.* **129** (2009) 465.

Lou X. M, Chen D. H, "Synthesis of $CaWO_4$:Eu^{3+} phosphor powders via a combustion process and its optical properties" *Mater. Lett.* **62** (2008) 1681.

Macalik L, Maczka M, Hanuza J, "Structure and properties of the $KNbW_2O_9$ hexagonal bronze doped with Eu^{3+} ions as an optically active probe" *J. Alloys Compds.* **380** (2004) 248.

Malta O. L, Brito H. F, Menezes J. F. S, Goncüalves e Silva F. S, "Spectroscopic properties of a new light converting device Eu(thenoyltrifluoroacetonate)$_3$ 2(dibenzyl sulfoxide). A theoretical analysis based on structural data obtained from a sparkle model" *J. Lumin.* **75** (1997) 255 (b).

Malta O. L, Couto dos Santos M. A, Thompson L. C, Ito N. K, "Intensity parameters of 4f—4f transitions in the Eu(dipivaloylmethanate)$_3$ 1, 10-phenanthroline complex" *J. Lumin.* **69** (1996) 77 (a).

Marrero Lopez D, Nunez P, Abril M, Lavin V, "Synthesis, electrical properties, and optical characterization of Eu^{3+}-doped $La_2Mo_2O_9$ nanocrystalline phosphors" *J. Non.Cryst. Solids*. **345 - 346** (2004) 377.

Menyuk N, Dwight K, Pierce J. W, "$NaYF_4$: Yb,Er- An efficient upconversion phosphor" *Appl. Phys. Lett.* **21** (1972) 159.

Minami T, Utsubo T, Miyata T, Suzuki Y, "PL and EL properties of Tm-activated vanadium oxide-based phosphor thin films" *Thin Solid Films.* **445** (2003) 377.

Moszynski M, Balcerzyk W, Czarnacki A, Nassalski T, Mikhailik I. M, Solskii, "Characterization of $CaWO_4$ scintillator at room and liquid nitrogen temperatures" *Nucl. Instrum. Methods Phys. Res. A* **553** (2005) 578.

Nagirnyi V, Feldbach E, Jonsson L, Kirm M, Lushchik A, Lushchik C, Nagornaya L. L, Ryzhikov V. D, Savikhin F, Svensson G, Tupitsina I. A, "Excitonic and recombination processes in $CaWO_4$ and $CdWO_4$ scintillators under synchrotron irradiation" *Radiat. Meas.* **29** (1997) 247.

Nakamura S, Fasol G, "*The Blue Laser Diode: GaN Based Light Emitters and Lasers*" Springer: Berlin, Germany (1997).

Nakamura S, Mukai T, Senoh M, "Candela class high brightness InGaN/AlGaN double heterostructure blue light emitting diodes" *Appl. Phys. Lett.* **64** (1994) 1687.

Nalwa H. S, Rohwer L. S, "Handbook of Luminescence, Display Materials, and Display Devices", *American Scientific Publishers*, California (2003).

Narukawa Y, "White light LEDs" *Opt. Photonics News* **4** (2004) 25.

Nassau K, Levinstein H, Loiacono G. M, "A comprehensive study of trivalent tungstates and molybdates of the type $L_2(MO_4)_3$" *J. Phys. Chem. Solids* **26** (1965) 1805.

Nazarov M. V, Jeon D. Y, Kang J. H, Popovici E, Muresan L. E, Zamoryanskaya M. V, Tsukerblat B. S, "Luminescence properties of europium terbium double activated calcium tungstate phosphor" *Solid State Commun.* **131** (2004) 307.

Nazarov M. V, Tsukerblat B. S, Popovici E. J, Jeon D.Y, "Optical lines in europium–terbium double activated calcium tungstate phosphor" *Phys. Lett. A* **330** (2004) 291.

Neeraj S, Kijima N, Cheetham A. K, "Novel red phosphors for solid-state lighting: the system $NaM(WO_4)_{2-x}(MoO_4)_x:Eu^{3+}$ (M=Gd, Y, Bi)" *Chem. Phys. Lett.* **387** (2004) 2 (a).

Neeraj S, Kijima N, Cheetham A. K, "Novel red phosphors for solid state lighting; the system $Bi_xLn_{1-x}VO_4$: Eu^{3+}/Sm^{3+} (Ln = Y, Gd)," *Solid State Commun.* **131** (2004) 65.

Nishida T, Ban T, Kobayashi N, "High color rendering light sources consisting of a 350 nm ultraviolet light emitting diode and three basal color phosphors" *Appl. Phys. Lett.* **82** (2003) 3817.

Nosenko A, Kostyk L, Koslovs'ka L, "Some peculiarities of the luminescence of the lead tungstate crystals" *J. Lumin*. **90**, (2000) 49.

Okamoto S, Yamamoto H, "Photoluminescent Properties of $(La,Eu,Sm)_2W_3O_{12}$ Red Phosphor for Near UV LED Based Solid State Lighting" *Electrochem. Solid State lett.* **10** (2007) 139.

Pang M. L, Lin J, Fu J, Cheng Z.Y, "Luminescent properties of $Gd_2Ti_2O_7$: Eu^{3+} phosphor films prepared by sol- gel process" *Mater. Res. Bull.* **39** (2004) 1607.

Parchur A. K, Ningthoujam R. S, Rai S. B, Okram G. S, Sing R. A, Tyagi M, Gadkari S. C, Tewari R, Vatsa R. K, "Luminescence Properties of Eu^{3+} Doped $CaMoO_4$ Nanoparticles," *Dalton Trans.* **40** (2011) 7595.

Pelant I, Valenta J, "Luminescence Spectroscopy of Semiconductors" *Oxford University Press*, New York (2012).

Peng C. Y, Zhang H. J, Yu J. B, Meng, Q. G, Fu L. S, "Synthesis, Characterization, and Luminescence Properties of the Ternary Europium Complex Covalently Bonded to Mesoporous SBA-15" *J. Phys. Chem. B* **109** (2005) 15278.

Peng H. S, Song H. W, Chen B. J, Wang J. W, Lu S. Z, Kong X. G, "Temperature Dependence of Luminescent Spectra and Dynamics in Nanocrystalline Y_2O_3: Eu^{3+}" J. *Chem. Phys.* **118** (2003) 3277.

Petricca F, Angloher G, Cozzini C, Frank T, Hauff D, Ninkovic J, Pröbst F, Seidel W, Uchaikin S, "Light detector development for CRESST II" *Nucl. Instrum. Method A* **520** (2004) 193.

Piao X, Horikawa T, Hanzawa H, Machida K, "Characterization and luminescence properties of$Sr_2Si_5N_8:Eu^{2+}$ phosphor for white light emitting diode illumination" *Appl. Phys. Lett.* **88** (2006) 161908.

Pode R. B, Dhoble S. J, "Photoluminescence in $CaWO_4$: Bi^{3+}, Eu^{3+} material" *Phys. stat. sol. (b)* **203** (1997) 571.

Quanmao Y. U, Yufeng L, Shan W. U, Xingdong L. U, Xinyang H, Xiaoxia L, "Luminescent properties of $Ca_2SiO_4:Eu^{3+}$ red phosphor for trichromatic white light emitting diodes" *J. Rare Earths*. **26** (2008) 783.

Raju G. S. R, Jung H. C, Park J. Y, Moon B. K, Balakrishnaiah R, Jeong J. H, Kim J. H, "The Influence of Sintering Temperature on the Photoluminescence Properties of Oxyapatite Eu^{3+} : $Ca_2Gd_8Si_6O_{26}$ Nanophosphors," *Sens. Actuators B Chem.* **146** (2010) 395.

Rao B. V, Kumar G. B, Jang K, Lee H. S, Shin D. S, Yi S. S, Jeong J, "Citric Based Sol-Gel Synthesis and Luminescence Characteristics of $CaLa_2ZnO_5$: Eu^{3+} Phosphors for Blue LED Excited White LEDs" *J. Alloys Compd.* **512** (2012) 264.

Rao R. P, "Preparation and Characterization of Fine Grain Yttrium Based Phosphors by Sol-Gel Process," *J. Electrochem. Soc.* **143** (1996) 189.

Ravindran Nair K, Rao P. P, Sameera S, Mohan V. S, Chandran M. R, Koshy P, "New powellite type oxides in Ca–R–Nb–Mo–O system (R = Y, La, Nd, Sm or Bi) : Their synthesis, structure and dielectric properties" *Mater. Lett.* **62** (2008) 2868.

Reddy K. R, Annapurna K, Buddhudu S, "Fluorescence spectra of Eu^{3+}: Ln_2O_2S (Ln = Y, La, Gd) powder phosphors" *Mater. Res. Bull.* **31** (1996) 1355.

Rohwer L. S, Srivastava A. M, "Development of Phosphors" *Electrochem. Soc. Interface* **12** (2003) 36.

Ronda C, "Luminescence from Theory to Applications" *Wiley-VCH Verlag GmbH & Co. KGaA*, Weinheim (2008).

Ronda C, "Luminescence: From Theory to Applications" *Wiley Publications*, Weinheim, (2007).

Ryu J. H, Yoon J. W, Lim C. S, Oh W. C, Shim K. B, "Microwave assisted synthesis of $CaMoO_4$ nano powders by a citrate complex method and its photoluminescence property" *J. Alloys Compd.* **390** (2005) 245.

Sa' Ferreira R. A, Carlos L. D, Goncülves R. R, Ribeiro S. J. L, de Zea Bermudez V, "Energy-Transfer Mechanisms and Emission Quantum Yields In Eu^{3+}-Based Siloxane-Poly (oxyethylene) Nanohybrids" *Chem. Mater.* **13** (2001) 2991.

Santos P. C. R, Nogueira H. I. S, Fe'lix V, Drew M. G. B, Sa' Ferreira R. A, Carlos L. D, Trindade T, "Novel lanthanide luminescent materials based on complexes of 3-hydroxypicolinic acid and silica nanoparticles" *Chem. Mater.* **15** (2003) 100.

Saradhi M. P, Pralong V, Varadaraju U. V, Raveau B, "Facile Chemical Insertion of Lithium in $Eu_{0.33}Zr_2(PO_4)_3$ - An Elegant Approach for Tuning the Photoluminescence Properties" *Chem. Mate.r* **21** (2009) 1793.

Schubert E. F, Kim J. K, "Solid-state light sources getting smart" *Science* **308** (2005) 1274.

Shi F, Meng J, Ren Y, Su Q, "Structure, luminescence and magnetic properties of $AgLnW_2O_8$ (Ln = Eu, Gd, Tb, Dy) compounds " *J. Phys. Chem. Solids* **59** (1998) 105.

Shi G, "Semiconductor light-emitting diodes and solid state lighting" *Science Press,* Beijing (2007).

Shi S, Gao J, Zhou J, "Effects of charge compensation on the luminescence behavior of Eu^{3+} activated $CaWO_4$ phosphor" *Opt. Mater.* **30** (2008) 1616 (a).

Shi S, Liu X, Gao J, Zhou J, "Spectroscopic properties and intense red light emission of (Ca, Eu, M)WO_4 (M = Mg, Zn, Li)" *Spectrochem. Acta, Part A* **69** (2008) 396 (b).

Shigeo Shionoya W. M. Y, "Phosphor Handbook" *CRC Press,* Boca Raton (1999).

Shin S. H, Jeon D. Y, Suh K. S, "Charge transfer nature in luminescence of $YNbO_4$: Bi blue phosphor" *J. Appl. Phys.* **90** (2001) 5986.

Shur M. S, Zukauskas A, "Solid-state lighting: Toward superior illumination" *Proc. IEEE* **93** (2005) 1691.

Singh N. S, Ningthoujam R. S, Singh S. D, Viswanath B, Manoj N, Vatsa R. K, "Preparation of Highly Crystalline Blue Emitting MVO_4: Tm^{3+} (M = Gd, Y) Spherical Nanoparticles: Effects of Activator Concentration Annealing Temperature on Luminescence, Lifetime and Quantum Yield" *J. Lumin.* **130** (2010) 2452.

Sivakumar V, Varadaraju U. V, "A Novel Orange- red phosphor under Near UV excitation for white LEDs" *J. Electrochem. Soc.* **154** (2007) J28.

Sivakumar V, Varadaraju U. V, "Intense red emitting phosphors for white LEDs" *J. Electrochem. Soc.* **152** (2005) H168.

Sivakumar V, Varadaraju U.V, "Synthesis, phase transition and photoluminescence studies on Eu^{3+} substituted double perovskites - A novel orange-red phosphor for solid state lighting" *J. Solid State Chem.* **181** (2008) 3344.

Sleight A. W, "Accurate cell dimensions for ABO_4 molybdates and tungstates" *Acta Crystallogr., Sect. B* **28** (1972) 2899.

Smet P. F, Parmentier A. B, Poelman D, "Selecting Conversion Phosphors for White Light-Emitting Diodes" *J. Electrochem. Soc.* **158** (2011) R37.

Sohn K. S, Lee J. M, Shin N. S, "A Search for New Red Phosphors Using a Computational Evolutionary Optimization Process" *Adv. Mater.* **15** (2003) 2081.

Sohn K. S, Park D. H, Cho S. H, Kwak J. S, Kim J. S, "Computational Evolutionary Optimization of Red Phosphor for Use in Tricolor White LEDs" *Chem. Mater.* **18** (2006) 1768.

Song H. W, Wang J. W, Chen B. J, Lu S. Z, "Size Dependent Electronic Transition Rates in Cubic Nanocrystalline Europium Doped Yttria" *Chem. Phys. Lett.* **376** (2003) 1.

Steigerwald D. A, Bhat J. C, Collins D, Fletcher R. M, Holcomb M. O, Ludowise M. J, Martin P. S, Rudaz S. L, "Illumination with solid state lighting technology" *IEEE J. Sel. Top. Quant.* **8** (2002) 310.

Stevens W. R, "Building Physics: Lighting" *Pergamon Press*, London (1969).

Strek W, Bednarkiewicz A, Dere'n P. J, "Power dependence of luminescence of Tb^{3+} doped $KYb(WO_4)_2$ crystal" *J. Lumin.* **92** (2001) 229.

Struck C. W, Fonger W. H, "Role of the Charge Transfer States in Feeding and Thermally Emptying the 5D States of Eu^{3+} in Yttriyum and Lanthanum Oxysulfides" *J. Lumin,* **1–2** (1970) 456.

Su Q, Lin J, Li B, "A Study on the Luminescence Properties of Eu^{3+} and Dy^{3+} in $M_2RE_8(SiO_4)_6O_2$ (M = Mg, Ca; RE = Y, Gd, La)," *J. Alloys Compd.* **225** (1995) 120.

Su Y, Li L, Li G, "Synthesis and Optimum Luminescence of $CaWO_4$ Based Red Phosphors with Codoping of Eu^{3+} and Na^{+}" *Chem. Mater*. **20** (2008) 6060.

Sun Y, Qi L, Lee M, Lee B. I, Samuels W. D, Exarhos G. J, "Photoluminescent properties of Y_2O_3: Eu^{3+} phosphors prepared via urea precipitation in non-aqueous solution" *J. Lumin.* **109** (2004) 85.

Thiyagarajan P, Kottaisamy M, Ramachandra Rao M. S, "Luminescent properties of near UV excitable Ba_2ZnS_3 : Mn red emitting phosphor blend for white LED and display applications" *J. Phys. D: Appl. Phys.* **39** (2006) 2701.

Thomas M, Rao P, Deepa M, Chandran M. R, Koshy P, "Novel Powellite-Based Red Emitting Phosphors: $CaLa_{1-x}NbMoO_8$: xEu^{3+} for White Light Emitting Diodes," *J. Solid State Chem.* **182 [1]** (2009) 203.

Thomas S. M, Rao P. P, Ravindran Nair K, Koshy P, "New Red- and Green-Emitting Phosphors, $AYP_2O_{7.5}$: RE^{3+} (A = Ca and Sr; RE = Eu and Tb) under Near UV Irradiation" *J. Am. Ceram. Soc.* **91** (2008) 473.

Toquin R. L, Cheetham A. K, "Red-emitting cerium based phosphor materials for solid state lighting applications" *Chem. Phys. Lett*. **423** (2006) 352.

Treadaway M. J, Powell R. C "Energy-transfer in samarium doped calcium tungstate crystals" *Phys Rev B* **11** (1975) 862.

Treadaway M. J, Powell R. C, "Luminescence of calcium tungstate crystals" *J. Chem. Phys.* **61** (1974) 4003.

Tyminski J. K, Lawson C. M, Powell R. C, "Energy transfer between Eu^{3+} ions in $LiNbO_3$, $CaWO_4$, and $Eu_xY_{1-x}P_5O_{14}$ crystals" *J. Chem. Phys.* **77** (1982) 4318.

Uheda K, Hirosaki N, Yamamoto Y, Naito A, Nakajima T, Yamamoto H, "Luminescence Properties of a Red Phosphor, $CaAlSiN_3:Eu^{2+}$, for White Light Emitting Diodes" *Electrochem. Solid State Lett.* **9** (2006) (a) H22.

Uhlich D, Plewa J, Jüstel T, "Phase formation and characterization of $Sr_3Y_2Ge_3O_{12}$, $Sr_3In_2Ge_3O_{12}$, and $Ca_3Ga_2Ge_3O_{12}$ doped by trivalent europium" *J. Lumin.* **128** (2008) 1649.

Wang H, Medina F. D,. Zhou Y. D, Zhang Q. N, "Temperature dependence of the polarized Raman spectra of $ZnWO_4$ single crystals" *Phys. Rev. B* **45** (1992) 10356.

Wang H. Y, Wang R. J, Sun X. M, Yan R. X, Li Y. D, "Synthesis of red luminescent Eu^{3+} doped lanthanides compounds hollow spheres" *Mater. Res. Bull.* **40** (2005) 911.

Wang J, Jing X, Yan C, Lina J, "$Ca_{1-2x}Eu_xLi_xMoO_4$: A novel red phosphor for solid state lighting based on a GaN LED" *J. Electrochem. Soc.* **152** (2005) G186.

Wang J. G, Jing X. P, Yan C. H, Lin J. H, "$Ca_{1-2x}Eu_xLi_xMoO_4$: A Novel Red Phosphor for Solid-State Lighting Based on a GaN LED" *J. Electrochem. Soc.* **152** (2005) G186.

Wang S. F, Rao K. K, Wang Y. R,. Hsu Y. F, Chen S. H, Lu Y. C, "Structural Characterization and Luminescent Properties of a Red Phosphor Series: $Y_{2-x}Eu_x(MoO_4)_3$ (x = 0.4 - 2.0)" *J. Am. Ceram. Soc.* **92** (2009) 1732.

Wang W, Yang P, Gai S, Niu N, He F, Lin J, "Fabrication and luminescent properties of $CaWO_4$: Ln^{3+} (Ln^{3+} = Eu, Sm, Dy) nanocrystals" *J. Nanopart. Res.* **12** (2010) 2295.

Wang X. X, Xian Y. L, Wang G, Shi T. X, Su Q, Gong M. L, "Luminescence investigation of Eu^{3+}- Sm^{3+} codoped $Gd_{2-x-y}Eu_xSm_y(MoO_4)_3$ phosphors as red phosphors for UV InGaN-based light emitting diode" *Opt. Mater.* **30** (2007) 521.

Wang Z, Liang H, Gong M, Su Q, "Luminescence investigation of Eu^{3+} activated double molybdates red phosphors with scheelite structure" *J. Alloys Compd.* **432** (2007) 308.

Wang Z, Liang H, Gong M, Su Q, "Novel red phosphor of Bi^{3+}, Sm^{3+} co activated $NaEu(MoO_4)_2$" *Opt. Mater.* **29** (2006) 896.

Wang Z. L, Liang H. B, Gong M. L, Su Q, "Novel red phosphor of Bi^{3+}, Sm^{3+} co-activated $NaEu(MoO_4)_2$" *Opt. Mater.* **29** (2007) 896.

Wang Z. L, Liang H. B, Zhou L, Wang J, Gong M. L, Su Q, "$NaEu_{0.96}Sm_{0.04}(MoO_4)_2$ as a promising red-emitting phosphor for LED solid-state lighting prepared by the Pechini process" *J. Lumin.* **128** (2008) 147.

Wang Z. L, Liang H. B, Zhou L. Y, Wu H, Gong M. L, Su Q, "Luminescence of $(Li_{0.333}Na_{0.334}K_{0.333})Eu(MoO_4)_2$ and its application in near UV InGaN based light emitting diode" *Chem. Phys. Lett.* **412** (2005) 313.

Warren B. E, "X ray Diffraction" *Dover Publications*, New York (1969).

Wei Q, Chen D, "Luminescence properties of Eu^{3+} and Sm^{3+} coactivated Gd(III) tungstate phosphor for light-emitting diodes" *Opt. Laser Technol.* **41** (2009) 783.

West A. R, "Solid State Chemistry and its Applications", *John Wiley and Sons*, Singapore (1984)

Williams D. K, Yuan H, Tissue B. M, "Size Dependence of the Luminescence Spectra and Dynamics of Eu^{3+}: Y_2O_3 Nanocrystals" *J. Lumin.* **83** (1999) 297.

Won Y, Jang H. S, Im W. B, Jeon D. Y, "Red-emitting $LiLa_2O_2BO_3$:Sm^{3+}, Eu^{3+} phosphor for near ultraviolet light emitting diodes based solid state lighting" *J. Electrochem. Soc*. **155** (2008) J226.

Wu H, Zhang X, Guo C, Xu J, Wu M., Su Q, "Three band white light from InGaN based blue LED chip precoated with green/red phosphors" *IEEE Photonics Technol. Lett.* **17 (**2005) 1160.

Xie A, Yuan X, Hai S, Wang J, Wang F, Li L, "Enhancement emission intensity of $CaMoO_4$: Eu^{3+}, Na^+ phosphor via Bi co-doping and Si substitution for application to white LEDs" *J. Phys. D: Appl. Phys.* **42** (2009) 105107.

Xie A, Yuan X. M, Hai S. J, Wang J. J, Wang F. X, Li L, "Enhancement emission intensity of $CaMoO_4$: Eu^{3+}, Na^+ phosphor via Bi co doping and Si substitution for application to white LEDs" *J. Phys. D* **42** (2009) 105107.

Xie A, Yuvan X, Shi Y, Wang F, Wang J, "Photoluminescence Characteristics of Energy Transfer Between Eu^{3+} and Bi^{3+} in $LiEu_{1-x}Bi_x(WO_4)_{0.5}(MoO_4)_{1.5}$" *J. Am. Ceram. Soc.* **92** (2009) 2254.

Xie R. J, Hirosaki N, Kiumra N, Sakuma K, Mitomo M, "2-phosphor converted white light emitting diodes using oxynitride/nitride phosphors" *Appl. Phys. Lett.* **90** (2007) 191101.

Xie R. J, Hirosaki N, Mitomo M, Yamamoto Y, Suehiro T, Sakuma K, "Optical Properties of Eu^{2+} in α-SiAlON" *J. Phys. Chem.* B **108** (2004) 12027.

Xie R. J, Mitomo M, Uheda K, .Xu F. F, Akimune Y, "Preparation and Luminescence Spectra of Calcium and Rare Earth (R = Eu, Tb, and Pr) Codoped α-SiAlON Ceramics" *J. Am. Ceram. Soc.* **85** (2002) 1229.

Yamada M, Narukawa Y, Tamaki H, Murazaki Y, Mukai T, "A Methodological Study of the Best Solution for Generating White Light Using Nitride Based Light Emitting Diodes" *IEICE Trans. Electron.* **E88C** (2005) 1860.

Yamashita N, Harada O, Nanamura K, "Photoluminescence Spectra of Eu^{2+} Centers in Ca(S, Se):Eu and Sr(S, Se):Eu" *Jpn. J. Appl. Phys.* **34** (1995) 5539.

Yan B, Lin L, Wu J, Lei F, "Photoluminescence of Rare Earth Phosphors $Na_{0.5}Gd_{0.5}WO_4$: RE^{3+} and $Na_{0.5}Gd_{0.5}(Mo_{0.75}W_{0.25})O_4$: RE^{3+} (RE = Eu, Sm, Dy)" *J. Fluoresc.* **21** (2011) 203.

Yan S. X, Zhang J. H, Zhang X, Lu S. Z, Ren X. G, Nie Z. G, Wang X. J, „Enhanced Red Emission in $CaMoO_4$:Bi^{3+},Eu^{3+}" *J. Phys. Chem. C* **111** (2007) 13256.

Yang H. K, Jeong J. H, "Synthesis, Crystal Growth, and Photoluminescence Properties of YAG: Eu^{3+} Phosphors by High Energy Ball Milling and Solid State Reaction" *J. Phys. Chem. C* **114** (2010) 226.

Ye S, Liu Z. S, Wang J. G, Jing X. P, "Luminescent properties of $Sr_2P_2O_7$:Eu,Mn phosphor under near UV excitation" *Mater. Res. Bull.* **43** (2008) 1057 (a).

Ye S, Wang C. H, Jing X. P, "Long Wavelength Extension of the Excitation Band of $LiEuMo_2O_8$ Phosphor with Bi^{3+} Doping" *J. Electrochem. Soc.* **156** (2009) J121.

Ye S, Wang C. H, Jing X. P, "Long Wavelength Extension of the Excitation Band of $LiEuMo_2O_8$ Phosphor with Bi^{3+} Doping" *J. Electrochem. Soc.* **156** (2009) J121.

Ye S, Wang C. H, Liu Z. S, Lu J, Jing X. P, "Photoluminescence and energy transfer of phosphor series $Ba_{2-z}Sr_zCaMo_{1-y}W_yO_6$:Eu,Li for white light UVLED applications" *Appl. Phys. B* **91** (2008) 551.

Ye S, X.M. Wang, X.P. Jing, "Energy transfer among Ce^{3+}, Eu^{2+}, and Mn^{2+} in $CaSiO_3$," *J. Electrochem. Soc.* **155** (2008) J143 (b).

Ye S, Xiao F, Pan Y. X, Ma Y. Y, Zhang Q. Y, "Phosphors in Phosphor Converted White Light Emitting Diodes: Recent Advances in Materials, Techniques and Properties" *Mater. Sci. Eng. R.* **71** (2010) 1.

Yen W. M, Weber M. J, "Inorganic phosphors: compositions, preparation, and optical properties" *The CRC Press*, New York (2004).

Yi G. R, Moon J. H, Manoharan V. N, Pine D. J, Yang S. M, "Packings of uniform microspheres with ordered macropores fabricated by double templating" *J. Am. Chem. Soc.* **124** (2002) 13354.

Ying Z, Linghong D, Xinling P , Weifeng Z, "Influence of annealing temperature on luminescent properties of Eu^{3+}/V^{5+} co doped nanocrystalline $Gd_2Ti_2O_7$ powder" *J. Rare Earths.* **27 (**2009) 900.

Yu F, Zuo J, Zhao Z, Jiang C, Yang Q, "Low temperature synthesis and photoluminescent properties of $CaMoO_4:Eu^{3+}$ red phosphor with uniform micro-assemblies" *Mater. Res. Bull.* **46** (2011) 1327.

Žalga A, Sažinas R, Garškaitė "Sol gel synthesis of RE^{3+} activated $CaWO_4$ phosphors" *Chemija.* **20 (**2009) 69.

Zalkin A, Templeton D. H, "X Ray diffraction refinement of the calcium tungstate structure" *J. Chem. Phys.* **40** (1964) 501.

Zeng J. H, Lou T. J, Wang Y. F, Guo J. C, Di D, Ma R. L, "Inorganic Single Source Precursor to Complex Fluoride and Oxyfluoride Nanocrystallines and Their Photoluminescence" *J. Phys. Chem. C*. **113** (2009), 597.

Zeng Q, Liang H, Gong M, Su Q, "Synthesis and Luminescence of $Ca_3Ln_2W_2O_{12}$: Eu^{3+} for near UV InGaN Based Red Emitting LED" *J. Electrochem. Soc.* **155** (2008) H730.

Zhang G. X, Jia R. P,. Wu Q. S, "Preparation, structural and optical properties of AWO_4 (A = Ca, Ba, Sr) nanofilms" *Mater. Sci. Eng. B* **128** (2006) 254.

Zhang N, Bu W. B, Xu Y. P, Jiang D.Y, Shi J. L, "Self assembled Flowerlike Europium-Doped Lanthanide Molybdate Micro architectures and Their Photoluminescence Properties" *J. Phys. Chem. C* **111** (2007) 5014.

Zhang Q. Y, Pita K, Buddhudu S, Kam C. H, "Luminescent properties of rare earth ion doped yttrium silicate thin film phosphors for a full color display" *J. Phys. D* **35** (2002) 3085.

Zhang Z. H, Huang Q, Zhao X, Huang Z. L, "Enhanced red emission of $CaMoO_4$: Eu^{3+} phosphor by structural adjustment for white light-emitting diodes application" *Phys. Status Solidi A* **206** (2009) 2839.

Zhang Z. J, Chen H. H, Yang X, Zhao J, "Preparation and luminescent properties of Eu^{3+} and Tb^{3+} ions in the host of $CaMoO_4$" *Mater. Sci. Eng. B* **145** (2007) 34.

Zhao X, Wang X, Chen B, Meng Q, Yan B, Di W, "Luminescent properties of Eu^{3+} doped α-$Gd_2(MoO_4)_3$ phosphor for white light emitting diodes" *Opt. Mater.* **29** (2007) 1680.

Zhao X. X, Wang X. J, Chen B. J, Meng Q. Y, Di W. H, Ren G. Z, Yang Y. M, "Novel Eu^{3+} doped red emitting phosphor $Gd_2Mo_3O_9$ for white light emitting diodes (WLEDs) application" *J. Alloy Compd.* **433** (2007) 352.

Zheludev N, "The life and times of the LED - a 100 year history" *Nat. Photonics* **1** (2007) 189.

Zhou Y, Liu J, Yang X, Yu X, J. Zhuang, "A promising deep red phosphor $AgLaMo_2O_8$: Pr^{3+} with blue excitation for white LED application" *J. Electro. Chem. Soc.* **157** (2010) H278.

Zhu C. Q, Xiao S. G, Ding B. W, Yang X. L, Qiang R. F, "Synthesis and photoluminescent properties of Eu^{3+} doped $(1-x)$ $CaO - xLi_2O - WO_3$ phosphors" *Mater. Sci. Eng. B* **150** (2008) 95.